# UNIVERSIDAD NACIONAL AUTÓNOMA DE MÉXICO

**Instituto de Geofísica**
**Pósgrado en Ciencias de la Tierra**

## ESTRUCTURA GEOELÉCTRICA DEL CRÁTER DE IMPACTO DE CHICXULUB, YUCATÁN, MÉXICO

# T E S I S

Que para Optar por el Grado de
**DOCTOR EN CIENCIAS (EXPLORACIÓN)**
P R E S E N T A :

**OMAR DELGADO RODRÍGUEZ**



**CD. UNIVERSITARIA**
**2001**

## AGRADECIMIENTOS

Agradezco al Señor Jesús, escudo y fortaleza, quien transforma mis problemas en victorias.

Agradezco a la Universidad Nacional Autónoma de México y en especial al Programa de Posgrado en Ciencias de la Tierra, por permitirme realizar este estudio de posgrado.

A la Dirección General de Asuntos del Personal Académico, por facilitar los recursos financieros destinados, tanto para la ejecución de los trabajos de campo, como en beca, haciendo posible este proyecto de investigación.

A la dirección del Instituto de Geofísica y Astronomía del CITMA de la República de Cuba, por el apoyo brindado para la continuación y culminación de los estudios doctorales.

Al Dr. Jaime Urrutia Fucugauchi, quien como asesor, dirigió el proyecto doctoral, por sus comentarios y experiencia transmitida.

A mis sinodales: Dr. José Oscar Campos Enríquez (quien propuso este tema de investigación y lo condujo en sus etapas iniciales), Dr. Jorge Arturo Arzate Flores, Dr. Fernando Ortega Gutiérrez, Dr. Juan Manuel Espíndola Castro, Dr. Arturo Diego Orozco y Dr. José María Chávez Aguirre, por revisar minuciosamente la redacción de este trabajo, contribuyendo al enriquecimiento del mismo.

Al personal del Instituto de Geofísica de la UNAM que me apoyaron significativamente en la conclusión de mis estudios, en especial: Frank García, Carlos Ortíz, Norma Bravo, Graciela Solache, Francois Graffe, Mónica Nava y Elizabeth Morales.

A las familias Morales de San Lucas, Coyoacán (Don Jorge, Jorgito, Luís, Lupita y Lupitica) y Arroyo-Varela de Prado Churubusco (Sara, Magaly y Miguel), quienes me aceptaron como integrante de sus respectivas familias, siendo esto de incalculable valor para mi.

A mi familia en Cuba (mi esposa Libertad, mi hijo Omar Jesús, mis padres y hermanos) por su incondicional apoyo en todo momento, sobrellevando mis cargas, compartiendo mis preocupaciones y anhelos.

Por último a todos aquellos que, aunque no menciono sus nombres, contribuyeron de manera alguna al logro de las tantas metas contenidas en este importante propósito.

GRACIAS

**DEDICATORIA**

*A mis padres:*

*Alfredo*

*y*

*Esther*

*Si fueres flojo en el día de trabajo,*
*tu fuerza será reducida.*
Prov. 24:10

## INDICE

## RESUMEN

Por más de una década varios estudios geológicos y geofísicos han sido realizados para investigar la estructura del cráter de impacto de Chicxulub, la cual está localizada en el sector noroeste de la península de Yucatán, México. En este trabajo, se aplica el método de sondeo magnetotelúrico (MT) con el objetivo de brindar un modelo geoeléctrico de dicha estructura. Un total de 22 sondeos MT fueron ejecutados a lo largo de dos perfiles radiales. Once sondeos se encuentran distribuidos a lo largo de un perfil N-S y diez a lo largo de un perfil NW-SE. En un primer análisis de la información MT del perfil NW-SE se pudo establecer un predominio del carácter 1-D del medio estudiado, con magnitudes de tipper (T) inferior a 0.2. Los sondeos MT 13, 14 y 15 presentan los mayores valores de T para frecuencias inferiores a 0.06 Hz. El comportamiento de la resistividad para períodos mayores a 16 s definen el limite estructural del cráter y la zona del anillo de cenote. Los valores de resistividad son mayores y menores a 150 ohm-m fuera y dentro del anillo de cenotes, respectivamente. Modelos 1-D, utilizando los esquemas de inversión de Bostick y Occam, fueron obtenidos con el fin de estudiar la distribución de la resistividad y la estructura interna del cráter. Aunque, en general, los sondeos MT presentan un carácter 1-D, las diferencias observadas en los modelos geoeléctricos $\rho_{xy}$ y $\rho_{yx}$, y los resultados de las secciones T y skew (k) indican la necesidad de realizar una inversión 2-D en ambos perfiles. Una inversión 2-D simultánea de los modos TE y TM fue realizada en ambos perfiles. Las secciones eléctricas obtenidas en ambos perfiles presentan diferencias significativas. En el perfil N-S, la frontera geoeléctrica que divide al basamento no fracturado del relleno del cráter muestra un pendiente más suave y se encuentra a más profundidad que en el perfil NW-SE. En este último perfil es observado, en su extremo NW, el alto estructural central expresado como un incremento de los valores de resistividad. Basado en los resultados obtenidos en ambos perfiles se propone un diámetro a la cavidad principal del cráter de 195 ± 4 km y a la base del alto estructural central de 80 ± 4 km. Las seudosecciones de T, k y skew regional ($\eta$) confirmaron características estructurales relacionadas con el cráter tales como el anillo de cenotes y la falla Ticul, las cuales no son evidentes en las secciones eléctricas obtenidas. Se realizó

una modelación sintética MT de la península de Yucatán y la plataforma marina que la circunda. Esta modelación indica la existencia de un efecto de costa despreciable sobre los sondeos MT ejecutados en ambos perfiles, además de proponer nuevas áreas para futuras mediciones MT con fines de estudio del cráter de Chicxulub.

## ABSTRACT

For more than a decade many geological and geophysical studies have been carried out to investigate on the subsurface structure of the Chicxulub impact crater, which is located at the northwestern sector of the Yucatan peninsula. In this work, the Chicxulub impact crater has been investigated by magnetotelluric (MT) soundings. A MT survey was carried out to assess the capabilities of the method to detect structural changes along two radial profiles (N-S and NW-SE) crossing the sinkholes ring. A total of 22 long period MT soundings were measured. One first analysis of the MT information was carried out in the NW-SE profile. In general, MT soundings are one-dimensional, with tipper magnitudes (T) well below 0.2. The MT soundings 13, 14 and 15 present the highest T values at frequencies lower than 0.06 Hz. The resistivity behavior for periods above 16 s defines the structural rim of the crater at the cenote ring zone. Resistivities are respectively higher and lower than 150 ohm-m outside and inside the cenote ring. One-dimensional modeling using Bostick and Occam inversion schemes gives similar geoelectrical models, which have been used to investigate on the subsurface structure and electrical conductivity distribution of the crater. Although, MT soundings present one-dimensional characteristics, the differences observed in the $\rho_{xy}$ and $\rho_{yx}$ and results of the T and Skew (k) sections indicate the need for a two-dimensional inversion of the MT soundings. A two-dimensional model was obtained for each profile from the simultaneous inversion of the TE and TM modes. The interpreted structural sections along the two measured profiles yielded significant differences. The N-S profile shows a smooth change of resistivity structure and a deeper undisturbed basement away from the crater center. However, the NW-SE profile renders a sharp electrical contact related to the major outer crater ring and a shallower undisturbed basement. In addition, a structural high is observed in this profile towards the postulated crater center. Based on

the two resistivity cross sections the crater diameter of the main cavity is set to 195 ± 4 km while the base of the crater central structural high to about 80 ± 4 km diameter. Pseudo sections of T, k and regional skew ($\eta$) were used to constrain structures related to the impact event such as the Ticul fault and the ring of sinkholes, which are not evident in the inverted resistivity sections. Three-dimensional synthetic modeling of magnetotelluric sounding data of the Yucatan peninsula, suggests that the coast effect on the magnetotelluric measurements carried out over the Chicxulub impact region is negligible. These results define other areas for future MT surveys in the Yucatan peninsula.

# 1.- INTRODUCCIÓN GENERAL

## 1.1.- El Límite Cretácico / Terciario

Los científicos relacionados con las Ciencias de la Tierra dedican gran parte de su tiempo y esfuerzo a tratar de entender los diferentes procesos que de una forma u otra han contribuido a la modificación del ambiente terrestre.

Específicamente, las extinciones masivas de la biota han acaparado la atención de la comunidad científica en todo el mundo. Se registran al menos 5 eventos mayores de extinción entre los períodos Cámbrico y el Presente (Albriton, 1989).

En el análisis de las causas de estas interrupciones paleontológicas se definen dos grupos fundamentales: uniformitaristas y catastrofistas.

Los uniformitaristas plantean que los cambios en la historia de la Tierra podrían ser explicados por la acumulación de eventos graduales, mientras que los catastrofistas sugieren que la historia geológica del planeta está constituida por cambios bruscos causados por grandes catástrofes.

Una de las más notables define el límite Cretácico / Terciario (K/T) hace aproximadamente 65 millones de años. La dramática diferencia entre la biota presente en ambos períodos es muy evidente, siendo esto objeto de estudio de los paleontólogos durante más de un siglo.

En la Figura 1 se muestra la variación del número de especies de amonites al final del Cretácico en una localidad de España. Mientras se aproxima en tiempo al Paleoceno (período Terciario), la presencia de amonites es practicamente nula, como evidencia de un período de extinción masiva (Fig. 1; Stanley, 1987).

Alvarez y colaboradores (1980) analizaron concentraciones anómalas de Iridio en el límite K/T en diferentes partes del mundo (Fig. 2), interpretándolas como indicadores de la existencia de una fuente de material extraterrestre en ese período. En la misma frontera K/T observaron una capa de arcilla oscura de algunos centímetros de espesor con un alto contenido de Iridio, el cual no es comun en la Tierra pero sí en ciertos tipos de meteoritos.

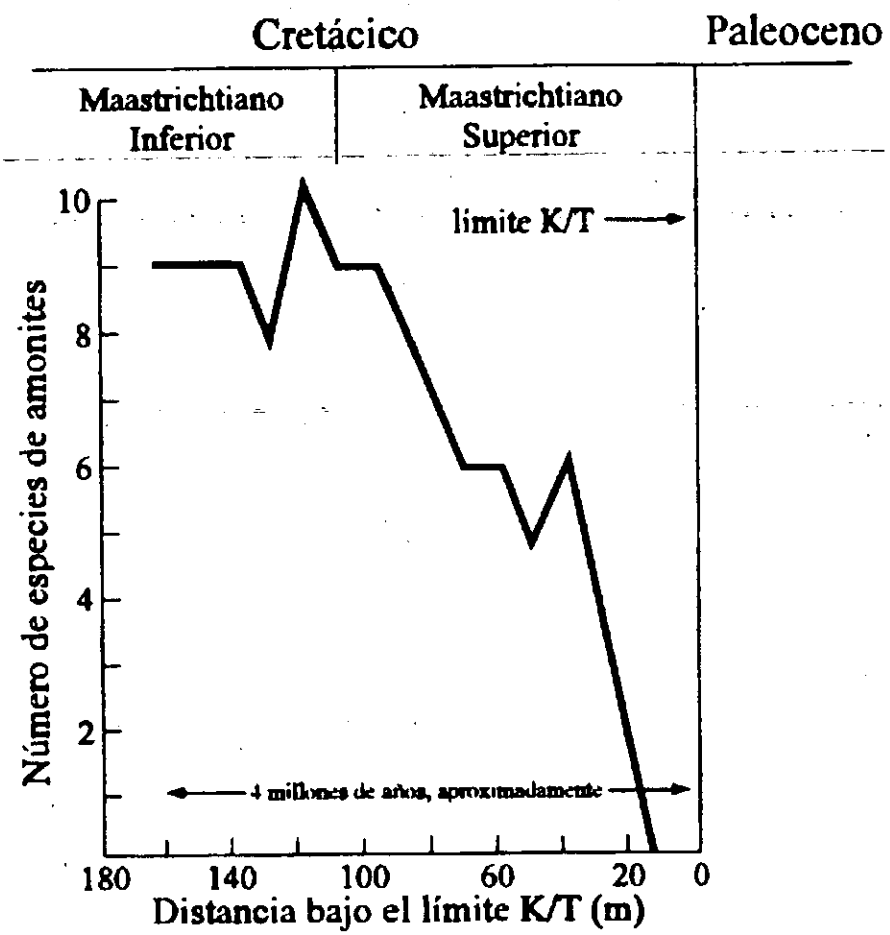


**Figura 1: Diversidad de especies de amonites en rocas maastrichtianas de Zumaya, España, según Stanley, 1987 (tomado de Vega-Vera y Perrilliat, 1997).**

Ellos propusieron como hipótesis que un meteorito de aproximadamente 10 km de diámetro impactó en la superficie terrestre, creando un cráter de diámetro estimado en 200 km. Al menos 1/3 del volumen total del polvo levantado penetró en la estratosfera. Esto provocó que se cubriera la atmósfera terrestre con una capa de polvo por un período de varios años, absorbiendo los rayos solares y afectando así el proceso de fotosíntesis. La consecuente ruptura de varias cadenas alimenticias provocó la extinción de muchas especies de animales y plantas

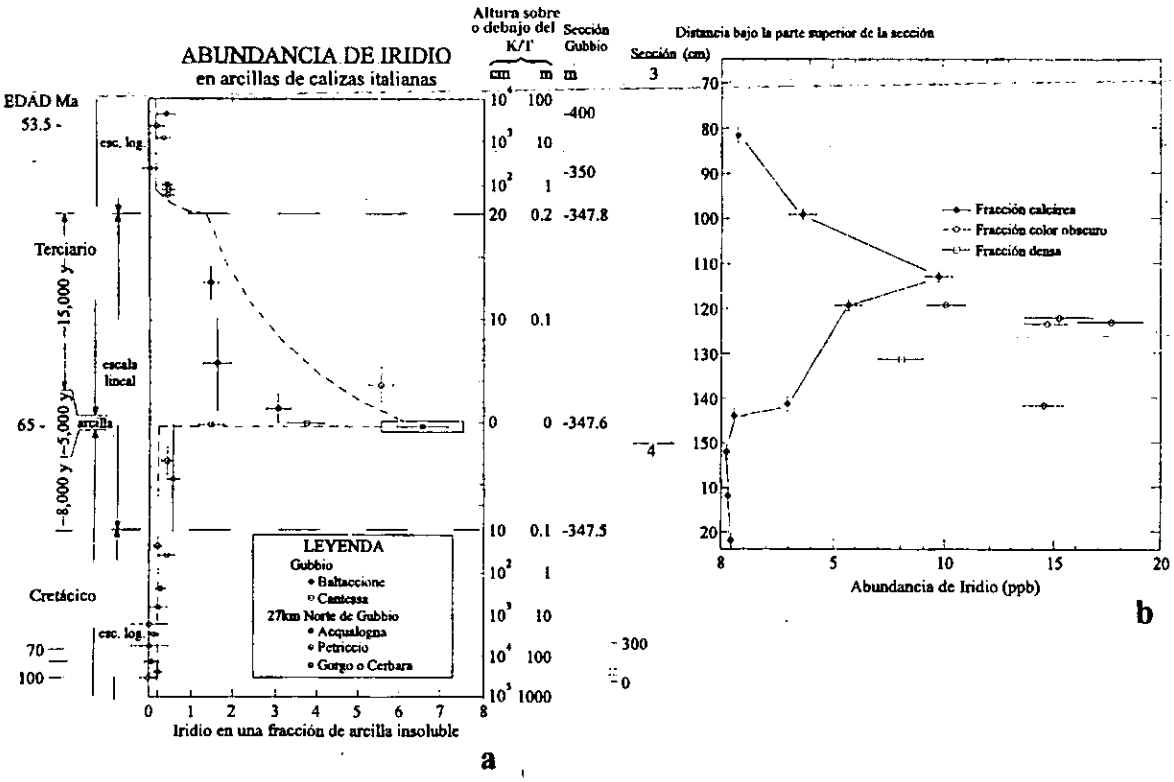


**Figura 2: Representación esquemática de la anomalía de Iridio en varias secciones en Umbria, Italia, según Alvarez y colaboradores (1982). a) Anomalía presente en la capa de arcilla que marca el límite K/T. b) Distribución de Iridio en la capa de arcilla perteneciente a las sección 3 (tomada de Urrutia-Fucugauchi y colaboradores, 1997).**

La hipótesis planteada por Alvarez y colaboradores (1980) puede ser convertida en tesis al descubrirse una estructura de impacto, cuya edad y dimensiones explique los cambios ocurridos en el período de transición K/T.

Las características de un estrato de sedimentos de 50 cm de espesor en la frontera K/T encontrado en Haití y depósitos de impacto en el resto de la región del Caribe, sugieren que el evento que ocurrió en esta frontera geológica debe estar entre América del Norte y América del Sur.

En la década de los 50´s PEMEX realizó un levantamiento gravimétrico en la península de Yucatán, México y a fines de los 70´s un levantamiento aero-magnético en la misma región, ambos con fines de prospección petrolera. Además, posteriormente se hicieron algunas perforaciones que ayudaron a establecer la estratigrafía de la región (Camargo-Zanoguera, 1997).

López-Ramos (1975) observó anomalías gravimétricas y magnéticas circulares de aproximadamente 200 km de diámetro en el margen noroeste de la península de Yucatán, lo que interpretó, de acuerdo a los registros litológicos de algunas de las perforaciones realizadas, como la presencia de rocas andesíticas asociadas a un centro volcánico. Sin embargo, Penfield y Camargo (1981) interpretaron estas anomalías como la señal de existencia de material asociado con un impacto meteorítico, en correspondecia con los resultados obtenidos y la hipótesis planteada por Alvarez y colaboradores (1980).

## 1.2.- El cráter de Chicxulub

### 1.2.1.- Antecedentes

En estas primeras perforaciones realizadas por PEMEX se pudo observar el predominio de secuencias carbonatadas y evaporíticas desde el Cretácico Inferior al Cuaternario que sobreyacen a un basamento cristalino poco conocido de edad probablemente Paleozoico (López-Ramos, 1983).

En la parte norte de la península, la secuencia de plataforma tiene no menos de 3500 m de espesor. La parte superior de esta secuencia es de edad Pleistoceno a Paleoceno. La fauna encontrada y las facies sedimentarias analizadas indican un ambiente de aguas más profundas que las encontradas en el resto de la plataforma. Las rocas encontradas son predominantemente calizas foraminíferas y margas. La unidad que subyace a la secuencia del Terciario está compuesta fundamentalmente de calizas foraminíferas, margas y pizarras arcillosas que han sido datadas como Cretácico Tardío (López-Ramos, 1973).

En la parte baja de esta segunda unidad se presentan pequeños estratos de vidrio andesíticos, el cual subyace a las brechas en los pozos C-1 y S-1 (Sharpton y colaboradores, 1992; Urrutia-Fucugauchi y colaboradores, 1994).

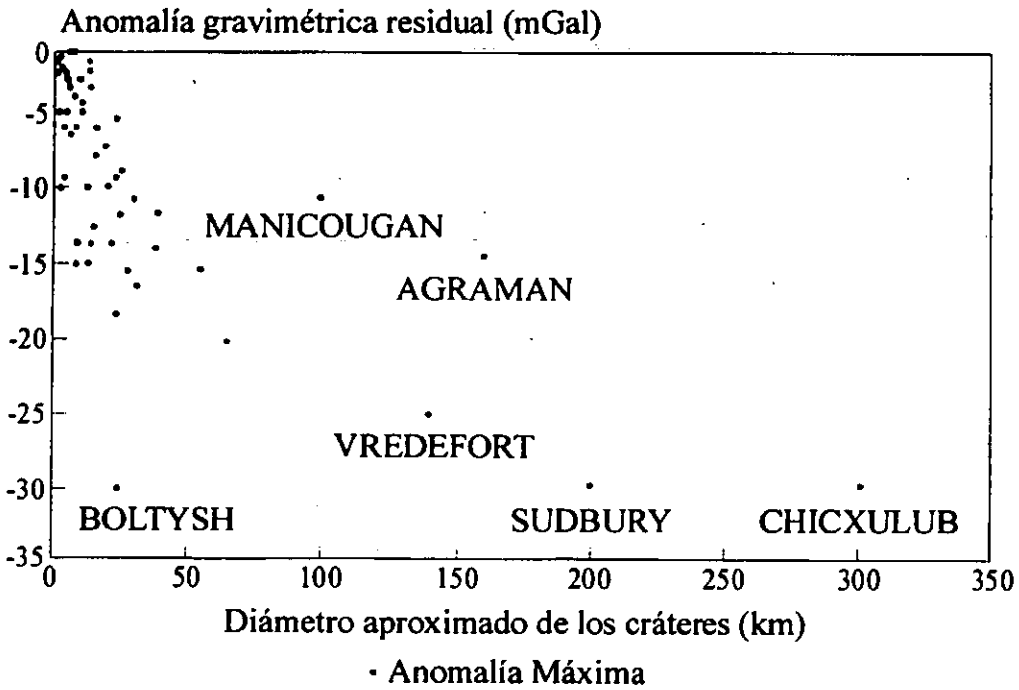


**Figura 3: Relación entre la amplitud de la anomalía gravimetrica y el diámetro del cráter (Pilkington y Grieve, 1992; modificado por Urrutia-Fucugauchi y colaboradores, 1997).**

El pozo Y-6 interseca andesitas microcristalinas las cuales terminan con la aparición de anhidrita laminada (Hildebrand y colaboradores, 1991).

En los cráteres de impacto es común la presencia de una anomalía gravimétrica negativa debido a la baja densidad que le corresponde al material resultante de los cambios litológicos y físicos asociados con el proceso de impacto, por ejemplo, la baja densidad de los sedimentos postimpacto que cubren el cráter, el alto grado de fracturamiento y por consiguiente la alta porosidad de los materiales que conforma el relleno del cráter (Pilkington y Grieve, 1992).

Por otro lado, la amplitud de la anomalía gravimétrica negativa aumenta con el incremento del diámetro del cráter. En la Figura 3 se muestra la relación existente entre las anomalías gravimétricas y el diámetros de estructuras de cráteres conocidos (Pilkington y Grieve, 1992; Urrutia-Fucugauchi y colaboradores, 1997).

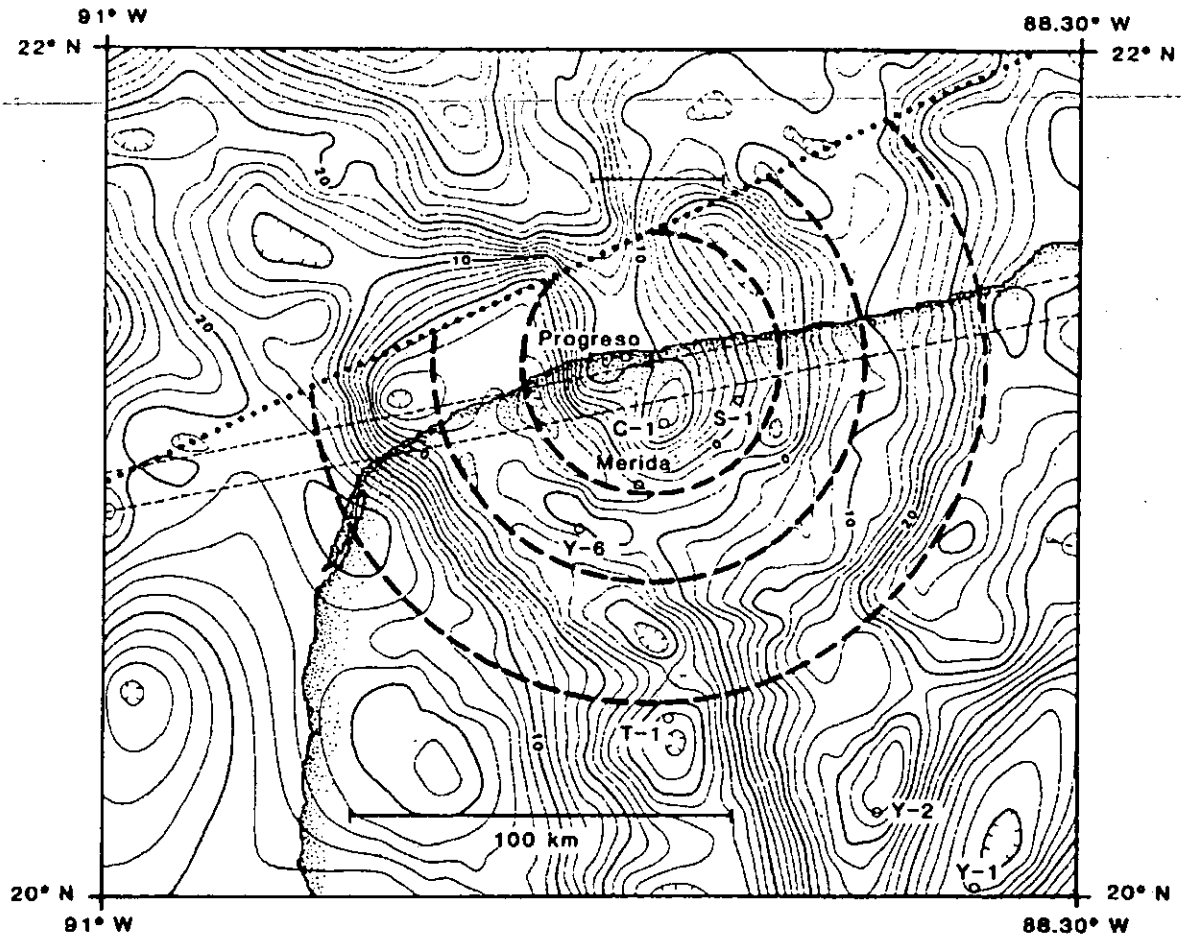


**Figura 4: Mapa de anomalía de Bouguer (tomado de Hildebrand y colaboradores, 1991). Los círculos discontinuos indican las características circulares del campo gravimétrico, truncadas notablemente al norte. C-1, S-I, Y1, Y-2, Y-6 y T-1 son los pozos perforados por PEMEX en el área de estudio.**

En el caso del Chicxlub, los datos gravimétricos muestran una anomalía circular de Bouguer de 30 mgals negativa (Fig. 4) similar en forma a la encontrada sobre el gran cráter de impacto de Manicougan, Canada (Fig. 5, Hildebrand y colaboradores, 1991).

Alrededor del centro, cerca del Puerto de Chicxulub, se define un alto central, donde la amplitud de la anomalía es sólo de 20 mgals. Este alto tiene un radio de 20 km. Además se definen dos bajos concéntricos de 35 y 60 km respectivamente (Fig. 4). El campo gravimétrico anómalo es truncado hacia el norte por un lineamiento orientado suroeste-noreste que cruza la plataforma de Yucatán.

Una anomalía negativa se extiende por 100 km al sur de la anomalía circular (Fig. 4).

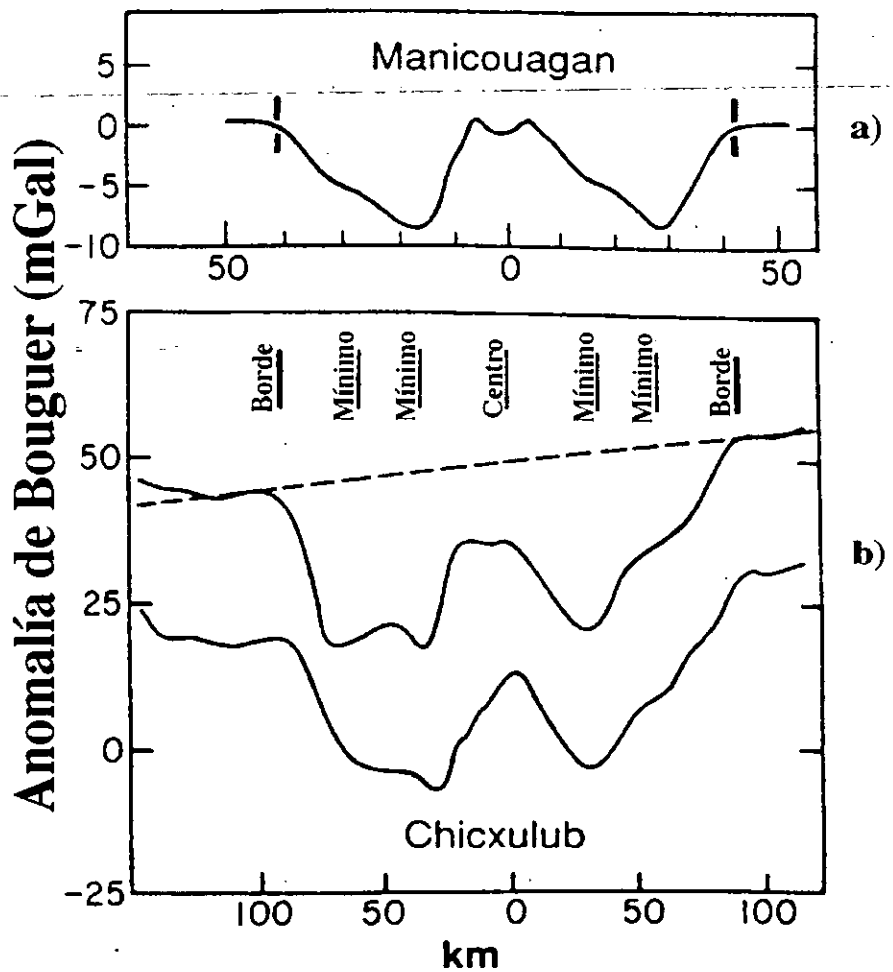


**Figura 5: Comparación entre los campos de anomalía de Bouguer pertenecientes a los cráteres Manicouagan, Canada a) y Chicxlub, México b). En el caso de Chicxulub b) se utilizan para la comparación dos perfiles paralelos y cercanos a la línea de costa (tomado de Hildebrand y colaboradores, 1991).**

El campo magnético total muestra una anomalía dipolar circular con un diámetro aproximado de 210 km, con un gradiente horizontal y algunas anomalías concéntricas que coinciden o están muy próximas a las anomalías concéntricas gravimétricas. Las anomalías magnéticas se extienden hacia el norte sin rupturas significativas, a través del lineamiento suroeste-noreste (Fig. 6).

Las rocas ígneas andesíticas fueron registradas en pozos que se encuentran dentro del circulo de las anomalías geofisicas.

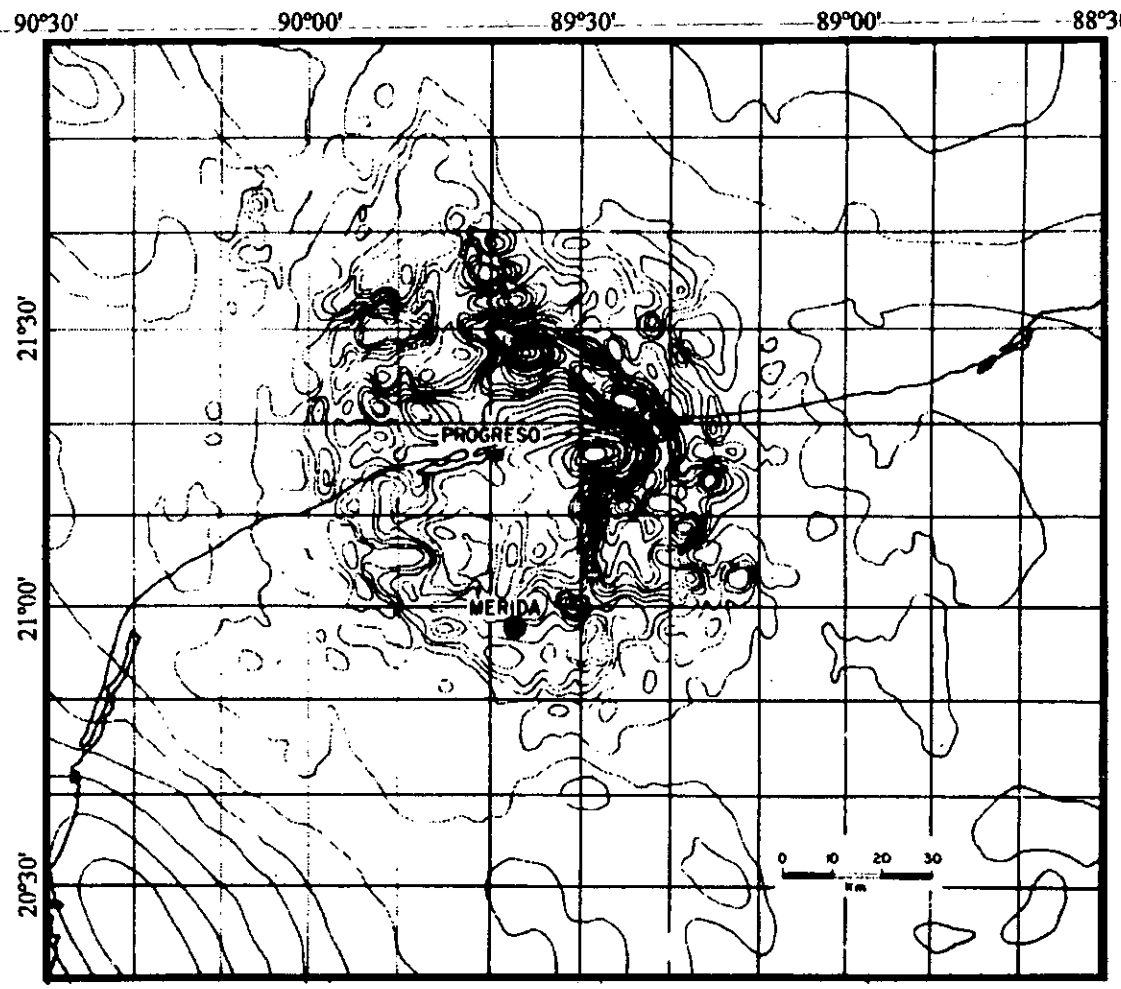


**Figura 6: Mapa de anomalía magnética de campo total (tomado de Camargo-Zanoguera, 1997).**

1.2.2.- Modelos Geofísicos.

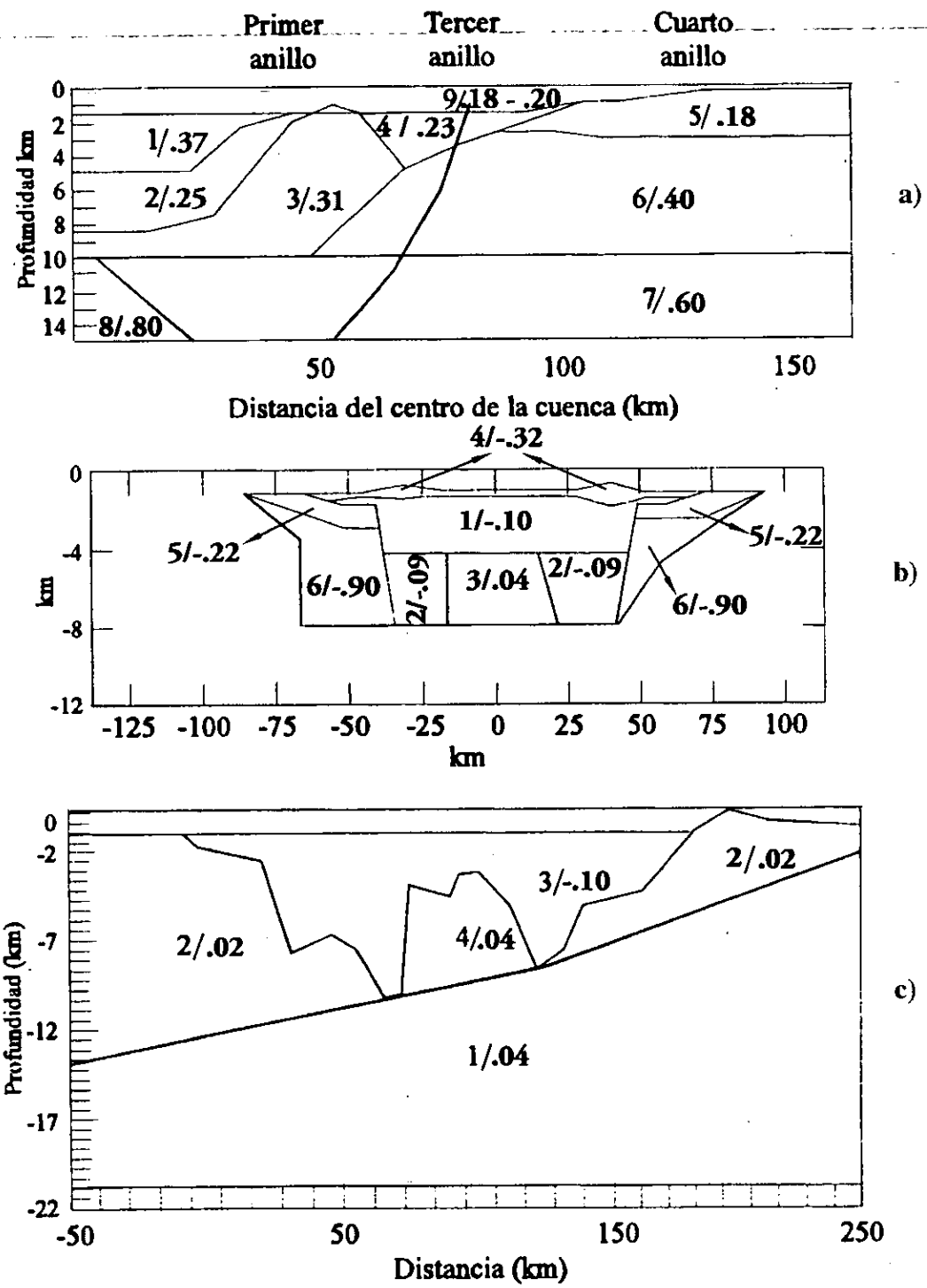


Figura 7: Principales modelos de la estructura subsuperficial del cráter de Chicxulub dado por el procesamiento de la información gravimétrica y de pozo (tomado de Espíndola y colaboradores, 1995). Los valores dentro de los modelos se refieren a las densidades o contrastes de densidades utilizadas en cada cuerpo dadas en $g/cm^3$.

Estas evidencias geofísicas y litológicas abrieron paso a múltiples trabajos de inversión de los campos potenciales con el objetivo de establecer un modelo geológico-geofísico de la estructura de impacto (Fig. 7).

Sharpton y colaboradores (1993) realizaron un análisis de los datos gravimétricos y propusieron la existencia de otro anillo exterior, además de los ya analizados, alcanzando un diámetro de casi 300 km (Fig. 7a). Basado en el análisis de las estructuras de impacto en planetas interiores del sistema solar, la posición de los diferentes anillos concéntricos guarda una relación proporcional a $(2)^{1/2}$. En el caso del Chicxulub se cumple esta regla de esparcimiento de los anillos.

Pilkington y colaboradores (1994) mostraron una sección preliminar del cráter del Chicxulub, la cual está elaborada a partir de la información de pozos, gravimétrica, magnética y de reflexión sísmica, además del conocimiento de otras estructuras de impacto. Los modelos de potencial son truncados a 8 km debido a la falta de información para profundidades mayores (Fig. 7b). La profundidad del techo del cráter se fijó a unos 1100 m, basándose en la información de pozo.

Espíndola y colaboradores (1995) también realizaron una modelación gravimétrica y magnética de la estructura de impacto. Ellos incluyeron la primera y segunda derivada de los campos potenciales para establecer los límites horizontales y resaltar las características del cráter enmascaradas en la anomalía de Bouguer. Se establece un modelo 2-D del cráter que se ajusta a la información gravimétrica. Se presenta en el modelo la existencia en el alto estructural central de lo que pudiera ser un pico gemelo (Fig. 7c).

Hildebrand y colaboradores (1995) realizaron un procesamiento de los datos gravimétricos, que condujo a observar una correlación entre el gradiente horizontal del campo gravimétrico y la distribución de los cenotes. El gradiente horizontal del campo enfatiza el efecto de los cambios laterales de densidad y suprime el gradiente regional del campo que esconde las evidencias gravimétricas del cráter.

Al menos 6 gradientes concéntricos ocurren entre los 20 y 90 km de radio. Los 4 más exteriores (entre 55 y 90 km de radio) se interpolan como evidencia de fallas concéntricas en la zona de hundimiento del cráter, las cuales son reveladas por los datos de reflexión sísmica. Los dos gradientes interiores representan el margen exterior del

alto estructural central (20-25 km de radio) y la cavidad trasiente colapsada (40-45 km de radio).

Las características del gradiente fuera del radio de 90 km no son concéntricas.

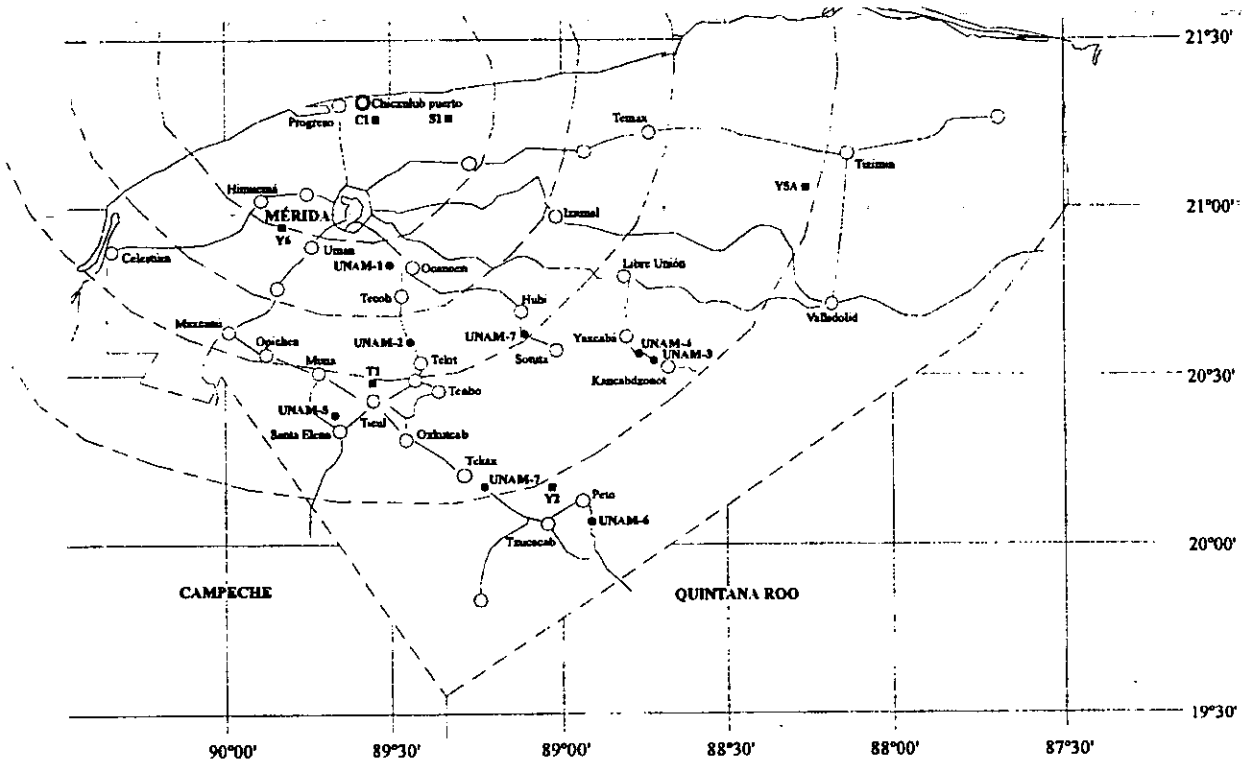


**Figura 8: Anillos del cráter de Chicxulub dados por los círculos discontinuos. Pequeños cuadrados oscuros representan los pozos perforados por PEMEX, pequeños círculos oscuros se refieren a la ubicación de los pozos UNAM (tomado de Marín y Trejo, 1997).**

Connors y colaboradores (1996) establecen una correlación entre las características superficiales del carso y los gradientes de gravedad cerca del anillo de cenotes. El anillo de cenotes se presenta como un arco de 80 km de radio con desviaciones de 3 km de su circularidad. Se compararon las alineaciones de las características del carso con evidencias de fracturas. Las alineaciones del carso junto con las del campo gravimétrico regional se asocian con el tectonismo de esta porción del área de estudio.

Urrutia-Fucugauchi y colaboradores (1996) analizan la estratigrafía y propiedades físicas de las brechas de impacto muestradas en el programa de perforaciones someras de la UNAM. Entre los resultados principales está el reportar la presencia de dos secuencias de brechas. Para esto se apoyaron en las perforaciones PETO UNAM-6 y TEKAX UNAM-7 ubicados al SSE del puerto de Chicxulub, a una distancia de 150 y

125 km respectivamente (Fig. 8). El pozo UNAM-7 se encuentra entre los anillos de anomalías gravimétricas 3 y 4 (el cuarto es según lo definido por Sharpton y colaboradores (1993)) y el pozo UNAM-6 se localiza fuera del anillo 4 (Fig. 8). La mayor diferencia entre ambas columnas litológicas es la presencia de una unidad de brechas caracterizadas por abundantes clastos de basamento, lo que se observa en el pozo UNAM-6. En el pozo UNAM-7 la brecha superior aparece a partir de los 226 m y la brecha rica en evaporitas está presente a partir de los 305.5 m. En el pozo UNAM-6 la brecha superior está ausente de clastos de basamento y la brecha rica en evaporitas se observa a partir de los 282.8 m. La correlación entre las brechas ricas en evaporitas de ambos pozos es consistente con la geometría planteada por Sharpton y colaboradores (1993).

Estos últimos resultados guardan una buena correspondencia con los obtenidos en los estudios geohidrológicos realizados por la Comisión Federal de Electricidad (CFE) en la península de Yucatán a partir de 1980, con el objetivo de poder abastecer de agua a las termoeléctricas de Mérida y Valladolid (Urrutia-Fucugauchi y colaboradores, 2000).

Durante estos trabajos se perforaron varios pozos entre Mérida y Valladolid, definiendose, en la parte somera, un espesor de 230 m de rocas carbonatadas del Terciario. A mayor profundidad se perfora una secuencia carbonatada de aproximadamente 34 metros de espesor, que se distingue por la presencia de brechas (fragmentos de tonalidades oscuras). El análisis químico de muestras de agua de estos pozos indicaron la presencia de altos valores de Estroncio (Sr), Arsénico (As) y Niquel (Ni), siendo estos dos últimos elementos comunes en meteoritos que, debido a procesos de lixiviación, fueron transportados hasta la interfase salina (Urrutia-Fucugauchi y colaboradores, 2000).

En otros trabajos, Morgan y colaboradores (1997) procesaron la información sísmica marina y proponen un modelo que sugiere la existencia de un cráter trasiente de 100 km de diámetro.

Morgan y Warner (1999) reprocesan los datos sísmicos con el objetivo de brindar la primera visión 3-D de la estructura de esta cuenca multianillada. Ellos establecen la siguiente nomenclatura para definir las características estructurales fundamentales del cráter de impacto:

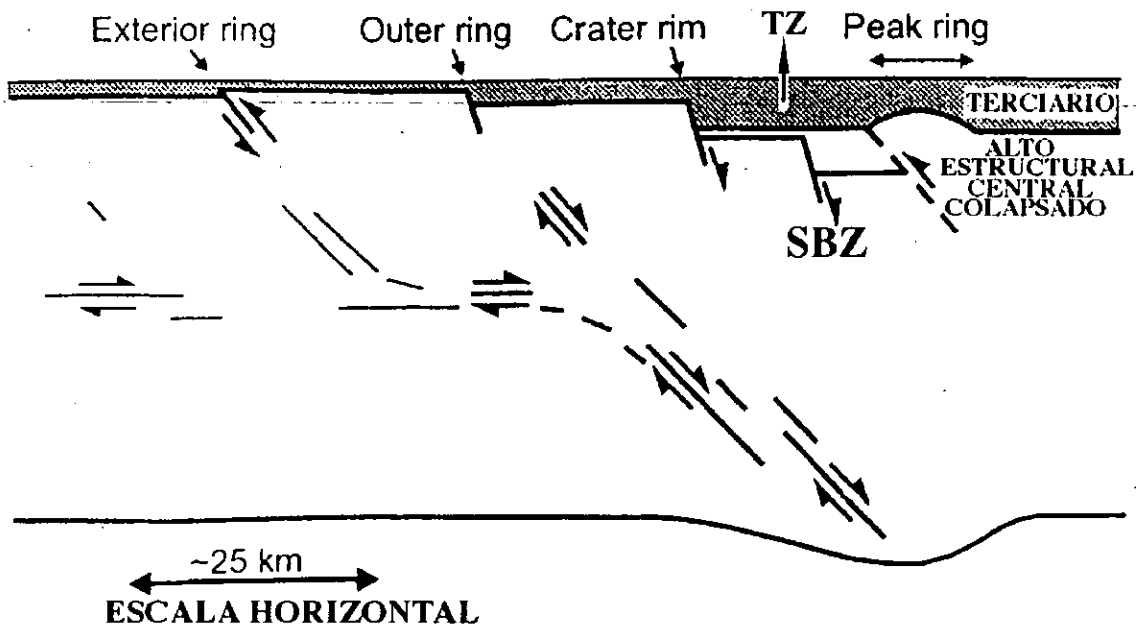


**Figura 9: Estructura esquemática del cráter de Chicxulub (tomado de Morgan y Warner, 1999).**

*Crater rim*: Se define como el escarpe o el borde de la cuenca post-impacto (Fig. 9). Constituye un alto estructural en forma de anillo circular o casi-circular. En Morgan y colaboradores (1997) fue definida como anillo interior (*inner ring*).

Tomando en cuenta los resultados obtenido de 4 perfiles sísmicos, se le otorga un diámetro promedio de 145 km, siendo este valor la extensión horizontal de la cuenca post-impacto.

*Peak ring*: Se forma por el material colapsado del alto estructural central, por lo que no se considera basamento elevado. Define una zona anular de diámetro aproximado de 80 km (Fig. 9).

Entre el *peak ring* y el *crater rim* la cuenca post-impacto alcanza su máxima profundidad (> 1 km), denominándose Zona de Terraza (Fig. 9, *TZ*) y se caracteriza por la existencia en su basamento de bloques fallados y escalonados en un sistema de fallas normales (Fig. 9, *SBZ*). Esta zona tiene un ancho variable entre 20 y 35 km.

*Major outer ring:* En el proceso de impacto, el colapso de toda la corteza hacia dentro y hacia abajo genera un sistema de fallas normales que su máxima expresión es este anillo principal con un diámetro aproximado de 190 km (Fig. 9).

*Exterior ring:* Aunque durante el colapso del cráter el movimiento predominante es hacia dentro y hacia abajo, en el inicio del proceso de impacto el movimiento es compresivo hacia fuera creando una serie de fallas inversas, cuya evidencia existente pudiera ser este cuarto anillo exterior, definido inicialmente por Sharpton y colaboradores (1992) y ratificado por Urrutia-Fucugauchi y colaboradores (1994). Su circularidad define un diámetro aproximado de 240 km (Fig. 9).

Al alto estructural central *(Central Uplift)* le asignan una forma acuñada, es decir, más ancho en su parte superior que en su base, con un diámetro promedio entre 40 y 50 km (Fig. 9).

Collins y colaboradores (2000) realizan simulaciones del impacto de Chicxulub, logrando reproducir en laboratorio las características esenciales del cráter. Este resultado permite inferir el desplazamiento real de los materiales involucrados y el origen de las características estructurales esenciales del cráter de Chicxulub. Estos resultados son corroborados en gran parte por Pilkington y Hildebrand (2000). Ellos realizaron una modelación 3-D del cráter utilizando la información magnética. Sugieren un diámetro de aproximadamente 40 km para el alto estructural central, negando la posibilidad de existencia de un diámetro entre 90 y 120 km, y la pertenencia del "peak ring" a un basamento elevado.

### 1.2.3.- Estudio Magnetotelúrico

En toda esta gama de trabajos se tiene el establecimiento de modelos geofísicos de densidad, suceptibilidad magnética y velocidad de ondas sísmicas que obviamente han contribuido a tener una idea más precisa de la estructura del cráter. Pero algo evidente es la ausencia de un modelo geoeléctrico.

Pilkinton y Grieve (1992) presentan las señales geofísicas que reflejan un cráter de impacto. Una de ellas es la brindada por el contraste de resistividad eléctrica entre el medio resistivo que le corresponde a las rocas poco o no fracturadas del exterior y basamento del cráter, y el relleno conductor dado por rocas muy fracturadas y porosas.

Tomando en cuenta este principio y el beneficio de poder obtener un nuevo modelo geofísico basado en una respuesta física diferente del medio a las ya analizadas, se decidió ejecutar un levantamiento magnetotelúrico en la región de impacto.

El método magnetotelúrico tiene la ventaja de lograr una gran profundidad de estudio. Su poder de resolución para brindar una imagen geoeléctrica precisa del medio a grandes profundidades, aun presentándose el inconveniente, para otros métodos eléctricos, de las llamadas pantallas resistidas (Vozoff, 1989), lo propone como la única vía eficiente para obtener la estructura geoeléctrica del cráter.

En junio de 1997 se completaron 22 sondeos magnetotelúricos distribuidos a lo largo de dos perfiles AA´ y BB´ (Fig. 10). Ambos perfiles están orientados de forma tal que cortan de manera perpendicular el anillo de cenotes.

La aplicación de este método requiere de un extenso procesamiento de la información magnetotelúrica, así como de la aplicación de varios algoritmos de inversión, a fin de obtener el modelo geoeléctrico que represente de manera más precisa la estructura del cráter de Chicxulub.

El trabajo desarrollado se ha divido en cuatro capítulos, los cuales serán descritos brevemente a continuación:

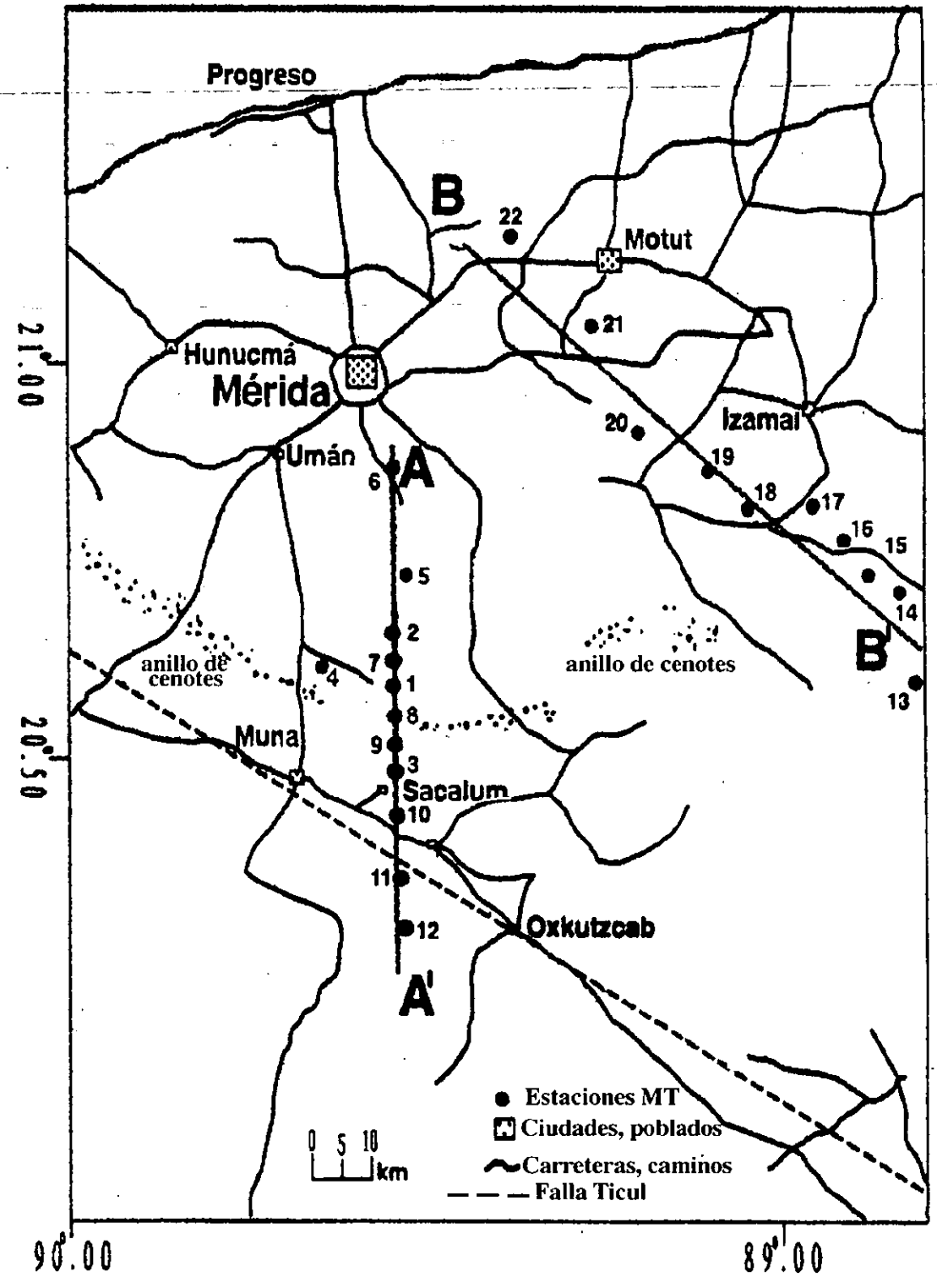


**Figura 10: Ubicación de los sondeos magnetotelúricos en el área de estudio.**

## 2.- EL MÉTODO MAGNETOTELÚRICO: RESULTADOS PRELIMINARES DEL LEVANTAMIENTO MT EN LA ZONA DE IMPACTO DEL CHICXULUB, YUCATÁN, MÉXICO.

Se presentan los primeros resultados, lo que constituye a la vez, el primer esfuerzo por investigar las propiedades eléctricas de la estructura de impacto de Chicxulub.

En este trabajo sólo se presentan los resultados preliminares obtenidos para el perfil BB'.

Se realizó un análisis cualitativo de los 20 pares de curvas de resistividad eléctrica aparente y de fase observadas en las 10 estaciones MT pertenecientes a este perfil.

Este análisis cualitativo demostró la efectiva respuesta de este método al estudio del cráter. Se observaron diferencias en el comportamiento de las curvas de resistividad y fases entre las estaciones que se ubicaron fuera del anillo de cenotes, hacia el exterior del cráter, y las ubicadas en el interior del mismo. Las curvas de resistividad aparente hacia el exterior del cráter mostraban un ligero comportamiento más resistivo que las curvas pertenecientes a las estaciones ubicadas en el interior del mismo.

Se presenta además, la sección 1-D dada por la inversión Bostick de las curvas observadas en el modo *xy*.

En general, se observa la existencia de una cuenca conductora de aproximadamente 190 km de diámetro y a una distancia radial de 40 km lo que pudiera ser la base del alto estructural central

## 3.- EFECTO DE COSTA EN SONDEOS MAGNETOTELÚRICOS REALIZADOS EN LA PENÍNSULA DE YUCATÁN, MÉXICO.

Los resultados alcanzados en los capítulos posteriores carecen de confiabilidad si no se realiza un análisis de efecto de costa sobre las estaciones MT consideradas.

Se realizó una modelación sintética 3-D de la península de Yucatán, utilizando el algoritmo de Park (Park, 1995) y considerando la plataforma marina que circunda la península.

Se pudo comprobar que el efecto de costa no es significativo. Solo para el extremo oeste y noroeste de la península se puede observar un efecto notable para períodos T ≥ 100s.

Este planteamiento es corroborado en el análisis de las flechas de inducción.

Los modelos geoeléctricos definidos de la aplicación del método magnetotelúrico pueden ser tomados en cuenta para el esclarecimiento de la estructura del cráter, con la confianza de que no existen distorsiones en los mismos por el efecto de costa. Por último, se proponen nuevas áreas igualmente confiables para la aplicación del método magnetotelúrico en el estudio del cráter de Chicxulub.

## 4.- INVERSIÓN 1-D BOSTICK Y OCCAM DE SONDEOS MAGNETOTELÚRICOS EN LA ZONA DE IMPACTO DE CHICXULUB, YUCATÁN, MÉXICO.

Después de haberse comprobado la efectividad del método magnetotelúrico en el estudio del cráter (Campos y colaboradores, 1997), se decidió realizar una inversión 1-D del perfil BB´ utilizando los algoritmos de Bostick (Bostick y Smith, 1961) y de Occam (Constable y colaboradores, 1987), para los modos *xy* y *yx*.

En este capítulo se realiza un análisis de distorsión a partir de las secciones de Tipper y Skew para este perfil, demostrando el predominio del carácter 1-D para el medio estudiado.

Las secciones de Bostick y OCCAM muestran una gran similitud. El comportamiento de la resistividad eléctrica en ambos modelos es correlacionado con el comportamiento del campo de anomalía de Bouguer para el área de estudio.

Se define un diámetro del cráter de aproximadamente 200 km y de 80 km para la base del alto estructural central, tomando como centro el puerto de Chicxulub.

No obstante estos resultados, se recomienda realizar una inversión 2-D de este perfil con el objetivo de garantizar resultados más precisos.

## 5.- ESTRUCTURA ELÉCTRICA DE LA CUENCA DE IMPACTO DE CHICXULUB A LO LARGO DE DOS PERFILES MAGNETOTELÚRICOS.

Una vez obtenidos los modelos unidimensionales Occam y Bostick pertenecientes al perfil BB´(Delgado y colaboradores, 2000) se procedió a determinar los modelos bidimensionales que le corresponden a los perfiles AA´ y BB´.

Para lograr este objetivo se utilizó el algoritmo de Relajación Rápida planteado por Smith y Booker (1987), el cual es muy eficiente y rápido.

El modelo 2-D del perfil AA´ no define con claridad las características esenciales de un cráter complejo. No obstante la influencia de las estructuras principales (limite de la cuenca de impacto y bajo estructural Norte-Sur) son observadas en el modelo dado.

La sección 2-D del perfil BB´ muestra de manera más precisa la estructura del cráter, sugiriendo un diámetro máximo de 195 km y de 80 km para la base del alto estructural central.

Se recomienda la realización de nuevos sondeos MT en la porción oeste del cráter de manera tal que, junto a los 22 sondeos existentes, permitan obtener un modelo geoeléctrico 3-D de toda el área de estudio.

## 1.3.- Referencias


ALBRITON C. Jr., 1989: Catastrophic episodes in Earth History. New York, Chapman & Hall.

ALVAREZ, L.W., W. ALVAREZ, F. ASARO y H. MICHEL, 1980. Extraterrestrial cause for the Cretaceous/Tertiary extinction. Science, **208**, 1095-1108.

ALVAREZ, L.W., W. ALVAREZ, F. ASARO y H. MICHEL, 1982. Current status of the impact theory for the terminal Cretaceous extintion. Geol. Soc. Am., Special paper **190**, 305-315.

BERDICHEVSKY, M. N. y V. I. DMITRIV, 1976. Basic principles of interpretation of magnetotelluric sounding curves. A. Adam (Editor). Geoel. Geoth. Studies. KAPG Geophysycal Monograph. Akademiai Kiado. Budapest, 165-221.

BOSTICK F. X. y H. W. SMITH 1961. An analysis of the magnetotelluric method for determining subsurface resistivities. Electrical Engineering Research Laboratory. The Univ. of Texas, Austin, Report No. 120.

BOURGEOIS, J., T. A. HANSEN, P. L. WILBERG y E. G. KAUFFMAN, 1988. A tsunami deposit at the Cretaceous-Tertiary boundary. Science, **241**, 567-570.

CAGNIARD, L., 1953. Basic theory of the magnetotelluric method of geophysical prospecting. Geophysics, **18**, 605-635.

COLLINS, G. S., H. J. MELOSH, J. V. MORGAN y M. R. WARNER, 2000. Hydrocode simulations of Chicxulub crater collapse. XXXI Lunar and Planetary Science Conference. Houston, Texas.

CAMARGO-ZANOGUERA, A., 1997. Los primeros estudios del cráter de Chicxulub. Unión Geofísica Mexicana, Monografía 4, 113-116.

CAMPOS-ENRÍQUEZ, J. O., J. A. ARZATE, J. URRUTIA-FUCUGAUCHI y O. DELGADO-RODRÍGUEZ, 1997. The subsurface structure of the Chicxulub crater (Yucatan, Mexico): Preliminary results of a magnetotelluric study. The Leading Edge. **16**, 1774-1777.

CONSTABLE, S. C., R. L. PARKER y C. G. CONSTABLE, 1987. Occam´s inversion: A practical algorithm for generating smooth models from electromagnetic sounding data. Geophysics, **52**, 3, 289-300.

DELGADO-RODRÍGUEZ, O., J. URRUTIA-FUCUGAUCHI, J. A. ARZATE y J. O. CAMPOS-ENRÍQUEZ, 2000. Coast effect in magnetotelluric soundings on the Yucatan peninsula, Mexico. Geofísica Internacional, en prensa.

ESPÍNDOLA, J. M., M. MENA, M. DE LA FUENTE y J. O. CAMPOS-ENRÍQUEZ, 1995. A model of the Chicxulub impact structure (Yucatan, Mexico) based on its gravity and magnetic signatures. Phys. Earth Plant. Inter., **92**, 271-278.

HENKEL, H., 1992. Geophysical aspects of meteorite impact craters in eroded shield environment, with special emphasis on electrical resistivity. Tectonophysics, **216**, 63-89.

HILDEBRAND, A. R., G. T. PENFIELD, D. A. KRING, M. PILKINGTON, A CAMARGO, S. JACOBSEN y W. BOYTON, 1991. Chicxulub crater: A possible Cretaceous/Tertiary boundary impact crater on the Yucatan Peninsula, Mexico. Geology, **19**, 9, 867-871.

HILDEBRAND, A. R., M. PILKINGTON, C. ORTÍZ-ALEMÁN, R. E. CHÁVEZ, J. URRUTIA-FUCUGAUCHI, M. CONNORS, E. GRANIEL, A. CAMARA, J. F. HALPENNY y D. NIEHAUS, 1998. Mapping Chicxulub crater structure with gravity and seismic reflection data. In: Grady, M.M. et al. (Eds.), Meteorites: Flux with Time and Impact Effects, Geol. Soc., London, Sp. Publ., **140**, 155-176.

LÓPEZ-RAMOS, E., 1973. Estudio geológico de la Península de Yucatán. Asoc. Mex. Geol. Petrol. Bol., **25**, 23-76.

LÓPEZ-RAMOS, E., 1975. Gelogical summary of the Yucatan peninsula. In The Ocean Basin and Magins, by A. Nairn and Stheli, **3**, 257-282, Plenum, NY.

LÓPEZ-RAMOS, E., 1983. Geología de México. Universidad Nacional Autónoma de México, México D.F., 3ª Edición.

MARÍN, L. y A. TREJO-GARCÍA 1997. El límite K/T y su exploración en el cráter de Chicxulub. Unión Geofísica Mexicana, Monografía 4, 171-174.

MORGAN, J. y M. WARNER,1999. Chicxulub: The third dimension of a multi-ring impact basin. Geology, **27**, 407-410.

MORGAN, J., M. WARNER y CHICXULUB WORKING GROUP, 1997. Size and morphology of the Chicxulub impact crater. Nature, **390**, 472-476.

PARK, S. R., 1985. Distortion of magnetotelluric sounding curves by three-dimensional structures, Geophysics, **50**, 785-797.

PENFIELD, G. T. y Z. A. CAMARGO,1981. Definition of a major igneos zone in the central Yucatan platform with aeromagnetics and gravity. 51st Ann. Internat. Mtg. SEG, Abstract, 37.

PILKINGTON, M. y R. GRIEVE, 1992. The geophysical signature of terrestrial impact craters. Rev. Geophys., **30**, 161-181.

PILKINGTON, M. y A. R. HILDEBRAND, 2000. XXXI Lunar and Planetary Science Conference. Houston, Texas.

PILKINGTON, M., A. R. HILDEBRAND y C. ORTÍZ-ALEMÁN, 1994. Gravity and magnetic field modeling and structure of the Chicxulub crater, Mexico. Journal Geophys. Resear. **99**, 147-162.

REBOLLEDO-VIEYRA, M., J. URRUTIA-FUCUGAUCHI, L. MARIN, A. TREJO-GARCÍA, V. L. SHARPTON y A. M. SOLER-ARECHALDE, 2000. UNAM scientific shallow drilling program of the Chicxulub impact crater. Int. Geol. Rev.,

SHARPTON, V. L., G. B. DALRYMPLE, L. MARIN, B. C. RYDER, B. C. SCHURAYTZ y J. URRUTIA-FUCUGAUCHI, 1992. New links between the Chicxulub impact structure and the Cretaceous/Tertiary boundary. Nature, **359**, 819-821.

SHARPTON, V. L., K. BURKE, A. CAMARGO, S. A. HALL, D. SCOTT-LEE, L. MARIN, G. SUÁREZ, J. M. QUEZADA, P. D. SPUDIS y J. URRUTIA-FUCUGAUCHI, 1993. Chicxulub multiring impact basin: Size and other characteristics derived from gravity analysis. Science, **261**, 1564-1567.

SNYDER, D. B., R. W. HOBBS, 1999 and CHICXULUB WORKING GROUP. Deep seismic reflection profiles across the Chicxulub crater. In: Dressler, B.O. and Sharpton, V.L. (Eds.), Large Meteorite Impacts and Planetary Evolution, Geol. Soc. Am. Sp. Paper, **339**, 263-268.

STANLEY, S. M., 1987. Extinction: Scientific American Library., **20**.

URRUTIA-FUCUGAUCHI, J., J. M. CHÁVEZ-AGUIRRE, L. MARÍN-STILLMAN y J. L. DE LA ROSA, 2000. Evidencias en la estructura de la rocas afectadas por el impacto del asteriode de Chicxulub. VI Reunión Nacional de Mecánica de Rocas. Museo Tecnológico de la CFE, México D.F.

URRUTIA-FUCUGAUCHI, J., L. M. ALVA-VALDIVIA y J. M. ESPÍNDOLA-CASTRO, 1997. Unión Geofísica Mexicana, Monografía 4, 137-146.

URRUTIA-FUCUGAUCHI, J., L. MARÍN y A. TREJO-GARCÍA, 1996. UNAM scientific drilling program of the Chicxulub impact structure – evidence for a 300 km crater diameter. Geophys. Res. Lett., **23**, 1565-1568.

URRUTIA-FUCUGAUCHI, J., L. MARÍN y V. L. SHARPTON, 1994. Reverse polarity magnetized melt rocks from the Cretaceous/Tertiary Chicxulub structure, Yucatan peninsula, Mexico. Tectonophysics, **237**, 105-112.

VEGA-VERA, F. J. y M. C. PERRILLIAT, 1997. Patrones de extinción (y radiación) en invertebrados a través del límite Cretácico-Terciario. Unión Geofísica Mexicana, Monografía 4, 49-54.

VOZOFF, K., 1972. The magnetotelluric method in the exploration of sedimentary basins. Geophysics, **37**, 1, 98-141.

VOZOFF, K., 1989. The magnetotelluric method. In: Nabigian, M.N. (Ed.), Electromagnetic Methods in Applied Geophysics, Soc. Expl. Geophys. Tulsa, OK, USA.

## 2.- El MÉTODO MAGNETOTELÚRICO: RESULTADOS PRELIMINARES DEL LEVANTAMIENTO MT EN LA ZONA DE IMPACTO DE CHICXULUB, YUCATÁN, MÉXICO.

*Resultados publicados en: The subsurface structure of the Chicxulub crater (Yucatan, Mexico): Preliminary results of a magnetotelluric study.* ***The Leading Edge, 16, 1997, 1774-1777.*** *(anexo 1).*

### 2.1.- Introducción

La existencia de una estructura de impacto en el norte de la península de Yucatán ha sido inferida basándose fundamentalmente en los estudios magnéticos y gravimétricos (Fig. 1). Esta estructura de impacto ha sido relacionada directamente con la extinción masiva de la biota en el período de transición Cretácico-Terciario (K/T) debido a los cambios climáticos inducidos por el impacto de un gran meteorito (Alvarez et al., 1980). En la actualidad, los estudios disponibles confirman tanto la existencia de la estructura de impacto como su asociación con la extinción de los dinosaurios.

No obstante esta afirmación, las características estructurales de este cráter de impacto aún no están claramente establecidas.

Estudios independientes han llegado a diferentes conclusiones acerca del tipo de cráter de impacto. De acuerdo con la interpretación inicial realizada por Penfield y Camargo (1981) el cráter tiene un diámetro de 180 km con una zona concéntrica de brechas magnéticas de 210 a 230 km de diámetro.

Diversos autores han considerado la estructura de impacto con diferentes características como son: una cuenca de 4 anillos, de anillo simple, con 300 km de diámetro, 180 km de diámetro, con un alto estructural central con pico gemelo, etc. (ej. Sharpton et al., 1993; Pilkington et al., 1994; Hildebrand et al., 1995; Espíndola et al., 1995).

Los diámetros estimados en los diferentes trabajos se encuentran en el rango de 170 a 300 km (Fig. 2). Esta diferencia en diámetro corresponde a una diferencia en la energía de impacto en más de un orden de magnitud.

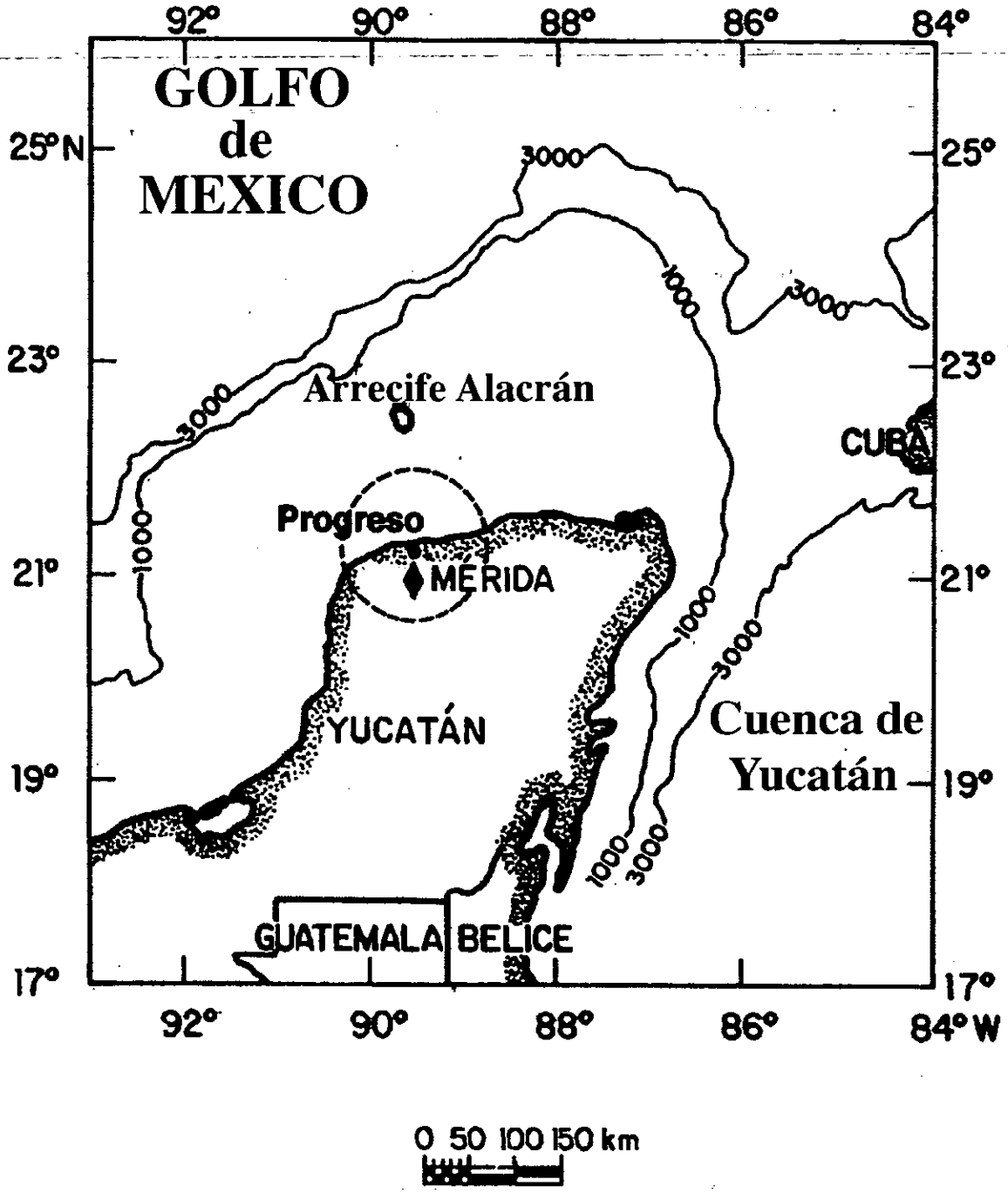


**Figura 1: Ubicación del área de impacto de Chicxulub. El círculo discontínuo representa uno de los diámetros planteados en los diferentes modelos geofísicos.**

Las diferencias entre los modelos propuestos radica en la ambigüedad de la información gravimétrica, lo cual se puede contrarrestar teniendo en cuenta la información sísmica y de pozo disponibles en el área de estudio.

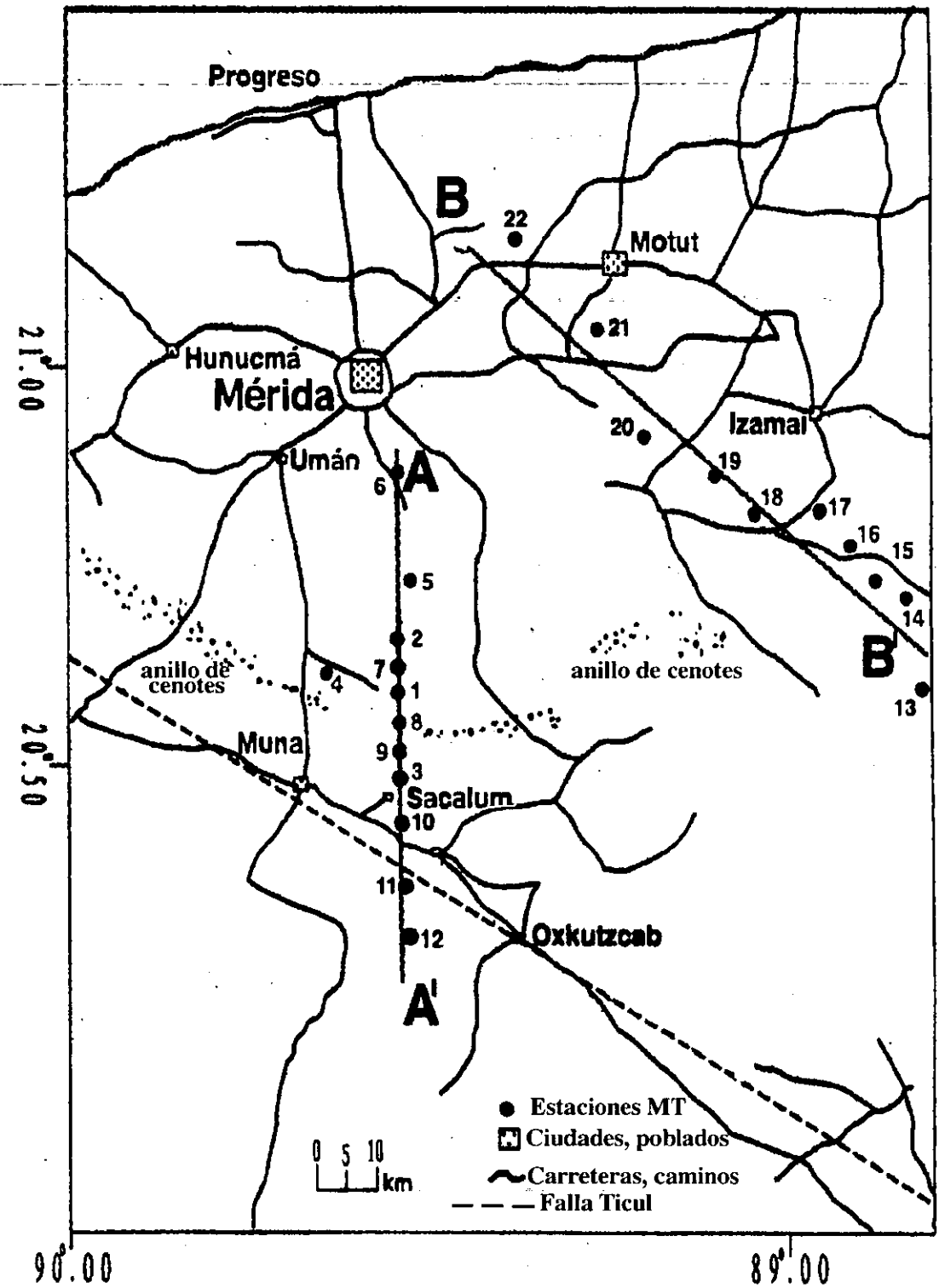


**Figura 2: Ubicación de los perfiles magnetotelúricos en el área de estudio.**

De lo anteriormente expuesto se puede asegurar la existencia de múltiples trabajos geofísicos dirigidos a establecer un modelo de la estructura del cráter de Chicxulub. No obstante, es evidente la ausencia de un modelo geoeléctrico que contribuya al esclarecimiento de las características estructurales no establecidas en acuerdo común por los diferentes grupos de investigadores.

El objetivo de este trabajo es, primero, comprobar la efectividad de aplicar el método magnetotelúrico en el estudio de esta estructura de impacto y, segundo, poder ofrecer los resultados preliminares alcanzados de esta etapa inicial de procesamiento e interpretación de la información magnetotelúrica adquirida.

## 2.2.- El Método Magnetotelúrico

### 2.2.1.- Breve ensayo histórico

Desde antes de 1850 los telegrafistas asociaban las perturbaciones del campo eléctrico terrestre (telúrico) con las variaciones del campo geomagnético (Fournier, 1969). En los momentos de grandes tormentas eléctricas las variaciones del campo magnético podían alcanzar tal magnitud que impedían las comunicaciones telegráficas.

En Noviembre de 1859 Johann Lamont comienza el registro visual de las variaciones telúricas y magnéticas en el Observatorio Astronómico de Munich (Fournier, 1969), situado al sur de Baviera, poniéndose de manifiesto el fenómeno de polarización de las corrientes telúricas.

En 1892 Ellis W. hace algunas observaciones generales sobre la simultaneidad de los fenómenos magnéticos y telúricos, y sobre la correspondencia que de ellos se deduce (Fournier, 1969).

Van Bemmelen (1908) asegura que las oscilaciones de las componentes magnéticas y telúricas ortogonales se corresponden, que la oscilación telúrica precede a la magnética y que la relación de sus amplitudes decrece cuando el período crece. Ofrece las primeras conclusiones válidas concernientes a las relaciones entre las variaciones de los campos magnéticos y electrotelúricos naturales por un lado, y por otro, a las variaciones de la

conductividad del suelo. También trató el aspecto de la fase, pero con menos desarrollo que el aspecto amplitud.

Hatekeyama y Hirayama (1934) presentan desarrollos análogos para el estudio de los ángulos de fase. El cálculo teórico se desarrolla admitiendo la hipótesis simplificadora de que la superficie terrestre es plana.

Hirayama (1935) propone el tensor tri-dimensional para caracterizar el campo eléctrico terrestre, determina la dirección horizontal de la conductividad máxima y plantea la ecuación del efecto skin: $(2\pi\mu\sigma\omega)^{1/2}$.

Tikhonov (1950) publica un ejemplo cuantitativo de profundidad de separación de dos capas en el manto. Muestra que para largos períodos existe una relación teórica de proporcionalidad entre los elementos que caracterizan los campos magnético y eléctrico considerados ortogonales. El modelo considerado por Tikonov se compone de una capa de resistividad finita que reposa sobre un substrato perfectamente conductor.

Cagniard (1953) patenta el método magnetotelúrico. Propone el empleo de la expresión:

$$\delta = \frac{1}{2\pi}\sqrt{\rho T}$$

Donde $\delta$ es la profundidad de penetración (metros), $\rho$ es la resistividad aparente (ohm-m) y T el período (segundos).

Esta expresión se asocia a:

$$\frac{E_y}{E_x} = \sqrt{\frac{2T}{\rho}}$$

Donde: $E_x$, $E_y$ son las componentes *x* e *y* del campo eléctrico dadas en mV/m.

Cagniard pone de relieve la simplicidad de las leyes que rigen el fenómeno en el caso general de capas sucesivas homogéneas de características diferentes (medio uni-dimensional).

Mediante la hipótesis de capas de corrientes tabular y horizontal, define el método de prospección llamado *método magnetotelúrico.*

El uso de las ecuaciones de Maxwell que vinculan estos campos conduce a Cagniard a la asociación de cuatro parámetros en un sistema de dos formulas prácticas y a un

ábaco de dos capas. Este ábaco permite calcular las resistividades (ρ) de los terrenos atravesados por las corrientes, así como la profundidad de separación (h) en metros de las dos capas. Las expresiones prácticas son:

$$\rho = 0.2T\left(\frac{E}{H}\right)^2 \qquad h = \frac{\sqrt{10\rho T}}{8}$$

Para el caso de los ángulos de fase existen desarrollos similares a los expuestos para las amplitudes, lo que constituye una importante ventaja frente al Sondeo Eléctrico Vertical.

Tikhonov y Sakhsuvarov (1956) amplían los conocimientos acerca del cálculo de la admitancia ($H_x/E_y$) en la superficie, con la suposición de capas horizontales y proponen ábacos para el caso de tres capas.

Lipskaja y colaboradores (1961) construyen curvas de sondeos magnetotelúricos para la prospección geológica. También en ese año Bostick y Smith (1961) presentan su técnica de análisis magnetotelúrico para el estudio del subsuelo.

Hoffman (1962) propone un análisis espectral de los fenómenos magnetotelúricos.

Moskvichev (1965) discute los diferentes aspectos del empleo del método magnetotelúrico.

Vozoff (1972) expone de manera explícita el procesamiento de la información obtenida en el método de sondeo magnetotelúrico. Demuestra las ventajas de la aplicación de este método en la exploración petrolera.

Esto es solo una síntesis de algunos de los principales trabajos que expresan las bases del desarrollo de este método electromagnético. En los últimos 20 años se ha acrecentado el número de trabajos en los cuales se presentan los resultados de la aplicación del sondeo magnetotelúrico, contribuyendo al desarrollo de los métodos vinculados al procesamiento e interpretación de la información adquirida, algunos de los cuales fueron utilizados en este proyecto de investigación y serán presentados en los capítulos siguientes.

## 2.2.2.- Principios básicos

El campo magnético de la Tierra está sometido a variaciones de origen interno y externo. Comenzando por lo períodos más largos tenemos las inversiones de polaridad (30 millones de años), la variación secular (500 años), ciclo solar (11 años), anual, rotación solar (27 días), diurna, y en períodos más cortos las perturbaciones de bahía (20 minutos a 2 horas) y las micropulsaciones.

El caso que nos interesa es el de las micropulsaciones cuyo rango de frecuencia es de $1.5*10^{-3}$ a 10 Hz (períodos de 600 a 0.2 s).

Las micropulsaciones se dividen en dos grupos principales: continuas e irregulares y tienen un origen extraterrestre.

Las fluctuaciones del viento solar dan origen a las ondas hidromagnéticas en los bordes e interior de la magnetosfera. Estas ondas al llegar al límite inferior de la ionosfera, se transforman en pulsos electromagnéticos que llegan a la superficie terrestre e inducen las corrientes telúricas.

En síntesis se puede definir el método magnetotelúrico como la deducción de las propiedades eléctricas del subsuelo partiendo de la clase de correlación que existe entre los registros efectuados, en un mismo lugar y tiempo, de las variaciones del campo geomagnético y de las corrientes telúricas asociadas a las primeras.

Para el caso de un terreno homogéneo la expresión del cálculo de la resistividad eléctrica es:

$$\rho_r = \frac{1}{\omega\mu}\left(\frac{E_x(\omega)}{H_y(\omega)}\right)^2$$

Donde: $\rho_r$ – resistividad eléctrica del terreno (ohm-m)

$\omega$ - frecuencia de la señal.

$\mu$ - permeabilidad magnética (H/m).

$E_x$ – componente x del campo eléctrico (mV/m).

$H_y$ – componente y del campo magnético (nT).

$\rho_r$ es constante para cualquier valor de frecuencia $\omega$ y corresponde con el valor real de resistividad del medio.

Si el medio no es homogéneo entonces se calcularán diferentes valores de resistividad para cada frecuencia seleccionada dentro del espectro de las micropulsaciones, constituyendo esto la curva de resistividad eléctrica aparente.

Si el medio puede ser representado por estratos planos paralelos (uni-dimensional) y a su vez se puede considerar el campo electromagnético como ondas planas que inciden normalmente en el terreno, entonces se puede definir:

$$Z_{xy} = \left(\frac{E_x}{H_y}\right) \qquad Z_{yx} = \left(\frac{E_y}{H_x}\right)$$

Donde: Z es la impedancia (ohm), la cual representa la función de respuesta del sistema Tierra. El elemento de impedancia $Z_{ij}$ (i,j= x o y) se refiere al coeficiente de la relación linear entre la componente eléctrica $E_i$ y la componente ortogonal magnética $H_j$ en la superficie de un semiespacio uniforme (Cagniard, 1953). La fase entre ambos en este caso es de 45°.

$$\rho_a = \frac{\mu_0}{f}\left|Z_{ij}\right|^2 = 0.2 * T\left|Z_{ij}\right|^2 \qquad \phi = tan^{-1}\left[\frac{\boldsymbol{Im}\, Z_{ij}}{\boldsymbol{Re}\, Z_{ij}}\right]$$

Como ya se mencionó, si el medio es homogéneo $\rho_a$ es constante e igual a $\rho_r$, mientras que $\phi$ es constante e igual a 45°.

Si el medio es uni-dimensional tanto $\rho_a$ como $\phi$ serán dependiente de la frecuencia $f$, pero es independiente del azimut del dispositivo, obteniéndose los mismos resultados para i,j=x,y como para i,j = y,x.

De no ser así, la causa principal sería la presencia de cambios laterales en las condiciones geológicas y el medio ya no sería uni-dimensional (bi o tri-dimensional). El cálculo de $\rho_a$ y $\phi$ se complica por ser imprescindible tener en cuenta el carácter tensorial de la resistividad y $Z$ será un valor complejo.

No obstante se puede definir el método de sondeo magnetotelúrico como la medición en superficie para una serie de frecuencias diferentes, en dos direcciones ortogonales *x* y *y*, de la impedancia *Z* del terreno.

2.2.3.- Procesamiento de la información

Tomando en cuenta el caso más general, cuando el medio no es ni homogéneo ni unidimensional, en el cual $E_x$ es debido en gran parte a $H_y$, pero también parcialmente a $H_x$, esto es por las corrientes inducidas por $H_x$ que son reflejadas en las estructuras, tenemos:

$$E_x = Z_{xy} H_y + Z_{xx} H_x \quad (1)$$

$$E_y = Z_{yx} H_x + Z_{yy} H_y \quad (2)$$

Transformando las series de tiempo obtenidas de los campos E y H al dominio de la frecuencia mediante la transformada de Fourier, se procede a multiplicar las ecuaciones (1) y (2) y determinándose los espectro de potencia y potencia cruzada conformando un sistema de 4 ecuaciones:

$$E_x E_x^* = Z_{xx} H_x E_x^* + Z_{xy} H_y E_x^* \quad (3)$$

$$E_x E_y^* = Z_{xx} H_x E_y^* + Z_{xy} H_y E_y^* \quad (4)$$

$$E_x H_x^* = Z_{xx} H_x H_x^* + Z_{xy} H_y H_x^* \quad (5)$$

$$E_x H_y^* = Z_{xx} H_x H_y^* + Z_{xy} H_y H_y^* \quad (6)$$

Donde: $E_x^*$, $E_y^*$, $H_x^*$y $H_y^*$ son las conjugadas complejas de $E_x$, $E_y$, $H_x$y $H_y$ respectivamente.

De las ecuaciones (3) a (6), se pueden obtener 6 ecuaciones para resolver $Z_{xx}$ y $Z_{xy}$.

$$Z_{xy} = ((H_xE_x^*)(E_xE_y^*) - (H_xE_y^*)(E_xE_x^*)) / ((H_xE_x^*)(H_yE_y^*) - (H_xE_y^*)(H_yE_x^*)) \quad (7)$$

$$Z_{xy} = ((H_xE_x^*)(E_xE_x^*) - (H_xH_x^*)(E_xE_x^*)) / ((H_xE_x^*)(H_yH_x^*) - (H_xH_x^*)(H_yE_x^*)) \quad (8)$$

$$Z_{xy} = ((H_xE_y^*)(E_xH_y^*) - (H_xH_y^*)(E_xE_x^*)) / ((H_xE_x^*)(H_yH_y^*) - (H_xH_y^*)(H_yE_x^*)) \quad (9)$$

$$Z_{xy} = ((H_xE_y^*)(E_xH_x^*) - (H_xH_x^*)(E_xE_y^*)) / ((H_xE_y^*)(E_xH_x^*) - (H_xH_x^*)(E_xE_y^*)) \quad (10)$$

$$Z_{xy} = ((H_xE_y^*)(E_xH_y^*) - (H_xH_y^*)(E_xE_y^*)) / ((H_xE_y^*)(H_yH_y^*) - (H_xH_y^*)(H_yE_y^*)) \quad (11)$$

$$Z_{xy} = ((H_xH_x^*)(E_xH_y^*) - (H_xH_y^*)(E_xH_x^*)) / ((H_xH_x^*)(H_yH_y^*) - (H_xH_y^*)(H_yH_x^*)) \quad (12)$$

De este sistema de ecuaciones (9) y (10) son inestables si el medio es unidimensional, ya que sólo se definen $H_xE_y^*$, $H_yE_x^*$ y las potencias de estas cuatro componentes, mientras que las demás potencias cruzadas se indeterminan.

Por lo que eliminado (9) y (10), se tiene un sistema de ecuaciones que permite determinar 4 valores de $Z_{xy}$, los cuales en teoría deben ser similares. De igual forma se pueden determinar los sistemas de ecuaciones que nos permiten encontrar los cuatros valores de $Z_{xx}$, $Z_{yy}$ y $Z_{yx}$. Por ejemplo, siguiendo el planteamiento de la ecuación (12) se obtiene:

$$Z_{xy} = ((H_xH_x^*)(E_xH_y^*) - (H_xH_y^*)(E_xH_x^*)) / ((H_xH_x^*)(H_yH_y^*) - (H_xH_y^*)(H_yH_x^*)) \quad (13)$$

$$Z_{xx} = ((H_xH_y^*)(E_xH_x^*) - (H_xH_y^*)(E_xH_y^*)) / ((H_xH_x^*)(H_yH_y^*) - (H_xH_y^*)(H_yH_x^*)) \quad (14)$$

$$Z_{yx} = ((H_yH_y^*)(E_xH_y^*) - (H_yH_x^*)(E_xH_x^*)) / ((H_xH_x^*)(H_yH_y^*) - (H_xH_y^*)(H_yH_x^*)) \quad (15)$$

$$Z_{yy} = ((H_xH_x^*)(E_yH_y^*) - (H_xH_y^*)(E_yH_x^*)) / ((H_xH_x^*)(H_yH_y^*) - (H_xH_y^*)(H_yH_x^*)) \quad (16)$$

Una vez determinadas las impedancias se pueden calcular mediante (1) y (2) valores estimados de $E_x$ y $E_y$ que, a través de un proceso de correlación con los valores observados, exponen de cierta manera el grado de contaminación con ruido en las mediciones del campo eléctrico.

No obstante, este proceso no garantiza una limpieza total de ruido en las componentes, sobre todo en las magnéticas. El método magnetotelúrico está diseñado para ser utilizado en zonas alejadas de todo ruido industrial y cultural, pero esto no siempre se cumple.

Con vista a compensar esta limitante se ha elaborado un procedimiento de campo en el cual se utiliza una segunda estación magnética, ubicada a cierta distancia (3 a 5 km) de la estación base. Esto es para utilizar las componentes magnéticas de referencia $H_{xr}$ y $H_{yr}$ en el proceso de cálculo de las impedancias mediante las ecuaciones (13) a (16), según:

$$Z_{xy} = ((H_xH_{xr}^*)(E_xH_{yr}^*) - (H_xH_{yr}^*)(E_xH_{xr}^*)) / ((H_xH_{xr}^*)(H_yH_{yr}^*) - (H_xH_{yr}^*)(H_yH_{xr}^*))$$

$$Z_{xx} = ((H_xH_{yr}^*)(E_xH_{xr}^*) - (H_xH_{yr}^*)(E_xH_{yr}^*)) / ((H_xH_{xr}^*)(H_yH_{yr}^*) - (H_xH_{yr}^*)(H_yH_{xr}^*))$$

$$Z_{yx} = ((H_yH_{yr}^*)(E_xH_{yr}^*) - (H_yH_{xr}^*)(E_xH_{xr}^*)) / ((H_xH_{xr}^*)(H_yH_{yr}^*) - (H_xH_{yr}^*)(H_yH_{xr}^*))$$

$$Z_{yy} = ((H_xH_{xr}^*)(E_yH_{yr}^*) - (H_xH_{yr}^*)(E_yH_{xr}^*)) / ((H_xH_{xr}^*)(H_yH_{yr}^*) - (H_xH_{yr}^*)(H_yH_{xr}^*))$$

Con el procedimiento anterior no era posible eliminar el ruido coherente en las componentes magnéticas, sobre todo cuando se calcula la potencia. En este caso al utilizar una estación remota de referencia, el ruido coherente debe ser nulo o muy poco, por lo que la mayor parte del ruido (no coherente) es eliminado en los procesos de potencia y potencia cruzada, obteniéndose una curva de resistividad y fase mejor definida.

Con los valores de impedancia calculados, es posible determinar una serie de funciones importantes para el proceso de interpretación

Otro paso sería rotar los ejes de medición con el objetivo de buscar la orientación en la cual se cumple la condición:

$(Z'_{xy}(\theta))^2 + (Z'_{yx}(\theta))^2 = \text{máximo}$

O lo que es lo mismo:

$(Z'_{xx}(\theta))^2 + (Z'_{yy}(\theta))^2 = \text{mínimo}$

Los valores de Z´ pueden ser hallados mediante las expresiones:

$2Z'_{xx}(\theta) = (Z_{xx} + Z_{yy}) + (Z_{xx} - Z_{yy}) \text{ Cos } (2\theta) + (Z_{xy} + Z_{yx}) \text{ Sen } (2\theta)$

$2Z'_{xy}(\theta) = (Z_{xy} - Z_{yx}) + (Z_{xy} - Z_{yx}) \text{ Cos } (2\theta) - (Z_{xx} - Z_{yy}) \text{ Sen } (2\theta)$

$2Z'_{yx}(\theta) = (Z_{xy} - Z_{yx}) + (Z_{xy} - Z_{yx}) \text{ Cos } (2\theta) - (Z_{xx} - Z_{yy}) \text{ Sen } (2\theta)$

$2Z'_{yy}(\theta) = (Z_{xx} + Z_{yy}) + (Z_{xx} - Z_{yy}) \text{ Cos } (2\theta) - (Z_{yx} + Z_{xy}) \text{ Sen } (2\theta)$

$\theta$ no es más que el ángulo para el cual se cumple que el medio estudiado se aproxima más a un medio bi-dimensional, es decir, se supone que uno de los ejes (el del ángulo $\theta$ o el perpendicular al mismo) coincide con el rumbo de las estructuras.

Con esto se calculan las curvas $\rho_{xy}$, $\rho_{xx}$, $\rho_{yy}$ y $\rho_{yx}$,. Los valores de $\rho_{xx}$ y $\rho_{yy}$ deben ser muy pequeños (próximos a cero) para que se pueda considerar la existencia de un medio bi-dimensional, de lo contrario puede esperarse la existencia de un medio tri-dimensional.

Una manera de cuantificar este problema es a través de la función **Skew (k)**, la cual se define como:

$$k = \frac{Z'_{xx} + Z'_{yy}}{Z'_{xy} - Z'_{yx}}$$

Si k toma valores diferentes de cero ($k \geq 0.4$) entonces el medio puede ser considerado como tri-dimensional para la frecuencia analizada.

Otro parámetro indicativo de la complejidad estructural del medio es el **Tipper (T).** Las heterogeneidades laterales producen un incremento de la densidad de corriente en los sectores más conductores. Las corrientes se concentran cerca de la superficie en el lado más conductor debido a que la profundidad nominal es menor.

En la frontera y las inmediaciones de la discontinuidad lateral se genera una componente vertical del campo magnético, debido a la existencia de un cambio lateral en la densidad de corriente. Esta componente vertical $H_z$ se relaciona con las componentes horizontales de la forma:

$H_z = A\ H_x + B\ H_y$

Donde A y B son elementos complejos, cuyas magnitudes representan la magnitud de la heterogenidad lateral o Tipper según:

$$T = \left[ |A|^2 + |B|^2 \right]^{\frac{1}{2}}$$

Si el medio es homogéneo o uni-dimensional A y B son nulos y por lo tanto T = 0. Cuando el Tipper toma valores diferentes de cero ($T \geq 0.2$), entonces se puede inferir un cambio lateral de la resistividad del medio que pudiera definir un rumbo en las estructuras estudiadas.

El Tipper y el Skew son parámetros esenciales para la determinación del grado de distorsión de la información MT, por lo que son de uso imprescindible en el proceso de análisis de los datos adquiridos en el campo.

Existen otros parámetros similares planteados por Bahr (1988) que supone que el medio estudiado se ajusta al modelo de superimposición (un medio regional 2-D con distorsión local 3-D), los cuales serán analizados en capítulo posterior.

Existen otras fuentes de distorsión que no están asociadas al carácter bi y/o tri-dimensional del medio estudiado. La distorsión galvánica, por ejemplo, tiene su fuente

en pequeñas heterogeneidades superficiales que son frecuentes en los diferentes ambientes geológicos reales.

La distorsión galvánica es el efecto que producen, sobre el campo electromagnético, las estructuras muy superficiales debido a la acumulación de cargas que se generan en las fronteras del cuerpo anómalo superficial (Vozoff, 1989).

Cuando esto ocurre sólo se afecta el campo eléctrico mediante un valor constante e independiente de la frecuencia que multiplica a los valores de resistividad eléctrica aparente ($\rho_a(\omega)$) observados, presentándose un desplazamiento constante en escala logarítmica de las curvas de $\rho_a(\omega)$.

Este efecto puede ser observado entre dos curvas $\rho_a(\omega)$ de un mismo sondeo o entre curvas $\rho_a(\omega)$ de diferentes sondeos (Fig. 3).

### 2.3.- Levantamiento MT

Un levantamiento magnetotelúrico fue realizado en el período Junio-Julio de 1997, lo cual constituye el primer esfuerzo por obtener la imagen geoeléctrica de la corteza en esta región del cráter de impacto.

En total se realizaron 22 sondeos magnetotelúricos. De éstos, 21 están distribuidos a lo largo de dos perfiles (Fig. 2) extendidos de manera radial con centro común en el puerto de Chicxulub, considerado como centro del cráter. El sondeo 4 no se encuentra a lo largo de ninguno de los dos perfiles, por lo que su aprovechamiento en futuros trabajos de inversión 3-D justifica su ejecución Las características fundamentales de estos perfiles se exponen en la Tabla 1.

Ambos perfiles cruzan de manera perpendicular el anillo de cenotes, garantizando el estudo de los cambios de resistividad eléctrica a través del mismo.

Durante la campaña de mediciones fueron utilizadas dos estaciones MT V-5 Phoenix (Scintrex). Ambos equipos trabajaron simultáneamente y sincronizados con relojes de alta precisión. Esto permitiría, en caso necesario, utilizar los registros obtenidos en un punto de medición como estación remota para corregir el ruido local que puediera estar afectando las mediciones registradas en la otra estación ubicada a cierta distancia (referencia).

Las observaciones magnetotelúricas se registraron en el rango de 384 Hz hasta un período de 1820 s.

| Perfil | Número de sondeos | Orientación | Longitud (km) | Estructuras principales estudiadas | Observaciones adicionales |
|---|---|---|---|---|---|
| A-A´ | 11 | Norte-Sur | ~70 | Atraviesa perpendicularmente el anillo de cenotes. Se extiende en su mitad sur sobre el bajo gravimétrico (bajo estructural). Los dos sondeos extremos sur (11 y 12 ) se encuentran sobre el escarpe de la falla Ticul. | Ningún sondeo se realiza sobre el máximo gravimétrico central. |
| B-B´ | 10 | Noroeste-Sureste | ~90 | Atraviesa perpendicularmente el anillo de cenotes | El sondeo extremo noroeste (22) se ejecuta sobre el borde del máximo gravimétrico central. |

**Tabla 1: Características fundamentales de los perfiles magnetotelúricos.**

Debido a la mayor complejidad estructural del perfil A-A´ (Tabla 1), sólo se expondrán en este trabajo los resultados preliminares del procesamiento e interpretación de la información MT registrada en los 10 sondeos magnetotelúricos pertenecientes al perfil B-B´.

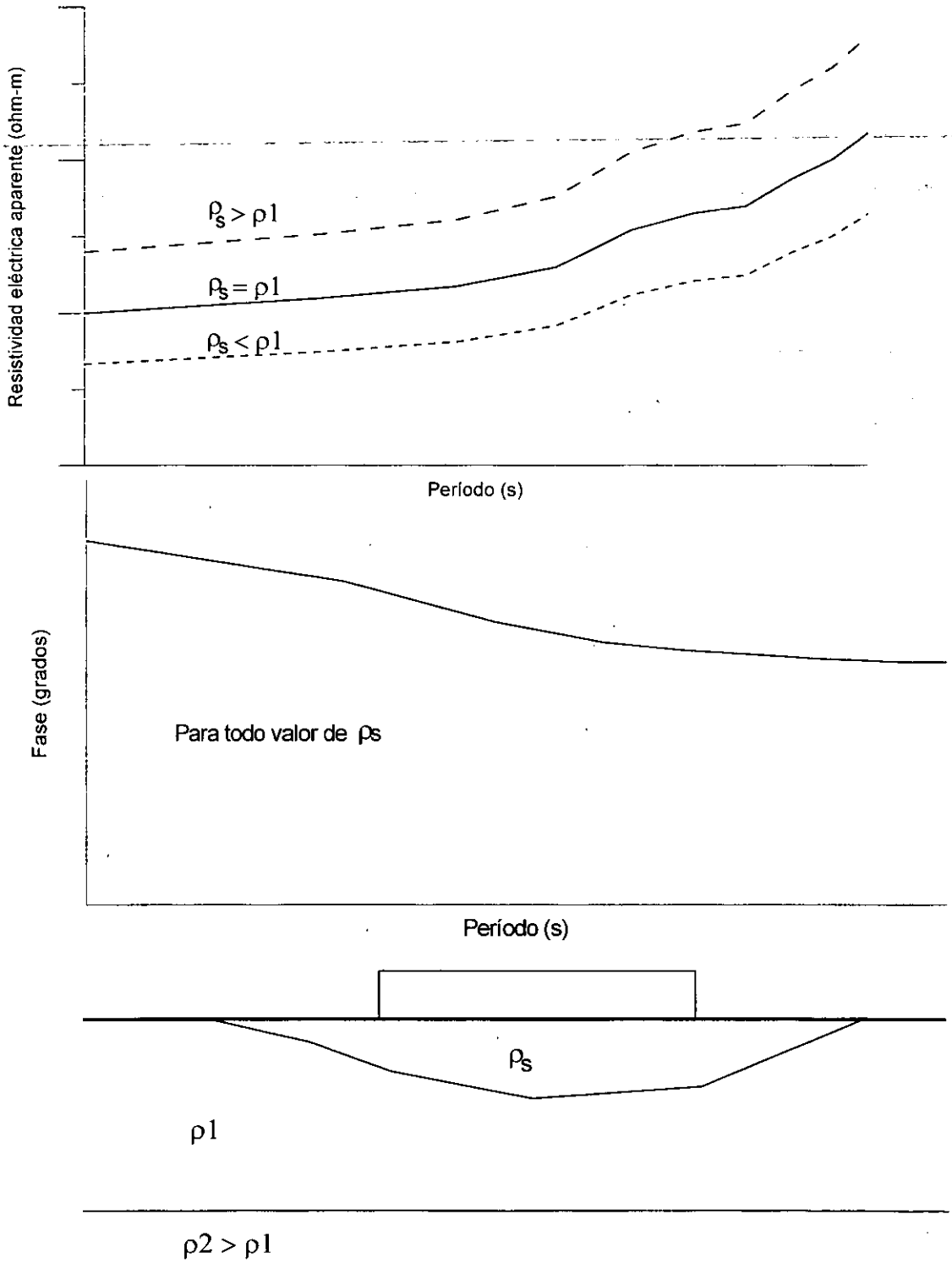


**Figura 3: Diagrama que ilustra el efecto de la distorsión galvánica sobre las curvas de campo observadas.**

## 2.4.- Análisis cualitativo

En la Figura 4 se exponen las curvas de resistividad eléctrica aparente ($\rho_a(\omega)$) y las fases observadas ($\phi(\omega)$) en los modos *xy* y *yx* de los 10 sondeos magnetotelúricos.

Según lo analizado anteriormente sobre el efecto de la distorsión galvánica en los valores registrados del campo electromagnético, podemos concluir que no se observa el efecto de este tipo de distorsión en las curvas de resistividad eléctrica aparente pertenecientes a este perfil MT, en correspondencia con el comportamiento de las fases, tanto en el modo *xy* como en el *yx* (Fig. 4).

Realizando un análisis cualitativo, estas curvas se pueden dividir en dos grupos de acuerdo al comportamiento de estos parámetros eléctricos.

Un grupo estaría comprendido por los sondeos localizados sobre y dentro del anillo de cenotes (sondeos 17, 18, 19, 20, 21 y 22); el segundo grupo comprende aquellos sondeos ubicados fuera del anillo de cenotes (sondeos 13, 14, 15 y 16).

Se puede observar que las curvas de ambos grupos son muy similares para los períodos $T \leq 0.1$ s. Para los períodos $T > 0.1$ s. el segundo grupo muestra valores mayores de $\rho_a(\omega)$ que el primero.

Este resultado es muy significativo ya que al menos cualitativamente, se puede apreciar una respuesta de la estructura del cráter en el comportamiento de los valores observados (Pilkington y Grieve, 1992).

Los sondeos 13, 14, 15 y 16, al estar ubicados fuera del anillo de cenotes, es de esperar que el medio estudiado por los mismos corresponda a rocas menos porosas y fracturadas que las que constituyen el medio analizado por el resto de los sondeos.

Fuera del anillo de cenotes el medio debe ser, en general, más resistivo que el que representa el relleno muy fracturado y poroso, perteneciente al interior del cráter.

Las curvas de $\rho_a(\omega)$ de los sondeos del primer grupo muestran una anomalía conductora en el rango de períodos de 1 a 10 s más pronunciada que para el resto de los sondeos, confirmando así el análisis antes expuesto.

Las curvas observadas en ambos grupos muestran un carácter predominante 1-D dada su similitudes en ambas polarizaciones.

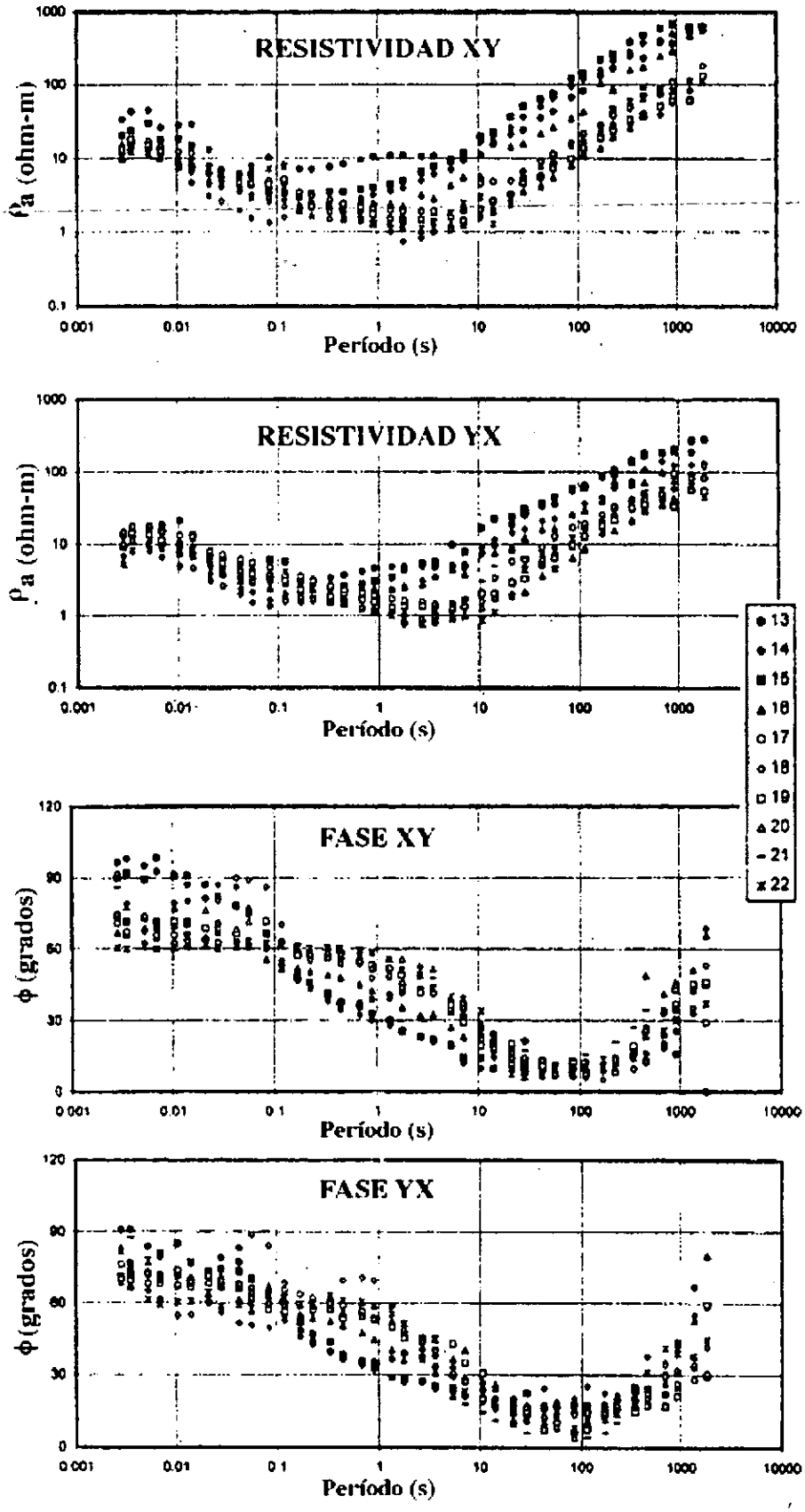


Figura 4: Curvas de resistividad aparente y fases observadas.

## 2.5.- Inversión Bostick

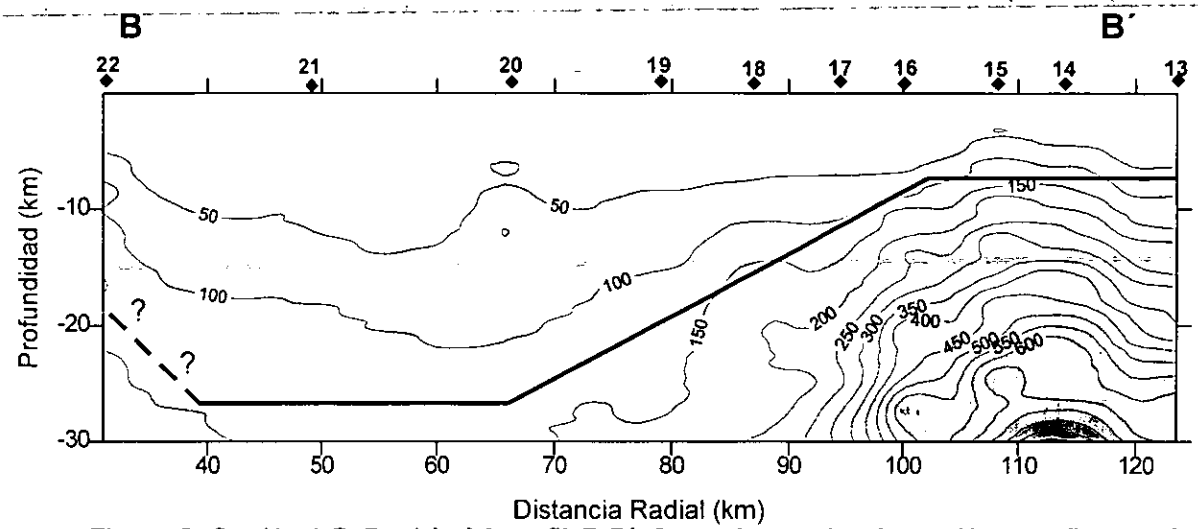


**Figura 5: Sección 1-D Bostick del perfil B-B´. Los valores sobre la sección se refieren a la resistividad eléctrica del medio dada en ohm-m. ♦: ubicación de las estaciones según su número.**

En la Figura 5 se presenta la sección geoeléctrica Bostick *xy*. Esta sección fue construida a partir de la correlación de los modelos de inversión 1-D de los pares de curvas $\rho_{axy}(\omega)$ y $\phi_{xy}(\omega)$ para cada sondeo, utilizando el algoritmo de Bostick (Goldberg y Rotstein, 1982).

Este procesamiento y resultado es realizado por la estación in situ (ver anexo 2, parámetros 43 y 58).

Como es de esperar, el análisis cualitativo de los sondeos 13, 14, 15 y 16 modela un medio muy resistivo, mientras que el resto de los sondeos modelan un medio relativamente conductor.

Los valores de $\rho(z)$ decrecen gradualmente hasta que se estabilizan entre los sondeos 20 y 21.

El sondeo 22 modela un incremento en los valores de $\rho(z)$ lo que puede significar, de acuerdo a su ubicación (Tabla 1, Fig. 2), que se deba a la influencia de las rocas menos fracturadas y más resistivas pertenecientes al alto estructural central, característica de los cráteres complejos (Pilkington y Grieve, 1992).

Esta distribución de $\rho(z)$ sugiere la existencia de una estructura de impacto de aproximadamente 190 km de diámetro.

De acuerdo con este modelo preliminar la zona de fracturas pudiera estar afectando la corteza superior e inferior. No se observa un levantamiento del manto, lo que contradice algunos trabajos anteriores que sugieren la existencia de un levantamiento del manto de manera tal que garantiza el equilibrio isostático.

## 2.6.- Conclusiones

La efectividad de la aplicación del método magnetotelúrico al estudio del cráter de Chicxulub pudo comprobarse en el análisis cualitativo de las curvas observadas. Los pares de curvas $\rho_a(\omega)$ y $\phi(\omega)$ se diferenciaron en su comportamiento de acuerdo a la ubicación del punto de medición respecto al anillo de cenotes.

El modelo geoeléctrico preliminar presentado sugiere la existencia de una estructura de impacto de aproximadamente 190 km de diámetro, mientras que un ligero incremento de $\rho(z)$ en el extremo NW del perfil pudiera indicar la influencia del alto estructural central en los registros obtenidos en el sondeo 22.

Los valores menores de resistividad eléctrica indican que las fracturas inducidas por el impacto alcanzan las partes inferiores de la corteza. La distribución de $\rho(z)$ en profundidad no concuerda con la presencia de un manto elevado.

Se recomienda realizar un análisis del grado de distorsión y un proceso de inversión 1-D más detallado de este perfil a fin de confirmar o corregir los resultados obtenidos.

## 2.7.- Referencias


ALVAREZ, L. W., ALVAREZ, W., ASSARO, F. y MICHEL, H., 1980. Extraterrestrial cause for the Cretaceous/Tertiary extinction. Science, **208**, 1095-1108.

BAHR, K., 1988. Interpretation of the magnetotelluric tensor: regional induction and local telluric distortion. J. Geophys., **62**, 119-127.

BOSTICK F. X. y SMITH H. W., 1961. An analysis of the magnetotelluric method for determining subsurface resistivities. Electrical Engineering Research Laboratory. The Univ. of Texas, Austin, Report No. 120.

CAGNIARD L., 1953. Basic theory of the magnetotelluric method of geophysical prospecting. Geophysics, **18**, 605-635.

ELLIS W., 1892. On the simultaneity of magnetic variations at different places on occasions of magnetic disturbance and on the relation between magnetic and earth-current phenomena. Proceed. Roy. Soc. London, **52**, 191.

ESPÍNDOLA, J. M.; M. MENA; M. DE LA FUENTE y J. O. CAMPOS-ENRÍQUEZ, 1995. A model of the Chicxulub impact structure (Yucatan, Mexico) based on its gravity and magnetic signatures. Phys. Earth Plant. Inter., **92**, 271-278.

FOURNIER H. G., 1969. Ensayo histórico sobre los conocimientos magnetotelúricos. Publicaciones del Observatorio del Ebro. Memoria **13**. Cons. Sup. Inv. Cient., Tarragona.

GOLDBERG, S. y Y. ROTSTEIN, 1982. A simple form of presentation of magnetotelluric data using the Bostick transform. Geophys. Prosp., **30**, 211-216.

HATAKEYAMA H. y HIRAYAMA M., 1934. On the phase difference between the pulsation of terrestrail magnetism and the current. Jour. Meteor. Soc. Japan, Sec. Ser. **12**, 449-459, Tokyo.

HILDEBRAND, A R.; PILKINGTON, M; CONNOR, C. ORTÍZ-ALEMÁN y R.E. CHÁVEZ, 1995. Chicxulub crater: Size and structure of the Chicxulub crater revealed by horizontal gravity gradients and cenotes. Letters to Nature, **376**, 415-417.

HIRAYAMA M., 1935. On the earth potential gradients induced by the magnetic variations in the anisotropic earth crust. Jour. of the Meteor. Soc. Japan, Sec. Ser. **13**, 456-465, Tokyo.

HOFFMAN A. A. J., 1962. Geophysical Interpretation of power spectral analysis of low frequency fluctuations in the magnetotelluric field. Texas.

LIPSKAJA, N. V., DENISKIN N. A. y EGOROV J. M., 1961. Construction des courbes du sondage electromagnétique d´aprés les observations des microvariations du champ

electromagnétique naturel de la Terre. *In* Probl. Theór. Prat. Electrométr. Moskva, Izdat. Akad. Nauk. USSR, 41-55.

MOSKVICHEV, Y. I., 1965. Amplitude-phase methods of interpretation in magnetotelluric methods of electrical surveyings. Prikl. Geofisika, **41**, 102-121.

PENFIELD G. T. y CAMARGO, Z. A., 1981. Definition of a major igneos zone in the central Yucatan platform with aeromagnetics and gravity. 51st Ann. Internat. Mtg. SEG, Abstract, 37.

PILKINGTON, M. y R.A.F. GRIEVE, 1992. The geophysical signature of terrestrial impact craters. Reviews of Geophysics, **30**, 161-181.

PILKINGTON, M., A. R. HILDEBRAND y ORTÍZ-ALEMÁN, C., 1994. Gravity and magnetic field modeling and structure of the Chicxulub crater, Mexico. Journal Geophys. Resear. **99**, 147-162.

SHARPTON, V. L.; K. BURKE, A. CAMARGO; S. A. HALL; D. SCOTT-LEE; L. E. MARÍN; G. SUÁREZ; J. M. QUEZADA; P. D. SPUDIS y J. URRUTIA-FUCUGAUCHI, 1993. Chicxulub multiring impact basin: Size and other characteristics derived from gravity analysis. Science, **261**, 1564-1567.

TIKHONOV A. N., 1950. Determination of the electrical characteristics of the deep strata of the earth's crust. Doklady, Akad. Nauk. SSSR, **73**, 295-299.

TIKHONOV A. N. y D.N. SHAKHSUVAROV, 1956. Concerning the possibility of using the impedance of the earth natural electromagnetic field for investigating its upper layers. Bull (IZV) Akad. Sc. USSR, Geophys. Ser., **4**, 410-418.

VAN BEMMELEN, W., 1908. Earth-current. Registration at Batavia, III part, Kon. Akad. Van Wetensch, Amsterdam, Proceed. of Octuber 31, 11-1, 242-248.

VOZOFF, K., 1972. The magnetotelluric method in the exploration of sedimentary basins. Geophysics, **37**, 98-141.

VOZOFF, K., 1989. The magnetotelluric method. *In* Electromagnetic methods in applied geophysics. Nabigian M. N.. S.E.G.

## 3.- EFECTO DE COSTA EN SONDEOS MAGNETOTELÚRICOS SOBRE LA PENÍNSULA DE YUCATÁN, MÉXICO

**Coast Effect in Magnetotelluric Soundings over the Yucatan Peninsula, Mexico**

Omar Delgado-Rodríguez[1,2], Jaime Urrutia-Fucugauchi[1], Jorge A. Arzate[3] and Oscar Campos-Enríquez[1]

*(1)* Departamento de Geomagnetismo y Exploración, Instituto de Geofísica, Universidad Nacional Autónoma de México, Coyoacán 04510, México D.F., México

*(2)* Instituto de Geofísica y Astronomía. CITMA, La Habana, Cuba

*(3)* Unidad de Investigación en Ciencias de la Tierra, UNAM-Campus Juriquilla, Juriquilla, Qro., C.P. 76230, México

*Aceptado para su publicación en Geofísica Internacional (anexo 1).*

### 3.1.- Abstract

Three-dimensional synthetic modeling of magnetotelluric sounding data of the Yucatan peninsula, suggests that the coast effect on the magnetotelluric measurements carried out over the Chicxulub impact region is negligible. The marine platform surrounding the Yucatan peninsula yields a moderate coast effect in a period range (T= 10 to 1000 s), outside of the period range associated wih the conductivity anomaly of the crater (T= 1 to 10 s). These results provide a framework for the interpretation of MT soundings previously obtained in the Chicxulub crater and define other areas for future MT surveys in the Yucatan peninsula.

**Key Words:** Magnetotelluric Soundings, 3-D Modeling, Coast Effect, Chicxulub Crater, Yucatan Peninsula.

### 3.2.- Resumen

A partir de la modelación sintética de la península de Yucatán, se pudo establecer que el efecto de costa sobre las mediciones magnetotelúricas realizadas en la región de impacto de Chicxulub, es despreciable.

La plataforma marina que circunda a la península produce un moderado efecto de costa en un rango de períodos (T= 10 a 1000 s.) que no se corresponde con las frecuencias (T= 1 a 10 s) que definen la anomalía conductora en las curvas de resistividad eléctrica aparentes observadas en las 22 estaciones MT.

Estos resultados le ofrecen una alta confiabilidad a los obtenidos del levantamiento MT por lo que se proponen otras áreas, igualmente confiables, para ejecutar nuevas mediciones MT.

**Palabras Claves:** Sondeo Magnetotelúrico, modelación 3-D, Efecto de Costa, Cráter de Chicxulub, Península de Yucatán.

## 3.3.- Introduction

Discovery of the Chicxulub crater on the Yucatan peninsula, Mexico (Fig. 1), with an age at the Cretaceous-Tertiary boundary (65 million years b.p.) supports the hypothesis of an extraterrestrial impact (Alvarez et al., 1980).

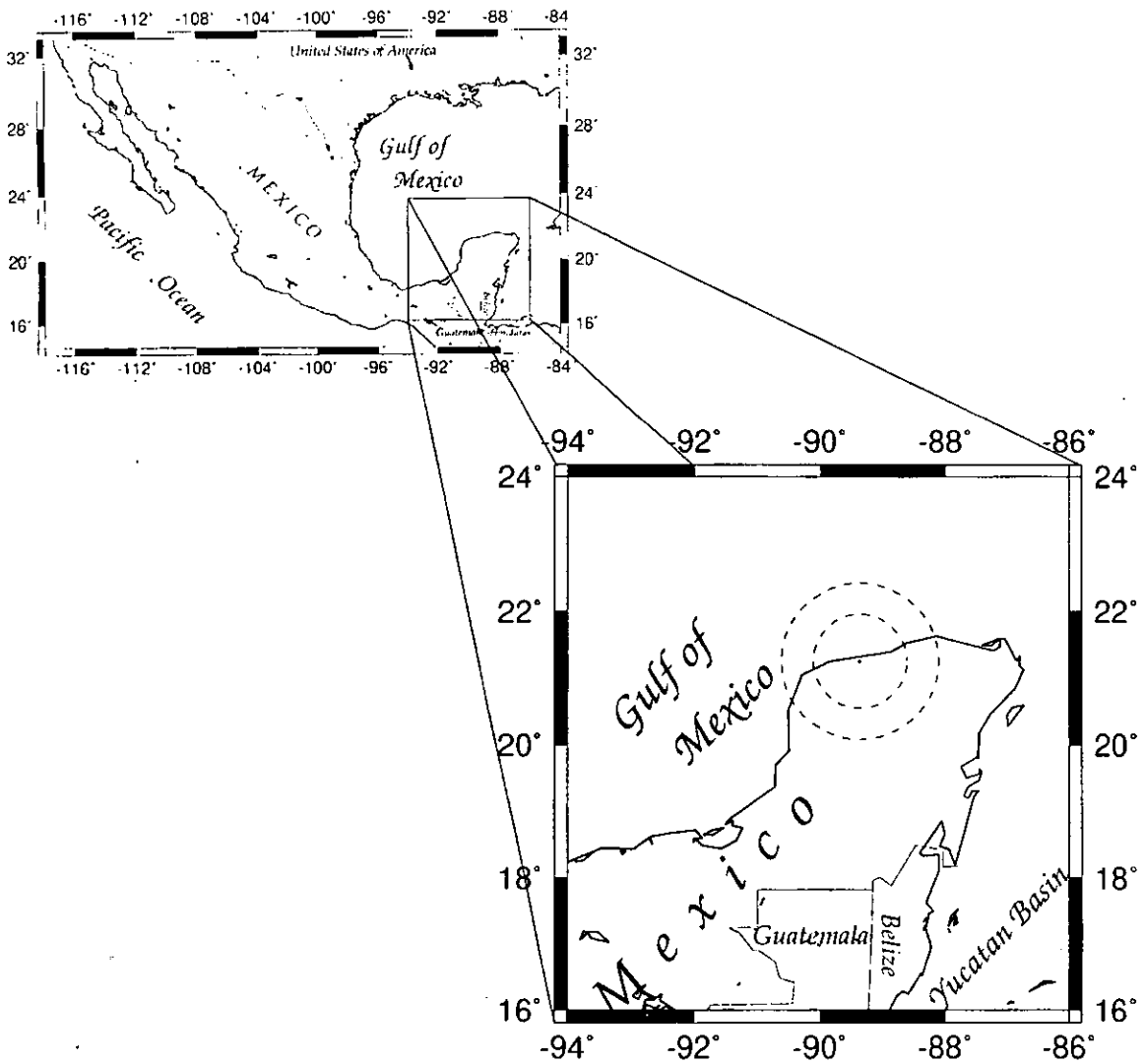


**Figure 1: Study area. Two of the proposed diameters of the structure are indicated with the town of Progreso in the center.**

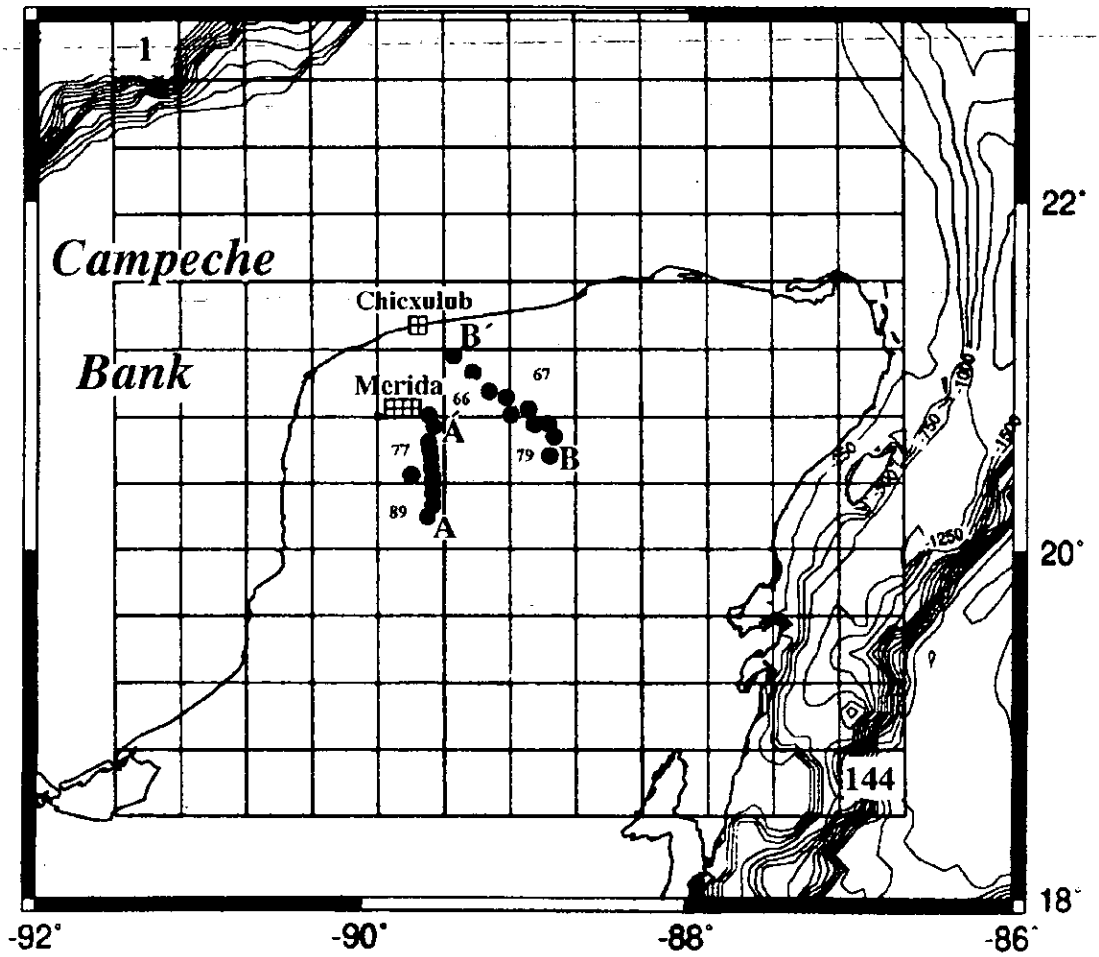


**Figure 2: Plan view of the synthetic 3-D model.**

During the past decade, geophysical studies have been carried out at the Chicxulub impact structure, including gravity and magnetic information (e. g., Hildebrand et al., 1991, 1998; Sharpton et al., 1993; Pilkington et al., 1994; Espíndola et al., 1995). Different models (e.g., four rings basin, simple ring, with diameter of 300 km, 180 km diameter, with central structural high with twin peaks) have been proposed.

Recently, models have been based on marine seismic reflection profiles (e. g., Morgan et al., 1997). In addition, lithological and geomorphological information has been analyzed in order to document the subsurface stratigraphy (e. g., Connors et al., 1996; Urrutia-Fucugauchi et al., 1996).

Magnetotelluric (MT) soundings provide information on the conductivity structure of the Yucatan peninsula (Campos-Enríquez et al., 1997). Twenty-two MT soundings were measured along two radial AA′ and BB′ profiles (Fig. 2). The survey showed the presence of fracture zones in the lower crust, and no evidence of a mantle uplift. Delgado-Rodríguez et al. (2000) carried out a 1-D inversion of profile BB′ using the Bostick (Golberg and Rotstein, 1982) and Occam algorithms (Constable et al., 1987). They provided support of a 1-D representation and they found a diameter of approximately 200 km for the crater. Arzate et al. (2000) carried out a 2-D inversion of both profiles, and established a maximum diameter of the structure of around 195 km.

The peninsular environment, raises the question of the dependence of the electromagnetic models on the coast effect (Dosso and Meng, 1992). This paper discusses the coast effect on the MT soundings performed over the Chicxulub impact structure.

### 3.4.- Coast Effect

The coast effect in electromagnetic observations was described by Parkinson (1959) as a result of the influence of the high electric conductivity of sea water (Kellet et al., 1991). The influence of a highly conductive body may affect geomagnetic measurements in a way that suggests a spurious presence of a conductive stratum in the interpretation of curves $\rho(\omega)$ and $\phi(\omega)$. In addition, it can mask the real effect of an anomalous conductive body, possibly associated with the Chicxulub impact crater.

Laboratory models have been constructed, which simulate conditions in different situations (Meng et al., 1979; Nienaber et al., 1979; Hebert et al., 1983; Chen et al., 1990). Dosso and Meng (1992) empirically determined some mathematical relations that estimate the effect for continental conditions and for islands.

The coast effect is measured by means of the relation $B_z/B_{yn}$. between the induced vertical magnetic field $B_z$ and normal magnetic field $B_{yn}$. A value of 1nT was assigned to $B_{yz}$. Bz/Byn depends on the distance from the coastline, it reaches its highest value at the coastline and decreases seaward as well as inland.

The influence of the coast effect a distance of the coastline $Y_r$ is long enough, so that the relation $B_z/B_{yn} = 0.2$. Otherwise, the coast effect is very difficult to calculate. $B_z/B_{yn}$ increases

with increasing ocean depth and decreases with the increase of period T. Dosso and Meng (1992) published sets of curves for different types of islands, providing the distance at which Bz/Byn = 0.2 is reached as well as the distance Yr.

### 3.5.- 3-D Modeling

A direct 3-D modeling scheme is used by means of the program 3DMT (Park, 1985).

The procedure consists of designing a network of blocks that contain the information on the distribution of the electric resistivities of the medium. In the design of the model three factors are considered:

1.- The thickness of any inhomogeneous layer should be smaller than the nominal depth (skin depth). Calculation of the skin depth uses the lowest electric resistivity and the highest frequency considered in the calculations. The thickness of any inhomogeneous layers should be less than 20% of the nominal calculated depth (Park, 1985).

We find a minimum skin depth of 350 m for model 3B; thus a cell thickness not larger than 70 m should be selected. We use a value of 50 m which factors integrally into 2 km and yields a total of 50 layers of 50 m thickness. For the model 3A the thickness is smaller.

2.- Lateral extension of the blocks should not be greater than the Minimal Adjustment Distance (AD). The AD parameter constitutes a nominal horizontal distance capable of influencing the non-homogeneities perturbing the 1-D solution in each block.

In order to calculate AD, average resistivities larger than 100 ohm-m present in the medium are considered by calculating the value of effective electric resistivity (Park, 1985).

$$\rho_{eff} = \frac{\sum \rho_i \Delta Z_i}{\Delta Z_{eff}},$$

$$\Delta Z_{eff} = \sum \Delta Z_i$$

where $\rho_i$ is the electric resistivity larger than 100 ohm-m in layer i, and

$\Delta Z_i$ is the thickness in km of layer i.

Thus, the AD distance is calculated by:

$$AD = \sqrt{\frac{\Delta Z_{block} * \rho_{eff} * \Delta Z_{eff}}{\rho_{block}}}$$

where $\rho_{block}$ is the electric resistivity of the inhomogeneous block in ohm-m, and.

$\Delta Z_{block}$ is the thickness km of the inhomogeneous block.

In our case $\rho_{eff}$ = 8921.6 ohm-m, $\Delta Z_{eff}$ = 51 km, $\rho_{block}$ = 500 ohm-m, $\Delta Z_{block}$ = 2 km and AD = 42.6 km. Thus it is possible to use a lateral dimension 40 x 40 km for each cell.

3.- Selection of the electric resistivity values for each layer, is subject to the solution of the two previous steps.

With these constraints, a 3-D resistivity model for the Yucatan peninsula and its margins is constructed. The magnetic and electric field components are calculated individually for each block. Next the values of the impedance tensor $Z(\omega)$ are determined as well the values of $\rho_{axy}(\omega)$, $\phi_{xy}(\omega)$ and $\rho_{ayx}(\omega)$, $\phi_{yx}(\omega)$ for each block and all periods.

The Yucatan Peninsula model is constructed by one inhomogeneous superficial layer, 2 km thick, that represents the carbonated rocks ($\rho$ = 500 ohm-m) covering the impact structure, and a marine platform around the peninsula (Fig. 3) The effect of the sea on MT measurements was modeled independently with a model including the marine platform (Fig. 3A), and another model based on a 1-D approximation of the platform (Fig. 3B).

Comparing both models should bring out the effect of a conductive sea on the apparent resistivity values for several periods.

The model is represented by a network of 12 x 12 cells with a size of 40 x 40 km each (Fig. 2).

At depth, it includes two layers with $\rho$=5000 ohm-m and $\rho$=10000 ohm-m, respectively. Their thicknesses are 11 and 40 km.

The 3-D modeling of both models was carried out for periods of 0.001, 0.004, 0.01, 0.04, 0.1, 0.4, 1, 4, 10, 40, 100, 400 and 1000 s.

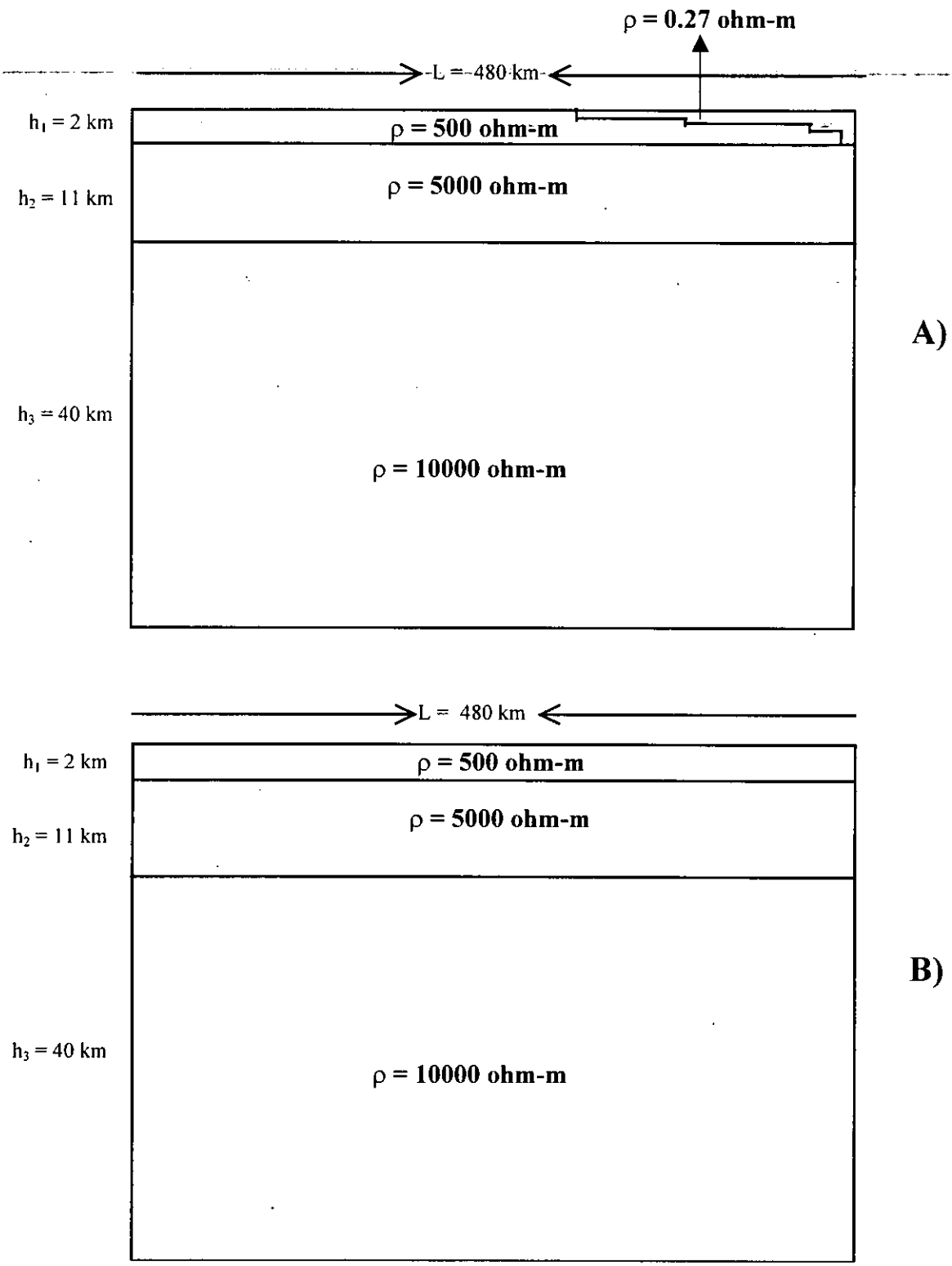


**Figure 3: Schematic sections of the models used in the 3-D synthetic modeling of the Yucatan peninsula. A) Model with marine platform, B) 1-D model.**

### 3.6.- Results and discussion

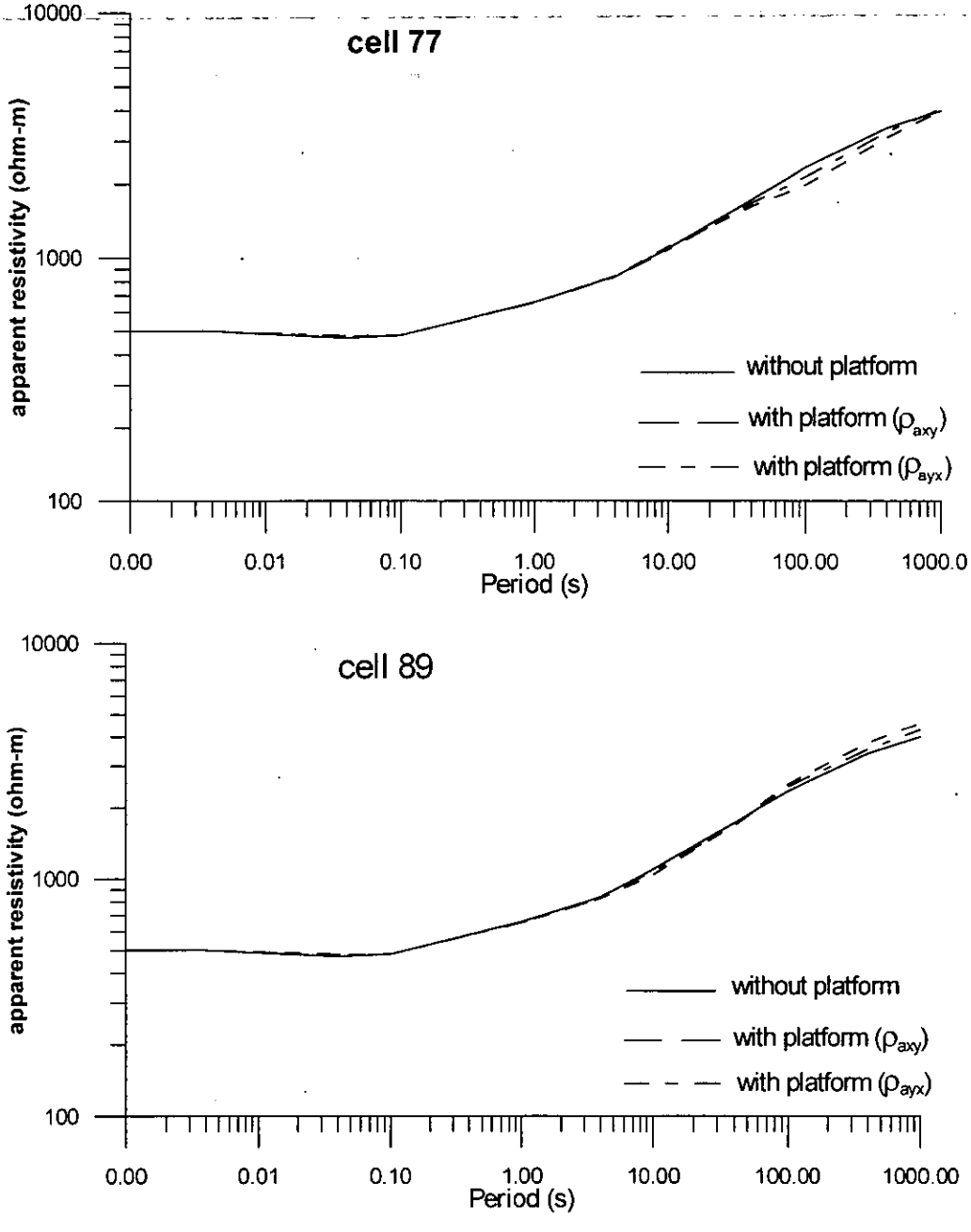


**Figure 4: Comparison of the apparent electric resistivity curves calculated from model 1-D and with marine platform. Cells 77 and 89 include the profile AA´.**

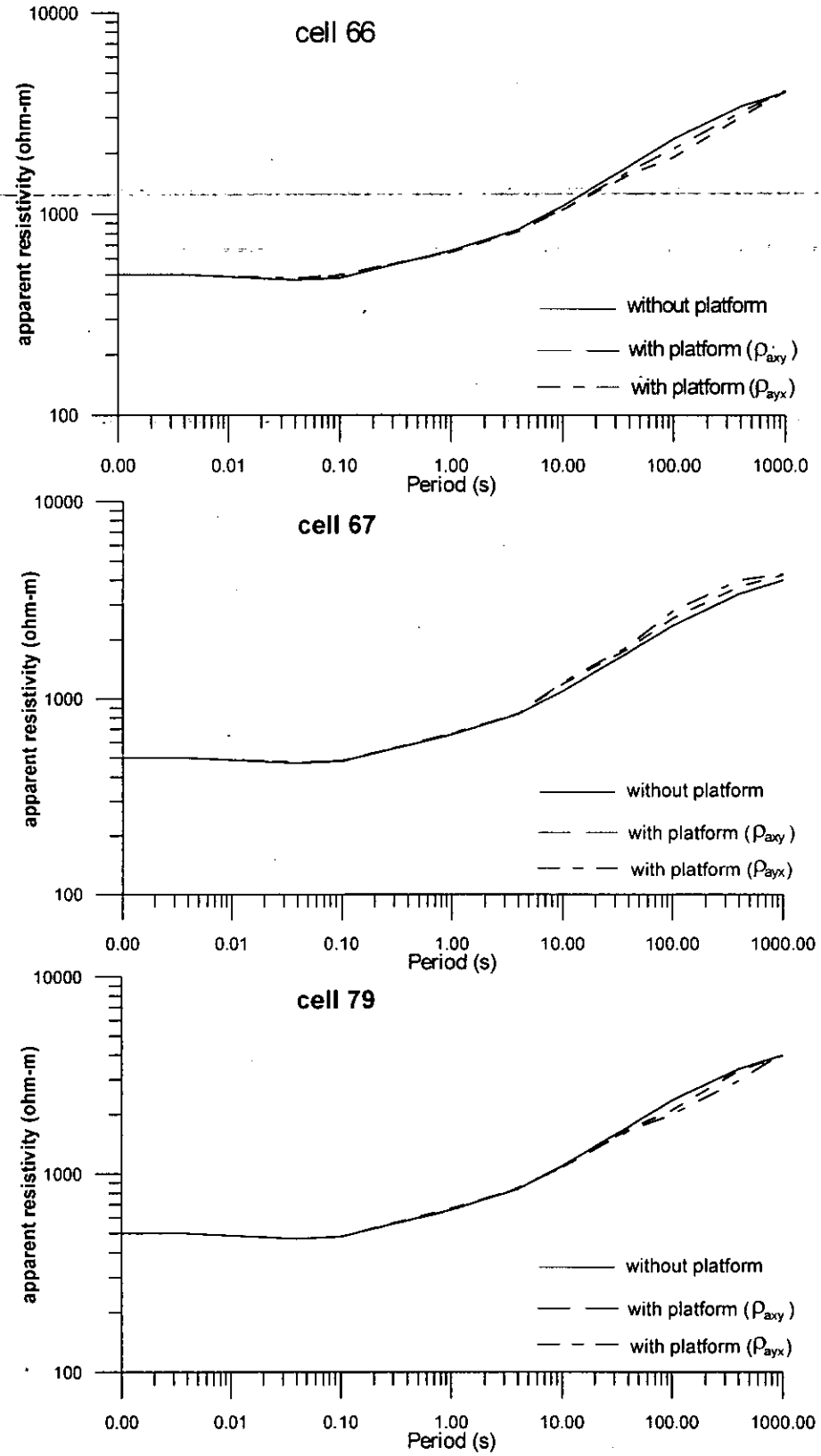


**Figure 5: Comparison of the apparent electric resistivity curves calculated from models 1-D and with marine platform. Cells 66, 67 and 79 include the profile BB′.**

Figure 2 shows the 22 MT soundings distributed along two profiles (AA′ and BB) contained in the cells 77 and 89 for profile AA′, and 66, 67 and 79 for the profile BB′.

Figure 4 shows the calculated apparent resistivity curves corresponding to cells 77 and 89, which include the profile AA′.

In both cells, the difference between the model that includes the marine platform and the 1-D model is small. This reflects the minor influence of the conductive sea on the profile. The most significant differences are observed in the period range of 10 to 100 s.

For the case of the profile BB′, the curves corresponding to the cells 66, 67 and 79 (Fig 5) show a similar phenomenon, with some differences in the period range of 20 to 1000 s. The period of T= 100 s seems to be the most representative of these differences.

In conclusion, the coast effect can only be seen in the range of periods of 10 to 1000 s, while the conductivity anomaly associated with the filling of the crater is present mainly in the periods of 0.01 to 10 s (Fig. 6).

The apparent resistivity differences between 1-D model and the model with a marine platform were calculated for T=100 s for each cell over the peninsula of Yucatan and the surrounding marine platform. These differences are summarized for the *xy* mode (N-S) and the *yx* mode (E-W).

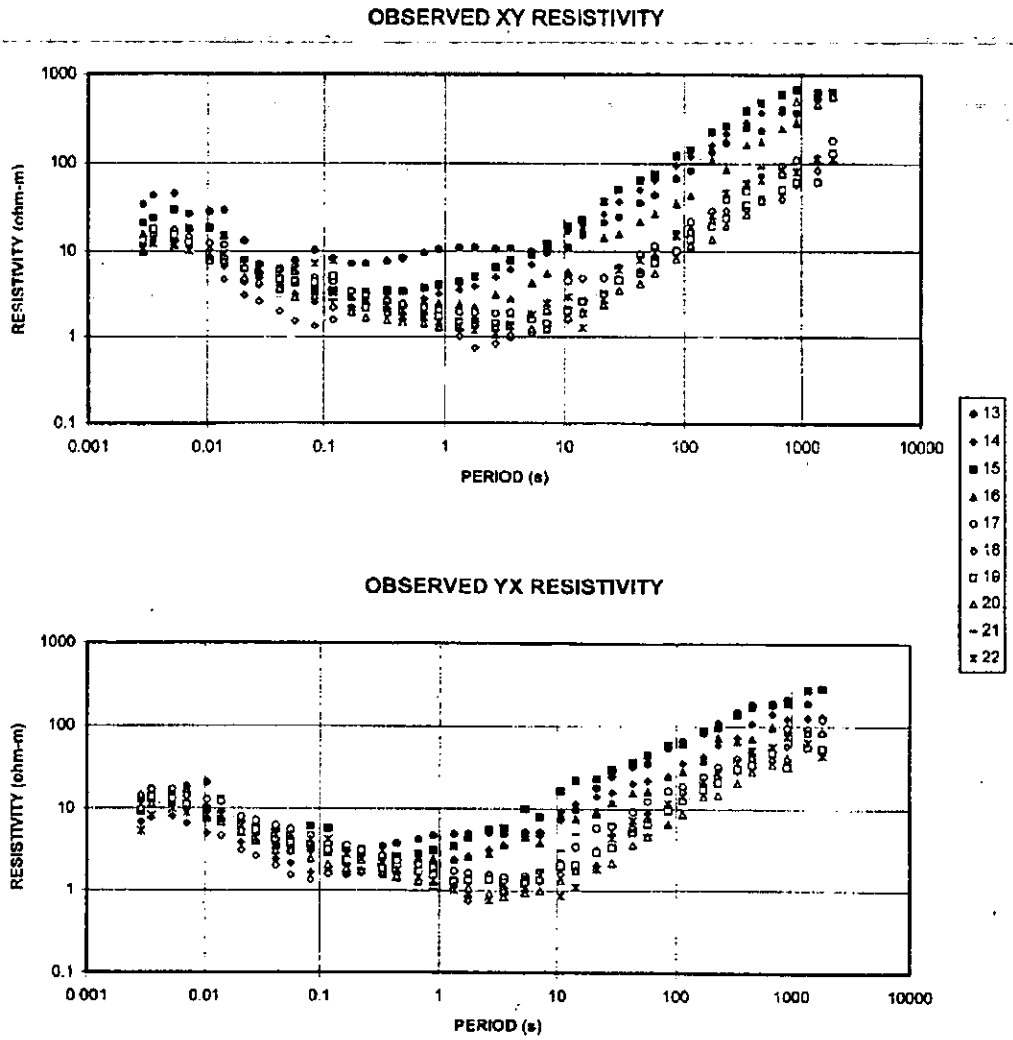


**Figure 6: Observed apparent resistivities curves fro the profile BB′.**

For the *xy* mode (Fig. 7A) the differences is less than 10% in the area that includes most of the stations belonging to profiles AA′ and BB′. The rest of the stations shows differences of around 10%. The greatest differences in the peninsula are found in the area where the marine platform vanishes and the margin of the Yucatan basin appears. The increase in water near the coast increases the coast effect. Thus the curve of apparent resistivity calculated with the model of Figure 3A shows a significant conductive anomaly at T = 100 s, that includes a large negative difference in percentage.

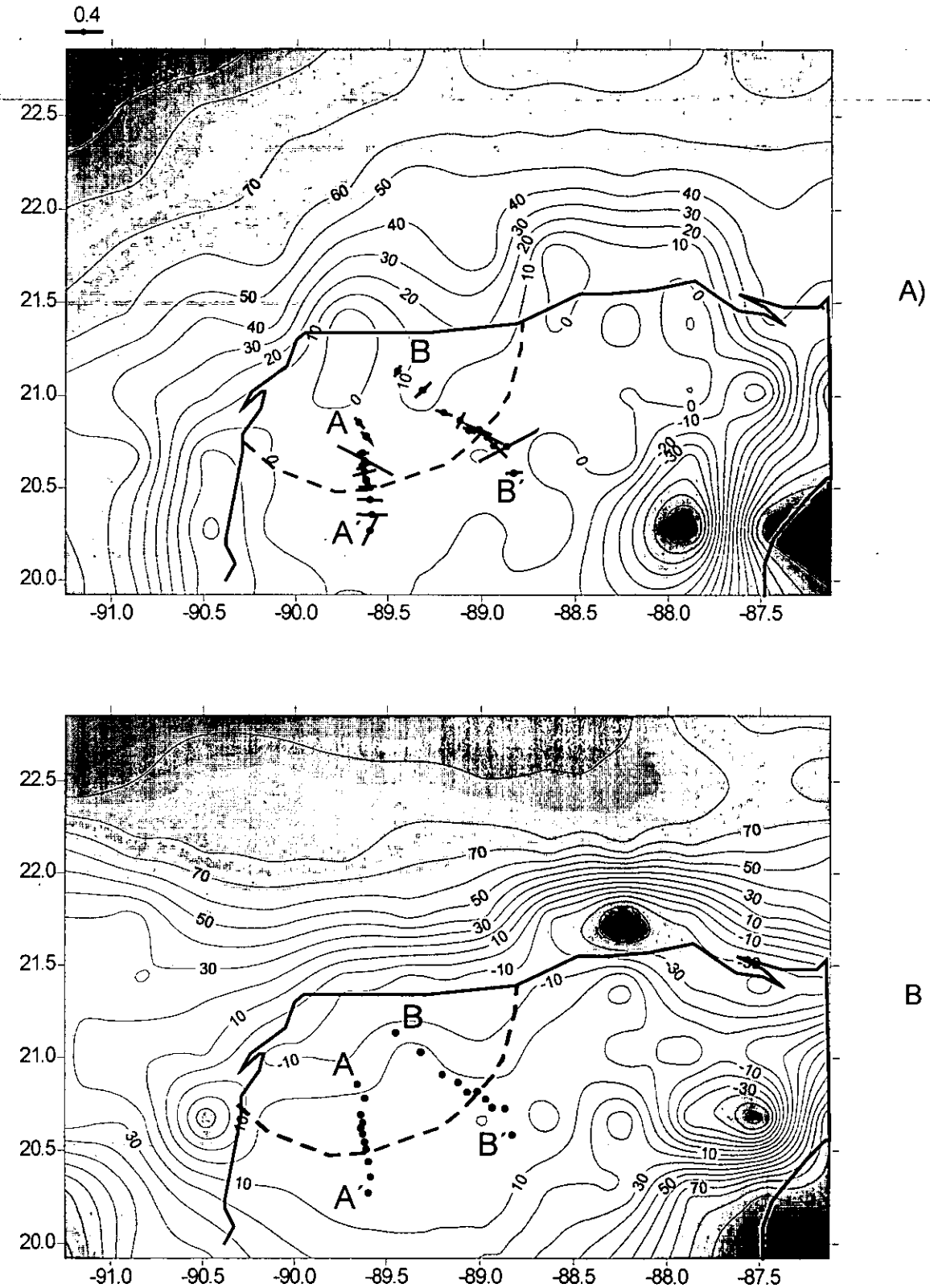


**Figure 7: Maps of coast effect for T = 100 s. A) xy mode, B) yx mode. The values on the maps are given in percent. The approximate location of cenote ring is represented in dash line. The induction arrows are represented in each stations for T = 100 s.**

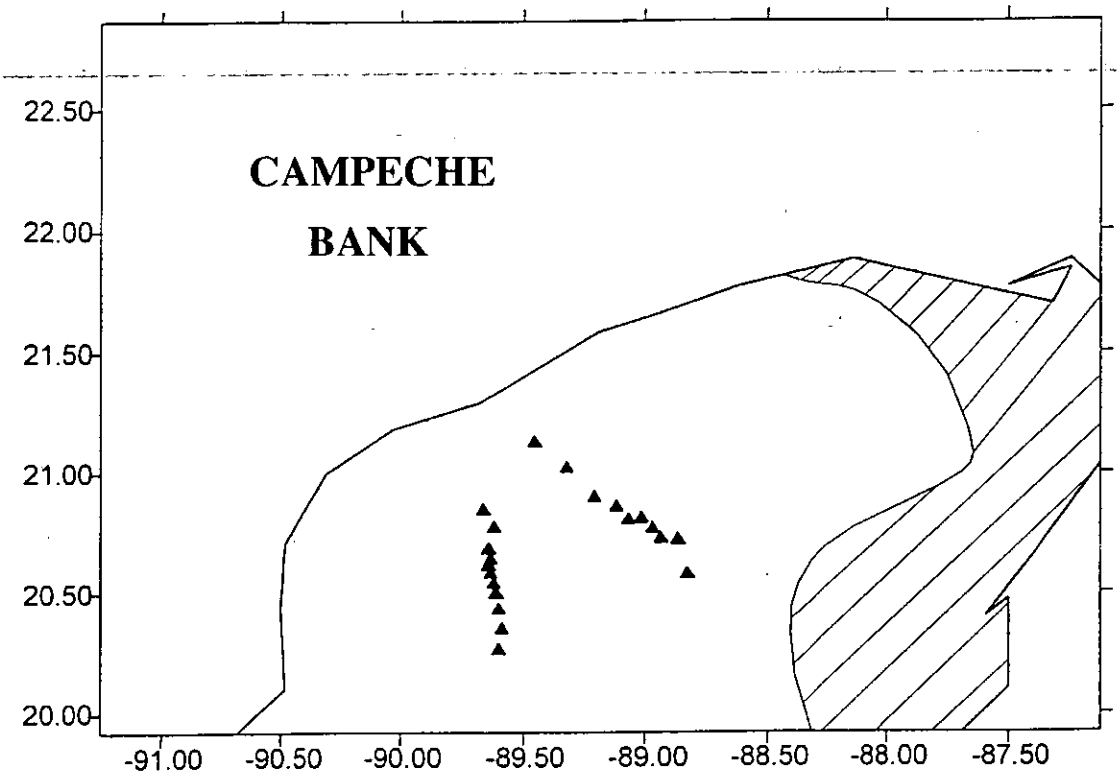


**Figure 8: Map of maximum coast effect for T = 100 s. The zones where the differences between the curves yield by both models are larger than 20 % are marked with diagonal lines.**

The induction arrows were determined at each of the MT stations for T = 100 s. In general, the induction magnitude is less than 0.4, being lower toward the interior of the cenote ring.

Northern Yucatan shows a higher density of fractures outside the cenote ring than inside it (Pilkington et al., 1994). This explains the difficult to establish a predominant way in the discontinuous conductivity body.

In the case of profile BB′, three stations (15, 16 and 17) have magnitudes and strikes that macht with the location of the cenote ring.

The cenote ring coincides with the larger horizontal gravity gradient, as well as with a topographical depression (Connors et al., 1996). The cenote ring is the surface expression of a zone of concentric faults associated with the crater structure.

This is less evident in the profile AA′, which is runs along the gravity depression that extends for more than 100 km south of the cenote ring. Thus there is a more complex structure in the zone where the profile AA′ is located, and therefore an undefined predominant direction is expected in the lateral heterogeneous discontinuities.

For the *yx* mode (Fig. 7B) the results are similar to those in the *xy* mode (Fig. 7A). The percentile differences are similar for the profiles AA′ and BB′, where the coast effect is important they cover a larger area toward the east of Yucatan peninsula. The TM mode is more affected by the coast effect (Vozoff, 1972). In this mode the current lines are normal to the coastline. Our *yx* mode is the TM mode for the eastern and western coastlines of the peninsula, while the *xy* mode is the TM mode for the northern coastline.

The areas of maximum coast effect on the TM mode in Figure 7 are mapped in Figure 8, showing the area of the Yucatan peninsula where MT soundings at periods larger than 100 s should not be carried out. The area of maximum coast effect is shaded. The coast effect increases to the east and northeast of the Yucatan peninsula, becuse of the presence of the margin of the Yucatan basin. The rapid increase of water depth in the Yucatan basin causes the coast effect to increase for higher values of T.

However, in the frequency range of interest (T< 100 s), the coast effect should become still smaller (see Figures 4 and 5), as the smaller area for the cells nearest to the eastern coastline of the Yucatan peninsula suggests.

### 3.7.- Conclusions

All MT stations are located in areas where the coast effect is very low. Our calculations define new suitable areas to carry out further MT measurements without significant coast effect, even for periods larger than 100 s.

The curves of apparent resistivity calculated from models of the Yucatan peninsula with a marine platform, and a simple 1-D resistivity model, were compared, and an insignificant effect of the sea on the MT soundings in the Chicxulub impact crater structure was observed.

A coast effect can only be appreciated in the range of periods of 10 to 1000 s. The anomaly associated with conductive filling of the crater is present mainly in the range of 0.01 to 10 s. The maximum coast effect for the area is found in the period T = 100 s.

A map of maximum coast effect for T= 100 s has been constructed. This map shows the influence of the margin of the Yucatan basin, which creates a zone of maximum coast effect in the eastern and northeastern end of the Yucatan peninsula.

We conclude that the coast effect on MT soundings in the Yucatan peninsula is negligible, and should have no significant effect on the interpretation of geoelectric models for Chicxulub crater.

Reliable MT soundings may be carried out everywhere, except in the marked areas with high coast effect, when MT observations for periods larger than 100 s are required.

**Acknowledgments**

We acknowledge useful comments by three reviewers. Partial economic support for this project has been provided by CONACyT grant G32526-T.

### 3.8.- References

ARZATE J. A., O. DELGADO-RODRÍGUEZ, J. O. CAMPOS-ENRÍQUEZ and J. URRUTIA-FUCUGAUCHI, 2000. Electric structure of the Chicxulub impact basin along two magnetotelluric profiles. Submitted to Can. J. Earth Sci.

BERDICHEVSKY, M. N. and V. I. DMITRIV, 1976. Basic principles of interpretation of magnetotelluric sounding curves. A. Adam (Editor). Geoel. Geoth. Studies. KAPG Geophysical Monograph. Akademiai Kiado. Budapest, 165-221.

CAGNIARD, L., 1953. Basic theory of the magnetotelluric method of geophysical prospecting. Geophysics, **18**, 605-635.

CAMPOS-ENRÍQUEZ, J. O., J. A. ARZATE, J. URRUTIA-FUCUGAUCHI and O. DELGADO-RODRÍGUEZ, 1997. The subsurface structure of the Chicxulub crater (Yucatan, Mexico): Preliminary results of a magnetotelluric study. The Leading Edge. **16**, 1774-1777.

CHEN, J., H. W. DOSSO and M. INGHAM, 1990 Electromagnetic induction in New Zealand: Analogue model and field results. Phys. Earth Plant. Inter., **62**, 257-270.

CONSTABLE, S. C., R. L. PARKER and C. G. CONSTABLE, 1987. Occam's inversion: A practical algorithm for generating smooth models from electromagnetic sounding data. Geophysics, **52**, 289-300.

DELGADO-RODRÍGUEZ, O., J. O. CAMPOS-ENRÍQUEZ, J. URRUTIA-FUCUGAUCHI and J. A. ARZATE, 2000. Occam and Bostick 1-D inversion of magnetotelluric soundings in the Chicxulub impact crater, Yucatan, Mexico. Submitted to Geof. Intern.

DOSSO, H. W. and Z. W. MENG, 1992 The coast effect response in geomagnetic field measurements. Phys. Earth Plant. Inter., **70**, 39-56.

CONNORS, M., A. R. HILDEBRAND, M. PILKINGTON, C. ORTÍZ-ALEMÁN, R. E. CHÁVEZ, J. URRUTIA-FUCUGAUCHI, E. GRANIEL-CASTRO, A. CAMARA-ZI, J. VASQUEZ and J. F. HALPENNY, 1996. Yucatan karst features and the size of Chicxulub crater. Geophys. J. Int., **27**, F11-F14.

ESPÍNDOLA, J. M., M. MENA, M. DE LA FUENTE and J. O. CAMPOS-ENRÍQUEZ, 1995. A model of the Chicxulub impact structure (Yucatan, Mexico) based on its gravity and magnetic signatures. Phys. Earth Plant. Inter., **92**, 271-278.

GOLDBERG, S. and Y. ROTSTEIN, 1982. A simple form of presentation of magnetotelluric data using the Bostick transform. Geophys. Prosp., **30**, 211-216.

HEBERT, D., J. A. WRIGTH, H. W. DOSSO and W. NIENABER, 1983. Comparison of analogue model and field station results for the Newfoundland region. J. Geom. Geoelectr., **35**, 673-682.

HILDEBRAND, A. R., G. T. PENFIELD, D. A. KRING, M. PILKINGTON, A CAMARGO, S. JACOBSEN and W. BOYTON, 1991. Chicxulub crater: A possible Cretaceous/Tertiary boundary impact crater on the Yucatan Peninsula, Mexico. Geology, **19**, 867-871.

HILDEBRAND, A. R., M. PILKINGTON, C. ORTÍZ-ALEMÁN, R. E. CHÁVEZ, J. URRUTIA-FUCUGAUCHI, M. CONNORS, E. GRANIEL, A. CAMARA, J. F. HALPENNY and D. NIEHAUS, 1998. Mapping Chicxulub crater structure with gravity and seismic reflection data. In: Grady, M.M. et al. (Eds.), Meteorites: Flux with Time and Impact Effects, Geol. Soc., London, Sp. Publ., **140**, 155-176.

KELLET, R. L., F. E. M. LILLEY and A. WHITE, 1991. A two-dimensional interpretation of the geomagnetic coast effect of southeast Australia, observed on land and seafloor. Tectonophysics, **192**, 367-382.

MENG, Z., H. W. DOSSO, L. K. LAW, F. W. JONES and V. RAMASWAMY, 1979. An analogue model study of E.M. induction in the North China-Korea coast region. Phys. Earth Planet. Inter., **60**, 25-39.

NIENABER, W., H. W. DOSSO, L. K. LAW, F. W. JONES and V. RAMASWAMY, 1979. An analogue model study of electromagnetic induction in the Vancouver Island region. J. Geomag. Geoelectr., **31**, 115-132.

MORGAN, J., M. WARNER and CHICXULUB WORKING GROUP, 1997. Size and morphology of the Chicxulub impact crater. Nature, **390**, 472-476.

PARKINSON, W. D., 1959. Directions of rapid geomagnetic fluctuations. Geophys. J. R. Astron. Soc., **2**, 1-14.

PARK, S. R., 1985. Distortion of magnetotelluric sounding curves by three-dimensional structures, Geophysics, **50**, 785-797.

PENFIELD, G. T. and Z. A. CAMARGO,1981. Definition of a major igneous zone in the central Yucatan platform with aeromagnetics and gravity. 51st Ann. Internat. Mtg. SEG, Abstract, 37.

PILKINGTON, M., A. R. HILDEBRAND and C. ORTÍZ-ALEMÁN, 1994. Gravity and magnetic field modeling and structure of the Chicxulub crater, Mexico. J. Geophys. Res. **99**, 147-162.

SHARPTON, V. L., K. BURKE, A. CAMARGO, S. A. HALL, D. SCOTT-LEE, L. MARIN, G. SUÁREZ, J. M. QUEZADA, P. D. SPUDIS and J. URRUTIA-FUCUGAUCHI, 1993. Chicxulub multiring impact basin: Size and other characteristics derived from gravity analysis. Science, **261**, 1564-1567.

URRUTIA-FUCUGAUCHI, J., L. MARIN and A. TREJO-GARCIA, 1996. UNAM scientific drilling program of Chicxulub impact structure. Evidence for a 300 kilometer crater diameter. Geophys. Res. Lett., **23**, 1565-1568.

VOZOFF, K., 1972. The magnetotelluric method in the exploration of sedimentary basins. Geophysics, **37**, 98-141.

# 4.- INVERSIÓN 1-D OCCAM Y BOSTICK DE SONDEOS MAGNETOTELÚRICOS EN EL CRÁTER DE IMPACTO DE CHICXULUB, YUCATÁN, MEXICO

## Occam and Bostick 1-D Inversion of Magnetotelluric Soundings in the Chicxulub Impact Crater, Yucatan, Mexico

Omar Delgado-Rodríguez* §, Oscar Campos-Enríquez*, Jaime Urrutia-Fucugauchi* and Jorge A. Arzate**

* Laboratorio de Paleomagnetismo y Geofisica Nuclear, Instituto de Geofísica. Universidad Nacional Autonoma de Mexico, Del. Coyoacán 04510 México D.F., MEXICO

§ Instituto de Geofísica y Astronomía. CITMA. Calle 212 No. 2906, entre 29 y 31, La Lisa. Ciudad de La Habana, CUBA

** Unidad de Investigación en Ciencias de la Tierra, Instituto de Geofisica, Universidad Nacional Autonoma de Mexico, Campus Juriquilla, Querétaro, MEXICO

*Sometido a Geofísica Internacional (anexo 1)*

### 4.1.- Abstract

The subsurface structure of the southeastern sector of the Chicxulub impact crater has been investigated by magnetotelluric (MT) soundings. This study is based on ten MT soundings distributed along a radial 92.5 km long profile oriented SE-NW from the approximate center of the crater at Chicxulub Puerto. In general, MT soundings are one-dimensional, with Tipper magnitudes well below 0.2. Soundings 13,14 and 15 present a slight anisotropy beyond 10 s. They also present the highest Tipper values at frequencies lower than 0.06 Hz. The resistivity behavior for periods above 16 s defines the structural rim of the crater at the cenote ring zone. Resistivities are respectively higher and lower than 150 ohm-m outside and inside the cenote ring. One-dimensional modeling using Bostick and Occam inversion schemes gives similar geoelectrical models, which have been used to investigate on the subsurface structure and electrical conductivity distribution of the crater. Although, MT soundings present one-dimensional characteristics, the differences observed in the $\rho_{xy}$ and $\rho_{yx}$ and results of the Tipper and Skew sections indicate the need for a two-dimensional inversion of the MT soundings.

Key words: Magnetotelluric soundings, 1-D inversion, cenote ring, Chicxulub impact crater

## 4.2.- Resumen

En este estudio se presenta la investigación realizada en el sector sureste del cráter de Chicxulub mediante la aplicación del método de Sondeo Mangetotelúrico (MT). El perfil MT analizado consta de diez sondeos MT distribuídos a lo largo de 92.5 km en la dirección radial SE-NW, tomando como centro el puerto de Chicxulub. En general, los sondeos MT exponen un medio uni-dimensional, con magnitudes de Tipper menores a 0.2. Los sondeos 13, 14 y 15 presentan una ligera anisotropía y los mayores valores de Tipper, para frecuencias inferiores a 0.1 y 0.06 Hz, respectivamente. El comportamiento de la resistividad, en estos sondeos, para períodos mayores a 16 s define el límite estructural del cráter, implicando para la estructura de impacto de Chicxulub un diámetro aproximado de 200 km. Modelos unidimensionales, utilizando los esquemas de inversión de Bostick y Occam, fueron utlizados para investigar la estructura del cráter. Resisitividades superiores e inferiores a 150 ohm-m caracterizan el medio dentro y fuera del anillo de cenotes, respectivamente. Aunque los sondeos MT presentan, en general, un comportamiento uni-dimensional, las diferencias observadas en los modelos $\rho_{xy}$ y $\rho_{yx}$, y los resultados de las secciones de Tipper y Skew indican la necesidad de realizar una inversion bi-dimensional de los sondeos MT pertenecientes a este perfil.

Palabras claves: Sondeo magnetotelúrico, inversión 1-D, anillo de cenotes, cráter de impacto de Chicxulub.

## 4.3.- Introduction

For more than a decade many geological and geophysical studies have been carried out to investigate on the subsurface structure of the Chicxulub impact crater, which is located at the northwestern sector of the Yucatan peninsula (Fig. 1). Penfield and Camargo (1981) first proposed the presence of an impact crater buried beneath a thick cover of Tertiary carbonate sediments, based on geophysical studies and oil exploration wells by Petroleos Mexicanos (Pemex). However, it still took several years to link the Chicxulub crater with the events of the Cretaceous/Tertiary (K/T) boundary (Hildebrand et al., 1991; Sharpton et al., 1992). Following the study by Alvarez et al. (1980) on the geochemical anomaly at the K/T boundary sediments and the proposal that a major impact occurred at the end of the Mesozoic that was associated with the extinction of biota, a world-wide search was lunched to locate the impact

site. Several candidate craters were considered before the search concentrated in the Gulf of Mexico and Caribbean (Bourgois et al., 1988).

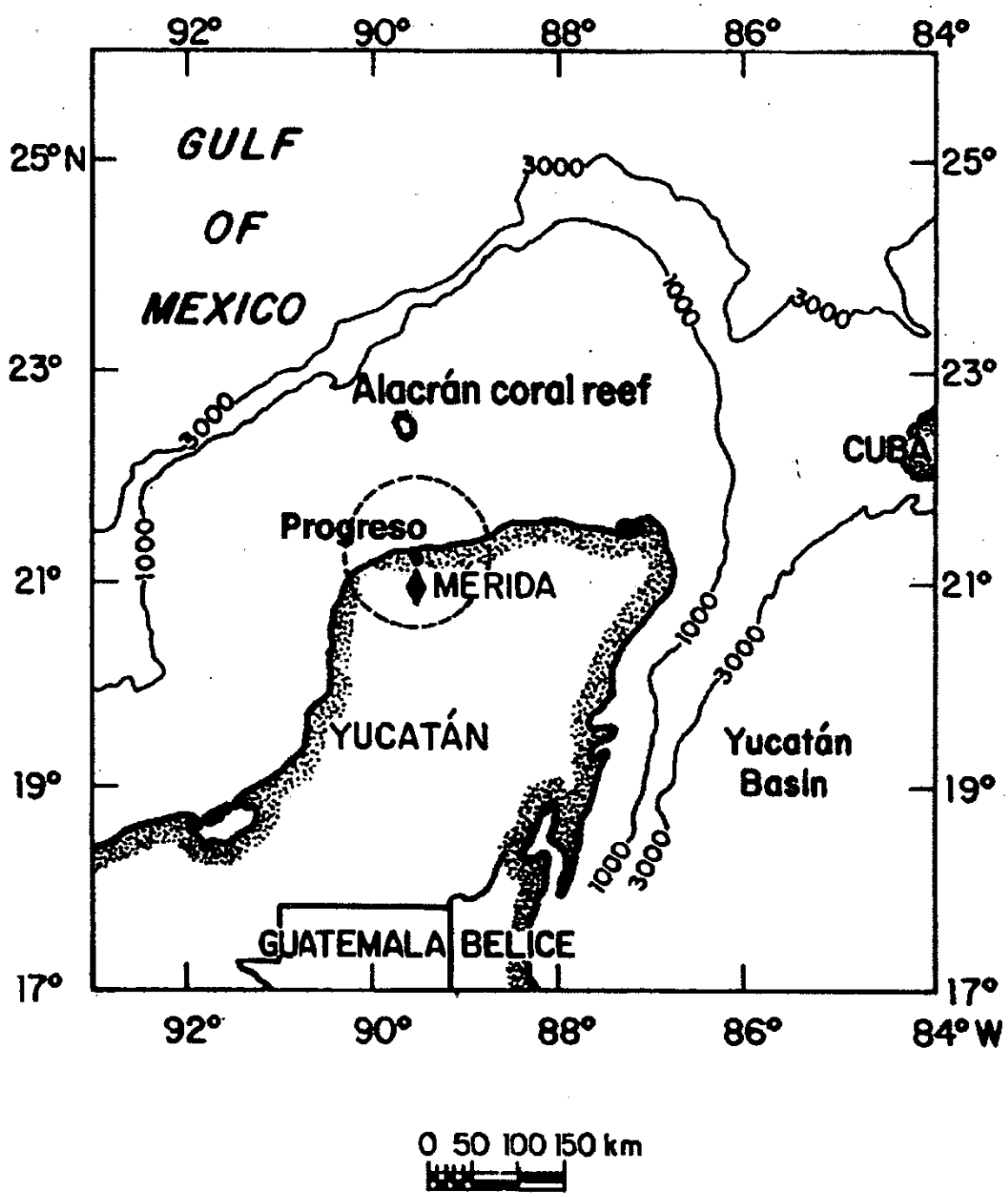


**Figure 1: Study area. The concentric circle indicate the limit proposed for the impact structure. Progreso town located in the center.**

Initial studies of the structure were mainly based on the gravity and magnetic anomaly data and on available core samples from the Pemex drilling program. Studies proposed different models for the crater size and nature, with crater diameters ranging from 180 km to 300 km and complex crater models with a peak-ring or a multi-ring structure (e.g., Hildebrand et al., 1991; Sharpton et al., 1993; Pilkington et al., 1994; Espindola et al., 1995; Hildebrand et al., 1998). The drilling program by UNAM, which included eigth boreholes located in the southern sector of the crater have recently made available new material from the impact breccias and Tertiary carbonates (Urrutia-Fucugauchi et al., 1996). Nearly complete lithological columns are now available for this sector of the crater, which permits to develop detailed geometrical models of the impact breccia distribution (Rebolledo-Vieyra et al., 2000). Recent marine seismic deep-reflection profiles and onshore wide-angle seismic profiles across the crater have supported a 180-210 km multi-ring impact basin (Morgan et al., 1997). Further analyses of the seismic data have resulted in refinements of the crater structure and the size and nature of the crater inner, peak and outer rings (e.g., Morgan and Warner, 1999; Snyder et al., 1999). High resolution geophysical data and new drilling with high recovery rates are required to improve our understanding of the crater and to test proposed models.

Several geophysical studies are being planned or conducted in the offshore and on-shore zones of the crater; they include for instance detailed new marine gravity and comprehensive aeromagnetic and aerogravity surveys. Similarly, new marine and land drilling projects have been designed and are being conducted. The Chicxulub scientific drilling project (CSDP) has selected as initial target zone the sector just SE of the Yucatan-6 Pemex well, inside the cenote ring (Figure 2). For the conduction of the CSDP, additional detailed studies of this sector of the crater with high resolution geophysical surveys and shallow drilling are being required. In this paper we present the results of the modeling and initial interpretation of a magnetotelluric (MT) study based on one-dimensional (1-D) inversion of ten MT soundings distributed along a SE-NW 92.5 km long profile (B-B´ profile) that crosses perpendiculy the cenote ring (Figure 2). We use Bostick (Bostick, 1977) and Occam (Constable et al., 1987) inversion algorithms for modeling of the MT data. The MT sounding profile is located to the east of the CSDP target zone, and provides new valuable data on the crater structure inside and outside of the cenote ring.

## 4.4.- Magnetotelluric Survey of the Chicxulub Crater

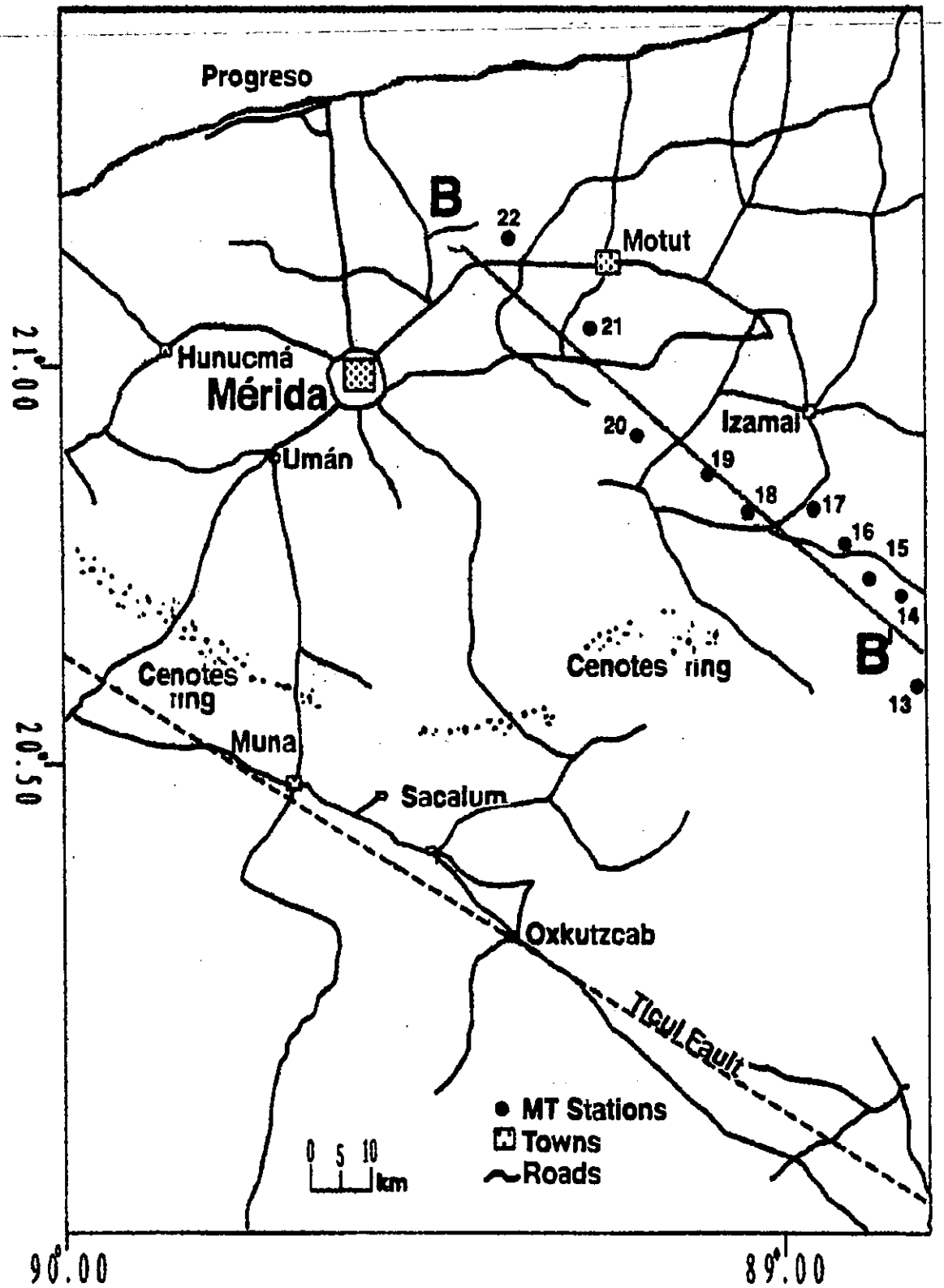


Figure 2: Location of the magnetotelluric stations in the study area.

Gravity, magnetic and seismic surveys have been widely used to study impact structures (Pilkington and Grieve, 1992). Geoelectrical methods have also been applied to investigate impact craters, as part of geophysical survey programs. Electrical resistivity data have proved particularly useful in mapping the extent of authigenic brecciation (Henkel, 1992). A range of electromagnetic methods has been developed for shallow and deep crustal investigations, and are being widely applied in a variety of geophysical problems. Among them, a particularly powerful method is the MT sounding method (Cagniard, 1953).

We recorded the three components hx , hy , and hz of the magnetic field and the horizontal components ex and ey of the electric field, in form of time series. In the conventional reference frame used in MT work, **x** points to the geomagnetic north, **y** points to the east, and **z** points vertically downwards.

With the data in the frequency domain, cross-spectra are calculated, which allow us to determine the impedance tensor (Z), which conveys the information about the subsurface (Vozoff, 1989).

In 1997 a magnetotelluric study comprising 22 MT soundings was conducted in the central and southern region of the impact crater (Campos-Enríquez et al., 1997). In this study, ten magnetotelluric soundings were obtained along a SE-NW 92.5 km long profile B-B´, crossing perpendicular to the zone where the 200-210 km limit of the crater structure is assumed to be located, which is marked by the cenote ring (Figure 2). This MT profile is located to the SE of Merida City. The interpretation of profile A-A´ will be reported elsewhere.

For the MT soundings, we used two V-5 MT acquisition instruments operating on a remote basis. MT observations cover the range between 384 Hz and a period of 1820 s.

The profile is located relatively far from the coast, to reduce its effect on the MT observations. Further, a recent quantitative evaluation of the coast effect on MT soundings in the Yucatan peninsula demonstrates that the effect is negligible in the crater region (Delgado et al., submitted).

The radial distance of the MT soundings shown in the sections were calculated taking the center of the impact structure on the Chicxulub puerto, located approximately 7 km to the E of Puerto Progreso (Figure 2).

A preliminary evaluation of MT data in the crater was presented in Campos-Enriquez et al. (1997). This was based on a Bostick inversion of the *xy* apparent resistivity and phases curves.

High resistivities were observed beneath the second group of soundings south of the cenote ring. Inside the cenote ring, resistivity decreased constantly and smoothly up to sounding 20; it then remains relatively constant with respect to depth; and then at the extreme of the profile it presents higher values. The high values towards the crater center beneath sounding 22 may correlate with the central structural uplift inferred from the gravity and magnetic anomalies.

In this study, each pair of curves $\rho_{axy}(\omega)$, $\phi_{xy}(\omega)$ and each pair of curves $\rho_{ayx}(\omega)$, $\phi_{yx}(\omega)$ will be interpreted in order to finally calculate, for each MT sounding, two independent geoelectric models.

For the interpretation of the observed MT data, the Bostick (Bostick, 1977) and Occam (Constable et al., 1987) inversion schemes have been used in this study. Here we present our data and results.

**4.5.- Data analysis**

Figure 3 shows the variance of the phase and resistivity observed values. Low variance values (SD < 5%) are observed for the electrical resistivity (Figures 3a and 3b), except for MT sounding 21, which presents values greater than 45% (data no useful for frequencies below 1Hz).

Figures 3c and 3d show the variance of the observed phases. Again the greatest values are observed around sounding 21. Besides, high variance values (SD > 45%) are observed for MT soundings 16, 18 and 20, contrasting with the variance of the corresponding electrical resistivity (Figures 3a and 3b). In general, these variance sections could indicate that phases are more sensitive to noise than the resistivity, mainly for lower frequencies.

Due to high variance values in the MT sounding 21, in the resistivity as well as in the phase, we decided not to take into account the observed values in this sounding for frequencies below 1 Hz. MT Sounding 21 will only be used to study the shallow part of the area.

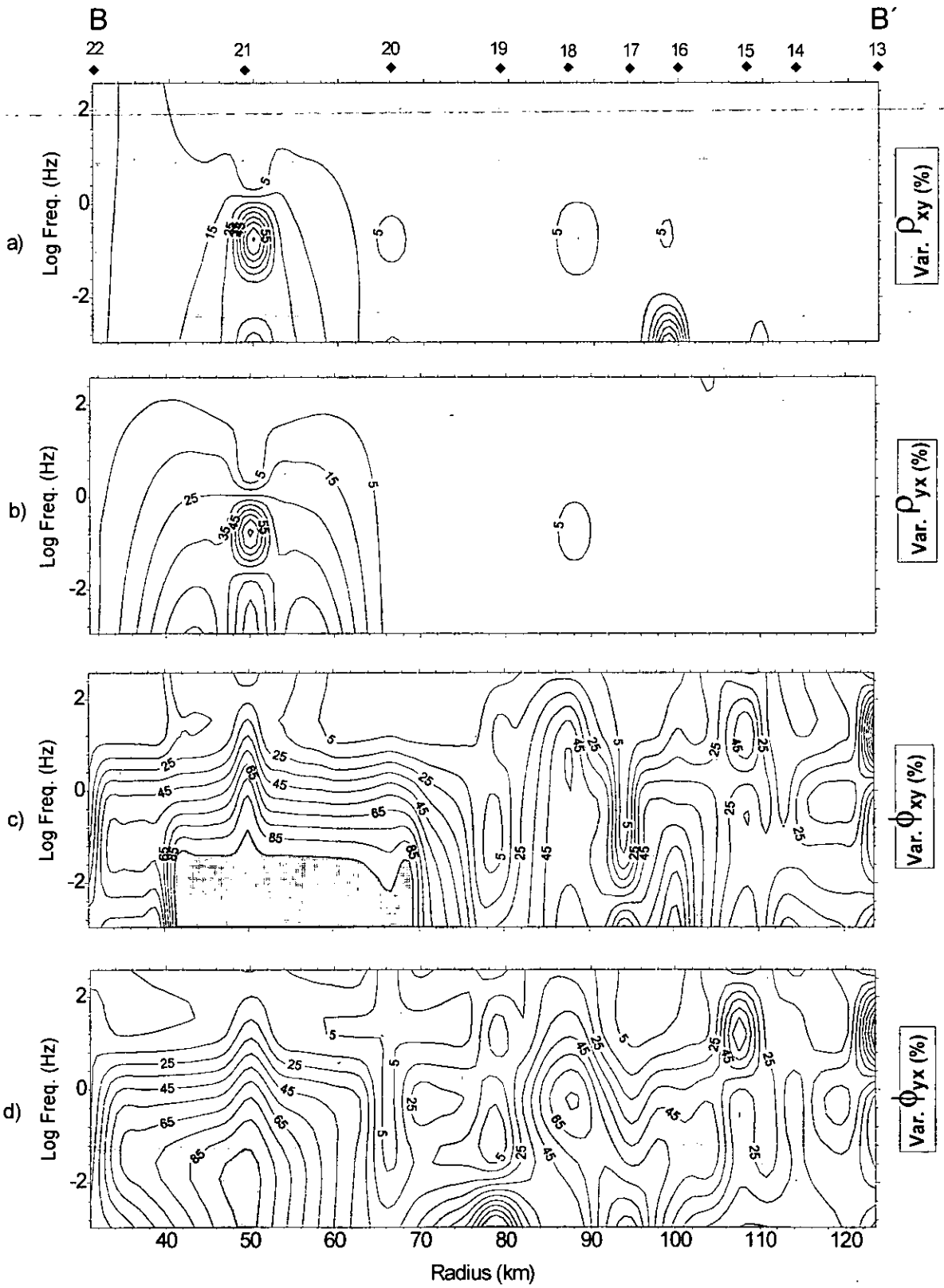


**Figure 3: Variance sections in %. a) apparent resisitivity xy, b) apparent resistivity yx, c) Phase xy and d) Phase yx.**

Figure 4 shows the apparent resistivity and phase sections. A good correspondence between the values of $\rho_{axy}(\omega)$ and $\rho_{ayx}(\omega)$ (Figures 4a and 4b) is observed in almost all the stations, except in the MT sounding 20 where for frequencies less than 0.4 Hz an increases is observed in the values of $\rho_{axy}(\omega)$ (Figure 4a), which is not present in $\rho_{ayx}$ section (Figure 4b).

In the case of the MT soundings 13, 14 and 15, the associated increase in the values of apparent resistivity could indicate the presence of the outer ring. The above mentioned soundings are located to south of the cenotes ring (Figure 2).

Figure 6 shows the Bouguer anomaly map with the location of the MT soundings. One could observe three characteristic zones where lies the MT profile:

Zone I of maximum gravity values. On this zone are located MT soundings 13, 14 and 15. Since this zone is outside of the cenotes ring the prevalence of little or not fractured carbonated rocks is expected.

Zone II of minimal gravity values. On this zone were carried out the MT soundings 18, 19, 20, and 21. It is expected the prevalence of very fractured rocks (breccias of several sizes), those constituting the main component of the crater filling.

Between the I and II zones is observed a high gravity gradient. In this transition region are the cenotes ring and the MT soundings 16 and 17.

Zone III associated with the denominated central maximum zone. This gravity maximum awards to the existence of a central structural high typical of the complex impact craters. The existence impact melt sheet and melt breccia contribute to the increment of the gravity values. On this zone, no MT soundings carried out. Sounding 21 is on the transition zone (high gravity gradient) between the II and III zones.

The increment in the magnitude of the apparent resistivity values observed in MT sounding 20 could indicate a change in the characteristics of the section not corresponding to a 1-D medium.

The phases sections (Figures 4c and 4d) also present a great similarity, except at the same portions as already mentioned.

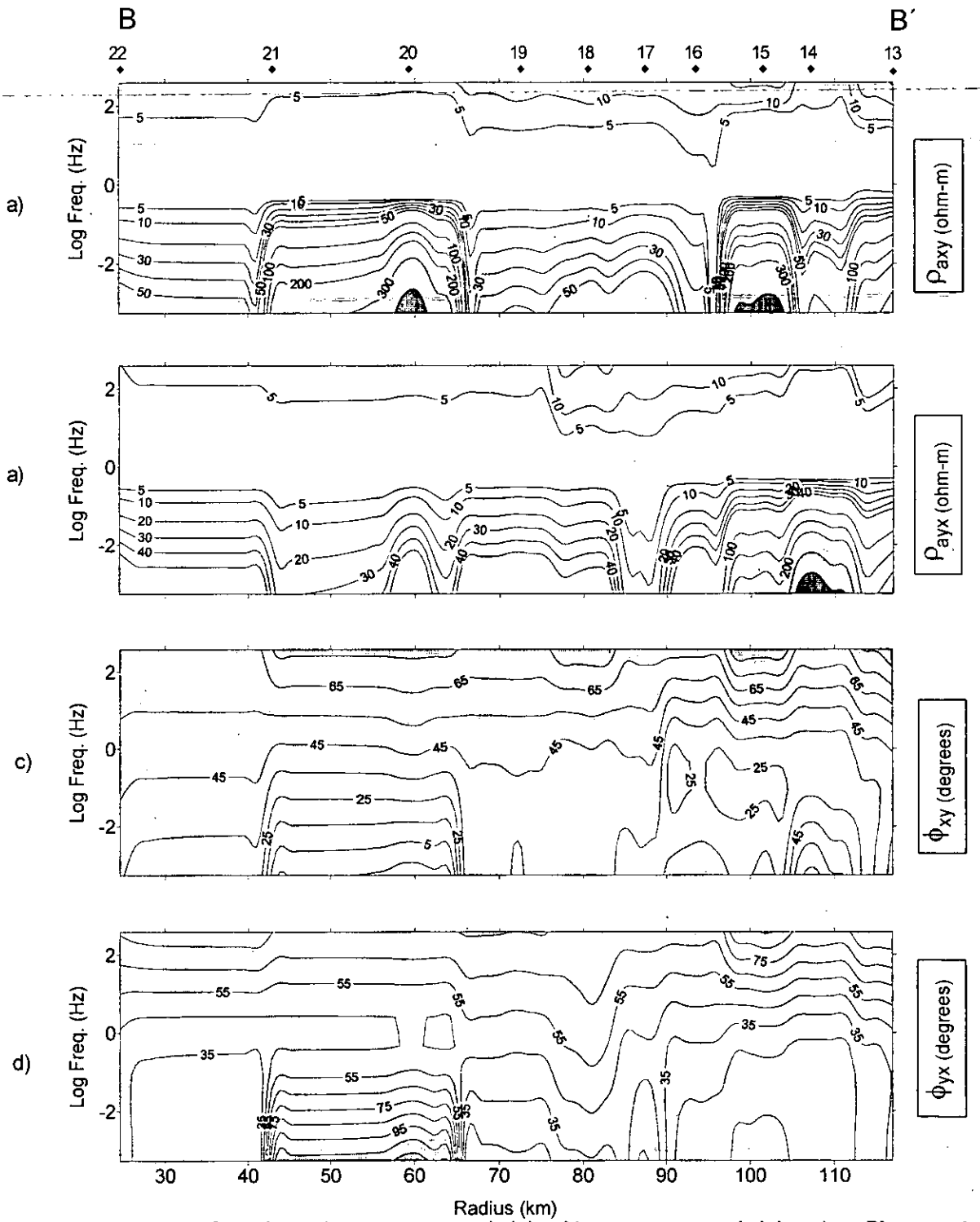


**Figure 4: Observed pseudosections. a) xy apparent resistivity, b) yx apparent resistivity, c) xy Phase and d) yx Phase.**

Tipper (T) and Skew (S) sections (Vozoff, 1989) were elaborated with the objective of analyzing the distortion degree present in the measurements (Figure 5).

Low values of Tipper ($T < 0.2$) are indicative of the presence of a 1-D structure, while higher values ($T \geq 0.2$) indicate that effects of 2-D or 3-D structures are present in the analyzed section.

On the other hand, the increment in the magnitude of the Skew ($k \geq 0.4$) shows the presence of 3-D structures in the studied medium.

In Figure 5a, the highest values of the Tipper ($Tip > 0.4$) are observed in the MT soundings 13, 14 and 15 for frequencies below 0.06 Hz.

According to the results obtained from the analysis of apparent resistivities and phases sections, this increasment in Tipper's magnitude could indicate the existence of a local strike determined by the outer ring of the impact structure. An altogether analysis of the Skew offers information about the possible presence of 3-D structures in the studied media. Figure 5b shows a 3-D distortion at MT sounding 16 for frequencies less than 0.3 Hz, as well as for the MT sounding 20 for frequencies less than 0.01 Hz.

So we can conclude for MT soundings 13, 14 and 15 that, according to their location and their $\rho_a(\omega)$ behavior for periods larger than 16 s, define a local strike.

The behavior of MT sounding 20 at lower frequencies could be due to the existence of a geoelectric contrast that yield rise to a 3-D distortion. This fact would explain at this site a strike, there is not define with clarity.

Nevertheless the analysis of apparent resistivity, phase, Tipper and Skew sections indicate the prevalence of a 1-D behavior for the studied medium, and justifies the use of 1-D inversion algorithms such as Bostick and Occam with the objective of establishing a preliminary 1-D geoelectric model for the impact structure.

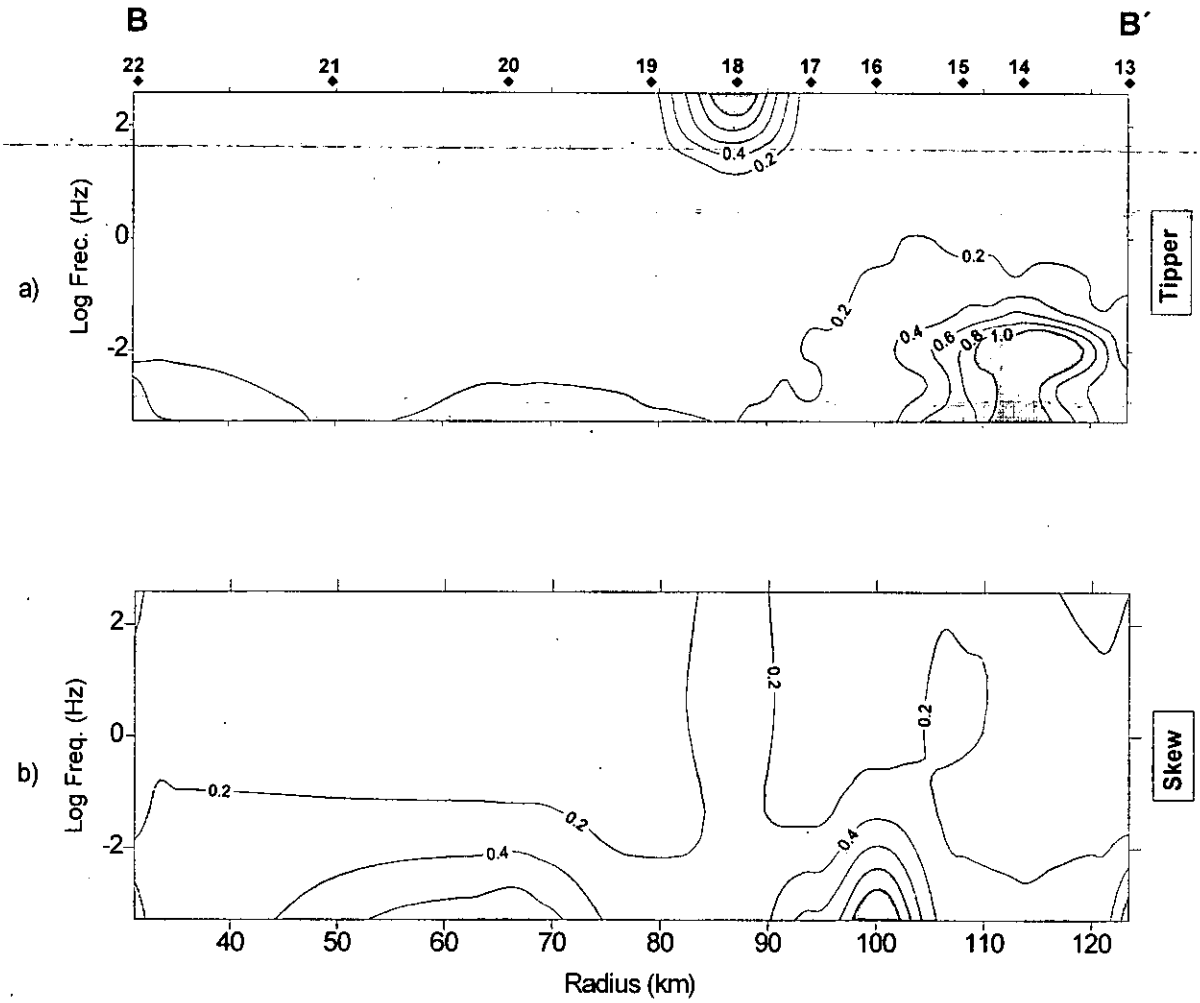


**Figure 5: Distortion analysis. a) Tipper section, b) Skew section.**

4.5.1.- Bostick's inversion

As a first step we conducted a Bostick inversion. This heuristic inversion scheme offers a continuous or semi-continuous resistivity distribution versus depth (Bostick, 1977). In this study, we estimated the resistivity is estimated by means of the apparent resistivity and the observed phase according to the relations:

$$\rho(z) = \rho_a(\omega)(\frac{\pi}{2\phi(\omega)} - 1)$$

$$z = (\frac{\rho_a(\omega)}{\mu\omega})^{\frac{1}{2}}$$

The values of depths, z, are the nominal depths corresponding to the skin depth of a half-space of apparent resistivity $\rho_a$ for a given frequency $\omega$.

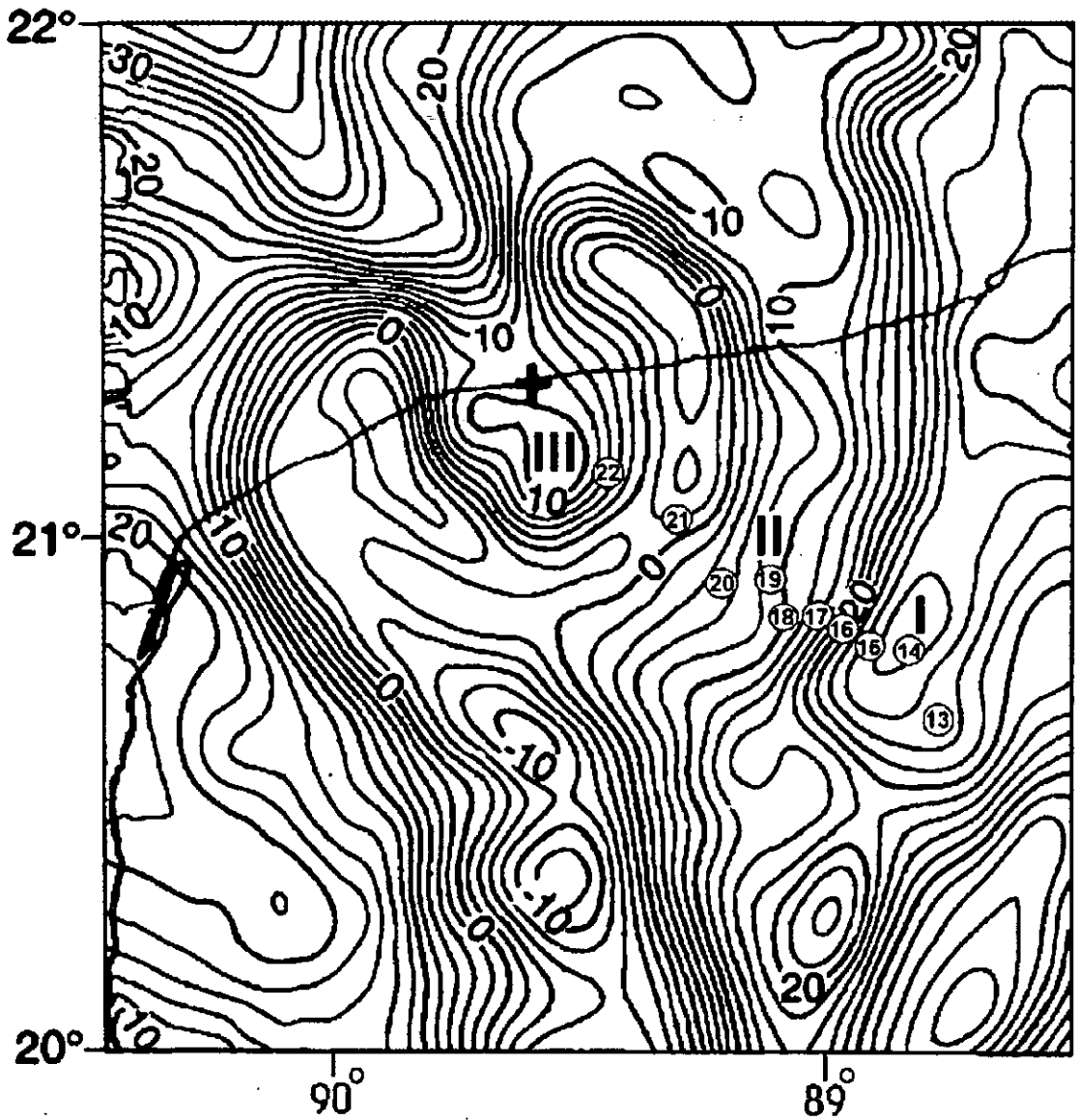


**Figure 6: Bouguer anomaly map. The values on the map are given in mgals. The location of MT soundings is indicated by encircled number.**

In Figures 7a and 7b, the $\rho_{xy}$ and $\rho_{yx}$ models resulting from the Bostick inversion are shown. Similar general characteristics are observed in both models. The prevalence of resistivity values $\rho(z) > 150$ ohm-m in the MT sounding 13, 14 and 15 (zone I, Figure 6),

indicate the basin limit, while resistivity values less of 150 ohm-m differentiate the filling of the crater for the rest of the MT soundings (zone II, Figure 6) (Campos-Enríquez et al., 1997).

The $\rho_{yx}$ section shows the outer ring between MT soundings 15 and 16 much more sharply. Also, a zone of minimum values of $\rho_{yx}(z)$ is observed from soundings 16 to 18, what is not clearly defined in $\rho_{xy}$ model.

This zone coincides with the external ring of minimum gravity values given in the Bouguer anomalies map (transition between I and II zones, Figure 6). Therefore, this result supports the existence of a structural feature around sounding 16, with a possible maximum diameter for the crater of approximately 200 km.

So both in the $\rho_{xy}$ model as well as in the $\rho_{yx}$, an increment with depth of the resistivity is observed in the vicinity of the MT sounding 22. If we keep in mind the vicinity of this station to the central maximum of Bouguer anomaly (zone III, Figure 6) and postulated central structural high, then one could suppose the influence from deeper and denser and less fractured materials conforming the base of the central structural high.

To minimize the effects of the lateral variations of the conductivity in the studied medium, it is convenient, once analyzed the $\rho_{xy}$ and $\rho_{yx}$ sections, to carry out an inversion of the effective values of the apparent resistivity and phase (Berdichevsky and Dmitriv, 1976). The effective impedance is determined according to:

$$Z_{eff} = \sqrt{(Z_{xx}Z_{yy}) - (Z_{xy}Z_{yx})}$$

Once $Z_{eff}$ is calculated, $\rho_{eff}(\omega)$ and $\phi_{eff}(\omega)$ are determined. Figure 7c shows the results of the Bostick inversion for $\rho_{eff}(\omega)$ and $\phi_{eff}(\omega)$. A good correspondence with the results obtained in models 7a and 7b supports the predominant 1-D character of the studied medium.

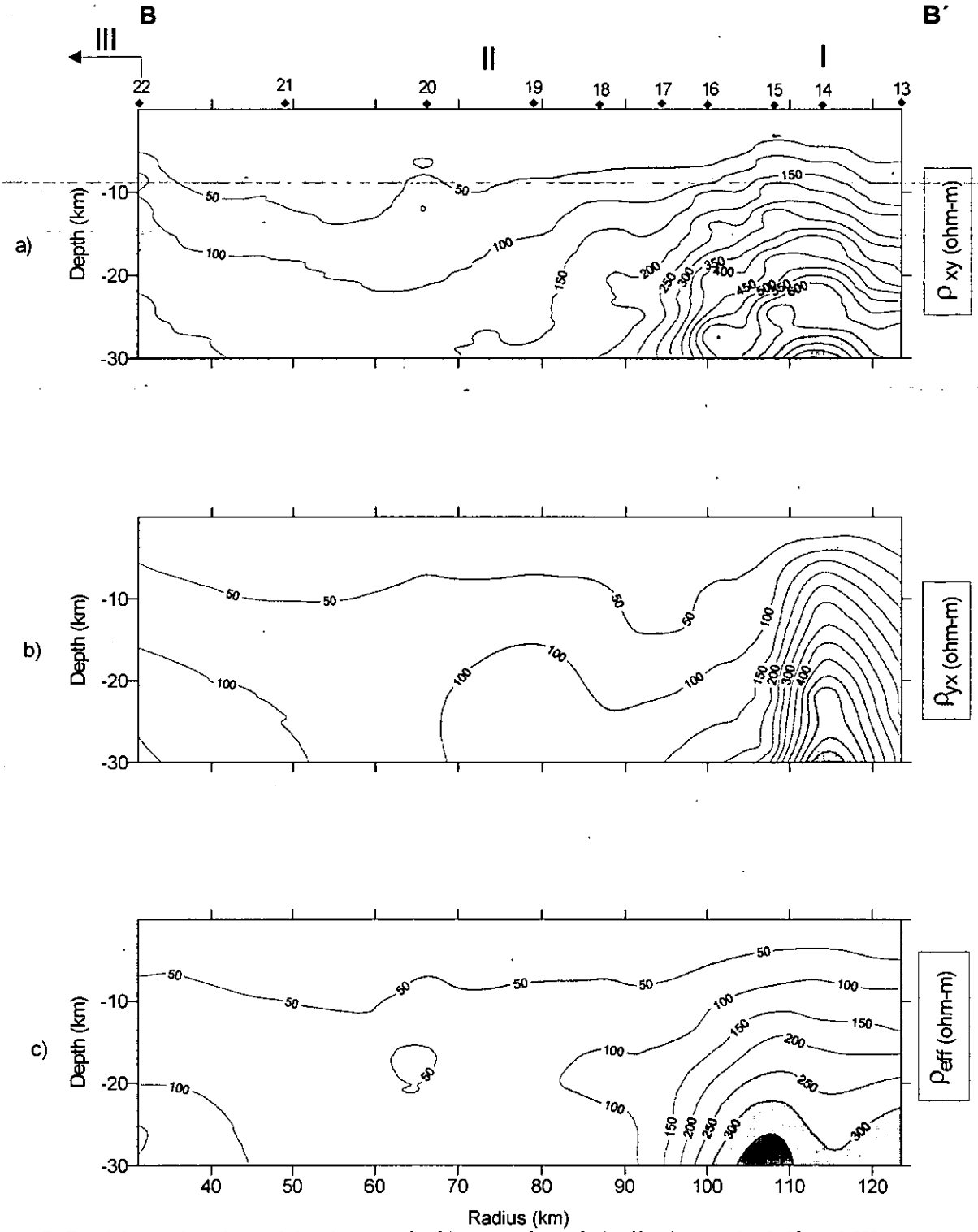


**Figure 7: Bostick geoelectric models. a) xy mode, b) yx mode and c) effective mode. I, II and III: gravity characteristic zones.**

4.5.2.- Occam's inversion

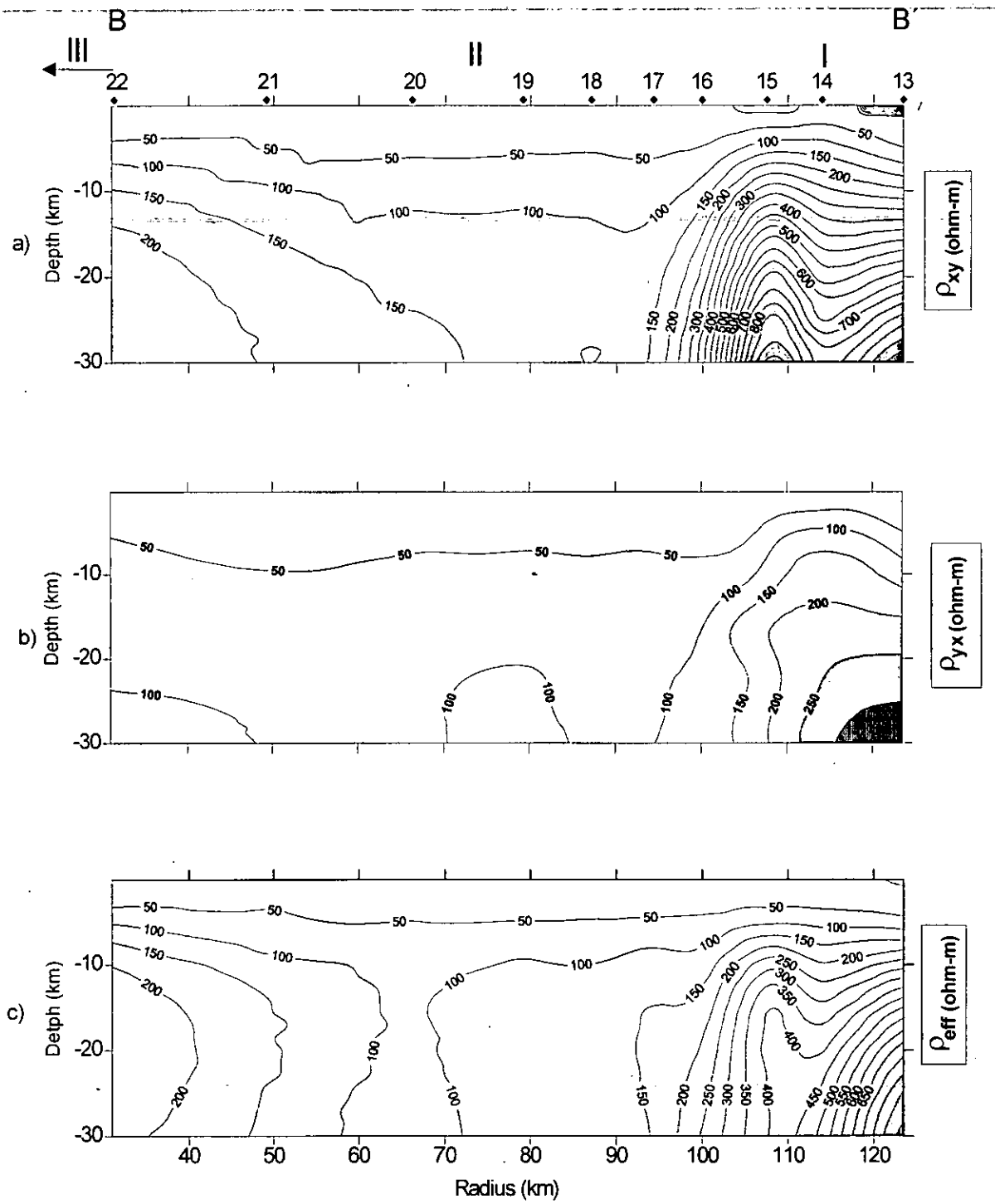


**Figure 8: Occam geoelectric models. a) xy mode, b) yx mode and c) effective mode. I, II and III: gravity characteristic zones.**

Application of the Occam's algorithm (Constable et al., 1987) enables one to obtain a simple model containing the essential characteristics present in all possible models fitting the field data. This method of inversion assists in dealing with ambiguity inherent in geophysical modeling. That is, a great number of geoelectric models could be match the observed data, some of which may be very complex.

In this way, the calculation of a model including no details guarantees in trying to achieve a better fit between small portions of the calculated and observed curve of $\rho(\omega)$, $\phi(\omega)$, the complexity of the obtained model increases and the results are not often reliable. That is to say, the obtained model could be as complex as the real medium, but never more complex than the latter.

The algorithm departs from a half-space and produces a multiestratified medium. The resistivities varies until it is achieved an adequate fit between the field curves and the calculated ones on the basis of a simple model.

The concept of roughness (or inverse of softness) of the considered model assit in obtaining the simplest model, and is related to the first and the second derivative of the medium electric resistivity of medium in relation to the depth according to:

$$R_1 = \int (dm/dz)^2 \, dz$$

$$R_2 = \int (d^2m/dz^2)^2 \, dz$$

where m (z): resistivity or log resistivity

z: depth

$R_1$ and $R_2$: roughness functions.

The strategy is to attain a model that minimizes $R_1$ and $R_2$.

Figure 8 shows the geoelectric sections obtained by stitching together the corresponding 1-D models resulting from Occam inversion.

The models presented in the Figures 8a, 8b and 8c are very similar to those given in Figures 7a, 7b and 7c supporting the already obtained models.

So, independently of the prevalence of the 1-D character of the studied medium, the differences between the $\rho_{xy}$ and $\rho_{yx}$ models (Figures 7 and 8), as well as the results of the analysis of Tipper and Skew sections (Figure 5), indicate the necessity to carry out a 2-D inversion of the ten MT soundings.

A 2-D model will permit to evaluate the structural model for the crater, particularly for the zone between soundings 13 and 16, Figures 7 and 8, where high values of Tipper and Skew (Figure 5) indicate a more complex structure. It will also help to improved the model between soundings 20 to 22 (Figures 7 and 8), where we observe an increase of resistivity with depth.

### 4.6.- Conclusions

One-dimensional inversion of the ten MT soundings performed in the Yucatan peninsula was carried out. We used the Bostick and Occam inversion schemes. A correspondence between both results is noticed. The established geoelectric sections show a structural limit for the impact structure around sounding 16, and indicate a diameter of approximately 200 km for this structure.

High resistivity values ($\rho > 150$ ohm-m) in the soundings located outside of cenotes ring contrasts with lower resistivity values ($\rho < 150$ ohm-m) modeled in the rest of soundings located inside the cenotes ring.

This electric characteristic corresponds to the prevalence of little or not fractured rocks outside of cenotes ring (beyond 100 km radial distance) and to considerable thickness of highly fractured and porous material that constitutes the impact structure filling.

A good correlation between the behavior of the sub-surface electric resistivity distribution and Bouguer anomaly field is observed. The gravity highs are associated with little fractured and resistive rocks, while gravity lows zones coincides with the presence of increased thickness of conductive and fractured filling.

One could observe the prevalence of a 1-D character for the studied medium. Similar $\rho_{axy}(\omega)$, $\rho_{ayx}(\omega)$, $\rho_{xy}(z)$, $\rho_{yx}(z)$ and $\rho_{eff}(z)$ sections confirm this result.

An analysis of the distortion degree of the magnetotelluric data of ten MT soundings was carried out based in the values calculated of the Tipper and Skew. This analysis indicates the need to conduct a 2-D inversion.

**Acknowledgments**

We want to acknowledge the valuable help in the field work campaign of Marino Pareja and Lener Sequeira. Funds were provided by grants 32434-T and G32526-T of the Consejo Nacional de Ciencia y Tecnología (CONACYT).

**4.7.- References**

ALVAREZ, L.W., W. ALVAREZ, F. ASARO and H. MICHEL, 1980. Extraterrestrial cause for the Cretaceous/Tertiary extinction. Science, 208, 1095-1108.

BERDICHEVSKY, M. N. and V. I. DMITRIV, 1976. Basic principles of interpretation of magnetotelluric sounding curves. A. Adam (Editor). Geoel. Geoth. Studies. KAPG Geophysycal Monograph. Akademiai Kiado. Budapest, 165-221.

BOSTICK, F. X., 1977. A simple almost exact method of magnetotelluric analysis, in Ward, S., Ed., Workshop of Electrical Methods in Geothermal Exploration, Univ. of Utah Res. Inst., U. S. Geol. Surv. Contract 14-08-0001-g-359.

BOURGEOIS, J., T. A. HANSEN, P. L. WILBERG and E. G. KAUFFMAN, 1988. A tsunami deposit at the Cretaceous-Tertiary boundary. Science, 241, 567-570.

CAGNIARD, L., 1953. Basic theory of the magnetotelluric method of geophysical prospecting. Geophysics, 18, 605-635.

CAMPOS-ENRÍQUEZ, J. O., J. A. ARZATE, J. URRUTIA-FUCUGAUCHI and O. DELGADO-RODRÍGUEZ, 1997. The subsurface structure of the Chicxulub crater (Yucatan, Mexico): Preliminary results of a magnetotelluric study. The Leading Edge, 16, 1774-1777.

CONSTABLE, S. C., R. L. PARKER and C. G. CONSTABLE, 1987. Occam´s inversion: A practical algorithm for generating smooth models from electromagnetic sounding data. Geophysics, 52, 289-300.

DELGADO-RODRÍGUEZ, O., J. URRUTIA-FUCUGAUCHI, J. A. ARZATE and J. O. CAMPOS-ENRÍQUEZ. Coast effect in magnetotelluric soundings on the Yucatan peninsula, Mexico. Submitted to Geofísica Internacional.

ESPÍNDOLA, J. M., M. MENA, M. DE LA FUENTE and J. O. CAMPOS-ENRÍQUEZ, 1995. A model of the Chicxulub impact structure (Yucatan, Mexico) based on its gravity and magnetic signatures. Phys. Earth Plant. Inter., 92, 271-278.

HENKEL, H., 1992. Geophysical aspects of meteorite impact craters in eroded shield environment, with special emphasis on electrical resistivity. Tectonophysics, 216, 63-89.

HILDEBRAND, A. R., G. T. PENFIELD, D. A. KRING, M. PILKINGTON, A CAMARGO, S. JACOBSEN and W. BOYTON, 1991. Chicxulub crater: A possible Cretaceous/Tertiary boundary impact crater on the Yucatan Peninsula, Mexico. Geology, 19, 867-871.

HILDEBRAND, A. R., M. PILKINGTON, C. ORTÍZ-ALEMÁN, R. E. CHÁVEZ, J. URRUTIA-FUCUGAUCHI, M. CONNORS, E. GRANIEL, A. CAMARA, J. F. HALPENNY and D. NIEHAUS, 1998. Mapping Chicxulub crater structure with gravity and seismic reflection data. In: Grady, M.M. et al. (Eds.), Meteorites: Flux with Time and Impact Effects, Geol. Soc., London, Sp. Publ., 140, 155-176.

MORGAN, J. and M. WARNER,1999. Morphology of the Chicxulub impact: Peak-ring crater or multi-ring basin? In: Dressler, B.O. and Sharpton, V.L. (Eds.), Large Meteorite Impacts and Planetary Evolution, Geol. Soc. Am. Sp. Paper, 339, 281-290.

MORGAN, J., M. WARNER and CHICXULUB WORKING GROUP, 1997. Size and morphology of the Chicxulub impact crater. Nature, 390, 472-476.

PENFIELD, G. T. and Z. A. CAMARGO,1981. Definition of a major igneos zone in the central Yucatan platform with aeromagnetics and gravity. 51st Ann. Internat. Mtg. SEG, Abstract,. 37.

PILKINGTON, M. and R. GRIEVE, 1992. The geophysical signature of terrestrial impact craters. Rev. Geophys., 30, 161-181.

PILKINGTON, M., A. R. HILDEBRAND and C. ORTÍZ-ALEMÁN, 1994. Gravity and magnetic field modeling and structure of the Chicxulub crater, Mexico. Journal Geophys. Resear. 99, 147-162.

REBOLLEDO-VIEYRA, M., J. URRUTIA-FUCUGAUCHI, L. MARIN, A. TREJO-GARCÍA, V. L. SHARPTON and A. M. SOLER-ARECHALDE, 2000. UNAM scientific shallow drilling program of the Chicxulub impact crater. Int. Geol. Rev.,

SHARPTON, V. L., G. B. DALRYMPLE, L. MARIN, B. C. RYDER, B. C. SCHUARAYTZ and J. URRUTIA-FUCUGAUCHI, 1992. New links between the Chicxulub impact structure and the Cretaceous/Tertiary boundary. Nature, 359, 819-821.

SHARPTON, V. L., K. BURKE, A. CAMARGO, S. A. HALL, D. SCOTT-LEE, L. MARIN, G. SUÁREZ, J. M. QUEZADA, P. D. SPUDIS and J. URRUTIA-FUCUGAUCHI, 1993. Chicxulub multiring impact basin: Size and other characteristics derived from gravity analysis. Science, 261, 1564-1567.

SNYDER, D. B., R. W. HOBBS and CHICXULUB WORKING GROUP, 1999. Deep seismic reflection profiles across the Chicxulub crater. In: Dressler, B.O. and Sharpton, V.L. (Eds.), Large Meteorite Impacts and Planetary Evolution, Geol. Soc. Am. Sp. Paper, 339, 263-268.

URRUTIA-FUCUGAUCHI, J., L. MARIN and A. TREJO-GARCÍA, 1996. UNAM scientific drilling program of the Chicxulub impact structure – evidence for a 300 km crater diameter. Geophys. Res. Lett., 23, 1565-1568.

VOZOFF, K., 1989. The magnetotelluric method. In: Nabigian, M.N. (Ed.), Electromagnetic Methods in Applied Geophysics, Soc. Expl. Geophys. Tulsa, OK, USA.

# 5.- ESTRUCTURA ELÉCTRICA DE LA CUENCA DE IMPACTO DE CHICXULUB A LO LARGO DE DOS PERFILES MAGNETOTELÚRICOS.

**Electric structure of the Chicxlub impact basin along two magnetotelluric profiles**

Jorge A. Arzate (1), Omar Delgado-Rodríguez (2,3), Oscar Campos-Enríquez (2), Jaime Urrutia-Fucugauchi (2)

(1) *Unidad de Investigación en Ciencias de la Tierra, UNAM-Campus Juriquilla, Juriquilla, Qro., C.P. 76230. arzatej@geminis.unicit.unam.mx*

(2) *Departamento de Geomagnetismo y Exploración, Instituto de Geofísica, Universidad Nacional Autónoma de México, Coyoacán 04510, México D.F., México*

(3) *Instituto de Geofísica y Astronomía. CITMA, La Habana, Cuba*

*Sometido a Canadian Journal of Earth Science (anexo 1).*

## 5.1.- Abstract

A magnetotelluric (MT) survey was carried out in the Yucatan Península to assess the capabilities of the method to detect structural changes along two radial profiles crossing the sinkholes ring, a surface feature thought to be directly associated to the Chicxulub impact crater. A total of 22 long period MT soundings were measured. Eleven of them were located along a N-S profile (or AA′) while the other ten were measured along a profile of azimuth NW-SE (or BB′). A two-dimensional model using the Smith and Booker (1991) algorithm was obtained for each profile from the simultaneous inversion of the TE and TM modes. The interpreted structural sections along the two measured profiles yielded significant differences. The NS profile shows a smooth change of resistivity structure and a deeper undisturbed basement away from the crater center. However, the NW-SE profile renders a sharp electrical contact related to the major outer crater ring and a shallower undisturbed basement. In addition, a structural high is observed in this profile towards the postulated crater center. Based on the two resistivity cross sections the crater diameter of the main cavity is set to 195 ± 4 km while the base of the crater central structural high to about 80 ± 4 km diameter. Pseudo sections of tipper (T), skew ($k$) and regional skew ($\eta$) were used to constrain structures related to the impact event such as the Tikul fault and the ring of sinkholes, which are not evident in the inverted resistivity sections.

## 5.2.- Introduction

There are evidences suggesting that from the Cambrian period to present have occurred, at least, five global biological disasters (Albriton, 1989) in which many groups of animals and plants disappeared. The most recent of these events, defined by the Cretaceous/Tertiary (or K/T) boundary, occurred about 65 million ago (Alvarez et al., 1980). The global excess of Iridium (Ir) in sediments at the K/T boundary has been attributed to either a meteorite impact or enhanced volcanism. However, Galer et al. (1989) demonstrated that the composition of the meteoritic Pb is isotopically quite distinct from Pb of volcanic or continental origin. The discovery of a 50 cm layer in Haiti with high Iridium (Ir) concentrations as well as impact products at the K/T boundary in several locations around the Caribbean region were compatible with the location of the impact at the Yucatan Península (Alvarez et al., 1992a and b; Bohor and Betterthon, 1994).

Several authors have found evidence of a fairly circular structure in the Yucatan Península (Fig. 1) from geophysical data, which was interpreted as the impact crater, carved by a 10 km diameter extraterrestrial meteor presumably responsible of the last mass extinction (Penfield and Camargo-Zanoguera, 1981). Based upon the analysis of magnetic and gravity field anomalies and information from bore holes drilled in the region and geological evidence, Hildebrand and colleagues (1991) suggested a buried 180 km impact crater diameter. They observed that stratigraphic sequence and target-rock composition satisfy many of the characteristics required for the Cretaceous-Tertiary (K/T) boundary.

Based on the analysis of gravity data over northern Yucatan, Sharpton and colleagues (1993) proposed a multiring impact basin structure, similar to those observed on other silicate planets in the inner solar system (Spudis, 1993). They analyzed radial profiles compiled for every 10 degrees increments of azimuth and interpreted three major rings and evidence of a fragmentary fourth one. A ~300 km diameter ring represents, according to their interpretation, the main rim of the Chicxulub multiring basin, suggesting that it may be one of the largest collisions in the inner solar system. With the exception of their third ring at about 200 km of diameter and a central peak ring of

around 40 km, Pilkington et al. (1994) see no evidence of additional rings. Using simultaneous inversion of gravity and magnetic data and first and second vertical derivatives, Espíndola et al. (1995) inferred the presence of a central peak and a single ring also constraining to 200 km the diameter of the structure, however, they found no evidence of a multiring basin. Pope et al. (1996) and Sharpton et al. (1996) provide additional data, and reinterpreted available geophysical data and drill core samples to argue in favor of a larger crater structure of 240 and 300 km respectively. However, Campos-Enríquez et al. (1997) interpreted magnetotelluric data acquired for the first time in the region, to conclude that the buried crater diameter was about 190 km.

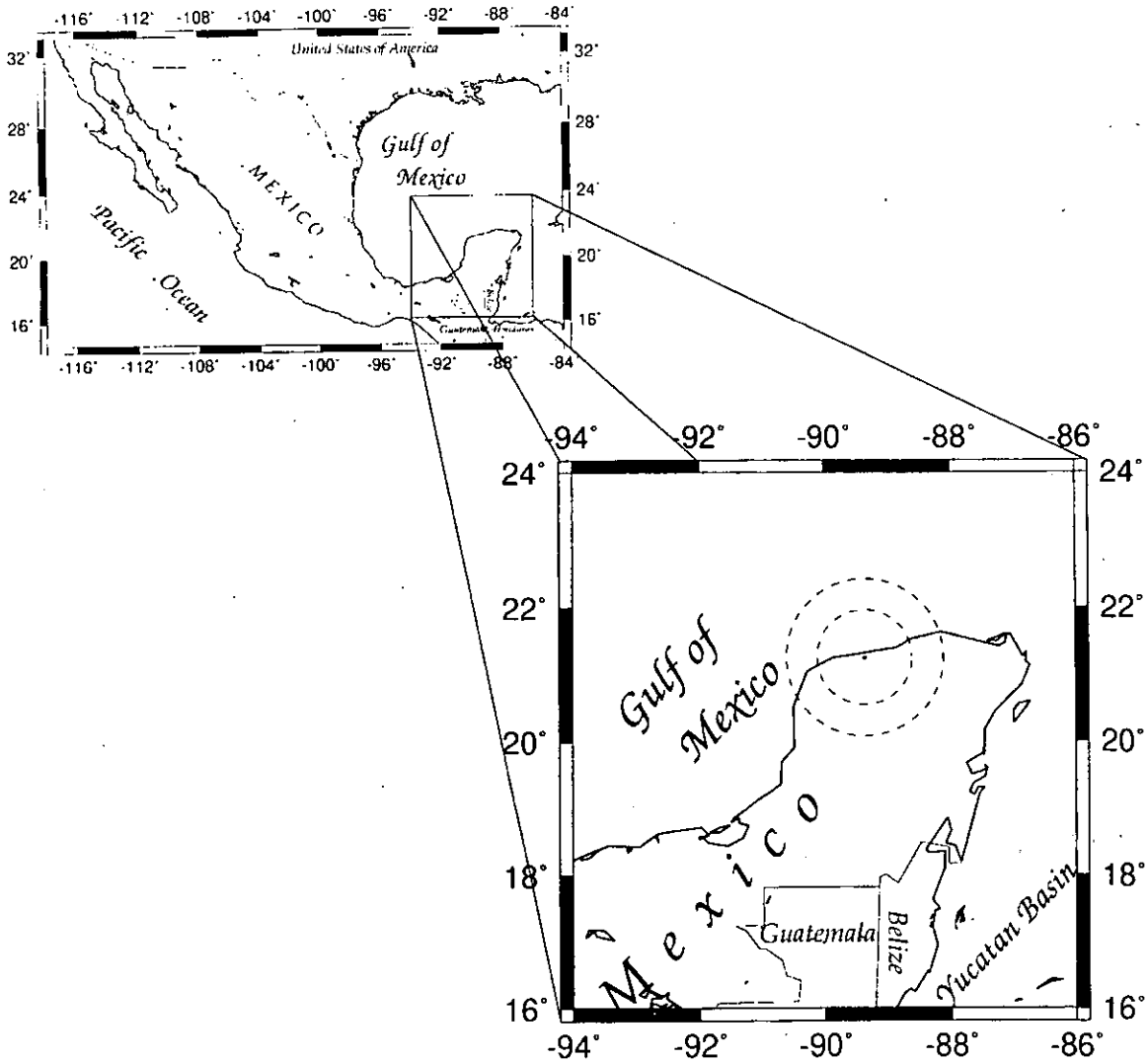


**Figure 1: Study area. Two of the proposed diameters of the structure are indicated with the town of Progreso in the center.**

Later, Hildebrand et al. (1998) combining the results of two offshore seismic reflection profiles and the onshore gravity anomaly map concluded that the crater of the buried impact structure is about 180 km and that apparently departs from circularity by up to 10 km. Based on newly acquired offshore seismic reflection data Snyder et al. (1999a) found two ringed structures defined by normal faults and inward dipping reflections of 110-130 km and 170-200 km diameter related to the central peak ring and the main crater cavity respectively. From the interpreted asymmetry of the cavity the authors speculate about the obliquity of the impact trajectory.

In this work we present the results of two radial-long period magnetoteluric profiles across the main surface structural evidence (the ring of sinkholes) and associated higher gradients of gravity field. The magnetotelluric survey was carried out to obtain the electrical response of the subsurface crater structure, and to evaluate its suitability for further research in the Yucatan Península. The ultimate goal of this study was to add complementary structural data to the general model of the Chicxulub impact zone known to date through the two dimensional modeling of the magnetotelluric transfer functions and elemental distortion analysis.

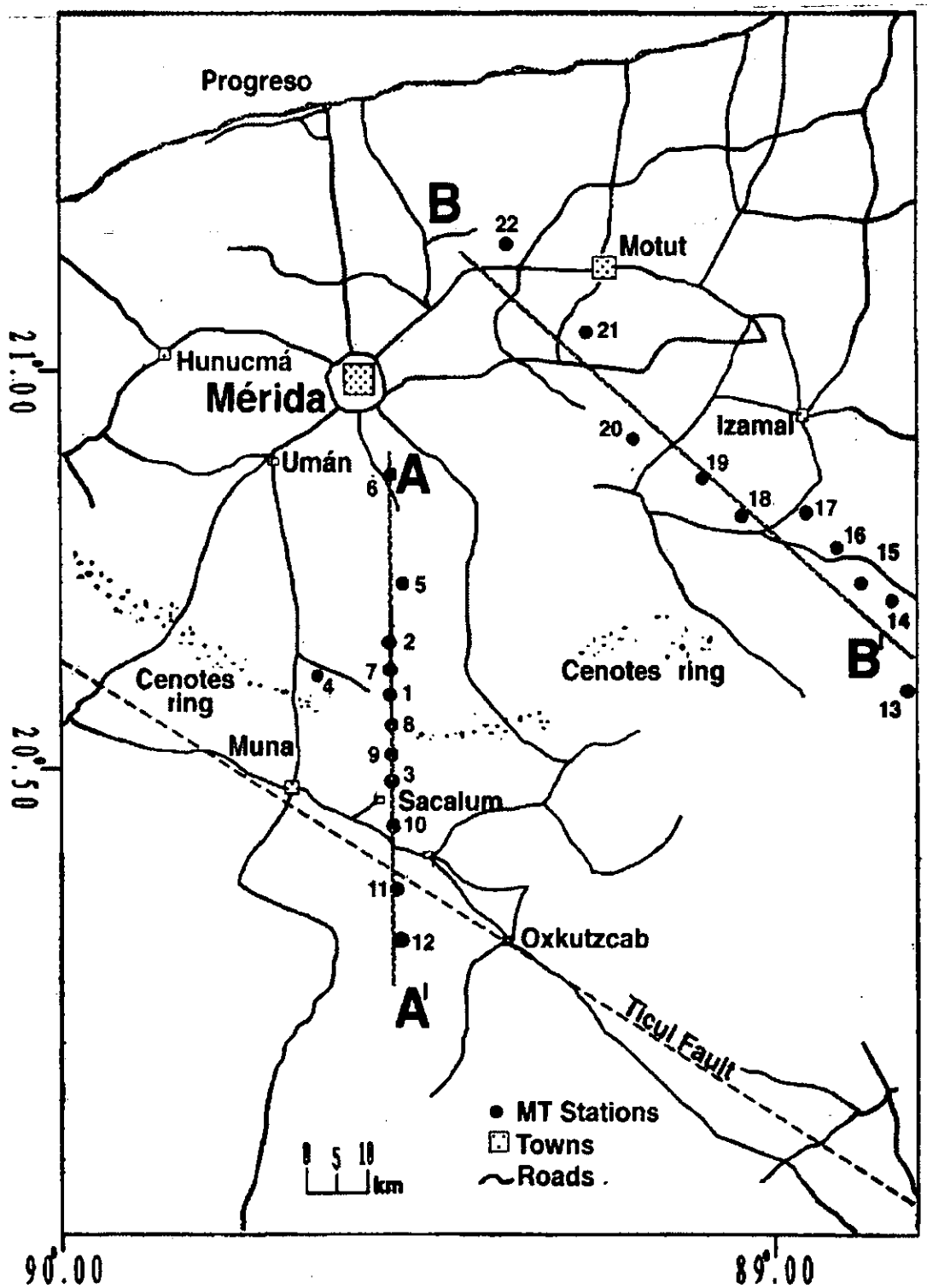


Figure 2: Magnetotelluric profiles indicating the location of the soundings.

### 5.3.- Magnetotelluric survey and data processing

In order to investigate if structural changes can be associated with changes in conductivity of the subsurface we have carried out 22 soundings in the Chicxulub impact zone. The soundings were executed along two radial profiles (Fig. 2) across the sinkholes ring where a structural change is expected to occur if this feature were related to the boundary of the buried crater. It is around this feature that several authors have found evidence of the main crater rim associated with the impact (Hildebrand et al., 1991; Pilkington et al., 1994; Espíndola et al., 1995; Campos-Enríquez et al., 1997; Hildebrand et al., 1998; Morgan and Warner, 1999).

Our survey was carried out using a Phoenix V5 Multipurpose system with a remote reference. Except for station 21 and for frequencies around 1 Hz for stations 16, 18, and 20, the observed variance for the transfer function was less than 10 %. However, the data of these stations were edited to suppress the noisy data to prevent errors in the interpretation process. The measurements were done in the frequency range of 384 – $5.5x10^{-4}$ Hz using recording times between 16 and 24 hours. Although the maximum separation between stations was around 15 km, most of the stations are within 8 km of distance from each other. However, this spacing prevented us to accurately pinpoint the precise location of the crater boundary with accuracy better than half this figure.

The calculated apparent resistivity, which is based on the relative amplitudes of the measured electric and magnetic field components, and the phase difference between them, were evaluated as a function of the period of the electromagnetic waves. The lower frequencies are used the deeper is the probing depth. We recorded the three components $h_x$, $h_y$, and $h_z$ of the magnetic field and the horizontal components $e_x$ and $e_y$ of the electric field. In the conventional reference frame used in MT work, **x** points to the geomagnetic north, **y** points to the east, and **z** points vertically downwards. The field components, measured in the form of individual time series, were later transformed using a Fast Fourier algorithm into the frequency domain. Then the cross-spectra were computed from which the MT transfer function **Z** was estimated.

The transformed horizontal components of the measured magnetic ($H_x$ , $H_y$) and electric fields ($E_x$, $E_y$) are related through the expression (e.g. Vozoff, 1989)

$$\begin{pmatrix} E_x \\ E_y \end{pmatrix} = \begin{pmatrix} Z_{xx} & Z_{xy} \\ Z_{yx} & Z_{yy} \end{pmatrix} \begin{pmatrix} H_x \\ H_y \end{pmatrix} \qquad (1)$$

where $Z_{ij}$ $(i,j = x \text{ or } y)$ are the components of the impedance tensor defining **Z**.

Maxwell's equations separate into two distinct cases if the induction problem is two dimensional. The off-diagonal impedances $Z_{yx}$ and $Z_{xy}$ represent these independent modes of polarization called transverse electric (TE) and transverse magnetic (TM) modes of polarization if the strike of the structure is EW. In such a case, i.e. in the principal axes, the diagonal components $Z_{xx}$ and $Z_{yy}$ are ~ 0. The TE mode is defined as having the electric currents parallel to strike, while the TM mode is defined as having currents across strike. The apparent resistivities $\rho_{xy}$ and $\rho_{yx}$ as a function of frequency and the impedance phases $\phi_{xy}$ and $\phi_{yx}$ are calculated from the complex elements $Z_{xy}$ and $Z_{yx}$ for subsequent interpretation from the following expressions

$$\rho_{xy}(\omega) = \frac{1}{\omega\mu_0}\left|Z_{xy}(\omega)\right|^2, \qquad \rho_{yx}(\omega) = \frac{1}{\omega\mu_0}\left|Z_{yx}(\omega)\right|^2 \qquad (2)$$

and

$$\phi_{xy}(\omega) = tan^{-1}\frac{\text{Im } Z_{xy}(\omega)}{\text{Re } Z_{xy}(\omega)}, \qquad \phi_{yx}(\omega) = tan^{-1}\frac{\text{Im } Z_{yx}(\omega)}{\text{Re } Z_{yx}(\omega)} \qquad (3)$$

where $\mu_0$ is the permeability of free space and $\omega$ the angular frequency $\omega = 2\pi f$. Figure 3 show the resistivity and phases curves of the soundings of both profiles.

### 5.4.- 2-D model

A 2-D inversion of the sounding curves using the rapid relaxation inverse (RRI) algorithm of Smith & Booker (1991) was applied to each profile separately. The simultaneous inversion of the TM and TE modes was carried out. As explained above, these represent the current flow across and along the main structure respectively, namely, the crater boundary. The associated standard deviation for all elements of the impedance tensor was less than or equal to 4 % in the period interval between 384 to 0.002 Hz. Errors, representative of the misfit between observed and calculated magnitudes and phases, are predominantly less than two standard deviations.

The static shift is a type of galvanic distortion related to near surface charge buildup, that affect the resistivity curves by shifting them vertically up or down by a factor, which is independent of frequency. Along profile BB´, only two curves were shifted respect to the remaining eight MT stations. These selective shift was regarded as local, frequency independent galvanic distortion, that was corrected for by shifting back these curves to the same level that the rest of the curves along this profile. This effect didn´t observed neither between the $\rho_a(\omega)$ curves of a same MT soundings, neither between $\rho_a(\omega)$ curves of several soundings.

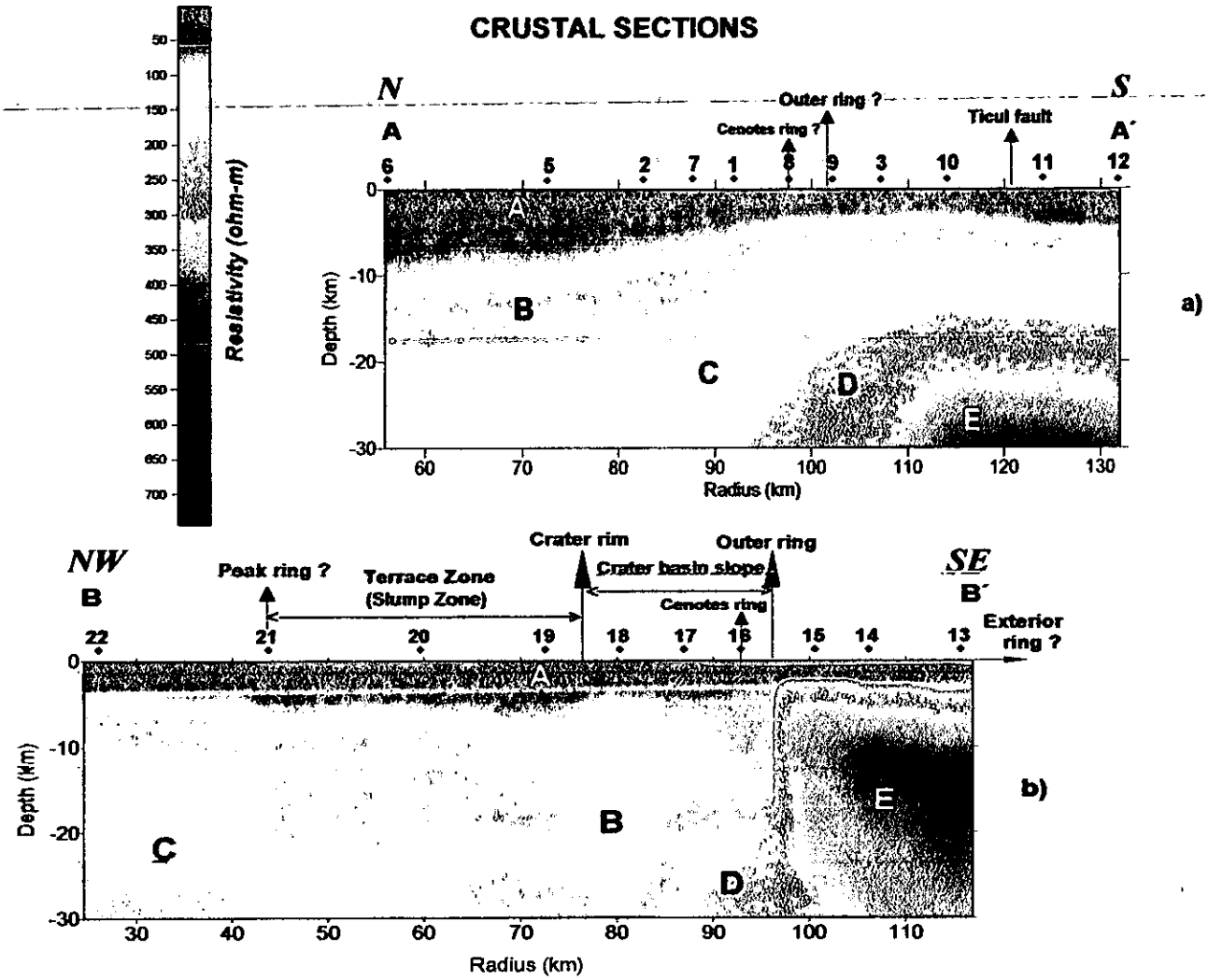


Figura 3: Inverted resistivity sections a) along a AA′ profile, b) along BB′ profile.

### 5.5.- Tipper

The vertical field component $H_z$ can be used, independently of the horizontal magnetic components $H_x$ and $H_y$, to observe lateral changes in conductivity. Near conductors, the relation between the vertical magnetic field and the horizontal field components at any frequency is given by

$$H_z = T_x H_x + T_y H_y \qquad (4)$$

where $T_X$ and $T_Y$ are complex because they may include phase shifting. The vertical component $H_Z$ is an anomalous field associated with lateral conductivity gradients in the Earth, whereas $H_X$ and $H_Y$ are dominated by the regional field. $T_X$ and $T_Y$ are given by

$$T_x = A_r + iA_i$$
$$T_y = B_r + iB_i \qquad (5)$$

and it is usual to plot the real ($A_r$ , $B_r$) and imaginary components ($A_i$ , $B_i$) separately. The former define an induction vector or tipper in the horizontal plane which correspond to the in-phase (p) and quadrature (q) components respectively. For a 2-D situation with the strike along the Y axis, as it is the case here, the $T_y$ component of the equation (4) vanishes and

$$H_z = T_x H_x \qquad (6)$$

In this case the in-phase tipper magnitude is simply given by $A_r$. The magnitude of the tipper is seldom larger than 1, with 0.1 to 0.5 being a common range. The measured tipper along profiles AA′ and BB′ is shown in Figures 4a and 5a respectively in the form of pseudo-sections. Large values of tipper in profile AA′ are common at frequencies below 1 Hz from station 12 to station 7 where it reaches its maximum value. Along profile BB′ there are only two anomalous regions. One under station 18 associated to frequencies larger than 1 Hz, and another under stations 13, 14, and 15 for frequencies below 0.1 Hz. While in this profile it is possible to associate these two anomalous tipper zones to the sinkholes ring and to the crater outer ring discontinuity respectively, in profile AA′ there is not a clear association of anomalous tipper values with the outer rim. In particular, there is not a clear correspondence of the high anomalous tipper values under station 7 in the AA′ profile.

### 5.6.- Skew

It is also often useful to prepare pseudo sections of distortion indicators to observe the behavior of the transfer functions as a function of frequency. These can assist in defining zones of complicated structure along the profile, which are often smoothed during the inversion of the data. Some distortion indicators are invariant under rotations, meaning

$$k = \frac{|Z_{xx} + Z_{yy}|}{|Z_{xy} - Z_{yx}|}$$

that the outcome is independent of the reference frame of measurement of the impedance. One of the more commonly used indicators (7) mpedance skew, $k$ (Swift, 1967), which provides a measure of a purely two dimensional model, and which is defined by

If $k$ is zero or close to zero (<0.2) then the tensor, and hence the structure at a particular frequency, is regarded to be at most two dimensional. Larger values of $k$ indicate a more complex structure. However, the EM fields could be locally distorted due to near surface discontinuities affecting a specific range of frequencies but behave as a regional two dimensional ground for the low frequency range. This is known as the "superposition model", which can be tested using the regional skew $\eta$ (Bahr, 1991) defined as

$$\eta = \frac{\sqrt{|[D_1, S_2] - [S_1, D_2]|}}{|D_2|} \qquad (8)$$

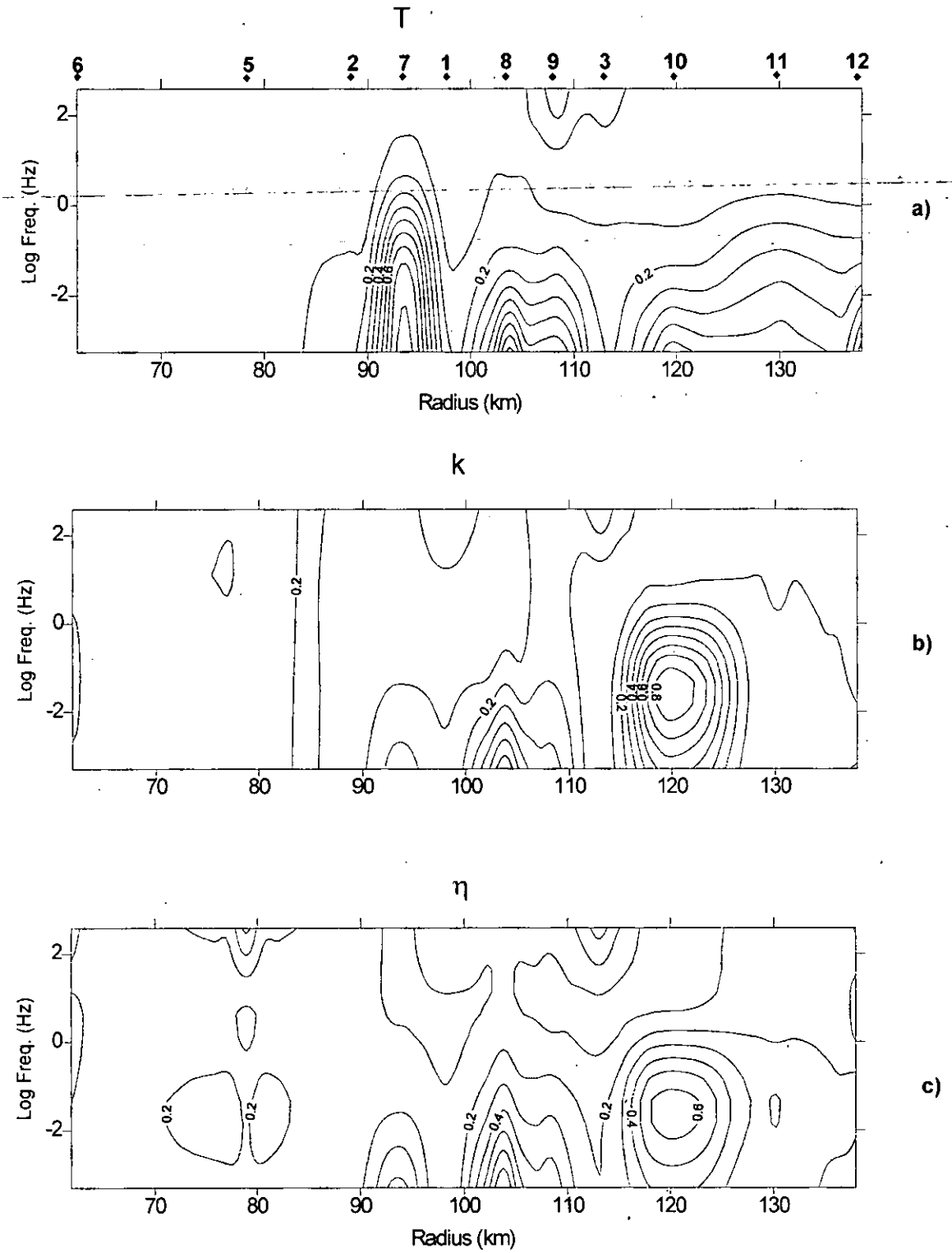


**Figure 4: Distortion analysis for NS profile. a) Tipper section, b) Skew section and c) Regional skew section.**

In this expression $S_1$, $S_2$, $D_1$, and $D_2$ are given by $S_1 = Z_{xx} + Z_{yy}$, $S_2 = Z_{xy} + Z_{yx}$, $D_1 = Z_{xx} - Z_{yy}$ and $D_2 = Z_{xy} - Z_{yx}$ .Values of $\eta$ larger than 0.4 are interpreted as a departure from the superposition model (2-D earth with local 3-D distortion). This parameter is

obtained from the condition that in the reference system of the 2-D regional structure, $Z_{xx}$ has the same phase as $Z_{yx}$ and $Z_{yy}$ has the same phase as $Z_{xy}$. Figures 4b and 4c show the Swift (k) and Bahr ($\eta$) skew plotted along profile AA′. These have similar shapes, both indicating anomalous skew values under station 8 at a frequency range below 0.1 to 0.01 Hz approximately. The high skew values suggest 3-D induction effects associated to the outer ring of the buried crater structure. This low frequency anomalous skew, located at about 100 km from the assumed crater center, could at first instance be associated to the sinkhole ring cutting off the profile around station 8. The anomalous skew zone at about 120 km radii observed in this profile can be associated to the E40S trending Tikul fault zone (Fig. 2) which has an observable 10-15 meter scarp close to the location of station 10.

Figures 5b and 5c are the corresponding Swift and Bahr's skews for profile BB′. Here the 100 km radii low frequency anomaly is also evident, this time nearby stations 16-17 and, although there is not a visible sinkholes ring at the surface in this sector it may be responding to a shallow buried fracture zone related to the subsidence of the crater fill. A wider low frequency anomalous skew zone, both $k$ and $\eta$, located around 60 km away from the accepted crater center is also observable. This feature could possibly be associated to the central uplift, which is not observed in profile AA′ because it does not extend far enough towards the center of the crater.

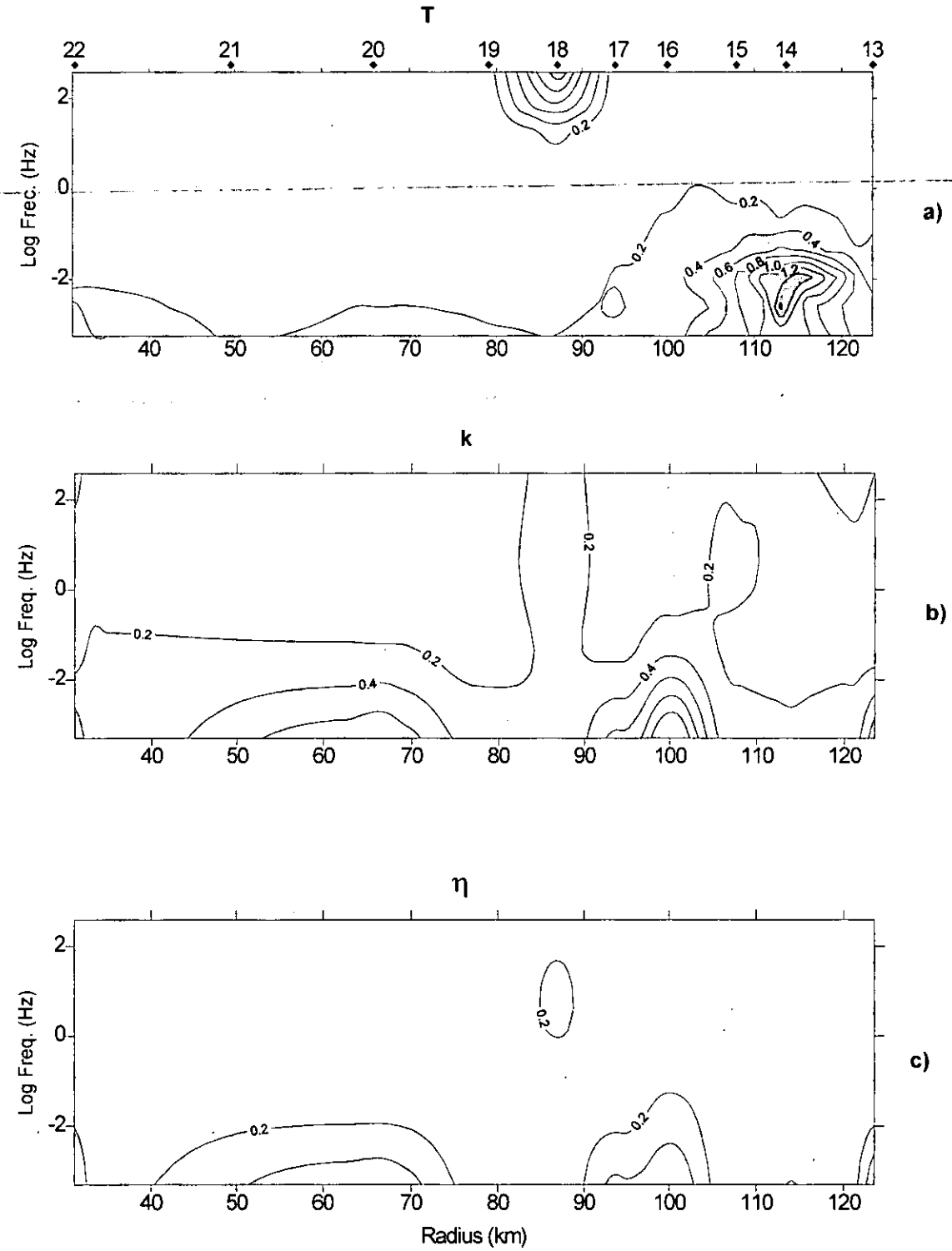


**Figure 5: Distortion analysis for NW-SE profile. a) Tipper section, b) Skew section and c) Regional skew section.**

### 5.7.- Discussion of results

The two interpreted resistivity sections (Fig. 3) have in common a highly conductive (10-20 ohm-m) upper unit, which according to available wells in the area is predominantly constituted by Tertiary sediments and breccia, ticking up towards the crater center (A). However, the two-dimensional inversions yield in general a relatively smoother structural model for profile AA′ (N-S) than for profile BB′ (NE-SW). In profile AA′ (Fig. 3a) for example, the transition zone between the undisturbed (E) and disturbed basement (C) is shown as a gently dipping slope. In contrast, profile BB′ (Fig. 3b) shows a sharp electrical contact between these two electrical units.

Another important difference is that the more resistive unit in section AA′ is deeper than along profile BB′. Taking arbitrarily the 150 ohm-m resistivity curve (B/C boundary), assumed characteristic of the upper crystalline basement, the difference in depth from its top to the surface is in average of 4 km. While in the AA′ profile this depth varies from about 7 to 9 km, in section BB′ it ranges from 3 to 5 km approximately. However this estimation is conservative. By taking a larger value for the upper crystalline basement, say 250 ohm-m (D), then this difference rises up to 12 km or so. Although only with an electrical well log register we could be in better position to estimate the depth to the undisturbed basement, what it is suggested by this data is that it may be tilted.

The difference in depths is supported by the Bouguer gravity profiles of Hildebrand et al. (1991) which show a regional field decreasing from east to west suggesting a shallower basement in the east. In addition, by modeling gravity and magnetic data Espíndola et al. (1995) suggested the existence of a westward dipping basement supporting further the idea of a shallower undisturbed basement to the east.

Another important difference between the interpreted 2-D sections, this however due to the different lengths of the profiles (see horizontal scales), is the relatively resistive topographic high towards the NW of profile BB′. This feature is associated to a central uplifted basement suggested by gravity and magnetic field data which has been modeled

previously by several authors (e.g. Hildebrand et al., 1994; Espíndola et al., 1995; Campos et al., 1996).

The fundamental structural characteristics of the crater are pointed out in the geoelectric section of the profile BB′ (Fig. 3b). For the correlation with the gravity information, the MT stations are plotted on the gravity gradient map (Hildebrand et al., 1998, Fig. 6).

The basin limit of the crater is evidently found around sounding 16, where a stepping structure can be appreciated, toward sounding 17 between the 20 and 30 km depth (Fig. 3b). In Figure 6 these stations coincide with the location of the cenotes ring and an extensive zone of maximum gradient, which Hildebrand et al. (1998) analyzed as crater basin slope. Sounding 19 established a step in the geoelectric model (Fig. 3b), where the resistive strata ($\rho$ > 100 ohm-m) reappear starting from the 10 km. In the gravity gradient maxims map (Fig. 6) this sounding is located in a poorly defined ring from the gravity information, however the geoelectric model in this part of crater assuring their existence. Sounding 21 is located at the peak ring zone according to the map in Figure 6, but no clear evidence is shown in the geoelectric model (Fig. 3b). This is because the lower signal-noise relation for this station grants a very low poids to the resistivity and phase values estimated for this station, so their influence in the determination of the geoelectric model is poor. Sounding 22 is located in the periphery of the central structural high (Fig. 6) and their geoelectric evidence is the increase of the electric resistivity starting from the 10 km depth (Fig. 3b). Sounding 18 is located in the zone of transition between the limit of the crater and the intermediate ring, showing the more conductive zone of the section of the crater (Fig. 3b).

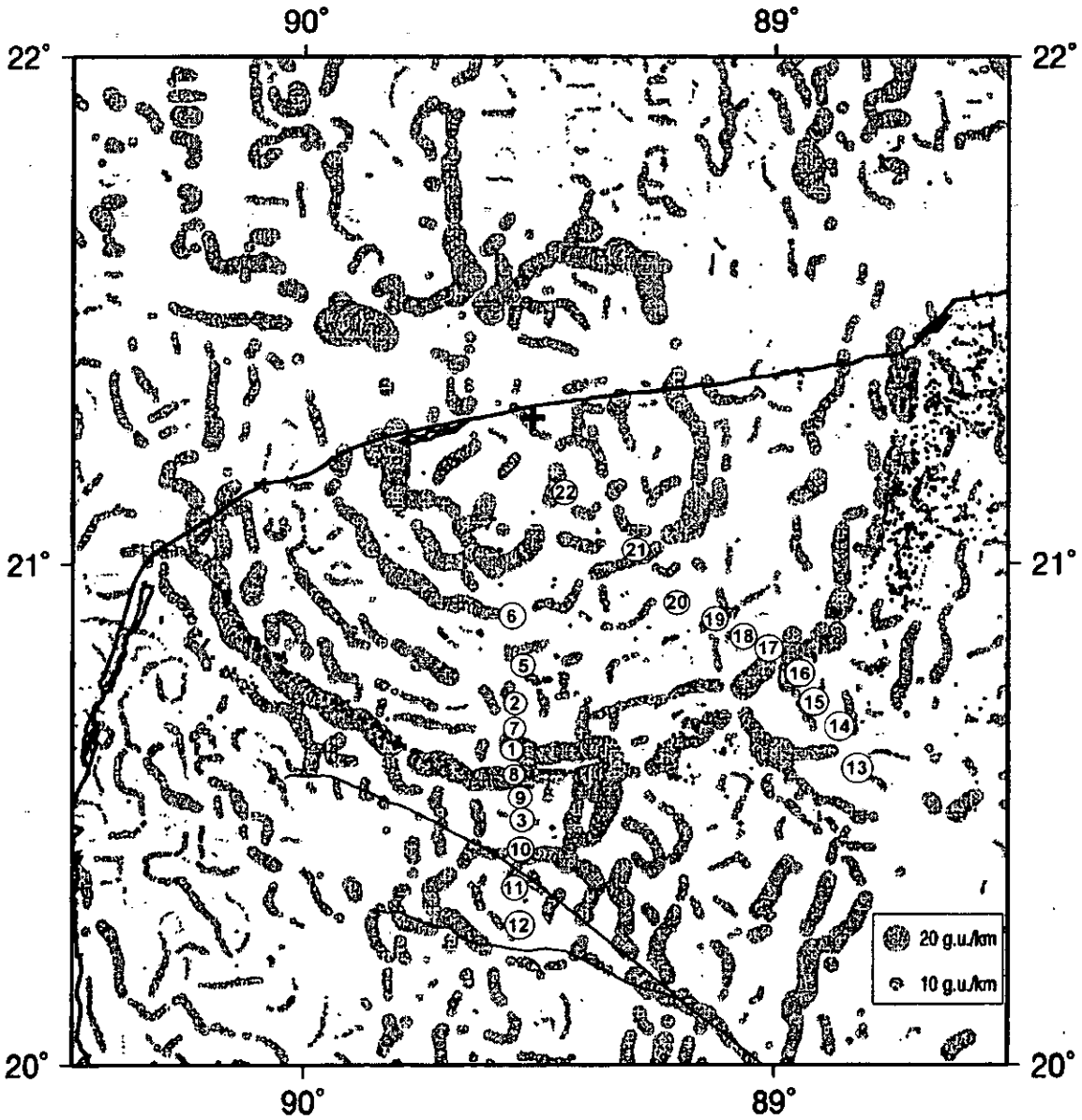


**Figure 6: Gravity gradient maxims map with cenotes (Hildebrand et al., 1998). Ticul fault is drawn as thin dark line and the center crater by the cross. MT soundings is indicated by encircled number.**

This is due to the prevalence of highly fractured materials belonging to the zone of slump.

The soundings 16, 17 and 18 register a very conductive zone (zone B) that lie on a stepping structure (Fig. 3b). This zone is limited by the crater rim and the external ring

and corresponds with the crater basin slope defined by Hildebrand et al. (1998), what in turn constitutes a slump zone. Morgan and Warner (1999) define the Terrace Zone between the peak ring and crater rim. In Figure 3b, this zone lies between the soundings 19 to 21, with an approximate width of 32 km. The position of the crater rim (between soundings18 and 19) confers a diameter to the post-impact basin of approximately 150 km, being this result very similar to the certain by Morgan and Warner (1999).

The structural interpretation of the two profiles is shown in Figure 7. The anomalies in the tipper and skew pseudo sections were used to incorporate structure to the smoothed resistivity sections. For example, the high values of skew at around 120 km of radius are though to be related to the Tikul fault. This feature in the southern end of the profile, is constrained at the surface by its actual location and extended to large depths according to observed long period skewness. The interpreted sections also merge characteristics of other interpretations such as the normal faulting related to the slump zone (Hildebrand et al., 1995), which cannot be resolved by the resistivity sections alone.

In Figure 7 , the central uplift is observed only in the BB´ profile and appears more conductive with respect to the Mesozoic basement. According to Hildebrand et al. (1995), the crater filling corresponds to the Cretaceous sediments and ejected breccia combined. The upper unit correspond to the Tertiary sedimentary cover, characterized by a high conductivity.

The pseudo sections of tipper, which reflect anomalous vertical field induced by lateral electrical discontinuities, are shown in Figures 4a and 5a. As observed above, there is a clear correlation of the observed anomalous tipper zone in profile BB´ with the location of the undisturbed basement (under stations 13, 14 and 15). Consistent with the smooth transition from the outer ring to the crater basin along profile AA´, there is not a sudden change of the anomalous tipper as observed in profile BB´. Instead it is observed a low frequency anomaly that extents from the southern end of the profile to station 2, located to the north. A particularly high tipper feature is present below station 7, which does not have an equivalent along profile BB´ nor a structural signature in the inverted profile. We have interpreted this anomalous tipper as the effect of a deep-rooted

conductive fault zone, although the sparse data set and the lack of additional information leave this argument as merely speculative.

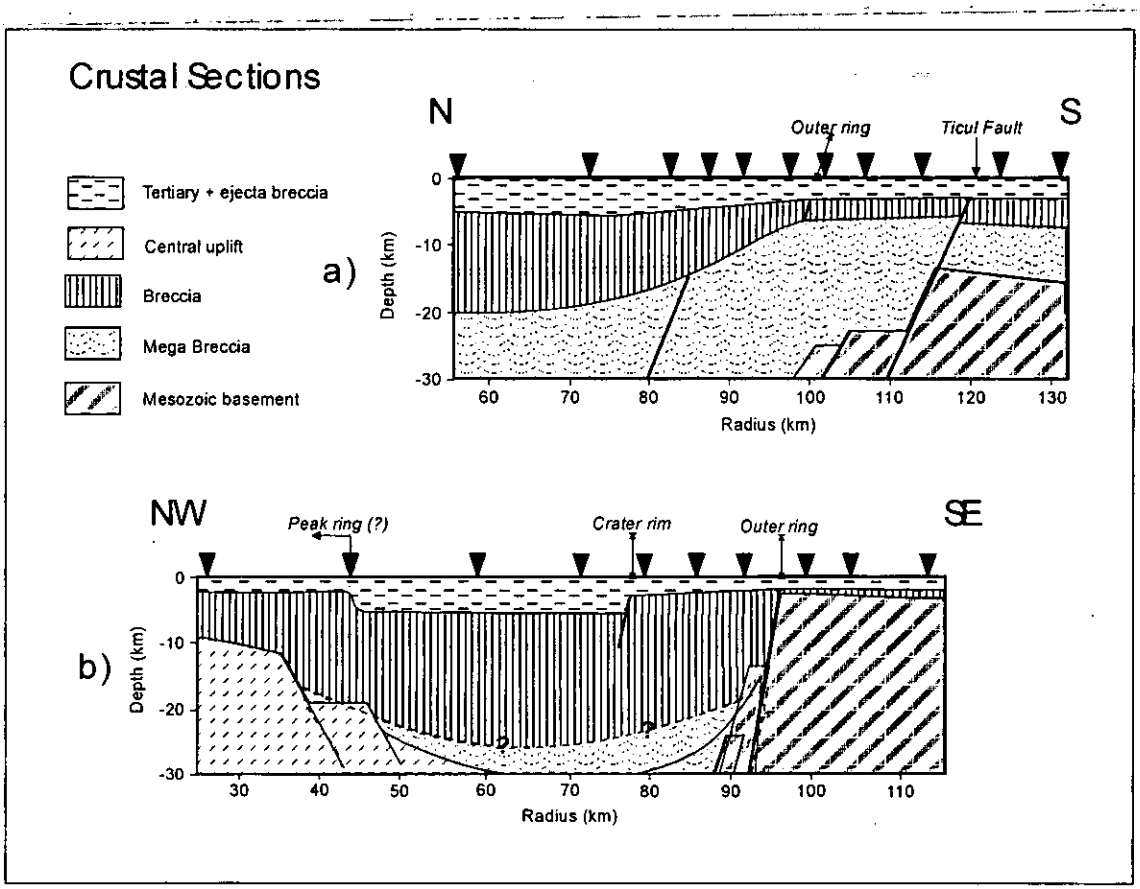


**Figure 7: Structural interpretation. a) along a NS profile, b) along a NW-SE profile.**

One of the still on-going discussions is focused on whether or not the Chicxulub crater has characteristics of a multi-ring basins (e.g. Pilkington and Grieve, 1992; Hildebrand et al., 1995; Sharpton et al., 1993, 1996; Snyder et al., 1999b). Recently, Snyder et al. (1999a) reported that only two out of four observed deformation zones, deduced from seismic reflection profiling, have inward facing scarps that are traditionally used to define multi-ring basins. Based on prominent reflectors the authors give diameters of 130 and 195 km for two ringed zones regarded as inner rings. The distortion parameters of the magnetotelluric data computed here and plotted on pseudo sections (Figs. 4 and 5) are consistent with the deformation zones observed by these authors. Both Swift and Bahr skew is anomalous ($k > 0.4$, $\eta > 0.2$) centered at about 65 and 100 km of radial distance along profile BB′. Although profile BB′ is fairly

consistent with the existence of two inner rings, profile AA´ shows a skew anomaly only around 100 km of radius and nothing noticeably at 65 km, however this is due to the limited length of this profile.

### 5.8.- Conclusions

Our results, based on magnetotelluric measurements, confirm the existence of a 180-200 km diameter crater buried in the Yucatán península. However, while this is quite clear along the NW-SE profile (~ 195 km), it is less obvious along the N-S profile, where there is a smoother contact slope of the Mesozoic resistive basement and the crater filling. The end of the slump zone defines the post impact basin that correlates with stations 18 from the first and station 2 from the later profile. This yields a diameter of 160 km approximately, which is in good agreement with the result obtained by Morgan and Warner (1999) for this feature.

There is a significant difference in depth to the top of the undisturbed basement in both profiles. While the resistive unit associated to the Mesozoic basement is observed at around 4 km along the NW-SE profile, the depth to the same resistive body corresponding to N-S profile is at around double. However, this estimation is based upon the assumption that the average resistivity of the undisturbed basement is 150 ohm-m. Without further control on the real resistivities from a well log register, which is not available in the zone, this result remains speculative. A larger value of the resistivity for the upper crystalline basement, say 250 ohm-m, triggers this difference up to 12 km.

Despite the uncertainty in establishing this difference more accurately it is evident from the resistivity sections this could be real. A tilted basement has been also suggested previously by gravity and magnetic data from Espíndola et al. (1995), suggesting the existence of a westward dipping basement supporting further the idea of a shallower undisturbed basement to the east. In addition, Hildebrand et al. (1991) have shown gravity profiles which show a regional field decreasing from east to west in agreement with our observations.

According to the interpreted resistivity sections, the observed disruption cavity along the NW-SE profile is apparently deeper than along the N-S profile and in general deeper

than it has been previously proposed. Former figures estimate maximum depth of disruption of 20 to 22 km (Snyder et al., 1999b; Hildebrand et al., 1998) however, the structural model of profile BB´ suggest depths of up to 30 km. This is represented by the relatively conducting zone under stations 17, 18, and 19, leveled with letter B. An alternative explanation of this conductor is that it may be due to the prevalence of highly fractured zone directly related with the zone of slump.

The marked differences in the conductivity structure between the two crustal sections necessary imply different structural boundaries between resistive and conductive units. Even if not conclusive, these differences provide elements to argue in favor of an oblique impact. Although our data hints more an equatorial trajectory of the impactor (probably SW-NE rather than S-N as suggested by Snyder et al., 1999a), the elements we have to constrain it are not enough at this point. So, this question is left open for the time being until more information is gathered in this region.

An ongoing ground AMT/MT field campaign as well as a planned marine EM induction experiment would provide additional elements to improve our model an to extend it towards a 3-D analysis.

**Acknowledgments**

We want to acknowledge the valuable help in the field work campaign of Marino Pareja, Lener Sequeira and David Alatriste. Funds were provided by grants 32434-T of the Consejo Nacional de Ciencia y Tecnología (CONACYT). Jorge Arzate wishes to thank Michael Chouteau from L'Ecole Polytechnique de Montrèal for providing the MT instruments used during the first field campaign.

## 5.9.- References


ALBRITON C. Jr., 1989: Catastrophic episodes in Earth History. New York, Chapman & Hall.

ALVAREZ, L.W., W. ALVAREZ, F. ASSARO and H. MICHEL, 1980. Extraterrestrial cause for the Cretaceous/Tertiary extinction. Science, **208**, 1095-1108.

ALVAREZ, L. W., GRAJALES J. M., MARTINEZ S. R., ROMERO P. R., RUÍZ L. E. GUZMÁN M. J., ZAMBRANO M., SMIT J., SWINBURNE N. H. M. and MARGOLIS S. V.,1992a. The Cretaceous-Tertiary boundary impact tsunami deposit in NE Mexico. GSA, Abstracts with programs, **24**, 331.

ALVAREZ, W., SMIT J., LOWRIE W., ASSARO F., MARGOLIS S. V., KASTNER M. and HILDEBRAND A. R., 1992b. Proximal impact deposits at the Cretaceous-Tertiary boundary in the Gulf of Mexico: a restudy of DSDP leg 77, sites 536 and 540. Geology, **20**, 697-700.

BAHR K., 1991. Geological noise in magnetotellurical data. A Classification of distortion types. Phys. Earth. Plant. Inter., **66**, 24-38.

BOHOR B. F. and BETTERTON W. J., 1994. Debris flow / Turbidite clastic units at the K/T boundary, northeastern Mexico, *in* New developments regarding the K/T event and other catastrophes in earth history: LPI Contribution **285**, Lun. Plant. Inst., Houston, Texas, 13-14.

CAMPOS-ENRÍQUEZ J.O., DIAZ-NAVARRO R., ESPÍNDOLA J.M., and MENA M., 1996. Chicxulub-Subsurface structure of impact crater infered from gravity and magnetic data. The Leading Edge, **15**,. 357-359

CAMPOS-ENRÍQUEZ, J. O., J. A. ARZATE, J. URRUTIA-FUCUGAUCHI and O. DELGADO-RODRÍGUEZ, 1997. The subsurface structure of the Chicxulub crater (Yucatán, Mexico): Preliminary results of a magnetotelluric study. The Leading Edge, **16**, 1774-1777.

CARREÑO, A. L. and M. MONTELLANO-BALLESTERO, 1997; Extinción masiva del límite Cretácico-Terciario: mitos y realidades. Unión Geofísica Mexicana. Monografía No. 4.

ESPÍNDOLA, J. M., M. MENA, M. DE LA FUENTE and J. O. CAMPOS-ENRÍQUEZ, 1995. A model of the Chicxulub structure (Yucatan, Mexico) based on its gravity and magnetic signatures. Phys. Earth. Plant. Inter., **93**, 271-278

GALER S.J.G., MACDOUGALL J.D. and ERICKSON III D.J., 1989; Pb isitopic tracers of the Cretaceous-Tertiary extinction event. Geophys. Res. Lett., **16**, 1301-1304

HILDEBRAND, A. R., G. T. PENFIELD, D. A. KRING, M. PILKINGTON, A CAMARGO, S. JACOBSEN y W. BOYTON, 1991. Chicxulub crater: A possible Cretaceous/Tertiary boundary impact crater on the Yucatan Península, Mexico. Geology, **19**, 867-871

HILDEBRAND A.R., CONNORS M., PILKINGTON M., ORTÍZ-ALEMÁN C., and CHÁVEZ R.E., 1994; Size and structure of the Chicxulub crater. Rev. Soc. Mex. Paleont., **7**, 59-68

HILDEBRAND A.R., PILKINGTON M., CONNORS M., ORTÍZ-ALEMÁN C., and CHÁVEZ R.E., 1995; Size and structure of the Chicxulub crater revealed by horizontal gravity gradients and cenotes. Nature, **376**, 415-417

HILDEBRAND, A. R., M. PILKINGTON, C. ORTÍZ-ALEMÁN, R. E. CHÁVEZ, J. URRUTIA-FUCUGAUCHI, M. CONNORS, E. GRANIEL, A. CAMARA, J. F. HALPENNY y D. NIEHAUS, 1998. Mapping Chicxulub crater structure with gravity and seismic reflection data. In: Grady, M.M. et al. (Eds.), Meteorites: Flux with Time and Impact Effects, Geol. Soc., London, Sp. Publ., **140**, 155-176.

MORGAN, J. y M. WARNER,1999. Chicxulub: The third dimension of a multi-ring impact basin. Geology, **27**, 407-410.

PENFIELD, G. T. y Z. A. CAMARGO,1981. Definition of a major igneous zone in the central Yucatán platform with aeromagnetics and gravity, *in* Technical Program, Abstracts and Biographies, 51st Annual Meeting,, **37**, Society of Exploration Geophysics, Tulsa, Okla.

PILKINGTON, M. y R. GRIEVE, 1992. The geophysical signature of terrestrial impact craters. Rev. Geophys., **30**, 161-181.

PILKINGTON, M., A. R. HILDEBRAND y C. ORTÍZ-ALEMÁN, 1994. Gravity and magnetic field modeling and structure of the Chicxulub crater, Mexico. J. Geophys. Res., **99**, 13147-13162

POPE K. O., OCAMPO C., KINSLAND G. L. and SMITH R., 1996; Surface expression of the Chicxulub crater. Geology, **24**, 527-530.

SHARPTON, V. L., K. BURKE, A. CAMARGO, S. A. HALL, D. SCOTT-LEE, L. MARIN, G. SUÁREZ, J. M. QUEZADA, P. D. SPUDIS y J. URRUTIA-FUCUGAUCHI, 1993. Chicxulub multiring impact basin: Size and other characteristics derived from gravity analysis. Science, **261**, 1564-1567

SHARPTON V., MARÍN L. E., CARNEY J., LEE S., RYDER G., SCHURAYTZ B., SIKORA P. and SPUDIS P., 1996; A model of the Chicxulub impact basin based on evaluation of geophysical data, well logs, and drill core samples. The Cretaceous-Tertiary event and other catastrophes in Earth history, Special Paper, GSA, **307**, 55-74.

SMITH J.T. and BOOKER R.B., 1991. Rapid inversion of two- and three-dimensional magnetotelluric data. J. Geophys Res., **96**, 3905-3922

SNYDER D. B., HOBBS R. W. and CHICXULUB WORKING GROUP, 1999a. Ringed structural zones with deep roots by the Chicxulub impact. J. Geophys Res., **104**, 5, 10743-10755.

SNYDER D. B., HOBBS R. W. and CHICXULUB WORKING GROUP, 1999b. Deep seismic reflection profiles across the Chicxulub crater. Large meteorite impacts and planetary evolution II, Special Paper, GSA, **339**, 263-268.

SPUDIS, P.D., 1993. Geology of multiring basins. Cambridge Univ. Press, Cambridge

SWIFT, C. M. Jr., 1967. A magnetotelluric investigation of an electrical conductivity anomaly in the southwestern United States. Ph Thesis, Massachusetts Institute of Tecnology.

VOZOFF, K., 1989; The magnetotelluric method. *In* Electromagnetic methods in applied geophysics, *by* Nabigian M.N. (ed.), Soc. Expl. Geophys.

## 6.- Conclusiones

La estructura del cráter de Chicxulub ha sido objeto de múltiples estudios geofísicos, geológicos y geoquímicos.

Este trabajo constituye el primer esfuerzo en establecer la estructura geoeléctrica del cráter de Chicxulub, partiendo del procesamiento e interpretación de la información MT contenida en 22 sondeos magnetotelúricos distribuidos a lo largo de los perfiles AA´ y BB´.

La inversión 1-D realizada en el perfil B-B´ confirmaron los resultados cualitativos obtenidos del análisis de las curvas de campo: el sondeo magnetotelúrico constituye un método efectivo para el estudio del cráter de Chicxulub. Un cráter de aproximadamente 200 km de diámetro fue modelado utilizando los algoritmos de inversión Bostick y Occam.

Sin embargo, secciones bidimensionales que fueron calculadas para ambos perfiles aplicando el algoritmo de inversión 2-D por Relajación Rápida, mostraron de manera mucho más precisa las características esenciales del cráter que las mostradas en las secciones 1-D. La sección 2-D del perfil B-B´ establece un diámetro de la cuenca de aproximadamente 195 km. Este límite define el anillo principal del cráter, ubicado inmediatamente al sur del anillos de cenotes. La ubicación del "crater-rim" propone la existencia de una cuenca post-impacto de 150 km de diámetro, mientras que el "peak-ring" se ubica a una distancia radial de 42 km. Una zona de bloques deslizados es definida entre los 42 y 75 km de distancia radial, siendo este el basamento de la zona de terraza (zona de máximo espesor de los sedimentos del Terciario). Estos resultados guardan una buena correspondencia con los obtenidos por Morgan y Warner (1999) del procesamiento de la información sísmica.

El modelo 2-D obtenido del perfil AA´ presenta diferencias significativas respecto al del perfil BB´. El techo de la unidad resistiva asociada con el basamento Mesozoico se encuentra a un profundidad mínima de ~ 4 km de profundidad, mientras que su profundidad en el perfil AA´ es de ~ 8 km. El perfil AA´ se encuentra ubicado sobre un bajo gravimétrico que se extiende por más de 100 km al sur de anillo de cenotes, lo que valida la existencia de un basamento cristalino más profundo en esta porción del perfil.

Comparando ambos modelos hacia el interior del anillo de cenotes, se pudo observar que el perfil BB´ presenta un mayor espesor de material conductor ( < 100 ohm-m) asociado con el relleno muy fracturado del cráter, otorgándole una profundidad máxima de la cavidad de ~ 30 km en la zona del "crater basin slope".

Las diferencias estructurales presentadas entre ambos perfiles pudieran ser el resultado de un impacto oblicuo, aunque la información MT no es suficiente para asegurar esta afirmación.

Realizando una modelación sintética 3-D de la península de Yucatán y la plataforma marina circundante, así como el análisis de las flechas de inducción, se pudo evaluar el efecto costa en las observaciones MT. Pudo comprobarse la existencia de un ligero efecto del mar sobre las observaciones registradas para los períodos T ≥ 100 s. Este resultado asegura la no existencia del efecto de costa en los 22 sondeos MT realizados para el rango de frecuencias de interés (T < 100 s), a la vez que propone nuevas áreas, igualmente confiables para futuras mediciones MT en la península de Yucatán.

Una de estas áreas es la porción oeste de la peninsula donde se recomienda la ejecución de un nuevo perfil radial (CC´) con orientación NE-SW que permita obtener una imagen eléctrica 2-D de esa porción del cráter y que, junto a los restantes 22 sondeos MT, constituyan la información MT suficiente para obtener un modelo 3-D que aporte nueva información acerca de la estructura de este gran cráter de impacto.

# ANEXO 7.1

**Publicación que incluye los resultados preliminares del levantamiento magnetotelúrico.**

**Cartas de sometimiento a arbitraje y aceptación para la publicación de los artículos involucrados en el trabajo de tesis**

# The subsurface structure of the Chicxulub crater (Yucatán, Mexico): Preliminary results of a magnetotelluric study

J.O. CAMPOS-ENRÍQUEZ, J.A. ARZATE, J. URRUTIA-FUCUGAUCHI, and O. DELGADO-RODRÍGUEZ, Instituto de Geofísica, UNAM, Mexico D.F.

The existence of an impact structure in northern Yucatán has been inferred based primarily on gravity and magnetic studies (Figure 1). This impact structure has been directly related with the massive biota extinction at the transition from the Cretaceous to the Tertiary (K/T) due to the global climatic changes induced by the impact of a major meteorite. At present, the available studies confirm both its existence and its association with extinction of the dinosaurs. Even if the existence of an impact structure in the subsurface in northern Yucatán has achieved near consensus, the subsurface features of this impact structure remain to be established. Independent studies have produced different conclusions about its type. According to the original interpretation of Penfield and Camargo (SEG *Extended Abstracts*, 1981), the crater has a 180-km diameter with a concentric zone of magnetic breccia 210-230 km in diameter. Different authors have considered the structure to be a four-ring basin, 300 km in diameter; a peak-ring crater, 180 km in diameter; or have inferred the presence of central twin peaks and a

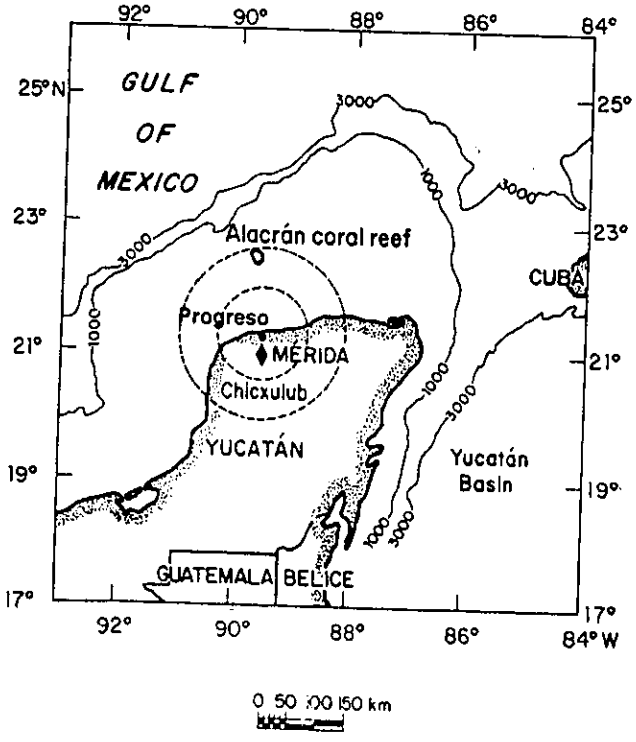


Figure 1. Study area. Two of the proposed diameters of the structure are indicated with the town of Progreso in the center.

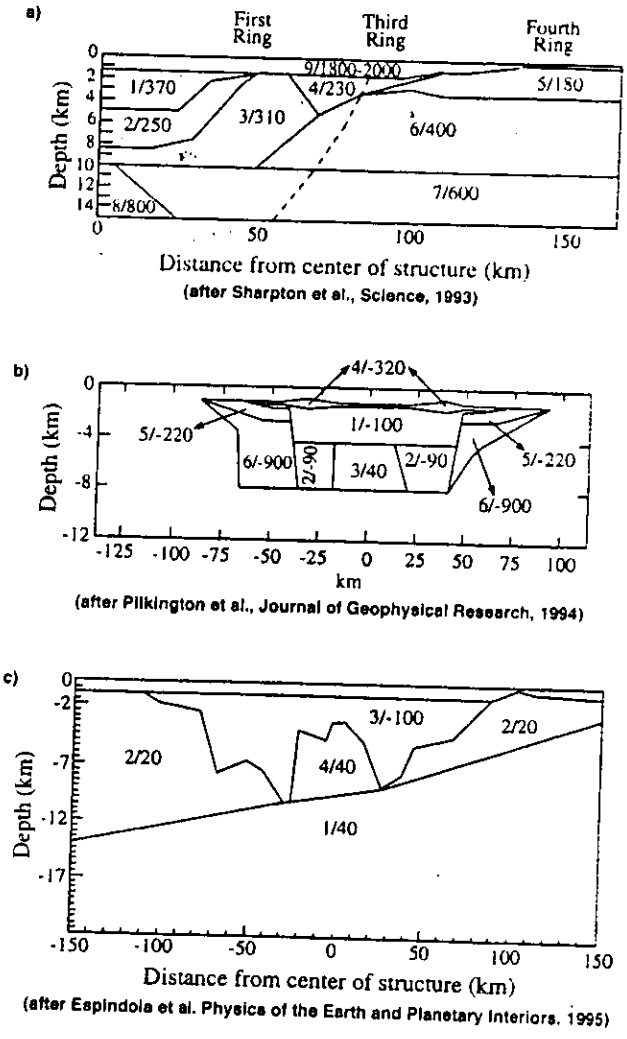


Figure 2. Subsurface models for the Chicxulub impact structure. Density or density contrasts are given in kg/m³. (a) 1= impact melt sheet and melt breccia, 2 = inner allogenic breccia unit, 3 = fractured uplifted crystalline basement, 4 = outer allogenic breccia, 5 = Cretaceous platform sediments, 6 = uppermost crystalline basement, 7 = intermediate basement, 8 = uplifted deep basement, and 9 = Tertiary carbonate rocks. (b) 1 = melt, 2 = megabreccia, 3 = central uplift, 4 = upper breccia, 5 = outer breccia, 6 = Cretaceous and basement. (c) 1 = basement, 2 = Mesozoic sedimentary sequence, 3 = filling material, breccias plus fractured basement, and 4 = impact melt sheet and/or uplifted basement.

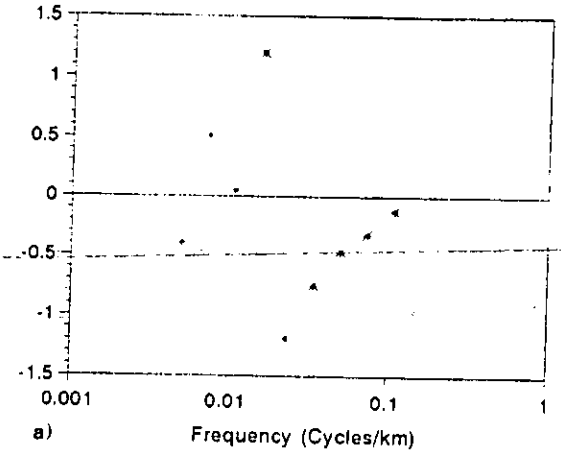


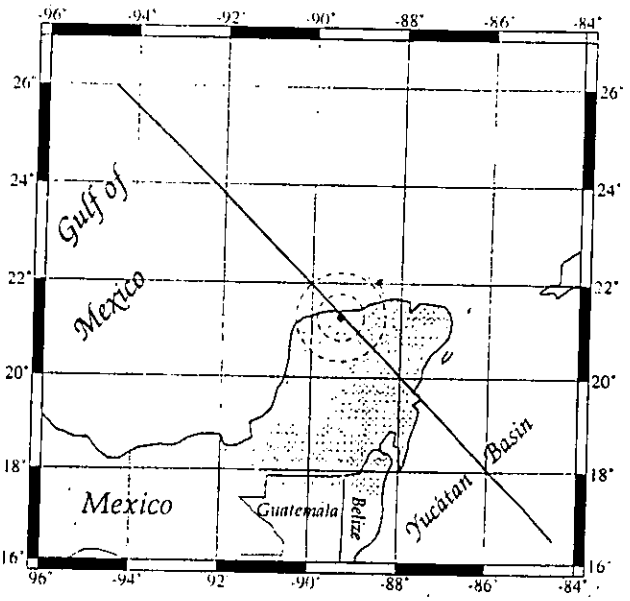


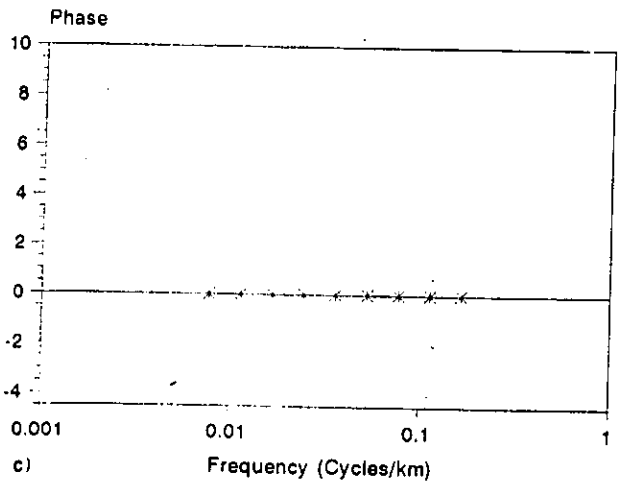


Figure 3. (a) Phase of the admittance function for the Yucatán Platform, based on the analysis of the gravity and topographic data along profile shown in (b). For comparison, the phase of the admittance function of a transect along the Tropic of Cancer is shown in (c).

single ring and constrained the diameter of the structure to less than 200 km. The present diameter estimates for the Chicxulub structure range between 170 and 300 km. The difference in diameter corresponds to a difference in impact energy of up to one order of magnitude. Figure 2 shows the differences between the models proposed so far. The differences between these models arise basically from the nonuniqueness associated with gravity data. This ambiguity can be reduced by constraining the modeling with seismic data and information from deep drilling.

The crust and mantle in the four-ring basin model were incorporated by Urrutia-Fucugauchi et al. (*Tectonophysics*, 1994). By analyzing the mass deficiency associated with this structure, Pilkington et al., inferred the absence of isostatic equilibrium for the Yucatán Peninsula. Campos-Enríquez et al. (*TLE*, 1996) analyzed the free air and Bouguer anomalies, and also determined the admittance function for the Yucatán Peninsula to analyze the isostatic equilibrium. The free-air anomaly has the same sign as the Bouguer anomaly and does not approach zero values, as expected for flat topography in isostatic equilibrium. The admittance function is the transfer function in a linear system where the input corresponds to the topography and the output is the gravity. The relationship between topography and gravity is only linear when there is isostatic equilibrium (i.e. the fase of the admittance function must be zero). However for the Yucatán Peninsula, the phase of the admittance

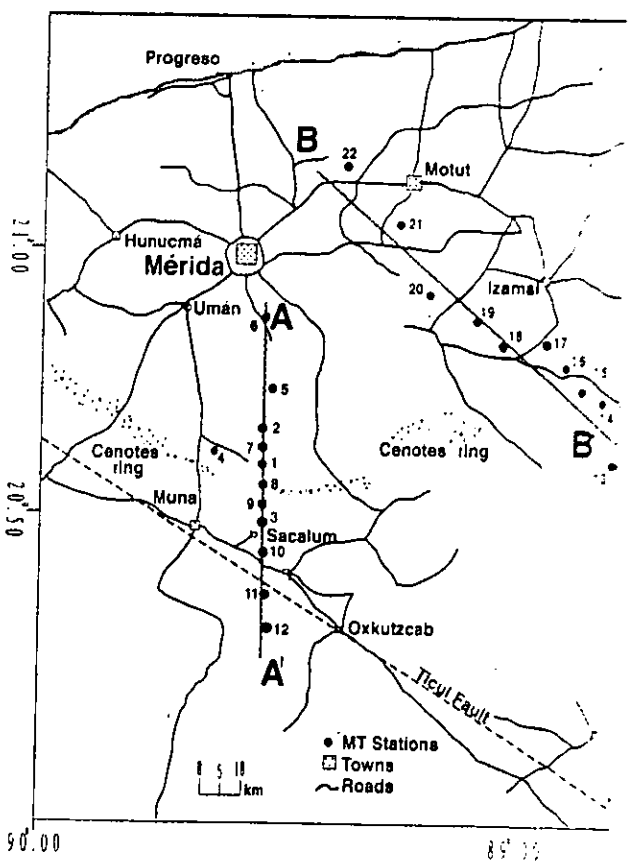


Figure 4. Magnetotelluric profiles indicating the location of the soundings.

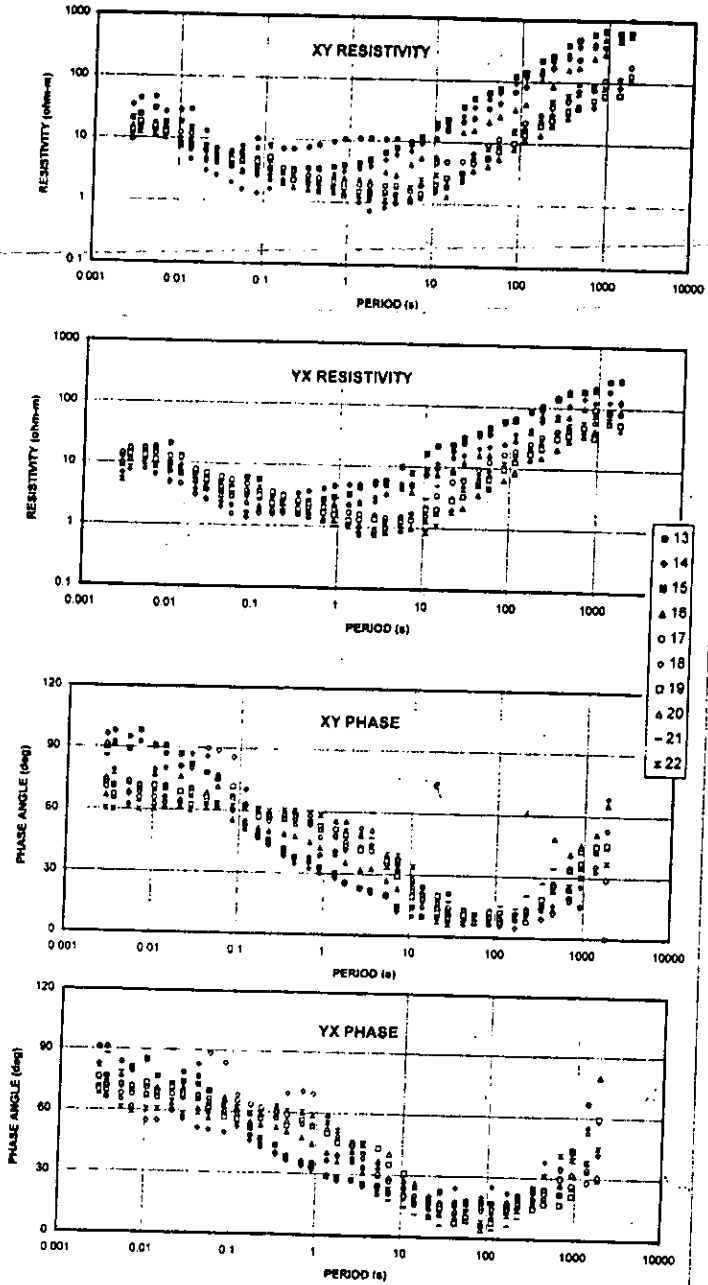


**Figure 5. Observed apparent resistivities and phase curves.**

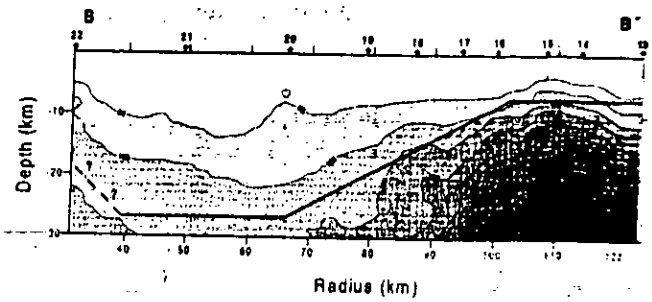


**Figure 6. Resistivity distribution along profile B-B' elaborated by stitching together the Bostick inversion of each of the *xy* mode apparent resistivity curves.**

function is not zero (Figure 3) as should be in regions in isostatic equilibrium.

Although we have some knowledge of the shallow features of the Chicxulub impact crater, its deep structure (lower crust, upper mantle) still waits to be established. Meanwhile, data of a magnetotelluric survey conducted in July-August 1997 are being studied, and what follows is a report of our findings so far.

**MT survey.** This was the first effort ever to image the electrical resistivity of the crust and upper mantle in the site of the Chicxulub impact structure. This survey comprises 22 MT soundings distributed along two radial profiles (Figure 4) whose northern extension would intersect approximately around Chicxulub Pueblo, the center of the crater. Both profiles are located outside the central structural high. Twelve soundings are distributed along profile A-A', which runs in a north-south direction for about 70 km. It crosses the ring of sinkholes (*cenotes*) and, 20 km further south, the Ticul Fault. Profile B-B' has an approximately 90-km length and a northwest-southeast orientation. This profile comprises 10 soundings. The location of the profiles was decided so as to study changes in the electrical resistivity across the sinkhole ring, which approximately marks the crater rim, according to most authors. The lines were located far from the coasts to avoid its effect as much as possible. We used two V-5 acquisition equipments operating in a remote reference basis. The observations covered the range between 384 Hz and a period of 1820 s. This progress report is related to profile B-B' only.

Almost all of the MT soundings are 1-D, with tipper magnitudes well below 0.2. Only the soundings 13, 14, 15, and 16, which are located outside the sinkhole ring, present a slight anisotropy beyond 10 s. In Figure 5, the apparent resistivity and phases of all the soundings are drawn together. The comparative analysis of the curves clearly indicates two distinct groups of soundings. These two groups bear a correlation with the surficial features of the impact structure. One group comprises the soundings inside the sinkhole ring (i.e, soundings 17, 18, 19, 20, 21, and 22); the second group is constituted by the soundings outside the sinkhole ring (soundings 13, 14, 15, and 16). The curves of both groups are similar up to 10 Hz. For larger periods, the curves in the second group show higher apparent resistivities.

As the very preliminary step, besides the qualitative analysis of the curves, we obtained the Bostick inversion of all our rho *xy* apparent resistivity curves. The different inversions are stitched together in Figure 6. South of the profile we observe a high resistivity below soundings 13, 14, 15, and 16. Northward the resistivity decreases constantly and smoothly, up to about sounding 20. From this point, the resistivity is more or less constant with respect to the depth. At the northern end of the profile the resistivity seems to get higher again.

We would need some more observation farther to the north to verify this last feature (it would correlate with the central structural high). This distribution of the electrical resistivity suggests the existence of a basin between soundings 16 and 22. This would correspond with an impact structure of about 190 km in diameter. The resistivity high would be associated with a zone of unaltered rock and marking the horizontal limits of the impact

structure. The high resistivity below sounding 22, on the other end, would also indicate a zone of unfractured material (the central structural high). According to this preliminary interpretation, the zone of fracturing would affect the upper lower crust. In other words, we do not observe a regional mantle uplift. This preliminary result is contrary to the working models of cratering, according to which the impact site would attain its isostatic equilibrium through a mantle uplift.

**Conclusions.** The preliminary electrical subsurface resistivity distribution indicates the existence of a basin about 190 km in diameter, which suggests an impact structure limited by the sinkhole ring. Relatively low resistivity values indicate that the impact-induced fracturing zone reached lower crustal levels. The deeper resistivity distribution does not correlate with the presence of the mantle uplift incorporated in the working models of cratering. Gravity data also indicate the absence of isostatic equilibrium in the Yucatán Platform.

*Jorge Arturo Arzate received his BSc (1983) in physics from the Universidad Autónoma de México, master's in geophysics from the Institute of Earth Sciences at Delft, Netherlands (1986) and the University of Toronto, Canada (1990), and a PhD (1994) in geophysics from the École Polytechnique de Montréal, Canada. He is presently working at the Instituto de Geofísica-UNAM. Arzate is interested in electromagnetic methods in general, and MT in particular, tectonics, and exploration geophysics.*

*Jaime Urrutia Fucugauchi received his BSc (1975) and MSc (1977) from the Faculty of Sciences of the UNAM, and his PhD (1980) from the University of Newcastle, United Kingdom. His main research interests are paleomagnetism, tectonics, and exploration geophysics. At present, he is conducting research concerning the Chicxulub impact crater.*

*Omar Delgado Rodríguez received his BSc (1985) in geophysical engineering from the J.A.E. Higher Polytechnic Institute in Habana, Cuba, and MSc (1995) in geophysical exploration from the UNAM, where he is presently pursuing his PhD at the Institute of Geophysics.*

*Corresponding author: ocampos@tonatiuh.igeofcu.unam.mx*

# ANEXO 7.2

**Ejemplo de procesamiento inicial de la información MT realizado por la estación V-5 Phoenix, utilizada en el presente trabajo.**

Archivo procesam. informacion Sondeo-21
Equipo: V-5 Phoenix
PLOT-COMP YUC-21, WGT=Rhova CUT=.00, REF=LOCH, ROT=0 deg.
STACKS:

| | | | | | | | |
|---|---|---|---|---|---|---|---|
| 918 | 918 | 918 | 918 | 459 | 459 | 894 | 894 |
| 910 | 910 | 455 | 455 | 9900 | 9900 | 4725 | 4725 |
| 2300 | 2300 | 1080 | 1080 | 525 | 525 | 240 | 240 |
| 100 | 100 | 42 | 42 | 42 | 42 | 16 | 16 |
| 6 | 6 | 3 | 3 | 0 | 0 | 0 | 0 |

PARAM.#1 RHOxy ohm-m.

| | | | | |
|---|---|---|---|---|
| 9.65E+00 | 1.21E+01 | 1.11E+01 | 6.51E+00 | 7.35E+00 |
| 6.38E+00 | 3.32E+00 | 2.66E+00 | 2.62E+00 | 1.04E+01 |
| 1.35E+01 | 1.12E+01 | 2.12E+00 | 1.86E+00 | 1.52E+00 |
| 4.73E-01 | 2.13E-01 | 1.34E-01 | 4.52E-01 | 4.38E-02 |
| 3.61E+00 | 4.95E-01 | 1.04E+00 | 6.30E+00 | 1.77E+02 |
| 1.74E+02 | 8.59E+00 | 3.58E+00 | 4.86E+00 | 5.06E+00 |
| 2.07E+01 | 1.01E+01 | 2.17E+01 | 3.40E+01 | 1.64E+00 |
| 2.30E+02 | 0.00E+00 | 0.00E+00 | 0.00E+00 | 0.00E+00 |

PARAM.#2 RHOyx ohm-m.

| | | | | |
|---|---|---|---|---|
| 8.03E+00 | 1.17E+01 | 1.27E+01 | 1.05E+01 | 8.60E+00 |
| 9.24E+00 | 6.31E+00 | 4.05E+00 | 4.32E+00 | 1.30E+01 |
| 4.12E+00 | 1.12E+01 | 2.71E+00 | 2.42E+00 | 2.06E+00 |
| 1.73E+00 | 1.46E+00 | 1.35E+00 | 2.22E+00 | 4.00E-01 |
| 3.96E+00 | 1.62E+00 | 1.86E+00 | 1.44E+01 | 7.95E+02 |
| 5.60E+02 | 2.66E+01 | 6.21E+00 | 6.17E+00 | 8.27E+00 |
| 3.32E+01 | 1.52E+01 | 3.65E+01 | 1.64E+01 | 2.13E+02 |
| 6.33E+01 | 0.00E+00 | 0.00E+00 | 0.00E+00 | 0.00E+00 |

PARAM.#3 PHASExy Deg.

| | | | | |
|---|---|---|---|---|
| 9.59E+01 | 7.86E+01 | 8.34E+01 | 8.55E+01 | 6.12E+01 |
| 6.30E+01 | 2.76E+01 | 8.08E+01 | 9.90E+01 | 1.14E+02 |
| 9.16E+01 | 1.07E+02 | 6.11E+01 | 6.12E+01 | 5.96E+01 |
| 3.97E+01 | 1.46E+02 | 1.08E+02 | 5.22E+01 | 1.80E+02 |
| -1.51E+02 | -1.59E+02 | 4.15E+01 | -6.97E+01 | 3.42E+01 |
| -1.61E+02 | -1.36E+02 | 2.60E+01 | 1.11E+01 | 1.13E+01 |
| -7.28E+01 | -2.95E+00 | 7.98E+00 | 2.49E+00 | 1.27E+02 |
| 3.38E+01 | 0.00E+00 | 0.00E+00 | 0.00E+00 | 0.00E+00 |

PARAM.#4 PHASEyx Deg.

| | | | | |
|---|---|---|---|---|
| -9.31E+01 | -1.03E+02 | -1.09E+02 | -1.10E+02 | -1.13E+02 |
| -1.14E+02 | -1.16E+02 | -1.06E+02 | -1.06E+02 | -1.14E+02 |
| -1.03E+02 | -9.21E+01 | -1.18E+02 | -1.19E+02 | -1.19E+02 |
| -1.23E+02 | -1.21E+02 | -1.23E+02 | -1.42E+02 | -1.30E+02 |
| -1.52E+02 | -1.34E+02 | -1.16E+02 | 6.19E+01 | 1.33E+02 |
| -4.57E+01 | -7.79E+01 | -1.65E+02 | -1.66E+02 | -1.66E+02 |
| -1.65E+02 | -1.40E+02 | -1.75E+02 | -1.71E+02 | -9.87E+01 |
| 1.32E+02 | 0.00E+00 | 0.00E+00 | 0.00E+00 | 0.00E+00 |

PARAM.#5 Z SKEW

| | | | | |
|---|---|---|---|---|
| 4.47E-02 | 2.63E-02 | 4.52E-02 | 5.15E-02 | 3.66E-02 |
| 5.12E-02 | 8.00E-02 | 9.83E-02 | 8.57E-02 | 6.67E-02 |
| 4.97E-02 | 7.10E-02 | 2.97E-02 | 3.86E-02 | 4.15E-02 |
| 1.71E-01 | 7.30E-01 | 4.05E-01 | 1.41E-01 | 1.53E+00 |
| 1.06E+01 | 7.09E-01 | 4.22E-01 | 3.99E-01 | 8.75E-01 |
| 7.29E-01 | 1.81E+00 | 1.69E-01 | 6.42E-02 | 3.23E-02 |
| 1.28E+00 | 4.09E-01 | 7.27E-02 | 3.23E-01 | 4.46E-01 |
| 9.07E-01 | 0.00E+00 | 0.00E+00 | 0.00E+00 | 0.00E+00 |

PARAM.#6 Z BETA

| | | | | |
|---|---|---|---|---|
| 3.95E-01 | 5.78E-01 | 3.58E-01 | 2.62E-01 | 4.32E-01 |
| 4.45E-01 | 2.25E-01 | 6.28E-01 | 3.72E-01 | 1.46E-01 |
| 1.60E-01 | 3.92E-01 | 4.25E-01 | 4.78E-01 | 4.19E-01 |
| 4.11E-01 | 5.32E-01 | 4.96E-01 | 3.62E-01 | 5.14E-01 |
| 2.41E-01 | 2.40E-01 | 4.37E-01 | 1.02E+00 | 6.87E-01 |
| 7.73E-01 | 5.03E-01 | 1.02E+00 | 5.67E-01 | 2.45E-01 |
| 5.07E-01 | 5.05E-01 | 4.47E-01 | 4.40E-01 | 5.30E-01 |
| 5.13E-01 | 0.00E+00 | 0.00E+00 | 0.00E+00 | 0.00E+00 |

PARAM.#7 Z-STRIKE Deg.

| | | | | |
|---|---|---|---|---|
| -2.03E+01 | -3.24E+01 | 1.71E+01 | 1.44E+01 | 1.38E+00 |
| -8.14E+00 | 1.77E+01 | 5.02E+00 | 8.13E+00 | 1.76E+01 |
| 1.78E+01 | 2.13E+01 | -1.87E+01 | -2.03E+01 | -1.44E+01 |
| 1.06E+01 | 1.58E+01 | 1.08E+01 | -7.37E+00 | 3.03E+01 |
| 3.04E+00 | 2.37E+00 | 1.08E+01 | 5.28E+01 | -2.50E+01 |
| 5.11E+01 | 1.08E+01 | -5.65E+00 | 4.23E+00 | -1.67E+01 |
| 2.35E+01 | -8.20E+00 | -2.03E+01 | -2.08E+01 | -6.34E+00 |
| 2.58E+00 | 0.00E+00 | 0.00E+00 | 0.00E+00 | 0.00E+00 |

PARAM.#8 Var TIP MAG

| | | | | |
|---|---|---|---|---|
| 1.43E-04 | 1.19E-05 | 2.38E-05 | 2.78E-05 | 2.07E-05 |
| 7.92E-05 | 4.48E-05 | 2.24E-05 | 1.75E-05 | 3.95E-05 |
| 1.15E-04 | 3.68E-04 | 1.61E-06 | 2.37E-06 | 3.97E-06 |
| 1.14E-05 | 6.18E-05 | 2.14E-05 | 4.07E-04 | 3.27E-04 |
| 2.42E-03 | 1.97E-03 | 7.96E-03 | 2.43E-02 | 7.33E-01 |
| 1.40E-01 | 3.30E-01 | 5.90E-02 | 7.56E-02 | 3.54E-03 |
| 1.06E-01 | 8.30E-02 | 1.59E-02 | 1.48E-01 | 7.14E+00 |
| 7.73E-01 | 0.00E+00 | 0.00E+00 | 0.00E+00 | 0.00E+00 |

PARAM.#9 TIP MAG

| | | | | |
|---|---|---|---|---|
| 2.71E-02 | 2.08E-02 | 1.24E-02 | 1.33E-02 | 8.88E-03 |
| 1.63E-02 | 1.14E-02 | 8.98E-03 | 8.14E-03 | 1.12E-02 |
| 1.19E-02 | 1.25E-02 | 7.26E-03 | 8.50E-03 | 9.91E-03 |
| 1.03E-02 | 1.20E-02 | 9.28E-03 | 2.71E-02 | 1.89E-02 |
| 1.05E-02 | 1.33E-02 | 9.45E-02 | 1.21E-01 | 2.83E-01 |
| 1.41E-01 | 8.62E-02 | 7.59E-02 | 6.42E-02 | 7.49E-02 |
| 2.09E-01 | 2.00E-01 | 1.17E-01 | 1.87E-01 | 1.63E-01 |
| 1.58E-01 | 0.00E+00 | 0.00E+00 | 0.00E+00 | 0.00E+00 |

PARAM.#10 RHOxx/ Ind-Vr

| | | | | |
|---|---|---|---|---|
| 0.00E+00 | 0.00E+00 | 0.00E+00 | 0.00E+00 | 0.00E+00 |
| 0.00E+00 | 0.00E+00 | 0.00E+00 | 0.00E+00 | 0.00E+00 |
| 0.00E+00 | 0.00E+00 | 0.00E+00 | 0.00E+00 | 0.00E+00 |
| 0.00E+00 | 0.00E+00 | 0.00E+00 | 0.00E+00 | 0.00E+00 |
| 0.00E+00 | 0.00E+00 | 0.00E+00 | 0.00E+00 | 0.00E+00 |
| 0.00E+00 | 0.00E+00 | 0.00E+00 | 0.00E+00 | 0.00E+00 |
| 0.00E+00 | 0.00E+00 | 0.00E+00 | 0.00E+00 | 0.00E+00 |
| 0.00E+00 | 0.00E+00 | 0.00E+00 | 0.00E+00 | 0.00E+00 |

PARAM.#11 RHOyy/ Ind-Vi

| | | | | |
|---|---|---|---|---|
| 0.00E+00 | 0.00E+00 | 0.00E+00 | 0.00E+00 | 0.00E+00 |
| 0.00E+00 | 0.00E+00 | 0.00E+00 | 0.00E+00 | 0.00E+00 |
| 0.00E+00 | 0.00E+00 | 0.00E+00 | 0.00E+00 | 0.00E+00 |
| 0.00E+00 | 0.00E+00 | 0.00E+00 | 0.00E+00 | 0.00E+00 |
| 0.00E+00 | 0.00E+00 | 0.00E+00 | 0.00E+00 | 0.00E+00 |
| 0.00E+00 | 0.00E+00 | 0.00E+00 | 0.00E+00 | 0.00E+00 |
| 0.00E+00 | 0.00E+00 | 0.00E+00 | 0.00E+00 | 0.00E+00 |
| 0.00E+00 | 0.00E+00 | 0.00E+00 | 0.00E+00 | 0.00E+00 |

PARAM.#12 TIP PHASE Deg

| | | | | |
|---|---|---|---|---|
| 1.33E+02 | 3.49E+01 | -1.37E+01 | -4.00E+01 | 2.63E+01 |
| -6.30E+00 | -1.43E+01 | 2.28E+01 | -5.26E+00 | 2.00E+01 |
| -1.59E+01 | 6.73E+00 | 4.41E+01 | 4.24E+01 | 2.68E+01 |
| 8.66E+01 | 1.34E+02 | -5.86E+01 | 1.45E+02 | -3.64E+01 |
| 1.71E+01 | 1.24E+02 | -2.39E+01 | 9.31E+01 | 8.76E+01 |
| 5.30E+01 | 1.06E+02 | 1.19E+02 | 1.37E+02 | 1.29E+02 |
| -5.58E+01 | -1.50E+02 | -5.42E+01 | 1.29E+02 | -9.72E+01 |
| 9.41E+01 | 0.00E+00 | 0.00E+00 | 0.00E+00 | 0.00E+00 |

PARAM.#13 PHAxx/ I-VrAng

| | | | | |
|---|---|---|---|---|
| 0.00E+00 | 0.00E+00 | 0.00E+00 | 0.00E+00 | 0.00E+00 |
| 0.00E+00 | 0.00E+00 | 0.00E+00 | 0.00E+00 | 0.00E+00 |
| 0.00E+00 | 0.00E+00 | 0.00E+00 | 0.00E+00 | 0.00E+00 |
| 0.00E+00 | 0.00E+00 | 0.00E+00 | 0.00E+00 | 0.00E+00 |
| 0.00E+00 | 0.00E+00 | 0.00E+00 | 0.00E+00 | 0.00E+00 |
| 0.00E+00 | 0.00E+00 | 0.00E+00 | 0.00E+00 | 0.00E+00 |
| 0.00E+00 | 0.00E+00 | 0.00E+00 | 0.00E+00 | 0.00E+00 |
| 0.00E+00 | 0.00E+00 | 0.00E+00 | 0.00E+00 | 0.00E+00 |

PARAM.#14 TIP SKEW

| | | | | |
|---|---|---|---|---|
| 2.92E-01 | 7.57E-01 | 4.29E-01 | 2.39E-01 | 1.96E-01 |
| 8.30E-01 | 1.21E-01 | 9.48E-01 | 4.90E-01 | 2.21E-01 |
| 2.76E-01 | 7.76E-01 | 9.54E-01 | 7.05E-01 | 4.16E-01 |
| 5.63E-01 | 7.19E-03 | 9.92E-01 | 3.48E-01 | 8.49E-01 |
| 4.41E-01 | 3.82E-01 | 8.55E-01 | 6.66E-01 | 8.88E-01 |
| 8.62E-01 | 3.66E-01 | 1.50E-01 | 3.04E-01 | 6.90E-01 |
| 8.83E-01 | 7.59E-02 | 7.83E-01 | 2.92E-01 | 5.37E-01 |
| 6.36E-01 | 0.00E+00 | 0.00E+00 | 0.00E+00 | 0.00E+00 |

PARAM.#15 TIP BETA

| | | | | |
|---|---|---|---|---|
| 2.40E+00 | 1.00E+00 | 3.32E+00 | 1.45E+00 | 3.89E-01 |
| 6.62E-01 | 5.19E+00 | 9.92E-01 | 2.36E+00 | 1.49E+00 |
| 1.98E+00 | 1.57E+00 | 1.35E+00 | 2.12E+00 | 3.95E+00 |
| 3.24E+00 | 5.21E+00 | 8.84E-01 | 2.09E+00 | 5.56E-01 |
| 1.71E+00 | 4.80E+00 | 1.21E+00 | 7.62E-01 | 1.50E+00 |
| 9.63E-01 | 1.51E+00 | 7.84E-01 | 1.12E+00 | 2.00E+00 |
| 7.43E-01 | 7.03E-01 | 7.22E-01 | 6.41E+00 | 1.10E+00 |
| 9.40E-01 | 0.00E+00 | 0.00E+00 | 0.00E+00 | 0.00E+00 |

PARAM.#16 TIP STRIKE

| | | | | |
|---|---|---|---|---|
| 2.24E+02 | 1.53E+02 | 1.20E+02 | 4.94E+01 | 2.01E+02 |
| 1.77E+02 | 1.12E+02 | 1.48E+02 | 1.19E+02 | 1.23E+02 |
| 6.43E+01 | 1.46E+02 | 1.13E+02 | 1.05E+02 | 8.36E+01 |
| 8.56E+01 | 1.30E+01 | 3.68E+01 | -5.30E+00 | 1.18E+02 |
| 1.06E+02 | 1.61E+02 | 5.30E+01 | 2.12E+02 | 1.41E+02 |
| 1.40E+02 | 1.40E+02 | 1.00E+02 | 3.55E+01 | 4.33E+01 |
| -5.23E+00 | -3.51E+01 | -1.69E+01 | -6.62E-01 | -1.91E+01 |
| 2.17E+02 | 0.00E+00 | 0.00E+00 | 0.00E+00 | 0.00E+00 |

PARAM.#17 ORD COH Hx-Ey

| | | | | |
|---|---|---|---|---|
| 7.92E-01 | 8.77E-01 | 8.74E-01 | 8.91E-01 | 8.92E-01 |
| 8.07E-01 | 5.73E-01 | 5.00E-01 | 4.96E-01 | 6.53E-01 |
| 4.12E-01 | 4.41E-01 | 5.41E-01 | 2.78E-01 | 4.29E-01 |
| 2.93E-01 | 2.41E-01 | 1.65E-01 | 1.07E-01 | 8.31E-02 |
| 9.54E-02 | 7.30E-02 | 7.89E-02 | 2.05E-02 | 1.22E-01 |
| 1.48E-01 | 1.16E-01 | 6.83E-01 | 5.71E-01 | 3.69E-01 |
| 3.80E-01 | 4.56E-01 | 8.85E-01 | 8.77E-01 | 8.70E-01 |
| 7.77E-01 | 0.00E+00 | 0.00E+00 | 0.00E+00 | 0.00E+00 |

| PARAM.#18 | ORD | COH | Hy-Ex | |
|---|---|---|---|---|
| 6.83E-01 | 7.40E-01 | 6.63E-01 | 5.99E-01 | 7.66E-01 |
| 6.15E-01 | 4.23E-01 | 3.79E-01 | 4.63E-01 | 6.78E-01 |
| 5.80E-01 | 5.75E-01 | 7.43E-01 | 5.10E-01 | 5.41E-01 |
| 2.63E-01 | 1.25E-01 | 1.05E-01 | 1.07E-01 | 2.67E-02 |
| 1.76E-01 | 6.09E-02 | 9.59E-02 | 2.67E-02 | 1.21E-01 |
| 1.01E-01 | 1.30E-01 | 7.18E-01 | 5.99E-01 | 4.76E-01 |
| 2.20E-01 | 6.70E-01 | 9.80E-01 | 9.78E-01 | 8.20E-01 |
| 8.03E-01 | 0.00E+00 | 0.00E+00 | 0.00E+00 | 0.00E+00 |

| PARAM.#19 | ORD | COH | Hx-Rx | |
|---|---|---|---|---|
| 1.00E+00 | 1.00E+00 | 1.00E+00 | 1.00E+00 | 1.00E+00 |
| 1.00E+00 | 1.00E+00 | 1.00E+00 | 1.00E+00 | 1.00E+00 |
| 1.00E+00 | 1.00E+00 | 1.00E+00 | 1.00E+00 | 1.00E+00 |
| 1.00E+00 | 1.00E+00 | 1.00E+00 | 1.00E+00 | 1.00E+00 |
| 1.00E+00 | 1.00E+00 | 1.00E+00 | 1.00E+00 | 1.00E+00 |
| 1.00E+00 | 1.00E+00 | 1.00E+00 | 1.00E+00 | 1.00E+00 |
| 1.00E+00 | 1.00E+00 | 1.00E+00 | 1.00E+00 | 1.00E+00 |
| 1.00E+00 | 0.00E+00 | 0.00E+00 | 0.00E+00 | 0.00E+00 |

| PARAM.#20 | ORD | COH | Hy-Ry | |
|---|---|---|---|---|
| 1.00E+00 | 1.00E+00 | 1.00E+00 | 1.00E+00 | 1.00E+00 |
| 1.00E+00 | 1.00E+00 | 1.00E+00 | 1.00E+00 | 1.00E+00 |
| 1.00E+00 | 1.00E+00 | 1.00E+00 | 1.00E+00 | 1.00E+00 |
| 1.00E+00 | 1.00E+00 | 1.00E+00 | 1.00E+00 | 1.00E+00 |
| 1.00E+00 | 1.00E+00 | 1.00E+00 | 1.00E+00 | 1.00E+00 |
| 1.00E+00 | 1.00E+00 | 1.00E+00 | 1.00E+00 | 1.00E+00 |
| 1.00E+00 | 1.00E+00 | 1.00E+00 | 1.00E+00 | 1.00E+00 |
| 1.00E+00 | 0.00E+00 | 0.00E+00 | 0.00E+00 | 0.00E+00 |

| PARAM.#21 | Ex | COH | Hx-Hy | |
|---|---|---|---|---|
| 6.84E-01 | 7.40E-01 | 6.69E-01 | 6.07E-01 | 7.67E-01 |
| 6.15E-01 | 4.40E-01 | 3.81E-01 | 4.68E-01 | 7.02E-01 |
| 5.89E-01 | 5.83E-01 | 7.43E-01 | 5.10E-01 | 5.41E-01 |
| 2.76E-01 | 2.06E-01 | 1.33E-01 | 1.13E-01 | 1.69E-01 |
| 1.79E-01 | 6.94E-02 | 1.01E-01 | 6.50E-02 | 1.87E-01 |
| 2.73E-01 | 1.74E-01 | 7.33E-01 | 5.99E-01 | 4.78E-01 |
| 2.98E-01 | 7.11E-01 | 9.82E-01 | 9.87E-01 | 9.10E-01 |
| 9.69E-01 | 0.00E+00 | 0.00E+00 | 0.00E+00 | 0.00E+00 |

| PARAM.#22 | Ey | COH | Hx-Hy | |
|---|---|---|---|---|
| 7.98E-01 | 8.78E-01 | 8.75E-01 | 8.92E-01 | 8.92E-01 |
| 8.08E-01 | 5.85E-01 | 5.03E-01 | 4.98E-01 | 6.84E-01 |
| 4.34E-01 | 4.45E-01 | 5.43E-01 | 2.80E-01 | 4.31E-01 |
| 2.94E-01 | 2.43E-01 | 1.66E-01 | 1.07E-01 | 9.22E-02 |
| 1.04E-01 | 7.41E-02 | 8.42E-02 | 4.79E-02 | 2.11E-01 |
| 2.71E-01 | 1.36E-01 | 6.83E-01 | 5.71E-01 | 3.71E-01 |
| 4.73E-01 | 4.70E-01 | 8.91E-01 | 8.89E-01 | 8.72E-01 |
| 8.86E-01 | 0.00E+00 | 0.00E+00 | 0.00E+00 | 0.00E+00 |

| PARAM.#23 | Hx | COH | Ex-Ey | |
|---|---|---|---|---|
| 7.93E-01 | 8.77E-01 | 8.78E-01 | 8.96E-01 | 8.92E-01 |
| 8.08E-01 | 5.78E-01 | 5.10E-01 | 4.98E-01 | 6.77E-01 |
| 4.13E-01 | 4.50E-01 | 7.13E-01 | 5.91E-01 | 5.79E-01 |
| 5.01E-01 | 3.97E-01 | 3.17E-01 | 3.65E-01 | 3.53E-01 |
| 1.36E-01 | 1.83E-01 | 3.03E-01 | 2.41E-01 | 2.56E-01 |
| 4.46E-01 | 7.60E-01 | 9.11E-01 | 8.92E-01 | 7.66E-01 |
| 7.91E-01 | 5.47E-01 | 9.12E-01 | 8.96E-01 | 9.38E-01 |
| 7.78E-01 | 0.00E+00 | 0.00E+00 | 0.00E+00 | 0.00E+00 |

PARAM.#24 Hy COH Ex-Ey

| | | | | |
|---|---|---|---|---|
| 6.91E-01 | 7.53E-01 | 6.84E-01 | 6.17E-01 | 7.67E-01 |
| 6.15E-01 | 4.67E-01 | 4.06E-01 | 4.66E-01 | 7.08E-01 |
| 5.81E-01 | 5.83E-01 | 8.47E-01 | 7.97E-01 | 6.55E-01 |
| 3.98E-01 | 1.47E-01 | 1.56E-01 | 3.76E-01 | 1.10E-01 |
| 2.65E-01 | 1.30E-01 | 4.01E-01 | 2.31E-01 | 1.55E-01 |
| 4.86E-01 | 7.12E-01 | 9.39E-01 | 9.24E-01 | 8.49E-01 |
| 4.06E-01 | 7.78E-01 | 9.89E-01 | 9.86E-01 | 8.94E-01 |
| 8.17E-01 | 0.00E+00 | 0.00E+00 | 0.00E+00 | 0.00E+00 |

PARAM.#25 Hz COH Ex-Ey

| | | | | |
|---|---|---|---|---|
| 5.66E-02 | 7.05E-02 | 7.73E-02 | 1.13E-01 | 5.54E-02 |
| 1.06E-01 | 8.40E-02 | 7.19E-02 | 3.19E-02 | 8.24E-02 |
| 1.40E-01 | 1.06E-01 | 6.79E-02 | 6.40E-02 | 4.21E-02 |
| 1.17E-02 | 4.29E-02 | 6.27E-03 | 3.84E-02 | 9.00E-02 |
| 1.24E-01 | 4.89E-02 | 1.47E-01 | 9.06E-02 | 2.33E-01 |
| 1.10E-01 | 1.62E-01 | 7.50E-01 | 5.03E-01 | 6.10E-01 |
| 4.53E-01 | 6.10E-01 | 9.30E-01 | 8.04E-01 | 7.00E-01 |
| 9.71E-01 | 0.00E+00 | 0.00E+00 | 0.00E+00 | 0.00E+00 |

PARAM.#26 Hz COH Hx-Hy

| | | | | |
|---|---|---|---|---|
| 6.72E-02 | 7.29E-02 | 7.58E-02 | 1.18E-01 | 6.93E-02 |
| 1.63E-01 | 1.15E-01 | 1.15E-01 | 1.22E-01 | 1.06E-01 |
| 1.46E-01 | 1.05E-01 | 7.36E-02 | 7.67E-02 | 7.41E-02 |
| 5.30E-02 | 5.57E-02 | 6.71E-02 | 1.51E-01 | 9.75E-02 |
| 3.41E-02 | 5.64E-02 | 2.52E-01 | 1.81E-01 | 2.60E-01 |
| 2.16E-01 | 3.10E-01 | 7.40E-01 | 5.67E-01 | 7.64E-01 |
| 6.45E-01 | 6.09E-01 | 9.41E-01 | 9.16E-01 | 5.82E-01 |
| 8.78E-01 | 0.00E+00 | 0.00E+00 | 0.00E+00 | 0.00E+00 |

PARAM.#27 Hx Gam/Hz^.5

| | | | | |
|---|---|---|---|---|
| 4.41E-04 | 5.20E-04 | 7.00E-04 | 6.48E-04 | 8.31E-04 |
| 8.32E-04 | 8.84E-04 | 9.22E-04 | 1.12E-03 | 1.21E-03 |
| 1.40E-03 | 1.27E-03 | 7.55E-04 | 7.95E-04 | 9.58E-04 |
| 1.15E-03 | 1.58E-03 | 1.99E-03 | 2.48E-03 | 2.96E-03 |
| 3.72E-03 | 5.60E-03 | 5.94E-03 | 5.31E-03 | 5.25E-03 |
| 1.82E-02 | 5.96E-02 | 2.14E-01 | 3.81E-01 | 6.34E-01 |
| 7.00E-01 | 7.04E-01 | 9.53E-01 | 1.54E+00 | 1.40E+00 |
| 4.85E+00 | 0.00E+00 | 0.00E+00 | 0.00E+00 | 0.00E+00 |

PARAM.#28 Hy Gam/Hz^.5

| | | | | |
|---|---|---|---|---|
| 4.78E-04 | 4.91E-04 | 6.24E-04 | 6.59E-04 | 6.50E-04 |
| 6.55E-04 | 1.11E-03 | 1.10E-03 | 1.29E-03 | 1.63E-03 |
| 1.61E-03 | 1.71E-03 | 1.03E-03 | 1.12E-03 | 1.25E-03 |
| 1.50E-03 | 2.16E-03 | 2.74E-03 | 3.24E-03 | 3.65E-03 |
| 5.17E-03 | 5.82E-03 | 6.58E-03 | 5.22E-03 | 5.88E-03 |
| 1.53E-02 | 4.81E-02 | 1.79E-01 | 3.11E-01 | 6.11E-01 |
| 2.91E-01 | 8.12E-01 | 2.58E+00 | 2.90E+00 | 2.72E+00 |
| 3.09E+00 | 0.00E+00 | 0.00E+00 | 0.00E+00 | 0.00E+00 |

PARAM.#29 Hz Gam/Hz^.5

| | | | | |
|---|---|---|---|---|
| 1.65E-04 | 1.27E-04 | 1.08E-04 | 7.93E-05 | 7.64E-05 |
| 7.62E-05 | 9.29E-05 | 8.15E-05 | 7.60E-05 | 1.37E-04 |
| 1.16E-04 | 1.63E-04 | 1.00E-04 | 1.12E-04 | 1.30E-04 |
| 2.27E-04 | 3.66E-04 | 3.22E-04 | 5.43E-04 | 6.68E-04 |
| 1.16E-03 | 1.34E-03 | 2.34E-03 | 2.47E-03 | 5.22E-03 |
| 7.02E-03 | 1.40E-02 | 2.43E-02 | 5.26E-02 | 6.12E-02 |
| 1.26E-01 | 1.71E-01 | 2.91E-01 | 3.45E-01 | 3.31E-01 |
| 9.30E-01 | 0.00E+00 | 0.00E+00 | 0.00E+00 | 0.00E+00 |

PARAM.#30 Ex uV/M/Hz^.5

| | | | | |
|---|---|---|---|---|
| 9.64E-02 | 8.75E-02 | 9.75E-02 | 7.60E-02 | 5.07E-02 |
| 5.18E-02 | 7.13E-02 | 6.36E-02 | 4.94E-02 | 7.40E-02 |
| 7.85E-02 | 6.69E-02 | 1.11E-02 | 1.44E-02 | 1.10E-02 |
| 1.40E-02 | 2.23E-02 | 2.70E-02 | 4.08E-02 | 3.15E-02 |
| 7.51E-02 | 7.77E-02 | 7.24E-02 | 2.05E-01 | 3.22E-01 |
| 3.94E-01 | 4.58E-01 | 2.13E-01 | 3.67E-01 | 8.56E-01 |
| 1.06E+00 | 8.56E-01 | 2.03E+00 | 2.37E+00 | 1.39E+00 |
| 4.23E+00 | 0.00E+00 | 0.00E+00 | 0.00E+00 | 0.00E+00 |

PARAM.#31 Ey uV/M/Hz^.5

| | | | | |
|---|---|---|---|---|
| 7.10E-02 | 7.84E-02 | 8.80E-02 | 6.33E-02 | 5.96E-02 |
| 5.86E-02 | 6.30E-02 | 5.04E-02 | 5.14E-02 | 6.28E-02 |
| 5.20E-02 | 6.51E-02 | 1.23E-02 | 2.05E-02 | 1.21E-02 |
| 1.71E-02 | 2.12E-02 | 3.25E-02 | 6.70E-02 | 4.31E-02 |
| 1.12E-01 | 1.15E-01 | 1.20E-01 | 3.53E-01 | 5.56E-01 |
| 6.82E-01 | 7.73E-01 | 3.31E-01 | 5.90E-01 | 1.40E+00 |
| 1.96E+00 | 1.14E+00 | 1.06E+00 | 1.37E+00 | 2.95E+00 |
| 4.49E+00 | 0.00E+00 | 0.00E+00 | 0.00E+00 | 0.00E+00 |

PARAM.#32 Hx N/(Sig+N)

| | | | | |
|---|---|---|---|---|
| 1.00E+00 | 1.00E+00 | 1.00E+00 | 1.00E+00 | 1.00E+00 |
| 1.00E+00 | 1.00E+00 | 1.00E+00 | 1.00E+00 | 1.00E+00 |
| 1.00E+00 | 1.00E+00 | 1.00E+00 | 1.00E+00 | 1.00E+00 |
| 1.00E+00 | 1.00E+00 | 1.00E+00 | 1.00E+00 | 1.00E+00 |
| 1.00E+00 | 1.00E+00 | 1.00E+00 | 1.00E+00 | 1.00E+00 |
| 1.00E+00 | 1.00E+00 | 1.00E+00 | 1.00E+00 | 1.00E+00 |
| 1.00E+00 | 1.00E+00 | 1.00E+00 | 1.00E+00 | 1.00E+00 |
| 1.00E+00 | 0.00E+00 | 0.00E+00 | 0.00E+00 | 0.00E+00 |

PARAM.#33 Hy N/(Sig+N)

| | | | | |
|---|---|---|---|---|
| 1.00E+00 | 1.00E+00 | 1.00E+00 | 1.00E+00 | 1.00E+00 |
| 1.00E+00 | 1.00E+00 | 1.00E+00 | 1.00E+00 | 1.00E+00 |
| 1.00E+00 | 1.00E+00 | 1.00E+00 | 1.00E+00 | 1.00E+00 |
| 1.00E+00 | 1.00E+00 | 1.00E+00 | 1.00E+00 | 1.00E+00 |
| 1.00E+00 | 1.00E+00 | 1.00E+00 | 1.00E+00 | 1.00E+00 |
| 1.00E+00 | 1.00E+00 | 1.00E+00 | 1.00E+00 | 1.00E+00 |
| 1.00E+00 | 1.00E+00 | 1.00E+00 | 1.00E+00 | 1.00E+00 |
| 1.00E+00 | 0.00E+00 | 0.00E+00 | 0.00E+00 | 0.00E+00 |

PARAM.#34 Hz N/(Sig+N)

| | | | | |
|---|---|---|---|---|
| 4.39E-03 | 6.61E-03 | 6.31E-03 | 1.64E-02 | 4.28E-03 |
| 2.50E-02 | 1.47E-02 | 1.80E-02 | 6.49E-03 | 1.12E-02 |
| 3.25E-02 | 1.77E-02 | 6.20E-03 | 6.41E-03 | 6.12E-03 |
| 1.08E-03 | 6.98E-03 | 1.23E-03 | 1.46E-02 | 5.84E-02 |
| 1.27E-02 | 1.45E-02 | 5.30E-02 | 4.39E-02 | 1.21E-02 |
| 2.94E-02 | 7.92E-02 | 5.76E-01 | 3.08E-01 | 5.43E-01 |
| 2.33E-01 | 4.98E-01 | 8.81E-01 | 7.75E-01 | 9.40E-02 |
| 1.21E+00 | 0.00E+00 | 0.00E+00 | 0.00E+00 | 0.00E+00 |

PARAM.#35 Ex N/(Sig+N)

| | | | | |
|---|---|---|---|---|
| 4.68E-01 | 5.48E-01 | 4.47E-01 | 3.68E-01 | 5.88E-01 |
| 3.79E-01 | 1.94E-01 | 1.45E-01 | 2.19E-01 | 4.92E-01 |
| 3.47E-01 | 3.40E-01 | 5.53E-01 | 2.60E-01 | 2.93E-01 |
| 7.64E-02 | 4.25E-02 | 1.77E-02 | 1.29E-02 | 2.85E-02 |
| 3.19E-02 | 4.81E-03 | 1.01E-02 | 4.22E-03 | 3.50E-02 |
| 7.48E-02 | 3.02E-02 | 5.38E-01 | 3.59E-01 | 2.29E-01 |
| 8.86E-02 | 5.05E-01 | 9.65E-01 | 9.75E-01 | 8.28E-01 |
| 9.40E-01 | 0.00E+00 | 0.00E+00 | 0.00E+00 | 0.00E+00 |

PARAM.#36 Ey N/(Sig+N)

| | | | | |
|---|---|---|---|---|
| 6.37E-01 | 7.70E-01 | 7.66E-01 | 7.96E-01 | 7.96E-01 |
| 6.52E-01 | 3.42E-01 | 2.53E-01 | 2.48E-01 | 4.67E-01 |
| 1.88E-01 | 1.98E-01 | 2.95E-01 | 7.85E-02 | 1.86E-01 |
| 8.63E-02 | 5.89E-02 | 2.76E-02 | 1.14E-02 | 8.50E-03 |
| 1.07E-02 | 5.50E-03 | 7.09E-03 | 2.30E-03 | 4.46E-02 |
| 7.34E-02 | 1.85E-02 | 4.67E-01 | 3.26E-01 | 1.38E-01 |
| 2.24E-01 | 2.21E-01 | 7.93E-01 | 7.90E-01 | 7.60E-01 |
| 7.85E-01 | 0.00E+00 | 0.00E+00 | 0.00E+00 | 0.00E+00 |

PARAM.#37 Var LOG RHOxy

| | | | | |
|---|---|---|---|---|
| 1.89E-03 | 8.37E-04 | 1.50E-03 | 1.66E-03 | 1.72E-03 |
| 6.17E-03 | 1.09E-02 | 1.29E-02 | 1.07E-02 | 3.76E-03 |
| 2.90E-02 | 3.63E-02 | 6.35E-05 | 2.40E-04 | 4.78E-04 |
| 3.56E-03 | 4.54E-02 | 1.10E-01 | 3.90E-01 | 3.73E+00 |
| 7.66E-01 | 6.48E+00 | 1.31E+01 | 7.79E+01 | 1.47E+01 |
| 4.51E+00 | 9.43E+01 | 4.74E-01 | 4.65E-01 | 3.57E-01 |
| 4.67E+00 | 6.27E-01 | 1.14E-02 | 3.16E-02 | 8.16E+01 |
| 1.78E-01 | 0.00E+00 | 0.00E+00 | 0.00E+00 | 0.00E+00 |

PARAM.#38 Var LOG RHOyx

| | | | | |
|---|---|---|---|---|
| 9.89E-04 | 3.13E-04 | 3.60E-04 | 2.39E-04 | 6.15E-04 |
| 1.89E-03 | 5.74E-03 | 6.62E-03 | 9.02E-03 | 4.10E-03 |
| 6.95E-02 | 7.68E-02 | 1.79E-04 | 9.40E-04 | 8.29E-04 |
| 2.43E-03 | 1.10E-02 | 2.94E-02 | 3.64E-01 | 1.19E+00 |
| 3.05E+00 | 4.67E+00 | 2.48E+01 | 9.83E+01 | 1.22E+01 |
| 2.96E+00 | 5.71E+01 | 5.27E-01 | 6.59E-01 | 6.09E-01 |
| 1.48E+00 | 1.55E+00 | 8.02E-02 | 6.40E-01 | 1.49E+01 |
| 1.05E+00 | 0.00E+00 | 0.00E+00 | 0.00E+00 | 0.00E+00 |

PARAM.#39 Var PHASExy

| | | | | |
|---|---|---|---|---|
| 8.21E+00 | 3.64E+00 | 6.54E+00 | 7.21E+00 | 7.48E+00 |
| 2.68E+01 | 4.76E+01 | 5.61E+01 | 4.66E+01 | 1.64E+01 |
| 1.26E+02 | 1.58E+02 | 2.76E-01 | 1.04E+00 | 2.08E+00 |
| 1.55E+01 | 1.98E+02 | 4.77E+02 | 1.70E+03 | 1.62E+04 |
| 3.33E+03 | 2.82E+04 | 5.70E+04 | 3.39E+05 | 6.42E+04 |
| 1.96E+04 | 4.11E+05 | 2.06E+03 | 2.02E+03 | 1.56E+03 |
| 2.03E+04 | 2.73E+03 | 4.97E+01 | 1.37E+02 | 3.55E+05 |
| 7.74E+02 | 0.00E+00 | 0.00E+00 | 0.00E+00 | 0.00E+00 |

PARAM.#40 Var PHASEyx

| | | | | |
|---|---|---|---|---|
| 4.30E+00 | 1.36E+00 | 1.57E+00 | 1.04E+00 | 2.68E+00 |
| 8.21E+00 | 2.50E+01 | 2.88E+01 | 3.93E+01 | 1.78E+01 |
| 3.02E+02 | 3.34E+02 | 7.77E-01 | 4.09E+00 | 3.61E+00 |
| 1.06E+01 | 4.80E+01 | 1.28E+02 | 1.58E+03 | 5.17E+03 |
| 1.33E+04 | 2.03E+04 | 1.08E+05 | 4.28E+05 | 5.29E+04 |
| 1.29E+04 | 2.48E+05 | 2.30E+03 | 2.87E+03 | 2.65E+03 |
| 6.42E+03 | 6.76E+03 | 3.49E+02 | 2.79E+03 | 6.47E+04 |
| 4.57E+03 | 0.00E+00 | 0.00E+00 | 0.00E+00 | 0.00E+00 |

PARAM.#41 Var TIP PHASE

| | | | | |
|---|---|---|---|---|
| 4.23E+06 | 5.35E+09 | 1.27E+10 | 1.95E+06 | 4.76E+08 |
| 2.23E+07 | 6.69E+06 | 1.05E+08 | 3.13E+07 | 9.90E+06 |
| 2.73E+08 | 2.27E+13 | 8.89E+08 | 3.34E+09 | 1.60E+07 |
| 1.59E+04 | 6.38E+06 | 8.30E+12 | 4.29E+06 | 5.18E+09 |
| 2.22E+10 | 2.50E+08 | 6.29E+08 | 1.80E+05 | 4.44E+04 |
| 8.03E+08 | 1.54E+12 | 5.84E+05 | 1.48E+06 | 1.42E+05 |
| 3.66E+05 | 3.79E+04 | 4.65E+05 | 3.53E+05 | 1.62E+06 |
| 7.55E+05 | 0.00E+00 | 0.00E+00 | 0.00E+00 | 0.00E+00 |

PARAM.#42 PHAyy/I-ViAng

| | | | | |
|---|---|---|---|---|
| 0.00E+00 | 0.00E+00 | 0.00E+00 | 0.00E+00 | 0.00E+00 |
| 0.00E+00 | 0.00E+00 | 0.00E+00 | 0.00E+00 | 0.00E+00 |
| 0.00E+00 | 0.00E+00 | 0.00E+00 | 0.00E+00 | 0.00E+00 |
| 0.00E+00 | 0.00E+00 | 0.00E+00 | 0.00E+00 | 0.00E+00 |
| 0.00E+00 | 0.00E+00 | 0.00E+00 | 0.00E+00 | 0.00E+00 |
| 0.00E+00 | 0.00E+00 | 0.00E+00 | 0.00E+00 | 0.00E+00 |
| 0.00E+00 | 0.00E+00 | 0.00E+00 | 0.00E+00 | 0.00E+00 |
| 0.00E+00 | 0.00E+00 | 0.00E+00 | 0.00E+00 | 0.00E+00 |

PARAM.#43 RHOxy BosInv.

| | | | | |
|---|---|---|---|---|
| 4.85E-02 | 3.35E-01 | 5.09E-01 | 8.71E-01 | 1.41E+00 |
| 1.94E+00 | 4.19E+00 | 2.20E+00 | 8.60E-01 | 2.10E-02 |
| 3.60E-02 | 5.85E-02 | 2.69E-01 | 6.27E-01 | 8.79E-01 |
| 7.51E-01 | 5.44E-02 | 1.20E-03 | 1.18E-03 | 6.95E-04 |
| 9.76E-01 | 8.52E+01 | 2.45E+02 | 2.94E+02 | 4.55E+02 |
| 1.15E+04 | 1.28E+04 | 3.48E+03 | 1.06E+03 | 2.04E+01 |
| 1.59E+03 | 2.03E+03 | 3.30E+03 | 6.82E+02 | 1.03E+01 |
| 1.53E+01 | 0.00E+00 | 0.00E+00 | 0.00E+00 | 0.00E+00 |

PARAM.#44 RHOyx BosInv.

| | | | | |
|---|---|---|---|---|
| 2.84E-01 | 9.48E-01 | 1.58E+00 | 2.79E+00 | 3.13E+00 |
| 3.14E+00 | 2.97E+00 | 2.03E+00 | 1.33E+00 | 1.62E+00 |
| 1.52E+00 | 1.44E+00 | 9.60E-01 | 1.19E+00 | 1.13E+00 |
| 1.06E+00 | 9.17E-01 | 8.42E-01 | 1.23E+00 | 9.20E-01 |
| 2.03E+00 | 1.61E+00 | 2.20E+00 | 1.76E-02 | 1.39E-01 |
| 9.32E-01 | 1.15E+00 | 3.25E+00 | 1.06E+01 | 3.55E+01 |
| 6.21E+01 | 4.67E+01 | 9.26E+01 | 8.46E+01 | 9.29E+01 |
| 3.04E-01 | 0.00E+00 | 0.00E+00 | 0.00E+00 | 0.00E+00 |

PARAM.#45 Zxx Re (ROT)

| | | | | |
|---|---|---|---|---|
| 4.85E+00 | -1.24E+00 | 1.23E+01 | 1.12E+01 | -1.51E+00 |
| 2.20E+00 | -6.26E+00 | -2.64E+00 | -3.16E-01 | 1.12E+01 |
| -4.10E-01 | 3.59E+00 | 1.15E-01 | 1.64E-01 | 6.67E-02 |
| -1.89E-01 | 1.19E+00 | 4.17E-01 | -5.67E-01 | 1.18E+00 |
| -5.06E-01 | 1.41E-01 | 2.13E-01 | 1.66E+00 | -5.79E+00 |
| 6.12E+00 | 9.95E-01 | -1.43E-01 | -4.92E-02 | -3.91E-02 |
| -2.78E-01 | -1.02E-01 | -1.58E-01 | 3.25E-01 | -6.57E-01 |
| 3.69E-01 | 0.00E+00 | 0.00E+00 | 0.00E+00 | 0.00E+00 |

PARAM.#46 Zxx Im (ROT)

| | | | | |
|---|---|---|---|---|
| 7.97E+00 | 3.55E-01 | -1.00E-01 | 3.38E+00 | 1.94E+00 |
| 5.92E-01 | 7.94E+00 | 5.95E-01 | 3.02E+00 | 1.16E-01 |
| -5.75E+00 | -3.58E+00 | -2.39E-01 | -2.52E-01 | -3.38E-02 |
| 1.06E+00 | 2.09E+00 | 1.09E+00 | 3.01E-01 | 1.40E+00 |
| 2.68E-01 | 4.43E-01 | -3.55E-01 | 2.14E+00 | 7.65E+00 |
| -5.77E+00 | -1.87E+00 | -2.31E-01 | 3.03E-03 | 4.07E-02 |
| -1.73E-01 | -3.63E-01 | 5.98E-02 | -1.52E-01 | -2.82E-01 |
| 6.69E-01 | 0.00E+00 | 0.00E+00 | 0.00E+00 | 0.00E+00 |

PARAM.#47 Zxy Re (ROT)

| | | | | |
|---|---|---|---|---|
| -1.41E+01 | 2.60E+01 | 1.20E+01 | 5.41E+00 | 2.86E+01 |
| 2.18E+01 | 2.50E+01 | 3.50E+00 | -2.76E+00 | -1.25E+01 |
| -7.99E-01 | -6.61E+00 | 3.86E+00 | 3.12E+00 | 2.41E+00 |
| 1.77E+00 | -1.04E+00 | -2.64E-01 | 7.99E-01 | -3.51E-01 |
| -2.29E+00 | -7.78E-01 | 7.38E-01 | 7.32E-01 | 7.54E+00 |
| -7.40E+00 | -1.01E+00 | 7.13E-01 | 7.40E-01 | 6.54E-01 |
| 3.25E-01 | 6.65E-01 | 7.90E-01 | 8.64E-01 | -9.27E-02 |
| 1.32E+00 | 0.00E+00 | 0.00E+00 | 0.00E+00 | 0.00E+00 |

PARAM.#48 Zxy Im (ROT)

| | | | | |
|---|---|---|---|---|
| 1.35E+02 | 1.29E+02 | 1.03E+02 | 6.82E+01 | 5.20E+01 |
| 4.27E+01 | 1.31E+01 | 2.16E+01 | 1.75E+01 | 2.79E+01 |
| 2.85E+01 | 2.15E+01 | 6.99E+00 | 5.68E+00 | 4.11E+00 |
| 1.47E+00 | 7.12E-01 | 8.26E-01 | 1.03E+00 | 7.70E-04 |
| -1.25E+00 | -3.03E-01 | 6.54E-01 | -1.97E+00 | 5.13E+00 |
| -2.55E+00 | -9.94E-01 | 3.48E-01 | 1.45E-01 | 1.31E-01 |
| -1.05E+00 | -3.42E-02 | 1.11E-01 | 3.75E-02 | 1.24E-01 |
| 8.83E-01 | 0.00E+00 | 0.00E+00 | 0.00E+00 | 0.00E+00 |

PARAM.#49 Zyx Re (ROT)

| | | | | |
|---|---|---|---|---|
| -6.67E+00 | -2.91E+01 | -3.60E+01 | -3.02E+01 | -2.49E+01 |
| -2.38E+01 | -1.72E+01 | -7.50E+00 | -6.38E+00 | -1.41E+01 |
| -3.55E+00 | -8.28E-01 | -4.28E+00 | -3.60E+00 | -2.74E+00 |
| -2.42E+00 | -1.69E+00 | -1.50E+00 | -2.29E+00 | -6.80E-01 |
| -2.41E+00 | -1.05E+00 | -5.84E-01 | 1.49E+00 | -1.32E+01 |
| 9.81E+00 | 5.23E-01 | -1.01E+00 | -8.24E-01 | -8.28E-01 |
| -1.35E+00 | -6.27E-01 | -1.03E+00 | -5.93E-01 | -2.66E-01 |
| -5.53E-01 | 0.00E+00 | 0.00E+00 | 0.00E+00 | 0.00E+00 |

PARAM.#50 Zyx Im (ROT)

| | | | | |
|---|---|---|---|---|
| -1.24E+02 | -1.27E+02 | -1.05E+02 | -8.14E+01 | -5.92E+01 |
| -5.25E+01 | -3.49E+01 | -2.59E+01 | -2.18E+01 | -3.12E+01 |
| -1.53E+01 | -2.24E+01 | -7.94E+00 | -6.43E+00 | -4.84E+00 |
| -3.68E+00 | -2.84E+00 | -2.31E+00 | -1.76E+00 | -8.14E-01 |
| -1.28E+00 | -1.08E+00 | -1.18E+00 | 2.80E+00 | 1.41E+01 |
| -1.00E+01 | -2.44E+00 | -2.79E-01 | -2.07E-01 | -2.05E-01 |
| -3.73E-01 | -5.25E-01 | -8.17E-02 | -9.45E-02 | -1.74E+00 |
| 6.24E-01 | 0.00E+00 | 0.00E+00 | 0.00E+00 | 0.00E+00 |

PARAM.#51 Zyy Re (ROT)

| | | | | |
|---|---|---|---|---|
| 5.08E+00 | 1.49E+00 | -3.88E+00 | -4.18E+00 | -1.24E+00 |
| 1.01E+00 | 1.30E+00 | -2.11E+00 | -1.80E+00 | -7.64E+00 |
| -1.14E+00 | -8.24E-01 | 2.90E-01 | 2.97E-01 | 1.51E-01 |
| 1.29E-01 | -2.64E-02 | -6.05E-04 | 3.63E-02 | -3.49E-01 |
| -8.30E-01 | 2.58E-01 | -6.91E-02 | -2.54E-01 | 1.47E+01 |
| -1.47E+01 | -2.06E+00 | -6.65E-02 | -5.26E-02 | 8.75E-02 |
| -3.92E-01 | 5.85E-02 | 4.31E-02 | 1.17E-01 | -1.11E-01 |
| 3.92E-02 | 0.00E+00 | 0.00E+00 | 0.00E+00 | 0.00E+00 |

PARAM.#52 Zyy Im (ROT)

| | | | | |
|---|---|---|---|---|
| -1.40E+01 | -7.22E+00 | 4.75E+00 | 2.59E-01 | 1.65E+00 |
| 3.75E+00 | -6.71E+00 | -1.22E+00 | -3.71E-01 | -1.89E+00 |
| 4.21E+00 | 2.08E+00 | 5.40E-01 | 5.20E-01 | 4.03E-01 |
| 7.97E-02 | 2.77E-01 | 2.06E-01 | -4.79E-02 | -3.39E-01 |
| -3.24E-01 | -1.48E-02 | -5.89E-01 | -3.46E+00 | 1.00E+01 |
| -4.85E+00 | -1.80E+00 | 3.03E-03 | -1.80E-02 | -3.23E-02 |
| -2.03E+00 | -2.01E-01 | 6.80E-03 | -1.60E-02 | -5.16E-02 |
| 9.96E-01 | 0.00E+00 | 0.00E+00 | 0.00E+00 | 0.00E+00 |

PARAM.#53 Zxx VAR (ROT)

| | | | | |
|---|---|---|---|---|
| 1.09E+02 | 3.43E+01 | 3.39E+01 | 2.13E+01 | 9.82E+00 |
| 2.33E+01 | 3.62E+01 | 2.33E+01 | 1.19E+01 | 1.69E+01 |
| 8.34E+01 | 8.89E+01 | 2.00E-02 | 5.33E-02 | 4.92E-02 |
| 8.48E-02 | 3.59E-01 | 4.13E-01 | 2.97E+00 | 1.85E+00 |
| 2.67E+01 | 1.30E+01 | 4.14E+01 | 8.85E+02 | 4.08E+03 |
| 5.14E+02 | 3.28E+02 | 5.49E-01 | 4.65E-01 | 3.92E-01 |
| 2.60E+00 | 9.83E-01 | 1.41E-01 | 2.21E-01 | 1.95E+01 |
| 4.81E-01 | 0.00E+00 | 0.00E+00 | 0.00E+00 | 0.00E+00 |

PARAM.#54 Zxy VAR (ROT)

| | | | | |
|---|---|---|---|---|
| 9.27E+01 | 3.86E+01 | 4.26E+01 | 2.06E+01 | 1.61E+01 |
| 3.76E+01 | 2.31E+01 | 1.64E+01 | 8.92E+00 | 9.32E+00 |
| 6.23E+01 | 4.86E+01 | 1.07E-02 | 2.67E-02 | 2.88E-02 |
| 5.02E-02 | 1.92E-01 | 2.18E-01 | 1.75E+00 | 1.22E+00 |
| 1.38E+01 | 1.20E+01 | 3.38E+01 | 9.16E+02 | 3.25E+03 |
| 7.31E+02 | 5.03E+02 | 7.91E-01 | 7.01E-01 | 4.22E-01 |
| 1.50E+01 | 7.37E-01 | 1.93E-02 | 6.26E-02 | 5.18E+00 |
| 1.19E+00 | 0.00E+00 | 0.00E+00 | 0.00E+00 | 0.00E+00 |

PARAM.#55 Zyx VAR (ROT)

| | | | | |
|---|---|---|---|---|
| 4.04E+01 | 1.40E+01 | 1.17E+01 | 4.77E+00 | 6.73E+00 |
| 1.67E+01 | 2.30E+01 | 1.28E+01 | 1.24E+01 | 1.27E+01 |
| 4.56E+01 | 1.02E+02 | 3.85E-02 | 1.36E-01 | 6.80E-02 |
| 1.25E-01 | 3.19E-01 | 5.90E-01 | 8.04E+00 | 3.54E+00 |
| 6.01E+01 | 2.82E+01 | 1.15E+02 | 2.63E+03 | 1.20E+04 |
| 1.55E+03 | 9.44E+02 | 1.53E+00 | 1.26E+00 | 1.17E+00 |
| 7.62E+00 | 2.75E+00 | 2.28E-01 | 6.13E-01 | 1.23E+02 |
| 1.93E+00 | 0.00E+00 | 0.00E+00 | 0.00E+00 | 0.00E+00 |

PARAM.#56 Zyy VAR (ROT)

| | | | | |
|---|---|---|---|---|
| 3.43E+01 | 1.57E+01 | 1.47E+01 | 4.61E+00 | 1.10E+01 |
| 2.69E+01 | 1.47E+01 | 8.99E+00 | 9.33E+00 | 7.03E+00 |
| 3.41E+01 | 5.60E+01 | 2.06E-02 | 6.78E-02 | 3.98E-02 |
| 7.40E-02 | 1.71E-01 | 3.13E-01 | 4.74E+00 | 2.33E+00 |
| 3.10E+01 | 2.60E+01 | 9.35E+01 | 2.72E+03 | 9.56E+03 |
| 2.20E+03 | 1.45E+03 | 2.20E+00 | 1.90E+00 | 1.26E+00 |
| 4.42E+01 | 2.07E+00 | 3.11E-02 | 1.74E-01 | 3.27E+01 |
| 4.78E+00 | 0.00E+00 | 0.00E+00 | 0.00E+00 | 0.00E+00 |

PARAM.#57 ROT Angle Deg

| | | | | |
|---|---|---|---|---|
| 1.00E-04 | 1.00E-04 | 1.00E-04 | 1.00E-04 | 1.00E-04 |
| 1.00E-04 | 1.00E-04 | 1.00E-04 | 1.00E-04 | 1.00E-04 |
| 1.00E-04 | 1.00E-04 | 1.00E-04 | 1.00E-04 | 1.00E-04 |
| 1.00E-04 | 1.00E-04 | 1.00E-04 | 1.00E-04 | 1.00E-04 |
| 1.00E-04 | 1.00E-04 | 1.00E-04 | 1.00E-04 | 1.00E-04 |
| 1.00E-04 | 1.00E-04 | 1.00E-04 | 1.00E-04 | 1.00E-04 |
| 1.00E-04 | 1.00E-04 | 1.00E-04 | 1.00E-04 | 1.00E-04 |
| 1.00E-04 | 0.00E+00 | 0.00E+00 | 0.00E+00 | 0.00E+00 |

PARAM.#58 DEPTHxy Km.

| | | | | |
|---|---|---|---|---|
| 1.75E+00 | 1.84E+00 | 1.93E+00 | 1.96E+00 | 2.01E+00 |
| 2.04E+00 | 2.08E+00 | 2.06E+00 | 2.09E+00 | 2.23E+00 |
| 2.44E+00 | 2.61E+00 | 2.58E+00 | 2.50E+00 | 2.44E+00 |
| 2.40E+00 | 2.33E+00 | 2.21E+00 | 2.30E+00 | 2.25E+00 |
| 2.57E+00 | 2.64E+00 | 2.96E+00 | 3.06E+00 | 3.58E+00 |
| 4.01E+00 | 4.12E+00 | 3.90E+00 | 3.73E+00 | 3.75E+00 |
| 3.97E+00 | 4.08E+00 | 4.28E+00 | 4.38E+00 | 4.33E+00 |
| 4.56E+00 | 0.00E+00 | 0.00E+00 | 0.00E+00 | 0.00E+00 |

PARAM.#59 DEPTHyx Km.

| | | | | |
|---|---|---|---|---|
| 1.71E+00 | 1.81E+00 | 1.92E+00 | 2.00E+00 | 2.07E+00 |
| 2.11E+00 | 2.16E+00 | 2.17E+00 | 2.20E+00 | 2.32E+00 |
| 2.41E+00 | 2.54E+00 | 2.51E+00 | 2.54E+00 | 2.50E+00 |
| 2.53E+00 | 2.58E+00 | 2.61E+00 | 2.72E+00 | 2.69E+00 |
| 2.86E+00 | 2.89E+00 | 3.09E+00 | 3.25E+00 | 3.79E+00 |
| 4.26E+00 | 4.39E+00 | 4.11E+00 | 3.87E+00 | 3.85E+00 |
| 4.06E+00 | 4.18E+00 | 4.38E+00 | 4.39E+00 | 4.67E+00 |
| 4.77E+00 | 0.00E+00 | 0.00E+00 | 0.00E+00 | 0.00E+00 |

PARAM.#60 LOG10(Frq) Hz

| | | | | |
|---|---|---|---|---|
| 2.58E+00 | 2.46E+00 | 2.28E+00 | 2.16E+00 | 1.98E+00 |
| 1.86E+00 | 1.68E+00 | 1.56E+00 | 1.38E+00 | 1.26E+00 |
| 1.08E+00 | 9.54E-01 | 7.78E-01 | 6.53E-01 | 4.77E-01 |
| 3.52E-01 | 1.76E-01 | 5.12E-02 | -1.25E-01 | -2.50E-01 |
| -4.26E-01 | -5.51E-01 | -7.27E-01 | -8.52E-01 | -1.03E+00 |
| -1.15E+00 | -1.33E+00 | -1.45E+00 | -1.63E+00 | -1.76E+00 |
| -1.93E+00 | -2.06E+00 | -2.23E+00 | -2.36E+00 | -2.53E+00 |
| -2.66E+00 | 0.00E+00 | 0.00E+00 | 0.00E+00 | 0.00E+00 |

# ANEXO 7.3

## Ejemplo de archivo de entrada al programa de inversión 1-D Occam

| Archivo | entrada al | programa | inversión 1D | OCCAM |
|---|---|---|---|---|
| | Descripción: | Los datos se | alternan de | la forma: |
| | Período (s) | Log10 RoaX | Var.Log10 ( | RoaXY) |
| | Período (s) | Fase | Var. Fase | |
| | | SONDEO# 9 | | |
| | 2.60E-03 | 1.115786 | 0.0018 | |
| | 2.60E-03 | 68.66288 | 0.8899 | |
| | 3.47E-03 | 1.204739 | 0.0016 | |
| | 3.47E-03 | 56.06478 | 0.4567 | |
| | 5.21E-03 | 1.192241 | 0.0004 | |
| | 5.21E-03 | 59.88708 | 0.7562 | |
| | 6.94E-03 | 1.093765 | 0.0002 | |
| | 6.94E-03 | 58.04021 | 0.3765 | |
| | 1.04E-02 | 1.055312 | 0.0004 | |
| | 1.04E-02 | 58.14627 | 0.4927 | |
| | 1.39E-02 | 1.055888 | 0.0006 | |
| | 1.39E-02 | 56.30276 | 0.6529 | |
| | 2.08E-02 | 0.9788459 | 0.0003 | |
| | 2.08E-02 | 61.86835 | 0.3021 | |
| | 2.78E-02 | 1.029041 | 0.0005 | |
| | 2.78E-02 | 60.01435 | 0.0934 | |
| | 4.17E-02 | 0.9977598 | 0.0007 | |
| | 4.17E-02 | 59.70089 | 0.0846 | |
| | 5.56E-02 | 0.9656936 | 0.0005 | |
| | 5.56E-02 | 60.42682 | 0.0754 | |
| | 0.0833334 | 0.8875075 | 0.0006 | |
| | 0.0833334 | 59.79062 | 0.0873 | |
| | 0.1111111 | 0.8157036 | 0.0008 | |
| | 0.1111111 | 59.80855 | 0.0948 | |
| | 0.1666667 | 0.6883973 | 0.0007 | |
| | 0.1666667 | 56.68941 | 0.2314 | |
| | 0.2222223 | 0.6443813 | 0.0007 | |
| | 0.2222223 | 54.06315 | 0.4327 | |
| | 0.3333333 | 0.6482979 | 0.0008 | |
| | 0.3333333 | 49.96964 | 0.5234 | |
| | 0.4444445 | 0.6236245 | 0.0006 | |
| | 0.4444445 | 47.74221 | 0.7325 | |
| | 0.6666666 | 0.5841405 | 0.0007 | |
| | 0.6666666 | 46.27504 | 0.8234 | |
| | 0.8888889 | 0.555925 | 0.0006 | |
| | 0.8888889 | 42.9839 | 0.6207 | |
| | 1.333333 | 0.5453403 | 0.0008 | |
| | 1.333333 | 38.58821 | 0.5083 | |
| | 1.777778 | 0.562124 | 0.0032 | |
| | 1.777778 | 33.16581 | 0.4378 | |
| | 2.666667 | 0.6643911 | 0.0026 | |
| | 2.666667 | 28.60236 | 0.7473 | |
| | 3.555556 | 0.7523699 | 0.0035 | |
| | 3.555556 | 21.31173 | 0.5483 | |
| | 5.333335 | 0.9463836 | 0.0045 | |
| | 5.333335 | 16.8269 | 0.8239 | |
| | 7.111111 | 0.8371858 | 0.0055 | |
| | 7.111111 | 17.53139 | 0.9749 | |
| | 10.66667 | 1.212757 | 0.0079 | |
| | 10.66667 | 15.84145 | 0.8456 | |
| | 14.22224 | 1.475746 | 0.0084 | |

| | | |
|---|---|---|
| 14.22224 | 10.50968 | 0.9345 |
| 21.33335 | 1.57041 | 0.0068 |
| 21.33335 | 11.94511 | 0.9945 |
| 28.44448 | 1.603717 | 0.0089 |
| 28.44448 | 7.116302 | 0.7439 |
| 42.6667 | 1.67342 | 0.0123 |
| 42.6667 | 9.920245 | 0.4172 |
| 56.88898 | 1.790838 | 0.0144 |
| 56.88898 | 9.857864 | 0.1937 |
| 85.33338 | 2.017533 | 0.0203 |
| 85.33338 | 8.282001 | 0.0635 |
| 113.7779 | 2.135054 | 0.0408 |
| 113.7779 | 12.75439 | 0.1323 |
| 170.6668 | 2.508064 | 0.0502 |
| 170.6668 | 2.652706 | 0.2385 |
| 227.5552 | 2.556189 | 0.0417 |
| 227.5552 | 2.914624 | 0.2016 |
| 341.3337 | 2.547929 | 0.0568 |
| 341.3337 | 10.59355 | 0.1993 |
| 455.1106 | 2.705835 | 0.0687 |
| 455.1106 | 19.62536 | 0.3935 |
| 682.667 | 2.62157 | 0.0579 |
| 682.667 | 15.84916 | 0.5872 |
| 910.2237 | 2.451299 | 0.0952 |
| 910.2237 | 17.01727 | 0.4327 |
| 1365.334 | 3.082502 | 0.1008 |
| 1365.334 | 45.40141 | 0.3289 |
| 1820.442 | 2.621606 | 0.0996 |
| 1820.442 | 52.2898 | 0.8657 |

# ANEXO 7.4

## Ejemplo de archivo de entrada al programa de inversión 2-D por Relajación Rápida.

Fichero de entrada al program de inversion 2D-IRR Smith and Booker

TEM CHICXULU MODEL FOR PROFILE AA

modes 2 2
stations, freq. 11 39

SITE POSITIONS (m)

| | 38100 | 30100 | 20100 | 12800 | 8300 | 3700 | -1700 | -6300 | -10800 | -20800 | -38100 | |
|---|---|---|---|---|---|---|---|---|---|---|---|---|
| FREQ | TE | | APP. | RES. | | | | | | | | |
| 384 | | 13.07 | 9.85 | 7.19 | 6.55 | 6.9 | 9.77 | 11.39 | 10.81 | 8.58 | 16.05 | [illegible] |
| 288 | | 15.62 | 13.73 | 12.62 | 11.75 | 11.87 | 14.37 | 7.99 | 20.49 | 15.56 | 15.75 | [illegible] |
| 192 | | 14.84 | 14.31 | 14.32 | 13.5 | 12.1 | 17.78 | 7.35 | 23.46 | 17.96 | 15.32 | [illegible] |
| 144 | | 12.45 | 15.66 | 13.81 | 12.5 | 11.84 | 15.81 | 6.82 | 22.19 | 12.1 | 12.97 | [illegible] |
| 96 | | 9.26 | 12 | 12.9 | 10.84 | 10.36 | 14.46 | 8.18 | 18.74 | 12.25 | 11.11 | [illegible] |
| 72 | | 8.83 | 9.43 | 12.91 | 10.77 | 9.4 | 14.41 | 7.77 | 16.91 | 10.34 | 10.24 | [illegible] |
| 48 | | 6.75 | 5.35 | 9.5 | 9.3 | 9.18 | 9.2 | 5.1 | 13.67 | 7.99 | 8.11 | [illegible] |
| 36 | | 5.72 | 5.05 | 7.27 | 8.94 | 8.97 | 8.9 | 4.52 | 10.88 | 7.47 | 7.75 | [illegible] |
| 24 | | 5.55 | 4.45 | 8.58 | 8.88 | 11.45 | 7.06 | 3.87 | 8.07 | 6.81 | 6.65 | [illegible] |
| 18 | | 6.55 | 3.67 | 7.04 | 8.21 | 9.86 | 8.67 | 3.4 | 7.56 | 6.18 | 5.55 | [illegible] |
| 12 | | 7.13 | 4.36 | 6.99 | 7.76 | 10.77 | 7.75 | 3.05 | 7.1 | 5.61 | 4.55 | [illegible] |
| 9 | | 7.05 | 3.55 | 5.92 | 5.57 | 10.41 | 6.65 | 2.37 | 6.77 | 4.29 | 3.49 | [illegible] |
| 6 | | 5.11 | 2.98 | 6.04 | 5.57 | 4.94 | 5.56 | 2.36 | 4.38 | 3.57 | 3.08 | [illegible] |
| 4.5 | | 5.14 | 2.76 | 5.75 | 5.08 | 4.73 | 4.78 | 2.13 | 3.99 | 3.06 | 2.94 | [illegible] |
| 3 | | 4.88 | 2.73 | 5.94 | 4.74 | 4.79 | 4.02 | 1.81 | 3.55 | 2.9 | 2.8 | [illegible] |
| 2.25 | | 4.48 | 2.38 | 6.18 | 4.59 | 4.79 | 3.64 | 1.62 | 3.22 | 2.43 | 2.61 | [illegible] |
| 1.5 | | 3.98 | 2.59 | 6.62 | 4.59 | 4.92 | 3.42 | 1.46 | 2.99 | 2.06 | 2.23 | [illegible] |
| 1.125 | | 3.46 | 2.4 | 6.69 | 4.51 | 5.04 | 3.32 | 1.34 | 2.64 | 1.99 | 2.03 | [illegible] |
| 0.75 | | 2.97 | 1.81 | 6.67 | 4.08 | 4.84 | 3.44 | 1.22 | 2.36 | 2 | 1.9 | [illegible] |
| 0.5625 | | 2.64 | 1.61 | 6.71 | 4.1 | 4.6 | 3.43 | 1.18 | 2.25 | 1.81 | 1.82 | [illegible] |
| 0.375 | | 2.22 | 1.36 | 7.04 | 4.55 | 4.87 | 3.38 | 1.06 | 2.01 | 1.77 | 1.78 | [illegible] |
| 0.2813 | | 1.91 | 1.33 | 7.53 | 4.4 | 5.55 | 3.35 | 0.92 | 1.98 | 1.74 | 2.02 | [illegible] |
| 0.1875 | | 1.75 | 1.37 | 8.51 | 6.91 | 5.74 | 3.85 | 1.11 | 2.4 | 1.68 | 2.13 | [illegible] |
| 0.1406 | | 1.43 | 1.41 | 9.88 | 6.16 | 7.63 | 4.46 | 1.35 | 2.58 | 2.61 | 2.5 | [illegible] |
| 0.0938 | | 2.55 | 1.65 | 14.35 | 8.5 | 12.97 | 6.36 | 1.78 | 3.71 | 2.84 | 2.95 | [illegible] |
| 0.0703 | | 3.01 | 1.85 | 16.08 | 10.06 | 9.93 | 6.33 | 2.1 | 6.22 | 3.33 | 3.29 | [illegible] |
| 0.0469 | | 3.83 | 2.05 | 17.84 | 9.78 | 12.08 | 8.83 | 2.85 | 9.06 | 4.8 | 3.31 | [illegible] |
| 0.0352 | | 4.3 | 2.37 | 21.3 | 9.99 | 14.91 | 10.5 | 3.48 | 8.22 | 6.2 | 5.03 | [illegible] |
| 0.0234 | | 7.07 | 3.44 | 25.22 | 12.1 | 14.3 | 14.13 | 4.09 | 11.75 | 7.57 | 6.33 | [illegible] |
| 0.0176 | | 8.54 | 5.02 | 31.48 | 12.44 | 23.89 | 21.2 | 4.8 | 14.88 | 9.79 | 7.95 | [illegible] |
| 0.0117 | | 10.66 | 7.05 | 34.18 | 11.86 | 23.45 | 19.85 | 4.9 | 23.93 | 13.03 | 8.87 | [illegible] |
| 0.0088 | | 15.58 | 7.51 | 42.35 | 12.04 | 23.91 | 25.43 | 4.94 | 27.29 | 15.29 | 11.15 | [illegible] |
| 0.0059 | | 19.7 | 11.91 | 54.05 | 11.98 | 31.62 | 31.72 | 4.23 | 30.5 | 20.81 | 6.74 | [illegible] |
| 0.0044 | | 25.5 | 12.53 | 61.96 | 7.37 | 38.2 | 45.5 | 3.46 | 35.5 | 26.83 | 7.99 | [illegible] |
| 0.0029 | | 35.5 | 38.26 | 86.45 | 5.18 | 71.65 | 73.26 | 2.17 | 45.5 | 32.55 | 5.08 | [illegible] |
| 0.0022 | | 44.51 | 40.5 | 108.25 | 4.7 | 49.75 | 100.5 | 1.51 | 52.58 | 37.89 | 4.65 | [illegible] |
| 0.0015 | | 60.45 | 45.5 | 131.73 | 4.5 | 61.98 | 186.27 | 1.05 | 55.5 | 43.43 | 3.26 | [illegible] |
| 0.0011 | | 53.29 | 50.5 | 118.57 | 4.2 | 65.5 | 222.13 | 0.6 | 65.5 | 50.29 | 1.05 | [illegible] |
| 0.0007 | | 60.5 | 55.5 | 138.88 | 3.5 | 70.5 | 250.5 | 0.3 | 70.5 | 72.91 | 1.05 | [illegible] |

| FREQ. | TE | ERROR (APP. | | RES.) | | | | | | | |
|---|---|---|---|---|---|---|---|---|---|---|---|
| 384 | 0.01 | 0.03 | 0.02 | 0 | 0.02 | 0.02 | 0.1 | 0.02 | 0.05 | | |
| 288 | 0.01 | 0.02 | 0.01 | 0 | 0.01 | 0.01 | 0.05 | 0.01 | 0.03 | | |
| 192 | 0.01 | 0.04 | 0.01 | 0 | 0.03 | 0.01 | 0.17 | 0.01 | 0.1 | 0.08 | |
| 144 | 0.01 | 0.03 | 0 | 0 | 0.02 | 0.01 | 0.03 | 0.01 | 0.02 | 0.02 | |
| 96 | 0.01 | 0.07 | 0 | 0.01 | 0.02 | 0.01 | 0.01 | 0.01 | 0.01 | 0.01 | |
| 72 | 0.02 | 0.13 | 0 | 0.01 | 0.04 | 0.02 | 0.02 | 0.02 | 0.02 | 0.03 | |
| 48 | 0.5 | 0.13 | 0 | 0.01 | 0.05 | 0.05 | 0 | 0.02 | 0.01 | 0.02 | |
| 36 | 0.02 | 0 | 0.01 | 0.01 | 0.04 | 0.04 | 0 | 0.02 | 0.01 | | |
| 24 | 0.5 | 0 | 0.01 | 0 | 0.04 | 0.06 | 0 | 0.03 | 0 | | |
| 18 | 0.5 | 0.24 | 0.01 | 0 | 0.05 | 0.07 | 0 | 0.03 | 0.01 | | |
| 12 | 0.05 | 0.4 | 0.02 | 0.01 | 0.08 | 0.5 | 0.01 | 0.09 | 0.01 | | |
| 9 | 0.06 | 0 | 0.02 | 0.01 | 0.16 | 0.5 | 0.01 | 0.12 | 0.01 | 0.05 | |
| 6 | 0 | 0.01 | 0 | 0 | 0 | 0 | 0 | 0 | 0 | | |
| 4.5 | 0 | 0.01 | 0 | 0 | 0 | 0 | 0 | 0 | 0.01 | | |
| 3 | 0 | 0.02 | 0 | 0 | 0 | 0 | 0 | 0 | 0.01 | | |
| 2.25 | 0 | 0.02 | 0 | 0 | 0 | 0 | 0 | 0 | 0.01 | 0.01 | |
| 1.5 | 0 | 0.03 | 0 | 0 | 0.01 | 0 | 0.01 | 0 | 0.03 | 0.01 | |
| 1.125 | 0 | 0.03 | 0 | 0 | 0.01 | 0 | 0.01 | 0 | 0.04 | 0.02 | |
| 0.75 | 0 | 0.06 | 0 | 0.01 | 0.01 | 0 | 0.02 | 0.01 | 0.08 | 0.06 | |
| 0.5625 | 0 | 0.06 | 0 | 0.01 | 0.01 | 0 | 0.02 | 0.01 | 0.04 | 0.09 | |
| 0.375 | 0.01 | 0.15 | 0 | 0.03 | 0.03 | 0.01 | 0.01 | 0.01 | 0.05 | 0.17 | |
| 0.2813 | 0.02 | 0.2 | 0 | 0.06 | 0.04 | 0.02 | 0.02 | 0.03 | 0.07 | 0.35 | |
| 0.1875 | 0.5 | 0.5 | 0.01 | 0.21 | 0.15 | 0.05 | 0.03 | 0.06 | 0.24 | 1.18 | |
| 0.1406 | 0.15 | 0.74 | 0.01 | 0.37 | 0.19 | 0.08 | 0.03 | 0.08 | 0.13 | 0.5 | |
| 0.0938 | 0.5 | 0.5 | 0.03 | 0.5 | 0.43 | 0.24 | 0.02 | 0.23 | 0.04 | 0.5 | |
| 0.0703 | 0.24 | 0.5 | 0.02 | 0.19 | 0.42 | 0.35 | 0.01 | 0.31 | 0.03 | 0.37 | |
| 0.0469 | 0.22 | 0.5 | 0.01 | 0.06 | 0.48 | 0.87 | 0.02 | 0.55 | 0.02 | 0.09 | |
| 0.0352 | 0.13 | 0.4 | 0.01 | 0.03 | 0.22 | 0.5 | 0.01 | 0.28 | 0.01 | 0.1 | |
| 0.0234 | 0.05 | 0.15 | 0.01 | 0.02 | 0.31 | 0.28 | 0.01 | 0.08 | 0.01 | 0.11 | |
| 0.0176 | 0.04 | 0.06 | 0.01 | 0.06 | 0.08 | 0.12 | 0.01 | 0.04 | 0.01 | 0.06 | |
| 0.0117 | 0.04 | 0.11 | 0.01 | 0.03 | 0.09 | 0.16 | 0.01 | 0.14 | 0.01 | 0.11 | |
| 0.0088 | 0.02 | 0.04 | 0.01 | 0.06 | 0.04 | 0.12 | 0.01 | 0.09 | 0.02 | 0.12 | |
| 0.0059 | 0.02 | 0.08 | 0.01 | 0.13 | 0.14 | 0.09 | 0.02 | 0.5 | 0.02 | 0.21 | |
| 0.0044 | 0.5 | 0.04 | 0.01 | 0.59 | 0.3 | 0.5 | 0.02 | 0.5 | 0.03 | 0.17 | |
| 0.0029 | 0.5 | 0.06 | 0.03 | 0.29 | 0.29 | 0.27 | 0.03 | 0.5 | 0.03 | 0.26 | |
| 0.0022 | 0.07 | 0.5 | 0.01 | 0.34 | 0.24 | 0.5 | 0.03 | 0.26 | 0.06 | 0.09 | |
| 0.0015 | 0.05 | 0.5 | 0.05 | 0.5 | 0.26 | 0.64 | 0.5 | 0.5 | 0.07 | 0.26 | |
| 0.0011 | 0.12 | 0.5 | 0.02 | 0.5 | 0.5 | 0.66 | 0.58 | 0.5 | 0.1 | 0.44 | |
| 0.0007 | 0.5 | 0.5 | 0.16 | 0.5 | 0.5 | 0.5 | 0.5 | 0.5 | 0.49 | 0.5 | |

| FREQ. | TE | PHASE (deg.) | | | | | | | | | |
|---|---|---|---|---|---|---|---|---|---|---|---|
| 384 | 69.15 | 70.31 | 59.49 | 65.5 | 68.98 | 79.26 | 75.16 | 69.81 | 71.53 | [illegible] | [illegible] |
| 288 | 66.06 | 70.14 | 56.12 | 60.5 | 57.32 | 74.58 | 69.2 | 66.37 | 64.88 | [illegible] | [illegible] |
| 192 | 68.18 | 73.83 | 55.7 | 58.5 | 56.74 | 72.16 | 65.21 | 71.77 | 67.58 | [illegible] | [illegible] |
| 144 | 68.29 | 64.6 | 55.05 | 57.9 | 55.64 | 66.78 | 68.21 | 68.5 | 68.01 | [illegible] | [illegible] |
| 96 | 68.36 | 70.84 | 56.6 | 57.44 | 52.48 | 65.12 | 64.51 | 69.49 | 63.82 | [illegible] | [illegible] |
| 72 | 66.38 | 71.93 | 56.22 | 57.49 | 47.31 | 64.56 | 64.01 | 69.86 | 63.21 | [illegible] | [illegible] |
| 48 | 55.5 | 79.9 | 58.5 | 54.85 | 56.13 | 62.04 | 63.03 | 61.66 | 62.47 | [illegible] | [illegible] |
| 36 | 46.96 | 75.5 | 60.71 | 54.55 | 55.49 | 62.16 | 63.11 | 60.19 | 62.25 | [illegible] | [illegible] |
| 24 | 45.5 | 70.5 | 58.06 | 55.75 | 51.95 | 72.41 | 62.79 | 61.49 | 61.04 | [illegible] | [illegible] |
| 18 | 45.5 | 65.29 | 61.9 | 56.4 | 48.26 | 79.02 | 61.69 | 63.67 | 60.72 | [illegible] | [illegible] |
| 12 | 45.04 | 54.14 | 60.65 | 57.06 | 47.9 | 72.5 | 60.7 | 59.77 | 61.88 | [illegible] | [illegible] |
| 9 | 38.64 | 60.5 | 56.73 | 52.44 | 55.07 | 65.5 | 59.46 | 61.64 | 55.6 | [illegible] | [illegible] |
| 6 | 49.96 | 62.31 | 51.43 | 57.17 | 53.72 | 61.42 | 61.26 | 60.38 | 61.24 | [illegible] | [illegible] |
| 4.5 | 52.01 | 58.66 | 47.98 | 55.26 | 50.77 | 59.66 | 60.7 | 59.22 | 60.23 | [illegible] | [illegible] |
| 3 | 54.2 | 57.11 | 44.54 | 51.96 | 46.82 | 56.49 | 59.2 | 58.42 | 59.99 | [illegible] | [illegible] |
| 2.25 | 55.28 | 55.59 | 42.73 | 50.05 | 44.77 | 52.73 | 58.09 | 57.5 | 62.23 | [illegible] | [illegible] |
| 1.5 | 57.54 | 55.02 | 42.17 | 48.33 | 43.68 | 49.43 | 55.41 | 55.15 | 63.51 | [illegible] | [illegible] |
| 1.125 | 57.74 | 56.32 | 42.08 | 47.91 | 42.88 | 46.36 | 54.63 | 53.43 | 59.53 | [illegible] | [illegible] |
| 0.75 | 56.85 | 54.9 | 41.18 | 45.76 | 42.07 | 44.8 | 52.12 | 51.51 | 64.08 | [illegible] | [illegible] |
| 0.5625 | 55.88 | 61.72 | 39.16 | 44.17 | 39.62 | 43.44 | 49.43 | 49.22 | 50.43 | [illegible] | [illegible] |
| 0.375 | 54.28 | 55.1 | 37.16 | 40.57 | 39.24 | 38.78 | 46.32 | 45.76 | 42.93 | [illegible] | [illegible] |
| 0.2813 | 51.63 | 57.48 | 34.78 | 36.69 | 35.04 | 34.7 | 43.18 | 40.91 | 40.63 | [illegible] | [illegible] |
| 0.1875 | 45.5 | 45.5 | 31.65 | 35.61 | 30.49 | 30.73 | 33.32 | 31.48 | 35.35 | [illegible] | [illegible] |
| 0.1406 | 37.37 | 35.49 | 32.24 | 32.17 | 29.2 | 27.04 | 29 | 27.63 | 21.26 | [illegible] | [illegible] |
| 0.0938 | 30.5 | 32.5 | 24.88 | 34.05 | 28.94 | 22.3 | 25.67 | 20.57 | 22.7 | [illegible] | [illegible] |
| 0.0703 | 22.15 | 29.5 | 26.01 | 35.2 | 18.28 | 24.46 | 22.75 | 18.67 | 19.01 | [illegible] | [illegible] |
| 0.0469 | 17.22 | 26.3 | 24.94 | 38.62 | 22.96 | 39.18 | 26.57 | 4.07 | 16.93 | [illegible] | [illegible] |
| 0.0352 | 14.71 | 23.76 | 25.95 | 39.87 | 25.9 | 30.5 | 31.01 | 23.36 | 15.8 | [illegible] | [illegible] |
| 0.0234 | 9.13 | 12.9 | 23.78 | 41.79 | 31.02 | 25.76 | 34.06 | 17.42 | 15.36 | [illegible] | [illegible] |
| 0.0176 | 12.38 | 19.95 | 24.05 | 45.94 | 22.73 | 22.06 | 40.36 | 17.23 | 16.39 | [illegible] | [illegible] |
| 0.0117 | 11.46 | 11.75 | 21.64 | 57.09 | 26.08 | 23.11 | 49.19 | 11.99 | 15.28 | [illegible] | [illegible] |
| 0.0088 | 10.65 | 13.97 | 22.07 | 63.29 | 17.94 | 27.11 | 58.35 | 17.19 | 15.76 | [illegible] | [illegible] |
| 0.0059 | 11.7 | 10.74 | 20.33 | 66.48 | 40.76 | 23.33 | 71.5 | 16.5 | 19.82 | [illegible] | [illegible] |
| 0.0044 | 14.5 | 14.15 | 19.39 | 85.84 | 38.09 | 25.5 | 75.73 | 15.5 | 16.87 | [illegible] | [illegible] |
| 0.0029 | 18.5 | 9.73 | 21.11 | 100.8 9 | 27.66 | 27.16 | 92.63 | 14.5 | 23.97 | [illegible] | [illegible] |
| 0.0022 | 22.17 | 8.5 | 23.65 | 111.6 | 38.45 | 35.5 | 98.35 | 12.36 | 24.46 | [illegible] | [illegible] |
| 0.0015 | 19.78 | 7.5 | 28.21 | 115.5 | 39.52 | 42.13 | 96.5 | 11.5 | 19.42 | [illegible] | [illegible] |
| 0.0011 | 26.58 | 6.5 | 36.7 | 120.5 | 40.5 | 20.28 | 94.9 | 10.5 | 33.06 | [illegible] | [illegible] |
| 0.0007 | 27.36 | 5.5 | 53.38 | 130.6 | 45.5 | 15.5 | 90.5 | 9.5 | 27.44 | [illegible] | [illegible] |

| FREQ. | TE | | ERROR (PHASE) | | | | | | | | |
|---|---|---|---|---|---|---|---|---|---|---|---|
| 384 | 0.89 | 1.84 | 1.31 | 1.05 | 1.6 | 1.49 | 6.27 | 1.46 | 3.53 | 0.5 | [illegible] |
| 288 | 0.72 | 1.4 | 0.68 | 0.65 | 0.9 | 0.79 | 3.56 | 0.73 | 1.77 | 0.5 | [illegible] |
| 192 | 0.74 | 2.55 | 0.34 | 0.7 | 1.74 | 0.95 | 11.19 | 0.92 | 6.37 | 3.87 | [illegible] |
| 144 | 0.62 | 1.65 | 0.26 | 0.75 | 1.03 | 0.78 | 2.08 | 0.66 | 1.38 | 1.48 | [illegible] |
| 96 | 0.94 | 4.79 | 0.24 | 0.8 | 1.19 | 0.8 | 0.87 | 0.9 | 0.93 | 0.74 | [illegible] |
| 72 | 1.25 | 8.82 | 0.25 | 0.92 | 2.61 | 1.39 | 1.09 | 1.29 | 1.47 | 1.87 | [illegible] |
| 48 | 0.5 | 8.25 | 0.5 | 0.65 | 3.53 | 3.4 | 0.26 | 1.39 | 0.43 | 1.29 | [illegible] |
| 36 | 1.36 | 0.5 | 0.84 | 0.38 | 2.49 | 2.7 | 0.22 | 1.17 | 0.39 | 0.5 | [illegible] |
| 24 | 0.5 | 0.5 | 0.61 | 0.16 | 2.31 | 4.04 | 0.24 | 1.78 | 0.31 | 0.5 | [illegible] |
| 18 | 0.5 | 15.82 | 0.83 | 0.22 | 3.47 | 4.6 | 0.29 | 2.21 | 0.36 | 0.5 | [illegible] |
| 12 | 3.39 | 26.21 | 1.05 | 0.39 | 5.1 | 0.5 | 0.51 | 5.79 | 0.67 | 0.5 | [illegible] |
| 9 | 4.03 | 0.5 | 1.39 | 0.64 | 10.33 | 0.5 | 0.61 | 8.03 | 0.96 | 2.97 | [illegible] |
| 6 | 0.08 | 0.69 | 0.04 | 0.04 | 0.15 | 0.08 | 0.06 | 0.13 | 0.22 | 0.15 | [illegible] |
| 4.5 | 0.09 | 0.78 | 0.04 | 0.06 | 0.17 | 0.09 | 0.08 | 0.14 | 0.33 | 0.17 | [illegible] |
| 3 | 0.11 | 1.46 | 0.04 | 0.14 | 0.3 | 0.14 | 0.2 | 0.18 | 0.53 | 0.28 | [illegible] |
| 2.25 | 0.11 | 1.45 | 0.04 | 0.16 | 0.32 | 0.15 | 0.27 | 0.19 | 0.82 | 0.33 | [illegible] |
| 1.5 | 0.16 | 2.11 | 0.05 | 0.27 | 0.39 | 0.23 | 0.68 | 0.31 | 1.9 | 0.8 | [illegible] |
| 1.125 | 0.17 | 2.18 | 0.06 | 0.33 | 0.39 | 0.23 | 0.73 | 0.3 | 2.34 | 1.03 | [illegible] |
| 0.75 | 0.3 | 4.18 | 0.09 | 0.49 | 0.67 | 0.25 | 1.39 | 0.37 | 5.19 | 3.73 | [illegible] |
| 0.5625 | 0.3 | 4.17 | 0.1 | 0.69 | 0.85 | 0.25 | 1.17 | 0.37 | 2.46 | 6.09 | [illegible] |
| 0.375 | 0.63 | 10.12 | 0.18 | 1.91 | 1.96 | 0.66 | 0.75 | 0.95 | 3.01 | 11.45 | [illegible] |
| 0.2813 | 1.11 | 13.44 | 0.26 | 4.13 | 2.83 | 1.12 | 1.04 | 1.7 | 4.35 | 22.8 | [illegible] |
| 0.1875 | 0.5 | 0.5 | 0.53 | 13.99 | 9.83 | 3.1 | 2.14 | 3.66 | 15.76 | 77.66 | [illegible] |
| 0.1406 | 10.22 | 48.94 | 0.77 | 24.59 | 12.68 | 5.09 | 1.8 | 5.12 | 8.47 | 0.5 | [illegible] |
| 0.0938 | 0.5 | 0.5 | 1.82 | 0.5 | 28.08 | 15.6 | 1.38 | 15.35 | 2.93 | 0.5 | [illegible] |
| 0.0703 | 15.54 | 0.5 | 1.2 | 12.76 | 27.74 | 22.82 | 0.97 | 20.39 | 2.22 | 24.7 | [illegible] |
| 0.0469 | 14.73 | 0.5 | 0.95 | 4.05 | 31.79 | 57.14 | 1.37 | 36.06 | 1 | 6.17 | [illegible] |
| 0.0352 | 8.74 | 26.57 | 0.78 | 2.26 | 14.28 | 0.5 | 0.98 | 18.4 | 0.82 | 6.84 | [illegible] |
| 0.0234 | 3.63 | 9.98 | 0.46 | 1.63 | 20.6 | 18.65 | 0.59 | 5.58 | 0.61 | 7.01 | [illegible] |
| 0.0176 | 2.33 | 4.23 | 0.4 | 4.2 | 4.98 | 7.99 | 0.7 | 2.62 | 0.62 | 4.13 | [illegible] |
| 0.0117 | 2.45 | 7 | 0.34 | 2.28 | 5.78 | 10.47 | 0.71 | 9.33 | 0.83 | 7.25 | [illegible] |
| 0.0088 | 1.48 | 2.88 | 0.77 | 4.08 | 2.73 | 7.76 | 0.82 | 5.91 | 1.21 | 8.23 | [illegible] |
| 0.0059 | 1.41 | 5.1 | 0.69 | 8.68 | 9.3 | 5.91 | 1.11 | 0.5 | 1.4 | 13.58 | [illegible] |
| 0.0044 | 0.5 | 2.84 | 0.83 | 38.67 | 19.7 | 0.5 | 1.53 | 0.5 | 2.06 | 11.31 | [illegible] |
| 0.0029 | 0.5 | 3.67 | 2.05 | 19.23 | 18.85 | 18.03 | 1.7 | 0.5 | 2.22 | 17 | [illegible] |
| 0.0022 | 4.77 | 0.5 | 0.79 | 22.58 | 15.84 | 0.5 | 1.66 | 17.04 | 3.7 | 5.72 | [illegible] |
| 0.0015 | 3.5 | 0.5 | 3.04 | 0.5 | 17.44 | 42.31 | 0.5 | 0.5 | 4.94 | 17.45 | [illegible] |
| 0.0011 | 7.78 | 0.5 | 1.38 | 0.5 | 0.5 | 43.42 | 38.32 | 0.5 | 6.84 | 29.11 | [illegible] |
| 0.0007 | 0.5 | 0.5 | 10.65 | 0.5 | 0.5 | 0.5 | 0.5 | 0.5 | 32.45 | 0.5 | [illegible] |

| FREQ | TM | (APP. | RES.) | | | | | | | | |
|---|---|---|---|---|---|---|---|---|---|---|---|
| 384 | 15.09 | 10.62 | 7.87 | 1 | 0.05 | 13.05 | 10.53 | 40.43 | 18.42 | 18.17 | [illegible] |
| 288 | 17.48 | 17.94 | 12.15 | 1 | 4.1 | 16.02 | 16.88 | 30.29 | 27.67 | 13.74 | [illegible] |
| 192 | 15.66 | 15.3 | 14.82 | 1 | 5.05 | 15.57 | 18.59 | 29.14 | 26.34 | 10.81 | [illegible] |
| 144 | 12.66 | 19.74 | 13.81 | 1 | 2.95 | 12.41 | 17.35 | 21.24 | 22.13 | 9.85 | [illegible] |
| 96 | 9.72 | 13.75 | 13.22 | | 9.02 | 11.36 | 15.4 | 12.33 | 18.1 | 9.84 | [illegible] |
| 72 | 8.9 | 12.56 | 12.78 | | 9.77 | 11.37 | 15.19 | 13.31 | 16.17 | 9.56 | [illegible] |
| 48 | 7.75 | 8.53 | 5.55 | | 8.13 | 9.53 | 12.01 | 5.06 | 11.29 | 7.33 | [illegible] |
| 36 | 6.58 | 7.75 | 8.87 | | 7.88 | 10.69 | 10.78 | 4.39 | 9.27 | 6.97 | [illegible] |
| 24 | 6.05 | 6.65 | 8.47 | | 7.39 | 9.95 | 9.62 | 3.85 | 7.36 | 6.4 | [illegible] |
| 18 | 5.95 | 5.72 | 7.24 | | 6.66 | 9.24 | 8.16 | 3.38 | 6.3 | 5.83 | [illegible] |
| 12 | 5.77 | 3.88 | 6.82 | | 5.88 | 7.72 | 7.75 | 2.9 | 5.16 | 5.2 | [illegible] |
| 9 | 4.37 | 3.75 | 5.84 | | 4.34 | 6.54 | 6.15 | 2.39 | 5.09 | 4.31 | [illegible] |
| 6 | 5.12 | 3.23 | 5.51 | | 4.1 | 4.88 | 4.38 | 2.08 | 4.17 | 3.97 | [illegible] |
| 4.5 | 5.07 | 3.2 | 5.23 | | 3.63 | 4.41 | 3.74 | 1.82 | 3.84 | 3.61 | [illegible] |
| 3 | 4.85 | 3.14 | 5.12 | | 3.29 | 4.45 | 3.15 | 1.53 | 3.46 | 3.24 | [illegible] |
| 2.25 | 4.54 | 2.95 | 5.03 | | 3.13 | 4.2 | 2.67 | 1.35 | 3.15 | 2.96 | [illegible] |
| 1.5 | 4.21 | 2.8 | 5.21 | | 3 | 3.84 | 2.33 | 1.19 | 2.87 | 2.54 | [illegible] |
| 1.125 | 3.85 | 2.63 | 5.45 | | 2.85 | 3.6 | 2.04 | 1.11 | 2.63 | 2.29 | [illegible] |
| 0.75 | 3.26 | 2.39 | 5.94 | | 2.75 | 3.51 | 1.76 | 1.01 | 2.38 | 2.01 | [illegible] |
| 0.5625 | 2.77 | 2.22 | 6.44 | | 2.76 | 3.65 | 1.74 | 0.9 | 2.34 | 1.88 | [illegible] |
| 0.375 | 2.25 | 2.14 | 7.42 | | 3.06 | 4.62 | 1.87 | 0.95 | 2.52 | 1.64 | [illegible] |
| 0.2813 | 1.9 | 1.81 | 8.49 | | 3.5 | 5.65 | 2.08 | 0.95 | 2.75 | 1.67 | [illegible] |
| 0.1875 | 1.9 | 1.79 | 10.28 | | 4.21 | 8.84 | 2.52 | 1.04 | 3.35 | 1.75 | [illegible] |
| 0.1406 | 1.97 | 1.75 | 12.74 | | 4.51 | 6.87 | 3.1 | 1.42 | 4.26 | 2.64 | [illegible] |
| 0.0938 | 2.02 | 1.75 | 19.94 | | 5.55 | 16.31 | 3.88 | 1.59 | 7.66 | 3.27 | [illegible] |
| 0.0703 | 2.2 | 1.75 | 25.62 | | 11.18 | 29.92 | 6.41 | 2.64 | 13.2 | 4.5 | [illegible] |
| 0.0469 | 2.21 | 2.5 | 40.78 | | 13.9 | 37.18 | 11.71 | 2.68 | 18.13 | 5.74 | [illegible] |
| 0.0352 | 3.43 | 4.31 | 52.84 | | 18.29 | 40.16 | 17.75 | 3.72 | 20.74 | 7.43 | [illegible] |
| 0.0234 | 4.18 | 7.09 | 71.05 | | 21.2 | 47.14 | 21.53 | 4.92 | 25.67 | 10.7 | [illegible] |
| 0.0176 | 5.24 | 8.47 | 91.88 | | 26.08 | 61.73 | 31.35 | 5.8 | 36.21 | 12.91 | [illegible] |
| 0.0117 | 8.25 | 12.09 | 134.4 | | 31.94 | 104.16 | 70.98 | 6.91 | 61.98 | 19.35 | [illegible] |
| 0.0088 | 11.79 | 15.42 | 173.72 | | 33.33 | 136.47 | 49.49 | 7.18 | 61.65 | 25.35 | [illegible] |
| 0.0059 | 17.13 | 22.4 | 246.14 | | 31.07 | 321.99 | 76.62 | 6.54 | 80.5 | 35.94 | [illegible] |
| 0.0044 | 22.5 | 34.21 | 288.99 | | 31.12 | 359.81 | 85.4 | 5.69 | 100.5 | 45.42 | [illegible] |
| 0.0029 | 28.5 | 34.75 | 409.51 | | 20.84 | 353.17 | 112 | 4.49 | 150.5 | 64.29 | [illegible] |
| 0.0022 | 37.52 | 34.5 | 448.21 | | 12.6 | 507.88 | 150.5 | 2.82 | 209.4 | 75.82 | [illegible] |
| 0.0015 | 34.24 | 34.5 | 597.99 | | 15.5 | 418.37 | 379.13 | 2.15 | 350 | 90.13 | [illegible] |
| 0.0011 | 31.17 | 34.5 | 561.34 | | 15.5 | 350 | 245 | 1.74 | 250 | 83.46 | [illegible] |
| 0.0007 | 30.5 | 34.5 | 593.92 | | 15.5 | 115 | 160 | 1.15 | 150 | 82.36 | [illegible] |

| FREQ. | TM | ERROR (APP. | | RES. | ) | | | | | | |
|---|---|---|---|---|---|---|---|---|---|---|---|
| 384 | 0.01 | 0.03 | 0.03 | 0.5 | 0.01 | 0.02 | 0.1 | 0.02 | 0.02 | [illegible] | [illegible] |
| 288 | 0.01 | 0.02 | 0.01 | 0.5 | 0 | 0.01 | 0.05 | 0.01 | 0.01 | [illegible] | [illegible] |
| 192 | 0 | 0.03 | 0.01 | 0.5 | 0.01 | 0.01 | 0.19 | 0.01 | 0.04 | [illegible] | [illegible] |
| 144 | 0 | 0.03 | 0 | 0.5 | 0 | 0.01 | 0.04 | 0 | 0.01 | [illegible] | [illegible] |
| 96 | 0.01 | 0.06 | 0 | 0.01 | 0.01 | 0.01 | 0.02 | 0 | 0.01 | [illegible] | [illegible] |
| 72 | 0.01 | 0.11 | 0 | 0.02 | 0.01 | 0.01 | 0.03 | 0.01 | 0.02 | [illegible] | [illegible] |
| 48 | 0.5 | 0.14 | 0.5 | 0.01 | 0.02 | 0.02 | 0.01 | 0.01 | 0.01 | [illegible] | [illegible] |
| 36 | 0.02 | 0.5 | 0.01 | 0.01 | 0.02 | 0.02 | 0.01 | 0.01 | 0 | [illegible] | [illegible] |
| 24 | 0.5 | 0.5 | 0.01 | 0 | 0.02 | 0.02 | 0.01 | 0.01 | 0 | [illegible] | [illegible] |
| 18 | 0.5 | 0.2 | 0.01 | 0 | 0.02 | 0.03 | 0.01 | 0.02 | 0 | [illegible] | [illegible] |
| 12 | 0.04 | 0.47 | 0.01 | 0.01 | 0.03 | 0.5 | 0.02 | 0.04 | 0.01 | [illegible] | [illegible] |
| 9 | 0.04 | 0.5 | 0.02 | 0.01 | 0.06 | 0.5 | 0.02 | 0.06 | 0.02 | [illegible] | [illegible] |
| 6 | 0 | 0.01 | 0 | 0 | 0 | 0 | 0 | 0 | 0 | [illegible] | [illegible] |
| 4.5 | 0 | 0.01 | 0 | 0 | 0 | 0 | 0 | 0 | 0 | [illegible] | [illegible] |
| 3 | 0 | 0.01 | 0 | 0 | 0 | 0 | 0.01 | 0 | 0 | [illegible] | [illegible] |
| 2.25 | 0 | 0.01 | 0 | 0 | 0 | 0 | 0.01 | 0 | 0 | [illegible] | [illegible] |
| 1.5 | 0 | 0.02 | 0 | 0 | 0.01 | 0 | 0.02 | 0 | 0.01 | [illegible] | [illegible] |
| 1.125 | 0 | 0.02 | 0 | 0 | 0.01 | 0 | 0.02 | 0 | 0.01 | [illegible] | [illegible] |
| 0.75 | 0 | 0.04 | 0 | 0.01 | 0.02 | 0.01 | 0.04 | 0 | 0.03 | [illegible] | [illegible] |
| 0.5625 | 0 | 0.04 | 0 | 0.01 | 0.03 | 0.01 | 0.04 | 0.01 | 0.03 | [illegible] | [illegible] |
| 0.375 | 0.01 | 0.06 | 0.01 | 0.02 | 0.07 | 0.02 | 0.03 | 0.01 | 0.05 | [illegible] | [illegible] |
| 0.2813 | 0.02 | 0.1 | 0.01 | 0.04 | 0.09 | 0.02 | 0.02 | 0.03 | 0.05 | [illegible] | [illegible] |
| 0.1875 | 0.5 | 0.5 | 0.01 | 0.11 | 0.23 | 0.07 | 0.04 | 0.04 | 0.16 | [illegible] | [illegible] |
| 0.1406 | 0.54 | 0.39 | 0.01 | 0.16 | 0.46 | 0.11 | 0.03 | 0.05 | 0.12 | [illegible] | [illegible] |
| 0.0938 | 0.5 | 0.5 | 0.02 | 0.5 | 0.98 | 0.47 | 0.03 | 0.15 | 0.08 | [illegible] | [illegible] |
| 0.0703 | 0.69 | 0.5 | 0.03 | 0.1 | 0.63 | 0.56 | 0.02 | 0.17 | 0.05 | [illegible] | [illegible] |
| 0.0469 | 0.66 | 0.5 | 0.02 | 0.02 | 0.51 | 0.98 | 0.03 | 0.34 | 0.02 | [illegible] | [illegible] |
| 0.0352 | 0.21 | 0.16 | 0.01 | 0.02 | 0.24 | 0.5 | 0.02 | 0.13 | 0.01 | [illegible] | [illegible] |
| 0.0234 | 0.18 | 0.05 | 0.01 | 0.01 | 0.6 | 0.45 | 0.01 | 0.04 | 0.02 | [illegible] | [illegible] |
| 0.0176 | 0.28 | 0.04 | 0.01 | 0.04 | 0.18 | 0.25 | 0.01 | 0.03 | 0.03 | [illegible] | [illegible] |
| 0.0117 | 0.31 | 0.07 | 0.01 | 0.02 | 0.12 | 0.21 | 0.02 | 0.07 | 0.02 | [illegible] | [illegible] |
| 0.0088 | 0.09 | 0.06 | 0.01 | 0.03 | 0.06 | 0.24 | 0.02 | 0.03 | 0.01 | [illegible] | [illegible] |
| 0.0059 | 0.21 | 0.08 | 0.01 | 0.04 | 0.12 | 0.2 | 0.02 | 0.5 | 0.01 | [illegible] | [illegible] |
| 0.0044 | 0.5 | 0.12 | 0.01 | 0.16 | 0.15 | 0.5 | 0.03 | 0.5 | 0.01 | [illegible] | [illegible] |
| 0.0029 | 0.5 | 0.15 | 0.02 | 0.08 | 0.2 | 0.59 | 0.03 | 0.5 | 0.03 | [illegible] | [illegible] |
| 0.0022 | 0.1 | 0.5 | 0.04 | 0.28 | 0.13 | 0.5 | 0.03 | 0.19 | 0.04 | [illegible] | [illegible] |
| 0.0015 | 0.19 | 0.5 | 0.05 | 0.5 | 0.27 | 1.11 | 0.5 | 0.5 | 0.05 | [illegible] | [illegible] |
| 0.0011 | 0.24 | 0.5 | 0.03 | 0.5 | 0.5 | 0.61 | 0.66 | 0.5 | 0.07 | [illegible] | [illegible] |
| 0.0007 | 0.5 | 0.5 | 0.07 | 0.5 | 0.5 | 0.5 | 0.5 | 0.5 | 0.36 | [illegible] | [illegible] |

| FREQ. | TM | PHASE (deg.) | | | | | | | | | |
|---|---|---|---|---|---|---|---|---|---|---|---|
| 384 | 71.79 | 76.27 | 63.33 | 65.78 | 68.67 | 75.83 | 68.19 | 70.43 | 63.89 | [illegible] | [illegible] |
| 288 | 65.47 | 69.54 | 59.08 | 62.78 | 56.06 | 69.85 | 65.27 | 68.56 | 66 | [illegible] | [illegible] |
| 192 | 68.66 | 75.78 | 56.86 | 61.89 | 59.88 | 66.09 | 68.08 | 71.39 | 65.19 | [illegible] | [illegible] |
| 144 | 68.5 | 65.24 | 56.15 | 59.75 | 58.04 | 64.22 | 56.12 | 70.34 | 63.22 | [illegible] | [illegible] |
| 96 | 68.57 | 76.08 | 57.37 | 57.43 | 58.15 | 63.56 | 66.05 | 72 | 57.35 | [illegible] | [illegible] |
| 72 | 66.68 | 72.94 | 57.04 | 56.23 | 56.3 | 64.31 | 65.44 | 71.05 | 55 | [illegible] | [illegible] |
| 48 | 60.5 | 79.64 | 57.75 | 55.62 | 61.87 | 62 | 63.73 | 68.58 | 57.97 | [illegible] | [illegible] |
| 36 | 58.86 | 60.5 | 58.1 | 56.14 | 60.01 | 61.66 | 64.88 | 65.53 | 59.2 | [illegible] | [illegible] |
| 24 | 50.5 | 57.05 | 57.98 | 57.35 | 59.7 | 63.23 | 64.74 | 63.95 | 58.93 | [illegible] | [illegible] |
| 18 | 45.05 | 56.22 | 58.71 | 58.63 | 60.43 | 64.29 | 63.9 | 62.1 | 59.39 | [illegible] | [illegible] |
| 12 | 36.09 | 59.3 | 59.99 | 58.24 | 59.79 | 64.5 | 62.78 | 61.42 | 58.83 | [illegible] | [illegible] |
| 9 | 36.84 | 56.67 | 57.69 | 55.58 | 59.81 | 64.5 | 54.99 | 58.04 | 56.75 | [illegible] | [illegible] |
| 6 | 49.23 | 53.56 | 50.25 | 59.05 | 56.71 | 64.17 | 64.33 | 59.46 | 58.9 | [illegible] | [illegible] |
| 4.5 | 50.07 | 52.23 | 47.87 | 56.94 | 54.07 | 62.8 | 63.98 | 57.52 | 58.43 | [illegible] | [illegible] |
| 3 | 52.19 | 51.61 | 45.03 | 53.52 | 49.97 | 60.79 | 61.43 | 56.02 | 58.04 | [illegible] | [illegible] |
| 2.25 | 52.99 | 51.67 | 42.16 | 51.54 | 47.73 | 58.17 | 59.38 | 54.26 | 56.92 | [illegible] | [illegible] |
| 1.5 | 55.13 | 52.08 | 38.62 | 48.91 | 46.27 | 54.97 | 58.8 | 52.39 | 56.46 | [illegible] | [illegible] |
| 1.125 | 56.23 | 53.17 | 35.84 | 47.01 | 42.98 | 52.63 | 55.9 | 49.76 | 55.21 | [illegible] | [illegible] |
| 0.75 | 57.46 | 54.98 | 32.75 | 42.6 | 38.59 | 47.61 | 50.86 | 45.65 | 51.05 | [illegible] | [illegible] |
| 0.5625 | 57.34 | 54.3 | 29.86 | 37.55 | 33.17 | 41.23 | 48.33 | 40.53 | 48.25 | [illegible] | [illegible] |
| 0.375 | 57.41 | 53.2 | 26.39 | 31.65 | 28.6 | 32.24 | 43.71 | 34.18 | 41.74 | [illegible] | [illegible] |
| 0.2813 | 53.85 | 49.77 | 23.86 | 28.74 | 21.31 | 28.67 | 35.18 | 26.9 | 37.89 | [illegible] | [illegible] |
| 0.1875 | 50.5 | 45.5 | 20.68 | 23.76 | 16.83 | 18.97 | 30.75 | 20.29 | 29.67 | [illegible] | [illegible] |
| 0.1406 | 45.31 | 34.27 | 17.83 | 16.14 | 17.53 | 12.99 | 25.52 | 17.46 | 20.49 | [illegible] | [illegible] |
| 0.0938 | 35.5 | 30.6 | 12.14 | 18.5 | 21.84 | 17.72 | 23.22 | 10.14 | 19.98 | [illegible] | [illegible] |
| 0.0703 | 25.14 | 27.5 | 10.95 | 21.96 | -3.65 | -5.24 | 21.66 | 9.73 | 14.48 | [illegible] | [illegible] |
| 0.0469 | 20.58 | 20.2 | 10.53 | 18.07 | 11.95 | 11.92 | 21.55 | 14.28 | 11.27 | [illegible] | [illegible] |
| 0.0352 | 19.75 | 14.99 | 9.13 | 21.15 | 7.12 | 9.5 | 22.95 | 8.09 | 10.45 | [illegible] | [illegible] |
| 0.0234 | 15.64 | 12.67 | 9.08 | 26.44 | -9.92 | 6.82 | 28.22 | 7.43 | 9.66 | [illegible] | [illegible] |
| 0.0176 | 12.06 | 10.83 | 9.86 | 30.28 | 9.86 | 9.62 | 32.2 | 5.99 | 13.17 | [illegible] | [illegible] |
| 0.0117 | 21.2 | 8.45 | 8.48 | 41.66 | 8.28 | 5.03 | 40.88 | 11.72 | 9.39 | [illegible] | [illegible] |
| 0.0088 | 13.9 | 12.22 | 8.45 | 49.99 | 12.75 | 5.02 | 47.88 | 9.54 | 9.05 | [illegible] | [illegible] |
| 0.0059 | 8.75 | 13.62 | 11.38 | 62.33 | 0.26 | 3 | 62.92 | 15.5 | 12.46 | [illegible] | [illegible] |
| 0.0044 | 15.5 | 18.45 | 12.49 | 73.42 | 2.91 | 15.5 | 72.04 | 25.5 | 12.83 | [illegible] | [illegible] |
| 0.0029 | 25.5 | 13.95 | 18.5 | 81.95 | 31.59 | 24.33 | 83.61 | 35.5 | 19.18 | [illegible] | [illegible] |
| 0.0022 | 32.26 | 25.5 | 22.11 | 88.99 | 19.63 | 5.5 | 91.36 | 43.14 | 19.91 | [illegible] | [illegible] |
| 0.0015 | 55.12 | 35.5 | 34.66 | 89.5 | 15.85 | -4.01 | 90.5 | 50.5 | 28.62 | [illegible] | [illegible] |
| 0.0011 | 42.19 | 45.5 | 32.46 | 90.5 | 25.5 | 3.44 | 89.69 | 55.5 | 36.41 | [illegible] | [illegible] |
| 0.0007 | 55.5 | 55.5 | 48.97 | 91.5 | 35.5 | 10.5 | 90.5 | 65.5 | 53.8 | [illegible] | [illegible] |

| FREQ. | TM | ERROR | (PHASE) | | | | | | | | |
|---|---|---|---|---|---|---|---|---|---|---|---|
| 384 | 0.94 | 2.07 | 1.66 | 0.5 | 0.9 | 1.19 | 6.47 | 1.09 | 1.44 | 0.5 | 1.86 |
| 288 | 0.55 | 1.51 | 0.68 | 0.5 | 0.27 | 0.58 | 2.98 | 0.51 | 0.76 | 0.5 | 1.63 |
| 192 | 0.33 | 2.08 | 0.35 | 0.5 | 0.46 | 0.49 | 12.61 | 0.37 | 2.56 | 10.81 | 4.73 |
| 144 | 0.25 | 1.9 | 0.26 | 0.5 | 0.33 | 0.38 | 2.39 | 0.26 | 0.74 | 4.26 | 1.93 |
| 96 | 0.34 | 3.85 | 0.23 | 0.86 | 0.34 | 0.38 | 1.38 | 0.3 | 0.66 | 2.7 | [illegible] |
| 72 | 0.37 | 6.94 | 0.25 | 1.06 | 0.5 | 0.51 | 1.71 | 0.34 | 1.11 | 5.52 | 2.45 |
| 48 | 0.5 | 9.35 | 0.5 | 0.5 | 1.52 | 1.59 | 0.66 | 0.7 | 0.38 | 3.06 | [illegible] |
| 36 | 1.25 | 0.5 | 0.44 | 0.33 | 1.05 | 1.28 | 0.56 | 0.57 | 0.32 | 0.5 | [illegible] |
| 24 | 0.5 | 0.5 | 0.48 | 0.23 | 1.02 | 1.48 | 0.62 | 0.88 | 0.28 | 0.5 | [illegible] |
| 18 | 0.5 | 13.34 | 0.59 | 0.27 | 1.2 | 2.14 | 0.61 | 1 | 0.32 | 0.5 | [illegible] |
| 12 | 2.42 | 30.91 | 0.91 | 0.8 | 2.07 | 0.5 | 1.08 | 2.5 | 0.66 | 0.5 | [illegible] |
| 9 | 2.94 | 0.5 | 1.16 | 0.79 | 3.85 | 0.5 | 1.6 | 3.72 | 1.01 | 0.5 | [illegible] |
| 6 | 0.03 | 0.43 | 0.04 | 0.04 | 0.09 | 0.06 | 0.12 | 0.05 | 0.09 | 0.14 | [illegible] |
| 4.5 | 0.03 | 0.49 | 0.04 | 0.04 | 0.11 | 0.07 | 0.18 | 0.05 | 0.12 | 0.18 | [illegible] |
| 3 | 0.05 | 0.96 | 0.06 | 0.08 | 0.26 | 0.12 | 0.4 | 0.06 | 0.24 | 0.33 | [illegible] |
| 2.25 | 0.05 | 0.88 | 0.06 | 0.1 | 0.31 | 0.15 | 0.52 | 0.06 | 0.32 | 0.43 | [illegible] |
| 1.5 | 0.09 | 1.36 | 0.09 | 0.16 | 0.47 | 0.24 | 1.24 | 0.09 | 0.68 | 0.93 | [illegible] |
| 1.125 | 0.1 | 1.31 | 0.1 | 0.21 | 0.55 | 0.27 | 1.37 | 0.11 | 0.86 | 1.37 | [illegible] |
| 0.75 | 0.26 | 2.44 | 0.16 | 0.41 | 1.19 | 0.49 | 2.79 | 0.23 | 2.06 | 4.78 | [illegible] |
| 0.5625 | 0.25 | 2.46 | 0.21 | 0.6 | 2.01 | 0.56 | 2.95 | 0.36 | 2.28 | 6.91 | [illegible] |
| 0.375 | 0.55 | 4.18 | 0.35 | 1.42 | 4.84 | 1 | 1.69 | 0.84 | 3.1 | 10.43 | [illegible] |
| 0.2813 | 1.24 | 6.45 | 0.43 | 2.52 | 6.14 | 1.57 | 1.57 | 1.79 | 3.62 | 22.37 | [illegible] |
| 0.1875 | 0.5 | 0.5 | 0.74 | 7.29 | 15.17 | 4.77 | 2.7 | 2.66 | 10.39 | 95.49 | [illegible] |
| 0.1406 | 35.44 | 25.84 | 0.8 | 10.66 | 30.03 | 7.34 | 2.1 | 3.12 | 7.65 | 0.5 | [illegible] |
| 0.0938 | 0.5 | 0.5 | 1.52 | 0.5 | 64.59 | 30.89 | 2.26 | 9.7 | 5.24 | 0.5 | [illegible] |
| 0.0703 | 45.27 | 0.5 | 1.69 | 6.27 | 41.77 | 37.11 | 1.57 | 10.92 | 3.39 | 22.29 | [illegible] |
| 0.0469 | 43.44 | 0.5 | 1.35 | 1.43 | 33.72 | 64.59 | 2.16 | 22.53 | 1.21 | 9.33 | [illegible] |
| 0.0352 | 14.04 | 10.26 | 0.78 | 1 | 15.78 | 0.5 | 1.49 | 8.35 | 0.81 | 8.24 | [illegible] |
| 0.0234 | 11.65 | 3.59 | 0.51 | 0.84 | 39.85 | 29.46 | 0.85 | 2.61 | 1.05 | 16.55 | [illegible] |
| 0.0176 | 18.21 | 2.42 | 0.42 | 2.51 | 11.97 | 16.66 | 0.77 | 2.11 | 1.84 | 5.82 | [illegible] |
| 0.0117 | 20.28 | 4.66 | 0.35 | 1.38 | 7.83 | 13.6 | 1.1 | 4.88 | 1.12 | 9.1 | [illegible] |
| 0.0088 | 5.9 | 3.65 | 0.53 | 1.95 | 4.12 | 15.64 | 1.11 | 1.96 | 0.88 | 9.79 | [illegible] |
| 0.0059 | 13.71 | 5.08 | 0.56 | 2.78 | 8.02 | 13.39 | 1.29 | 0.5 | 0.94 | 12.22 | [illegible] |
| 0.0044 | 0.5 | 8.05 | 0.59 | 10.84 | 9.83 | 0.5 | 2.06 | 0.5 | 0.9 | 16.51 | [illegible] |
| 0.0029 | 0.5 | 9.95 | 1.08 | 5.58 | 12.87 | 39.19 | 1.71 | 0.5 | 1.72 | 18.74 | [illegible] |
| 0.0022 | 6.89 | 0.5 | 2.32 | 18.45 | 8.84 | 0.5 | 1.79 | 12.3 | 2.39 | 9.94 | [illegible] |
| 0.0015 | 12.26 | 0.5 | 3.18 | 0.5 | 17.8 | 73.05 | 0.5 | 0.5 | 3.44 | 34.53 | [illegible] |
| 0.0011 | 15.85 | 0.5 | 2.3 | 0.5 | 0.5 | 40.18 | 43.32 | 0.5 | 4.91 | 16.72 | [illegible] |
| 0.0007 | 0.5 | 0.5 | 4.71 | 0.5 | 0.5 | 0.5 | 0.5 | 0.5 | 23.68 | 0.5 | [illegible] |

| INCLUDE | MATRIX | TE | MODE | MAGN. | | | | | |
|---|---|---|---|---|---|---|---|---|---|
| 1 | 1 | 1 | 0 | 1 | 1 | 1 | 1 | 1 | 0 |
| 1 | 1 | 1 | 0 | 1 | 1 | 1 | 1 | 1 | 0 |
| 1 | 1 | 1 | 0 | 1 | 1 | 1 | 1 | 1 | 1 |
| 1 | 1 | 1 | 0 | 1 | 1 | 1 | 1 | 1 | 1 |
| 1 | 1 | 1 | 1 | 1 | 1 | 1 | 1 | 1 | 1 |
| 1 | 1 | 1 | 1 | 1 | 1 | 1 | 1 | 1 | 1 |
| 0 | 1 | 0 | 1 | 1 | 1 | 1 | 1 | 1 | 1 |
| 1 | 0 | 1 | 1 | 1 | 1 | 1 | 1 | 1 | 0 |
| 0 | 0 | 1 | 1 | 1 | 1 | 1 | 1 | 1 | 0 |
| 0 | 1 | 1 | 1 | 1 | 1 | 1 | 1 | 1 | 0 |
| 1 | 1 | 1 | 1 | 1 | 0 | 1 | 1 | 1 | 0 |
| 1 | 0 | 1 | 1 | 1 | 0 | 1 | 1 | 1 | 1 |
| 1 | 1 | 1 | 1 | 1 | 1 | 1 | 1 | 1 | 1 |
| 1 | 1 | 1 | 1 | 1 | 1 | 1 | 1 | 1 | 1 |
| 1 | 1 | 1 | 1 | 1 | 1 | 1 | 1 | 1 | 1 |
| 1 | 1 | 1 | 1 | 1 | 1 | 1 | 1 | 1 | 1 |
| 1 | 1 | 1 | 1 | 1 | 1 | 1 | 1 | 1 | 1 |
| 1 | 1 | 1 | 1 | 1 | 1 | 1 | 1 | 1 | 1 |
| 1 | 1 | 1 | 1 | 1 | 1 | 1 | 1 | 1 | 1 |
| 1 | 1 | 1 | 1 | 1 | 1 | 1 | 1 | 1 | 1 |
| 1 | 1 | 1 | 1 | 1 | 1 | 1 | 1 | 1 | 1 |
| 0 | 0 | 1 | 1 | 1 | 1 | 1 | 1 | 1 | 1 |
| 1 | 1 | 1 | 1 | 1 | 1 | 1 | 1 | 1 | 0 |
| 0 | 0 | 1 | 0 | 1 | 1 | 1 | 1 | 1 | 0 |
| 1 | 0 | 1 | 1 | 1 | 1 | 1 | 1 | 1 | 1 |
| 1 | 0 | 1 | 1 | 1 | 1 | 1 | 1 | 1 | 1 |
| 1 | 1 | 1 | 1 | 1 | 0 | 1 | 1 | 1 | 1 |
| 1 | 1 | 1 | 1 | 1 | 1 | 1 | 1 | 1 | 1 |
| 1 | 1 | 1 | 1 | 1 | 1 | 1 | 1 | 1 | 1 |
| 1 | 1 | 1 | 1 | 1 | 1 | 1 | 1 | 1 | 1 |
| 1 | 1 | 1 | 1 | 1 | 1 | 1 | 1 | 1 | 1 |
| 1 | 1 | 1 | 1 | 1 | 1 | 1 | 0 | 1 | 1 |
| 0 | 1 | 1 | 1 | 0 | 1 | 0 | 1 | 1 | 1 |
| 0 | 1 | 1 | 1 | 1 | 1 | 1 | 0 | 1 | 1 |
| 1 | 0 | 1 | 1 | 1 | 0 | 1 | 1 | 1 | 1 |
| 1 | 0 | 1 | 0 | 1 | 1 | 0 | 0 | 1 | 1 |
| 1 | 0 | 1 | 0 | 0 | 0 | 1 | 0 | 1 | 1 |
| 1 | 0 | 0 | 0 | 0 | 0 | 0 | 0 | 1 | 0 |

| INCLUDE | MATRIX | TE | MODE | PHASE | | | | | | |
|---|---|---|---|---|---|---|---|---|---|---|
| 1 | 1 | 1 | 0 | 1 | 1 | 1 | 1 | 1 | 0 | · |
| 1 | 1 | 1 | 0 | 1 | 1 | 1 | 1 | 1 | 0 | · |
| 1 | 1 | 1 | 0 | 1 | 1 | 1 | 1 | 1 | · | · |
| 1 | 1 | 1 | 0 | 1 | 1 | 1 | 1 | 1 | · | · |
| 1 | 1 | 1 | 1 | 1 | 1 | 1 | 1 | 1 | · | · |
| 1 | 1 | 1 | 1 | 1 | 1 | 1 | 1 | 1 | · | · |
| 0 | 1 | 0 | 1 | 1 | 1 | 1 | 1 | 1 | · | · |
| 1 | 0 | 1 | 1 | 1 | 1 | 1 | 1 | 1 | 0 | · |
| 0 | 0 | 1 | 1 | 1 | 1 | 1 | 1 | 1 | 0 | · |
| 0 | 1 | 1 | 1 | 1 | 1 | 1 | 1 | 1 | 0 | · |
| 1 | 1 | 1 | 1 | 1 | 0 | 1 | 1 | 1 | 0 | · |
| 1 | 0 | 1 | 1 | 1 | 0 | 1 | 1 | 1 | · | · |
| 1 | 1 | 1 | 1 | 1 | 1 | 1 | 1 | 1 | · | · |
| 1 | 1 | 1 | 1 | 1 | 1 | 1 | 1 | 1 | · | · |
| 1 | 1 | 1 | 1 | 1 | 1 | 1 | 1 | 1 | · | · |
| 1 | 1 | 1 | 1 | 1 | 1 | 1 | 1 | 1 | · | · |
| 1 | 1 | 1 | 1 | 1 | 1 | 1 | 1 | 1 | · | · |
| 1 | 1 | 1 | 1 | 1 | 1 | 1 | 1 | 1 | · | · |
| 1 | 1 | 1 | 1 | 1 | 1 | 1 | 1 | 1 | 1 | · |
| 1 | 1 | 1 | 1 | 1 | 1 | 1 | 1 | 1 | · | · |
| 1 | 1 | 1 | 1 | 1 | 1 | 1 | 1 | 1 | 0 | · |
| 0 | 0 | 1 | 1 | 1 | 1 | 1 | 1 | 1 | 1 | 0 |
| 1 | 1 | 1 | 1 | 1 | 1 | 1 | 1 | 1 | 0 | 0 |
| 0 | 0 | 1 | 0 | 1 | 1 | 1 | 1 | 1 | 0 | 0 |
| 1 | 0 | 1 | 1 | 1 | 1 | 1 | 1 | 1 | 1 | · |
| 1 | 0 | 1 | 1 | 1 | 1 | 1 | 1 | 1 | 1 | · |
| 1 | 1 | 1 | 1 | 1 | 0 | 1 | 1 | 1 | · | · |
| 1 | 1 | 1 | 1 | 1 | 1 | 1 | 1 | 1 | 1 | · |
| 1 | 1 | 1 | 1 | 1 | 1 | 1 | 1 | 1 | 1 | · |
| 1 | 1 | 1 | 1 | 1 | 1 | 1 | 1 | 1 | 1 | · |
| 1 | 1 | 1 | 1 | 1 | 1 | 1 | 1 | 1 | 1 | · |
| 1 | 1 | 1 | 1 | 1 | 1 | 1 | 0 | 1 | 1 | · |
| 0 | 1 | 1 | 1 | 0 | 1 | 0 | 1 | 1 | 1 | · |
| 0 | 1 | 1 | 1 | 1 | 1 | 1 | 0 | 1 | 1 | · |
| 1 | 0 | 1 | 1 | 1 | 0 | 1 | 1 | 1 | 1 | · |
| 1 | 0 | 1 | 0 | 1 | 1 | 0 | 0 | 1 | 1 | · |
| 1 | 0 | 1 | 0 | 0 | 0 | 1 | 0 | 1 | 1 | · |
| 1 | 0 | 0 | 0 | 0 | 0 | 0 | 0 | 1 | 0 | · |

| INCLUDE | MATRIX | TM | MODE | MAGN. | | | | | | |
|---|---|---|---|---|---|---|---|---|---|---|
| 1 | 1 | 1 | 0 | 1 | 1 | 1 | 1 | . | . | . |
| 1 | 1 | 1 | 0 | 1 | 1 | 1 | 1 | . | . | . |
| 1 | 1 | 1 | 0 | 1 | 1 | 1 | 1 | . | . | . |
| 1 | 1 | 1 | 0 | 1 | 1 | 1 | 1 | . | . | . |
| 1 | 1 | 1 | 1 | 1 | 1 | 1 | 1 | . | . | . |
| 1 | 1 | 1 | 1 | 1 | 1 | 1 | 1 | . | . | . |
| 0 | 1 | 0 | 1 | 1 | 1 | 1 | 1 | . | . | . |
| 1 | 0 | 1 | 1 | 1 | 1 | 1 | 1 | . | . | . |
| 0 | 0 | 1 | 1 | 1 | 1 | 1 | 1 | . | . | . |
| 0 | 1 | 1 | 1 | 1 | 1 | 1 | 1 | . | . | . |
| 1 | 1 | 1 | 1 | 1 | 0 | 1 | 1 | . | . | . |
| 1 | 0 | 1 | 1 | 1 | 0 | 1 | 1 | . | . | . |
| 1 | 1 | 1 | 1 | 1 | 1 | 1 | 1 | . | . | . |
| 1 | 1 | 1 | 1 | 1 | 1 | 1 | 1 | . | . | . |
| 1 | 1 | 1 | 1 | 1 | 1 | 1 | 1 | . | . | . |
| 1 | 1 | 1 | 1 | 1 | 1 | 1 | 1 | . | . | . |
| 1 | 1 | 1 | 1 | 1 | 1 | 1 | 1 | . | . | . |
| 1 | 1 | 1 | 1 | 1 | 1 | 1 | 1 | . | . | . |
| 1 | 1 | 1 | 1 | 1 | 1 | 1 | 1 | . | . | . |
| 1 | 1 | 1 | 1 | 1 | 1 | 1 | 1 | . | . | . |
| 0 | 0 | 1 | 1 | 1 | 1 | 1 | 1 | . | . | . |
| 1 | 1 | 1 | 1 | 1 | 1 | 1 | 1 | . | . | . |
| 0 | 0 | 1 | 0 | 1 | 1 | 1 | 1 | . | . | . |
| 1 | 0 | 1 | 1 | 1 | 1 | 1 | 1 | . | . | . |
| 1 | 0 | 1 | 1 | 1 | 1 | 1 | 1 | . | . | . |
| 1 | 1 | 1 | 1 | 1 | 0 | 1 | 1 | . | . | . |
| 1 | 1 | 1 | 1 | 1 | 1 | 1 | 1 | . | . | . |
| 1 | 1 | 1 | 1 | 1 | 1 | 1 | 1 | . | . | . |
| 1 | 1 | 1 | 1 | 1 | 1 | 1 | 1 | . | . | . |
| 1 | 1 | 1 | 1 | 1 | 1 | 1 | 1 | . | . | . |
| 1 | 1 | 1 | 1 | 1 | 1 | 1 | 0 | . | . | . |
| 0 | 1 | 1 | 1 | 0 | 1 | 0 | 1 | . | . | . |
| 0 | 1 | 1 | 1 | 1 | 1 | 1 | 0 | . | . | . |
| 1 | 0 | 1 | 1 | 1 | 0 | 1 | 1 | . | . | . |
| 1 | 0 | 1 | 0 | 1 | 1 | 0 | 0 | . | . | . |
| 1 | 0 | 1 | 0 | 0 | 0 | 1 | 0 | . | . | . |
| 1 | 0 | 0 | 0 | 0 | 0 | 0 | 0 | . | . | . |

| INCLUDE | MATRIX | TM | MODE | PHASE | | | | | | |
|---|---|---|---|---|---|---|---|---|---|---|
| 1 | 1 | 1 | 0 | 1 | 1 | 1 | 1 | . | . | . |
| 1 | 1 | 1 | 0 | 1 | 1 | 1 | 1 | . | . | . |
| 1 | 1 | 1 | 0 | 1 | 1 | 1 | 1 | . | . | . |
| 1 | 1 | 1 | 0 | 1 | 1 | 1 | 1 | . | . | . |
| 1 | 1 | 1 | 1 | 1 | 1 | 1 | 1 | . | . | . |
| 1 | 1 | 1 | 1 | 1 | 1 | 1 | 1 | . | . | . |
| 0 | 1 | 0 | 1 | 1 | 1 | 1 | 1 | . | . | . |
| 1 | 0 | 1 | 1 | 1 | 1 | 1 | 1 | . | . | . |
| 0 | 0 | 1 | 1 | 1 | 1 | 1 | 1 | . | . | . |
| 0 | 1 | 1 | 1 | 1 | 1 | 1 | 1 | . | . | . |
| 1 | 1 | 1 | 1 | 1 | 0 | 1 | 1 | . | . | . |
| 1 | 0 | 1 | 1 | 1 | 0 | 1 | 1 | . | . | . |
| 1 | 1 | 1 | 1 | 1 | 1 | 1 | 1 | . | . | . |
| 1 | 1 | 1 | 1 | 1 | 1 | 1 | 1 | . | . | . |
| 1 | 1 | 1 | 1 | 1 | 1 | 1 | 1 | . | . | . |
| 1 | 1 | 1 | 1 | 1 | 1 | 1 | 1 | . | . | . |
| 1 | 1 | 1 | 1 | 1 | 1 | 1 | 1 | . | . | . |
| 1 | 1 | 1 | 1 | 1 | 1 | 1 | 1 | . | . | . |
| 1 | 1 | 1 | 1 | 1 | 1 | 1 | 1 | . | . | . |
| 0 | 0 | 1 | 1 | 1 | 1 | 1 | 1 | . | . | . |
| 1 | 1 | 1 | 1 | 1 | 1 | 1 | 1 | . | . | . |
| 0 | 0 | 1 | 0 | 1 | 1 | 1 | 1 | . | . | . |
| 1 | 0 | 1 | 1 | 1 | 1 | 1 | 1 | 1 | . | . |
| 1 | 0 | 1 | 1 | 1 | 1 | 1 | 1 | 1 | . | . |
| 1 | 1 | 1 | 1 | 1 | 0 | 1 | 1 | 1 | . | . |
| 1 | 1 | 1 | 1 | 1 | 1 | 1 | 1 | . | . | . |
| 1 | 1 | 1 | 1 | 1 | 1 | 1 | 1 | 1 | . | . |
| 1 | 1 | 1 | 1 | 1 | 1 | 1 | 1 | 1 | . | . |
| 1 | 1 | 1 | 1 | 1 | 1 | 1 | 1 | 1 | . | . |
| 1 | 1 | 1 | 1 | 1 | 1 | 1 | 0 | 1 | . | . |
| 0 | 1 | 1 | 1 | 0 | 1 | 0 | 1 | 1 | . | . |
| 0 | 1 | 1 | 1 | 1 | 1 | 1 | 0 | . | . | . |
| 1 | 0 | 1 | 1 | 1 | 0 | 1 | 1 | 1 | . | . |
| 1 | 0 | 1 | 0 | 1 | 1 | 0 | 0 | 1 | . | . |
| 1 | 0 | 1 | 0 | 0 | 0 | 1 | 0 | 1 | . | . |
| 1 | 0 | 0 | 0 | 0 | 0 | 0 | 0 | . | . | . |

```
.02 TE      MAG              RELATI ERROR  FLOOR
.02 TE      PHASE            RELATI ERROR  FLOOR
.02 TM      MAG              RELATI ERROR  FLOOR
.02 TM      PHASE            RELATI ERROR  FLOOR

DISTORTION CONTROL  MATRIX MODE   1;
        0          0        0        0        0        0        0        0        :        :        :

DISTORTION CONTROL  MATRIX MODE   2;
        0          0        0        0        0        0        0        0        :        :        :

DISTORTION  PARAM.,   MODE   1;
        0          0        0        0        0        0        0        0        :        :        :

DISTORTION PARAM.,    MODE   2;
        0          0        0        0        0        0        0        0        :        :        :

STARTING   MODEL      FILE;
..\2DINV   \MOD-IN    \CHICX

NEW GRID   INFORMA.
8 NAIR     FOR TE     MODE

Z' IN AIR      FOR GRID   ARE;
     -50000      -20000     -5000   -1128.2      -862     -420     -200     -100

          31          62 ny   ,      nz

y's
        38100      35560      33020      30480      27940      25400
        22860      20320      17780      15240      12700      10160
         7620       5080       2540          0      -2540      -5080
        -7620     -10160     -12700     -15240     -17780     -20320
       -22860     -25400     -27940     -30480     -33020     -35560
       -38100

z's
            0         10         20         31       43.1
         56.4         71       87.1      104.8      124.3
        145.7      169.3      195.3      223.8      255.2
        289.7      327.7      369.4      415.4      465.9
        521.5      582.7        650        724      805.4
        894.9      993.4     1101.8     1221       1352.1
       1496.3     1654.9     1829.4     2021.3     2232.5
       2464.7     2720.2     3001.2     3310.3     3650.4
       4024.4     4435.9     4888.5     5386.3       5934
       6536.4       7199     7927.9     8729.7     9611.7
      10581.9      11649      12823    14114.3    15534.7
      17097.2    18815.9    20706.5    22786.1    25073.7
      27590.1    30358.1
```